DEEP SEATED MAGMATISM,
Its sources and plumes

Глубинный магматизм, его источники и плюмы

VLADIVOSTOK
IRKUTSK
2008

Russian Academy of Sciences
Vinogradov Institute of Geochemistry
Siberian Branch
Far Eastern Geological Institute
Far Eastern Brach
Russian Foundation of Basic Research

Deep-seated magmatism, its sources and plumes

(Глубинный магматизм, его источники и плюмы)

PROCEEDING
of VIII International Workshop
« Deep-seated magmatism, its sources and plumes *»*

Edited by Dr. N.V. Vladykin

VLADIVOSTOK

IRKUTSK

2008

UDK 552.33+ 552.33

Deep-seated magmatism, its sources and plumes

Proceedings of the VIII Interntional Conference. Publishing House of the Institute of Geography SB RAS, 2008, 237 p., ISBN 978-5-94797-130-9. Vol.1.

This book offers invited papers of the international workshop organized in Vladivostok. The invited reports discuss the features of alkaline, carbonatite and kimberlite magmatism. They also disclose the influence of the fluid on the thermal regime of mantle plumes. The model of mechanism of forming the core and silicate Earth's cover is given. The evolution of structure of the continental lithosphere under the influence of plume processes is discussed using the data of numerous thermobarometers, obtained from different minerals of mantle xenoliths from kimberlites of the Siberian Platform and the composition of xenoliths. The fluid regime of the lithosphere mantle of the Siberian Platform is proved using the data on the mineral composition and volatile components of the mantle xenoliths in kimberlites. The mineralogical and petrographic composition of the kimberlites of the Upper Muya field, Yakutia was studied and the features of the composition of the lithosphere mantle under this field were calculated. The evolution of the upper mantle from the Riphean to the Carbonaceous was discussed using the data on xenoliths of volcanic rocks of the Nyurba pipe (Yakutia). Geochemical types of kimberlites and their mantle sources are compared for the Yakutian and Arkhangelsk provinces. Inclusions in diamonds from Yakutian kimberlites are investigated. 4 formation types of carbonatites are described; mantle types of their sources are defined using Nd-Sr and C-O isotopes. Coefficients of distribution of rare elements between rhoenite and silicate melt in volcanics are calculated. Mantle sources are considered for peridotites of the archipelago from Sal Island, Cape Verde Archipelago in the Atlantic using data on Re-Os isotopes. Geochemical features of alkaline rocks of the Paleozoic magmatism of Belarus are discussed. Variations in Pt and Au compositions (mineralization of unique alkaline-ultrabasic massif, Konder, Eastern Aldan) are studied.

The book is of great importance for petrologists, geochemists, and specialists studying deep alkaline and kimberlite magmatism, students and teaching staff of Universities.

Published following the decision of the Scientific Council of Vinogradov Institute of Geochemistry SB RAS

Editor: Prof. N.V. Vladykin

Reviewers: *Prof. V.S. Antipin*
Original-model: *S.S.Tsipukova*

Institute of Geography SB RAS
664033, Irkutsk, Ulanbatorskaja str. 1

Published in Glazkovskaya printing House
Irkutsk, Gogol str., 53.
Order № 1960. Edition 100 copies.

ISBN 978-5-94797-130-9

Photo on the cover page volcanj Pectusan in Primorsky krai (after V.G.Sakhno)

TABLE OF CONTENTS

1. Anfilogov V.N., Khachay Y.V. The mechanism of the Earth core and silicate envelopes formation. **5**

2. Vladykin N.V. Formation types of carbonatites: geochemistry and genesis **14**

3. Ryabchikov I.D.,Kogarko L.N.,Brügmann G. Mantle sources of highly reduced melts in peridotites from Sal Island,Cape Verde Archipelago **25**

4. Kogarko L.N., Hellebrand E., Ryabchikov I.D. Trace element partitioning between rhönite and silicate melt in Cape Verde volcanics **32**

5. Pokhilenko N.P. Permo-Triassic Superplume and its influence to the Siberian lithospheric mantle **41**

6. Logvinova A.M., Wirth R., Fedorova E.N., Sobolev N.V. Multi-phase assemblages of nanometer-sized inclusions in cloudy Siberian diamonds: evidence from TEM **53**

7. Sablukov S.M. , Sablukova L.I. , Stegnitsky Yu.B. , Karpenko M.A., Spivakov S.V. Volcanic rocks of the Nyurbinskaya pipe: a portrayal of regional upper mantle evolution from the Riphean to the Carboniferous time, and its geodynamic relationship **71**

8. Ashchepkov I.V., Pokhilenko N.P. , Vladykin N.V. , Logvinova A.M., Rotman A.Y. , Afanasiev V.P., Pokhilenko L.N. , Kuligin S.S. , Malygina L.V. , Alymova N.V., , Stegnitsky Y.B. , Khmelnikova O.S. Plume interaction and evolution of the continental mantle lithosphere **104**

9. Pokhilenko L.N., Pokhilenko N.P., Fedorov I.I., Tomilenko A.A., Usova L.V., Fomina L.N., Sobolev V.S. Fluid regime peculiarities of the lithosphere mantle of the Siberian platform **122**

10. Spetsius Z.V., Zezekalo M.Yu., Tarskhix O.V. Pecularities of mineralogy and petrography of the Upper-Muna field kimberlites: application to the lithospheric mantle composition **137**

11. Lapin A.V., Tolstov A.V. Geochemical types of kimberlites and their mantle sources **147**

12. Mikhailov N.D., Vladykin N.V., Laptsevich A.G. Geochemical features of alkali rocks of Palaeozoic magmatism of Belarus **169**

13. Lennikov A.M., Zalishchak B.L., Oktyabrsky R.A., Ivanov V.V. Variations of Chemical composition in platinum-group minerals and gold of the Konder alkali-ultrabasic massif, Aldan Schield, Russia **181**

14. Stoppa F. Alkaline and ultramafic lamprophyres in Italy: distribution, mineral phases and bulk rock data **209**

FOREWORD

The fact is well accepted that alkaline rocks represent unique formations on the Earth. They have been long attractive for research because large Nb, Ta, Zr, Y, TR, Cu and P deposits, gemstones of charoite, Cr-diopside, dianite are associated with them. For instance, in Australia diamonds are recovered in lamproites. The complicated processes of their formation provoked scientific disputes still going on. The newly developed analytical methods and techniques provided abundant information on the composition of alkaline rocks. The data on geochemistry of isotopes confirm the evidence on the mantle sources of the substance of alkaline rocks. The new concepts of plume tectonics are applied by scientists when studying alkaline rocks as the deep-seated geodynamics of the Earth is interpreted based on these data.

These problems were discussed at the international workshops held in 2001 at the Institute of Geochemistry in Irkutsk; in 2002 at the Far-East Geological Institute, Vladivostok; in 2003 at the Institute of Tectonics and Geophysics in Khabarovsk, in 2004 at Geological Institute in Ulan-Ude, in 2005 at the Institute of Volcanology and Seismology in Petropavlovsk-Kamchatsky), in 2006 in TSNIGRI JC "ALROSA" in Mirny, in 2007 in Irkutsk and Naples (Italy). We are very grateful to the Italian colleagues, the Department Director Università di Perugia Prof. Walter Dragoni for arranging the geological excursion to visit alkaline volcanoes in Italy and Prof. A.Peccerillo for conducting the above excursion. The workshop on 2008 was held at the Geological Institute, Far East Branch, Vladivostok, the invited reports of which are presented in this book.

The model of mechanism of forming the core and silicate Earth's cover is given. The evolution of structure of the continental lithosphere under the influence of plume processes is discussed using the data of numerous thermobarometers, obtained from different minerals of mantle xenoliths from kimberlites of the Siberian Platform and the composition of xenoliths. The fluid regime of the lithosphere mantle of the Siberian Platform is proved using the data on the mineral composition and volatile components of the mantle xenoliths in kimberlites. The mineralogical and petrographic composition of the kimberlites of the Upper Muya field, Yakutia was studied and the features of the composition of the lithosphere mantle under this field were calculated. The evolution of the upper mantle from the Riphean to the Carbonaceous was discussed using the data on xenoliths of volcanic rocks of the Nyurba pipe (Yakutia). Geochemical types of kimberlites and their mantle sources are compared for the Yakutian and Arkhangelsk provinces. Inclusions in diamonds from Yakutian kimberlites are investigated. 4 formation types of carbonatites are described; mantle types of their sources are defined using Nd-Sr and C-O isotopes. Coefficients of distribution of rare elements between rhoenite and silicate melt in volcanics are calculated. Mantle sources are considered for peridotites of the archipelago from Sal Island, Cape Verde Archipelago in the Atlantic using data on Re-Os isotopes. Geochemical features of alkaline rocks of the Paleozoic magmatism of Belarus are discussed. Variations in Pt and Au compositions (mineralization of unique alkaline-ultrabasic massif, Konder, Eastern Aldan) are studied.

The book might present interest to specialists involved in petrological and geochemical investigations as well as those studying deep alkaline and kimberlite magmatism.

Chairman of Organizing Committee,
Chief Editor Dr. N.V. Vladykin

UDK 523.3

The mechanism of the earth core and silicate envelopes formation

Anfilogov V.N.[1], Khachay Y.V.[2]

[1]*Institute of mineralogy Ural division of Russian Academy of Sciences, Miass, Russia*
[2]*Institute of geophysics Ural division of Russian Academy of Sciences. Ekaterinburg, Russia*

ABSTRACT

The mechanism of core formation and possible mantle composition are considered with using the two stage model of the Earth formation. The model is presumed that the solid particles accumulation and primary embryo formation happens coincidentally with condensation of the solid compounds from gas phase. The embryos are warmed up to the melting temperature of iron by energy of ^{26}Al decay. The liquid iron core is formed by the integration of smelt iron embryo envelopes at their collision. The portion of embryo material goes out from the growing Earth feeding zone and the Moon is formed from it. The two stages model has a clear mechanism of liquid iron core on the early stage of the Earth formation. It allows to explain the Earth magnetic field occurrence and MGD dynamo start-up mechanism. The silicate Earth envelope is formed from the material, which composition is consistent with ordinary chondrites. As the Earth size increased its composition changed from H-chondrites to LL chondrites. The carbonaceous chondrite material took part in the Earth formation on the final stage and was concentrated in the outer part of upper mantle. As a result this part of mantle was enriched by water. The active function of water in the processes of differentiation brought to big volume acid magmatites formation, which werefixed in Archean rocks as “grey gneisses”

Keywords: Earth, core, silicate envelope, mantle

The composition of the Earth core and its silicate envelopes depend on the way of the Earth accumulation and later differentiation. The modern hypothesis are assumed that protoplanetary material had gone through two consecutive stages: the stage of the solid phases condensation from gas phase and the stage of solid particle agglomeration in gas-dust cloud [8], which was accomplished with planet formation [24].The currently available data of the time of potopanetary cloud cool (10^4 -10^5 years) [6,8] shows that there is no way to separate these processes by time and by distance from the Sun. It is beyond reason to exclude the possibility that the solid phase condensation and solid particle agglomeration can work concurrently. It permits to use the sequence of the solid phase condensation, which is founded in laboratory experiment to description of the planet formation mechanism [11,18].

The assumption that the solid particle agglomeration process began after the process of the primary gas material condensation was completed and had gone in

cold cloud allows homogenous Earth accretion variant only. This variant leads to primary homogenous cold planet. The portioning of homogenous planet material on the iron core and silicate mantle is conceivable in the final stages of its formation, which exist happen be after the secondary warming-up of the upper planet strata only. There is a problem on the energy contributor to start-up the process of the primary homogenous Earth differentiation. The decay of radioactive elements is able to warm-up the Earth two billion years after its formation only. The assumption that the warming- up of the Earth was caused by impact with the space body, which was Mars-sized is speculative and it will not be the subject of discussion. Moreover the homogenous accretion models do not agree with data on the geochemisrty of isotopes, which has been realized at lately time. These data evidence, that the separation of the core and mantle chemical reservoirs took place on the beginning stage of the Earth formation [10].

The heterogenous accretion is the alternative to homogenous one. It proposes that the composition of material from which the Earth has been formed was not constant, but changes as the size of the Earth increase. This idea was supported by many investigators [1,2,5,6,11,23,25]. The most radical point of view was stated by Anderson, who proposed that the inner core was built up from the early condensates, which had been condensed before iron. [2].The possible composition of the Earth envelopes and their evolution are discussed on the basis of the two stage model of the Earth formation in this paper.

Simultaneous condensation and solid particle agglomeration permits to propose that the composition of the central part of the planets was close to CAI – white inclusions in the Allende meteorite on the first stage of planet formation [3]. These inclusions are the most high temperature and ancient condensates in the Solar system [4]. As the embryos grows and the protoplanetry cloud cool the condensate composition changes, Fig. 1 and in the wake of the high temperature iron and iron-silicate fractions will be precipitated on the embryo surface. The planet embryos, which size is the first hundred kilometers, will be formed as a result of the impacts and partially integration of the planetesimales. The structure of these embryos is shown on the Figure 2.

The warming-up of the embryos as a result of the short-live radioactive isotope decay take place during the process of growing. The main short-live isotope is ^{26}Al, which half decay period, t = $7.38 \cdot 10^5$ years. The $^{26}Al/^{27}Al$ ratio in protoplanetary material is equal $5 \cdot 10^{-5}$ [15,16]. The temperature in the embryo center may be as much as 1850-2200K at this ^{26}Al content if the embryo size is 200 km [3]. It is large enough for partial melting alumino-silicate mixture in the central part of embryo and full melting of the Fe-Ni mixture in its middle envelope. The outer envelope, which is complicated by olivine-pyroxene chondritic material remains solid at this time, Figure 2.

The further evolution of the planet formation process goes in following manner. In line with Safronov's model of the planet accumulation [19] the embryo quantities, which are formed on initial stage of agglomeration is large and they will

impact one to other often. The impact of two embryos, having close size, partially molted core, smelt iron middle envelope and hard silicate outer one terminate to

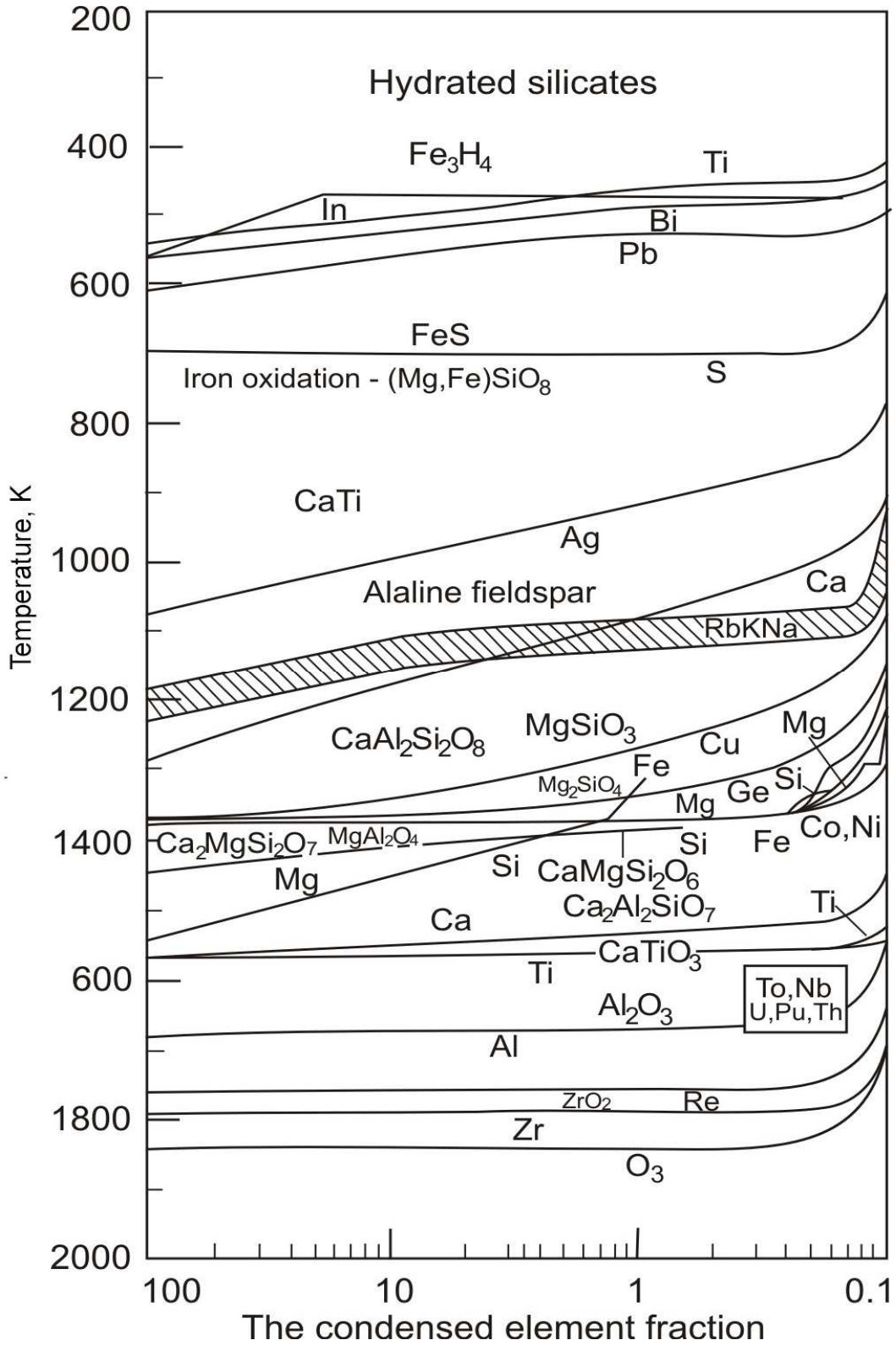

Fig. 1, **The sequence of solid phases condensation from gas phase [11,18],**

their failure. Middle smelt iron envelopes will coalesce after impact and form a new embryo complicated from Fe-Ni molted allow. Material of alumino-silicate cores will be press-out from inner part of the primary embryos and throw out partially beyond new embryo. The outer solid envelopes will be failured and part of their fragments goes out beyond the growing planet. The two primary embryo impact is represented schematically in Fig 3. The duration of the first stage accordingly dynamic assessment [12] not more then 10^6 years, what is in agreement with time of chemical reservoirs the Earth core and mantle separation [10].

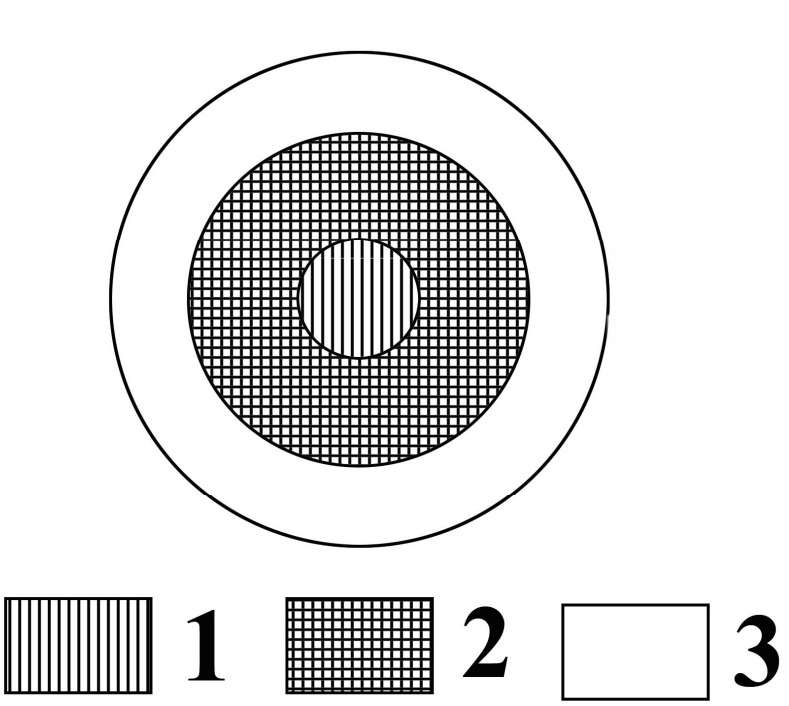

Figure **2The schematic structure of the primary Earth embryo.**

1- the high aluminum core; 2 – the smelt ron envelope; 3 – the outer hard envelope.

The integration of iron envelopes after impact of the primary embryos gives rise to the second embryo generation, the most part of which is represented by the Fe-Ni smelt core. Two the most complete problems are solved by his way: the core formation on the initial stage of the Earth formation, the possibility of MHD dynamo start-up and geomagnetic field formation, which are inducted in smelt iron core by the outer magnetic field [12]. Dynamics of further process of the Earth formation is described by Safonov's model. When the Fe-Ni core reaches the most part of its modern mass it becomes able to hold and to form asilicate envelope round itself.

The discussed above two stages model of the Earth formation is represented the heterogenous accretion variant. Contrary to variants proposed before [18] it gives the real mechanism of the smelted iron core formation on the initial stage of the Earth formation, removal of the primary light alumino-silicate material from

the center of embryo and explains the origin of high temperature in the growing Earth.

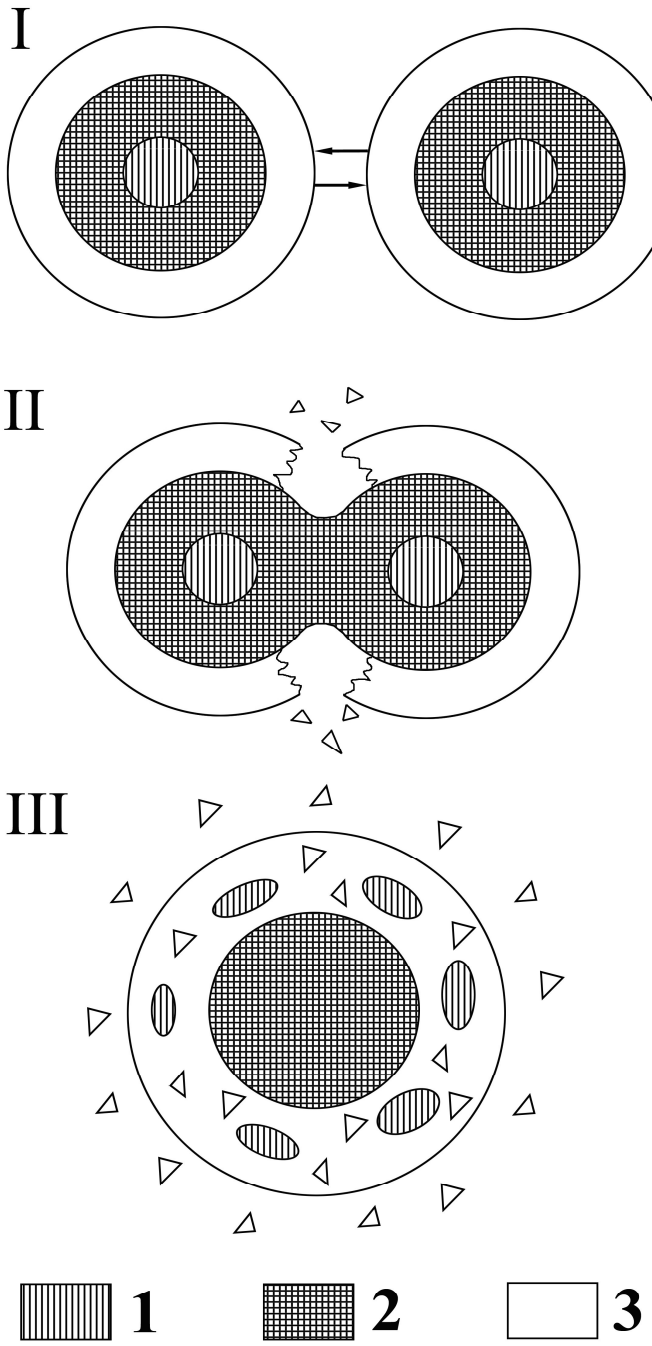

Fig. 3. **The new Earth embryo formation as a result of the two primary embryos collision.**

1 - high aluminum material; 2 –smelt iron material; ordinary chondritic material.

The two stages mechanism of the Earth formation allows to propose the possible variant of the Moon formation together with the Earth, explain the absence of metallic iron in the Moon and high primary temperature in the Moon interior. The major source of material for the Moon formation is the fragments formed at the primary Earth embryos destruction and gone out from area of the

growing Earth feeding. Because the main part of iron is among the Earth core there is a lack of material for the Moon formation. Aside from iron the Moon material accessibled to investigation is depleted of potassium. In line with condensation sequence (Fig.1) it allows to exclude the alkaline fieldspars and other solid phases, which condensed at temperature lower than 1100K . This suggests that the material of the Moon was separated from the Earth one before accretion of the Earth was completed. If this is the case the most part of potassium must accumulate by the Earth at the last stage of its formation and is concentrated in the upper mantle.

Let us consider possible composition of the silicate envelopes of the Earth. Meteoritic material is the primary source of information about mantle composition. Whereas the iron meteorites gives us solid data about core composition the stone meteorites considered as a possible material of silicate Earth envelopes have rather different composition and choosing of meteorite type, which is represented mantle composition is ambiguous. The problem is complicated because some part of meteorites is the fragments knocked from the Moon and nearest planets surface [22] and can not be the material for the Earth formation. A similar statement is true for meteorites which age is younger then the Earth [13].

A.E. Ringwood has analyzed the complex of physical and mineralogical criterions: the distribution of seismic waves velocities, springiness, density, mineralogical composition and phase transformation of minerals at high pressure got the conclusion that two alternative models can be considered [17].

1. The lower mantle has pyrolite composition and its density excess is conditioned by phase transitions.
2. The lower mantle is enriched by FeO and possible SiO_2 [17].

We believe that these variants are not alternative. Firstly there is no evidence for composition of material for the Earth formation was constant during all time its accumulation and that it was consistent to carbonaceous chondrites. Secondly the phase transformations of the mantle minerals are investigated experimentally and it is impossible to build up the correct model of lower mantle not having regard these transformations.

Based on the sequence of solid phase condensation, Fig 1, more likely the lower mantle must have composition not carbonaceous, but olivine-pyroxene chondrites. These chondrites are distinguishing from carbonaceous ones by the absence of water and presence of large quantity of iron and troilite, Table 1. In analogous way the base of mantle would be expected conforms to composition of H-chondrites, which have large quantity of iron. As the Earth mass increases H-condrite composition changes on L- and LL-chondrite one. The proposed chondritic lower mantle is no strong difference from the pyrolite one. As may be seen from table 1 the middle composition of chondrites without Fe and FeS is close to pyrolite. It differs from pyrolite by high concentration of FeO nd more low concentration of MgO. It well to bear in mind, that it is initial composition formed in the Earth growing process. As the temperature and pressure increased the

material of lower mantle was differentiated and Fe and FeS move to the core. Part of iron oxide by the way of disproportioning transform to magnetite and metallic iron:

$$\mathbf{4FeO = Fe_3O_4 + \alpha Fe,}$$

Then it moves to the core too [18]. The result composition of the lower mantle became to pyrolite one still further as a result.The pyrolite model of the upper mantle put forward by A.E. Ringwood gained general acceptance [18]. It is built-up on the base of correlation of of carbonaceous chondrites composition, alpine hyperbasites and deep-earth kxenolites in kimberlites and alkaline basalts. In spite of general acceptance the pyrolite model has some contradictions. It is agreed that the Earth material is conformed to the middle meteorite composition. But there is no meteorites, except Allende one and the rear ureilites having as high concentration of MgO and as low concentration of FeO as pyrolite. It rises the question where leaves the excess of FeO and from where appears the excess of MgO in mantle. By this is meant that pyrolite and other mantle composition models are approximate.

Table 1.

The composition of chondrites and Ringwood's pyrolite

	Type H [14] (53)	**Type L [14] (79)**	**Type LL [13] (17)**	**Pyrolite Ringwood [18]**
SiO_2	**47, 0**	**45,2**	**42,8**	**45,1**
Al_2O_3	**3,0**	**2,9**	**2,7**	**3,3**
FeO	**12,9**	**17,7**	**21,5**	**8,0**
MgO	**30,1**	**28,6**	**27,8**	**38,1**
CaO	**2,5**	**2,2**	**2,0**	**3,1**
Na_2O	**1,1**	**1,0**	**0,9**	**0,4**
FeS	**5,6**	**5,8**	**5,3**	
Fe	**17,3**	**6,7**	**1,3**	

We will now look at the origin of catarchtan crust. It is made up of basic volcanic, and acid magmatic and metamorphic rocks [21]. V.E. Hain and N.A Boshko advocate that the "grey gneises" not only constantly present in Archean rocks, but is prevalent quantitative [9]. These rocks could form by the way of primary mantle composition partial melting with the specific toward Archean active constraint of water only.

The sequence of solid phase condensation, which is used by two stages model of the Earth formation is proposed that water and carbon appeare in the material for the Earth formation in the closing stage this process. Absence of carbon in the early condensates is due to CO_2 generation, which remains in gas phase of the protoplanetary cloud:

$$\mathbf{C + O_2 = CO_2 \qquad (\Delta G_{1400K} = -396.17\ kJ/mol\ [19])}$$

Coincidentally with CO_2 production the oxidation of Fe occurs. The free energy changes in this process at 1400K is equal -180.44 kJ/ mol [19] and oxidation of Fe is not in competition with CO_2 production.

Carbon, H_2O and organic compounds appear in protoplanetary material and in meteorites as the temperature decreases, hydrogen concentration increased and carbon restored:

$$\mathbf{CO_2 + H_2 + C + 2H_2O\ (\Delta G_{600\ K} = -95.70\ kJ/mol\ [19])}$$

It is followed from this that the process of the Earth formation is to be ended by the formation of the enriched water and carbon outer envelope having chondritic composition of its silicate component. Two processes may be in this envelope at high temperature. 1 – degassing of outer envelope, which gave rise to atmosphere and ocean formation. 2 – production of big volume of dioritic and granitic melt, which able to form at presence of water.

The outlined considerations about the sources of material for silicate envelopes formation allows to propose the hypothesis on the mantle composition at all and upper mantle one in particular. The average mantle composition more likely is consistent with olivine-pyroxene chondrites composition without metallic Fe and FeS. Compared to Rinwood's pyrolite it enriched with FeO and depleted with MgO. The material of carbonaceous chondrites takes part in upper mantle. Three types of geochemical reservoirs can be in outer part of upper mantle: the material of primitive mantle consistenting with average mantle composition, partial depleted mantle consistenting with Ringwood's pyrolite and depleted mantle. The last composition is formed after basaltic magma smelted from pyrolite.

CONCLUSION

1. The smelt iron core is formed on the initial stage of the Earth formation. It is formed by the integration of smelt iron envelopes of the primary embryos at their collision.

2. The overwhelming bulk of mantle made up from chondritic material, which composition is changed from H-chondrite to LL-chondrite.

3. The carbonaceous chondrite material took place in outer part of upper mantle formation only. The active function of water in the processes of differentiation brought to big volume acid magmatites formation, which are fixed in Archean rocks as "grey gneisses"

This investigation is supported by RFBR. Grant № 07-05-00395

REFERENCES

1. **Anders E.** Chemical processes in the early solar system, as inferred from meteorites// Account Chem. Res. 1968. No 1. P.289-298.
2. **Anderson D.L., Sammis C., Jordan T.** Composition of the mantle and core// E.C. Robertson (ed.). The nature of the solid Earth. McGraw-Hill. New York, 1972. P. 41-66.

3. **Anfilogov V.N., Khachay Y.V.,** 2005. A possible scenario of material differentiation at the initial stage of the Earth's formation. Doklady Earth Sci. . 403A, 954-957..
4. **Brearley A.J, Jones R.H.** Chondrite meteorites // Rev. Min. 1998. V. 36. P. 3-83- 3-190
5. **Cameron A.G.W.** Accumulation processes in the primitive solar nebula// Icarus. 1973. V. 18. P. 407-450.
6. **Clark S.P., Turekian R.R., Grossman L.** Model of the early history of the Earth // Nature of the solid Earth / Ed. E.C. Robertson. N.Y.: McGraw-Hill,1972. p.3-18.
7. **Dodd R.T**. Meteorites. A petrologic-chemical synthesis. Cambrige Univ. Press. New York. 1981. 384 p.
8. **Dorofeeva V.A., Makalkin A.B.** The evolution of the early solar system. The cosmochemical and physical aspects. Moscow. UPSS. 2004. 264 p.
9. **Hain V.E., Bozhko H.A.** Historical geotectoniks. Pre-Cambrian. Moscow. Nedra. 1988. 382 p. (Russian).
10. **Harper C, Jacobsen S.** Evidence for ^{182}Hf in early Solar system and constraints the timescale for terrestrial accretion and core formation// Geochim. Cosmochim. Acta. 1996. V.60 No 7. C. 1131-1153.
11. **Grossman L.** Condensation in the primitive solar nebula. Geochim. et Cosmochim. Acta. 1972. V. 36. P. 597-619.
12. **Khachay U.V., Anfilogov V.N.** About condition an d process of the Earth formation on the early stage of accumulation. The Fundamental problems of geotectonic. V.II. Moscow. 2007. P. 330-333. (Russian)
13. **Marakushev A.A.** The early Earth's crust from meteorite composition research// The early crust: the composition and edge. Moscow. Nauka. 1991. P. 27-38. (Russian)
14. **Mason B.** Meteorites. John Wiley and Sons Inc. New York. 1962. 283 p.
15. **Merk R.,Breuer D., Spohn T.,** 2002. Numerical modeling of ^{26}Al – Induced radioactive melting of asteroids concerning accretion, Icarus, 159, 183-191.
16. **Nichols R. H Jr.** Short lived radionuclides in meteorites: constraints on nebuar time scales to the production of solids// Space Sci. Rev. 2000 № 1-2б. P. 113-122.
17. **Ringwood A.E.** Composition and petrology Of the Earth's mantle. McGraw-Hill. New York. 1975.
18. **Ringwood A.E**. Origin of the Earth and Moon. Springer-Verlaqg. 1979.
19. **Robie R.A,Hemingway B.S., Fisher J.R.** Thermodynamic properties of minerals and related substances at 298.15 K and 1 bar(10^5 Pascals) pressure and at high temperatures. Geol. Surv. Bull. 1978. No 1452. 456 p.
20. **Safronov V.S.** Protoplanetary cloud evolution and The Earth and planet formation. Moscow. Nauka. 1969. 244 p. (Russian)
21. **Salop L.I.** The grological development of the Earth in Pre-Cembrian. Leningrad. Nedra. 1982. 343 p.(Russian)
22. **Shukolukov U.A.** A isotope-cosmochemical evidence of the native material transport between terestrial planets. Geochemistry International. 2003. No 11.
23. **Turekian K., Clark S.P.** Inhomogeneous accumulation of the Earth from the primitive solar nebula// Earth Planet. Sci. Lett. 1969.V. 6. P. 346-348.
24. **Vitiazev A.V. Pechernikova G.V. Safronov V.S .** The terestrial planets. Moscow. Nauka. 1990. 296 p.
25. **Voitkevich G.V.** The foundation of Earth origin theory. Moscow. Nedra. 1979. (Russian)

UDK 552.33+ 550.42

Formation types of carbonatites: geochemistry and genesis

Vladykin N.V.

Vinogradov Institute of Geochemistry SB RAS, Irkutsk, vlad@igc.irk.ru

INTRODUCTION

The "carbonatite" problem is one of the largest problems in modern petrology, geochemistry and geology of deposits [1]. The carbonatite complexes are related to the largest deposits of rare elements: niobium, tantalum, rare earths, zircon, strontium, barium, iron, copper, apatite, fluorite, phlogopite, vermiculite, forsterite, K-richterite-asbestos, gem stones – charoite, dianite and other minerals [5,7,8,19,21,23].The carbonatite problem originated at the beginning of the 20th century when the so-called "intrusive limestone" were given attention. In 1920-ies

W.C.Brogger proved the magmatic genesis of carbonatites. However, 1930-ies N.L.Bowen using the experimental data showed impossible formation of dry carbonate melts, and thus, carbonatites were regarded as metasomatic and hydrothermal formations. The greatest splash in studying carbonatites took place in 1950-1960-ies when high concentration of rare elements required for the developing industry. This splash lasted up to 1980-ies. A great number of new massifs and provinces of carbonatites and related deposited were discovered at that time. Different scientific geologic schools available in the USSR: Leningrad (Leningrad State University, NIIGA), Moscow (VIMS, IMGRE, IGEM), Irkutsk – IGC, SB RAS much contributed to studies of carbonatites; a number of monographs devoted to carbonatites were published [11, 15]. The carbonatite occurrences of the Kola Peninsula and Siberia were intensively studied (Fig. 1). Classification of carbonatites has been developed. **So, endogenous carbonate rocks containing over 50 % of the carbonate component, demonstrating a certain set of rare elements, and related to complexes of ultrabasic-alkaline formations were regarded as carbonatites.** As regard to the composition of major rock-forming carbonate the following carbonatites have been distinguished: calcite, dolomite, ankerite, siderite as well as transitional varieties, e.g. calcite-dolomite, ankerite-dolomite and others. Some young scientists recently involving into this problem have ignored this classification, replacing the name "carbonatites" by fashionable western terms – sevites, beforsites; though these names were given not to carbonatites as a type, but carbonatites from certain localities, which are characterized by regional differences as compared with typical carbonatites. Therefore, the more rational names of these carbonates are calcite and dolomite taking into account the composition of the major carbonates. Later on carbonates were found together with complexes of alkaline rocks, though it was doubtful to refer the latter to carbonates. Detailed studies of new carbonatite occurrences associated with potassium complexes led to discovery of calcite-fluorite [7,8] and unusual Ba-Sr benstonite carbonatites [23,24]. As regard to their genesis in 1960-1970-ies the majority of geologists considered carbonatites as metasomatic formations (rare exceptions- e.g. L.S. Egorov always considered carbonatites as magmatic formations [3]). The comprehensive geologic, mineralogic-petrographic,

geochemical, isotope studies confirmed the endogenous nature of carbonatites and their magmatic genesis. Carbonatite lavas of active Oldoinyo Lengai volcano (Tanzania) [1] and findings of melted inclusions in carbonatite minerals using the thermobarogeochemical method were of particular significance for interpreting the genesis of carbonatites. Studies of volcanogenic carbonatites (carbonatite tuffs and lavas of Oldoinyo Lengai volcano) revealed new mineral types of carbonatites i.e. ultra-alkaline carbonatites, consisting of soda and potassium (with calcium) carbonates, while the studies of Mushugai-Khuduk complex in Mongolia discovered K-Fe-sulfate-carbonate jarozite-cerussite tuffs containing to 18 % Pb [21]. The Tomtor massif contains explosive Fe-phosphate—carbonate tuffs, containing to 15%Nb and 10 % TR. In some rare-metal carbonatites the rock-forming minerals include monazite (Africa, India), bastnesite-sinkhisite (Lugingol, Mongolia [6] and Bayan-Obo, China) and a number of other rare-metal minerals (Biraya, Siberia). Similar formations correspond to all classification features of carbonatites.

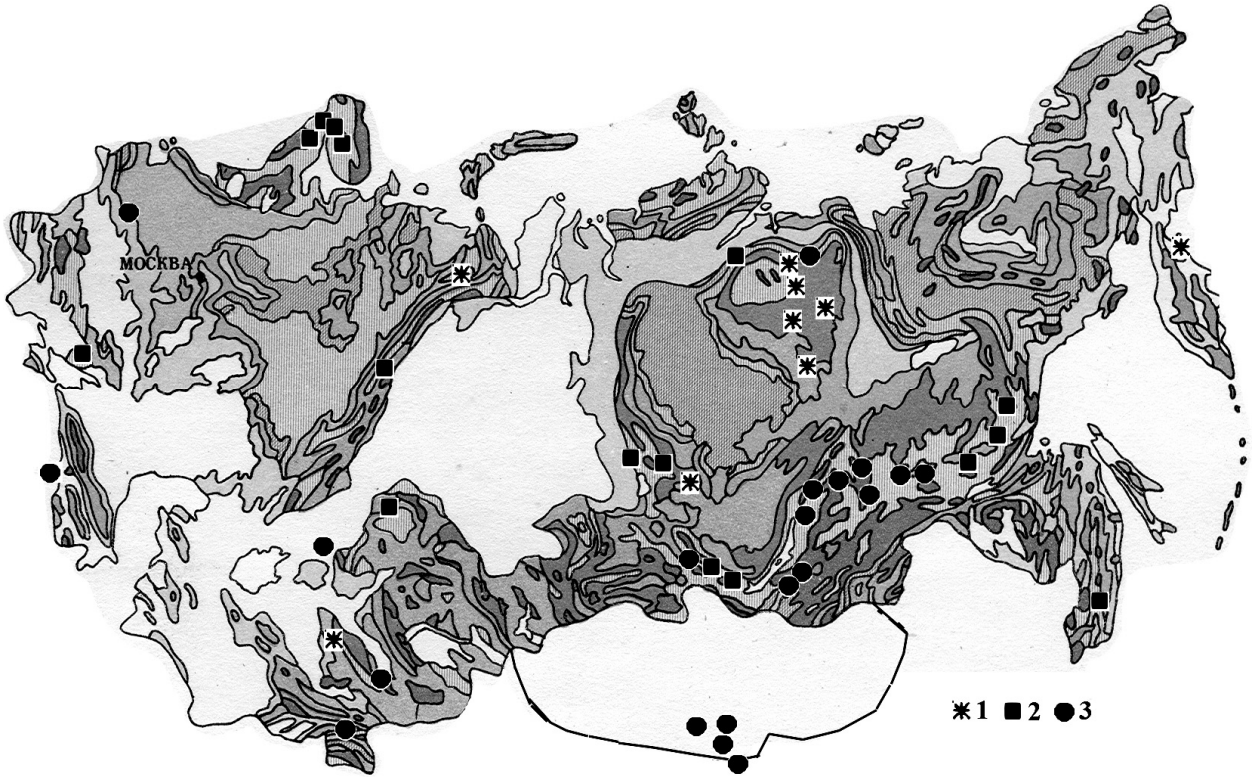

Fig.1. **Location of carbonatite complexes of Russia and adjacent countries.**
1- the first formation types (kimberlite-picrite complexes), 2- the second formation type (Na-alkaline complexes), 3- the third formation type (K-alkaline complexes)

FORMATION TYPES OF CARBONATITES

There are still a lot of disputable questions concerning the genesis of separate carbonatite occurrences and classification of carbonatites.

An attempt to resolve many disputable questions was the article [4] which gives quantitative parameters to refer carbonate rocks to carbonatites and characterizes 3 formation types of carbonatites. A fundamental monograph [1], which discusses a number of carbonatite problems appeared in late 1980-ies. The

interest to this problem slightly decreased in 1990-ies due to difficult situation with geology in Russia. However, at the beginning of the XXI century owing to the evolution of plate tectonics concept the studies of carbonatites as rocks related to deep-seated magmatism which can be used for interpreting deep geodynamic settings, continued [9, 10]. Specialists in other fields of research joined to these studies; however they were less familiar with results of the previous investigations, so they regarded the rocks which do not meet all the criteria revealed to carbonatites that resulted in a confusion and misunderstanding between various authors. Thus, there is a necessity to summarize data concerning carbonate complexes obtained recently. It is in particular urgent due to new analytical methods to study the matter and development of new criteria to classify endogenous carbonate rocks as carbonatites. We have been engaged in studying the petrology and geochemistry of alkaline rocks and carbonatites for 40 years [18-24]. We studied alkaline and carbonatite complexes of the Kola Peninsula, surrounding of the Siberian platform, Aldan and Anabar shields, the Far East, Mongolia, Brazil, India (). We will discuss some questions of classification of various carbonatite complexes using geochemical and genetic criteria.

A.I. Ginsburg and V.S. Samoilov distinguished three formation types of carbonatite complexes related to [4]: 1) complexes of ultrabasic-alkaline rocks; 2) complexes of K-alkaline rocks; 3) linear zones of alkaline metasomatites. This classification is based on different factors: the first formation type considers geologic-petrographic factor, the second - chemical features and the third - genetic, that is not so correct. Moreover, ultrabasic rocks have been recently found in K-alkaline complexes (Vladykin, 2005), while linear zones are related to younger metamorphism as compared with carbonatites, but not to metasomatism. Basically, we agree with these three types, which were of great importance for classification of carbonatites; however new data and sites require further development and supplementation of this classification.

We suggest to use the following criteria as the basis for distinguishing formation types of carbonatites: alkalinity type (Na or K) of alkaline rocks and the time when the carbonatite liquid separated from silicate magma of different differentiation degree. These two parameters are genetically connected, and the type of ore in carbonatite complexes depends on the above parameters. As the previous studies indicate, **all carbonatites are late differentiates of deep-seated alkaline complexes**, having mantle sources. Recently, due to findings of drop-like carbonates in mantle xenoliths of various composition, there is an opinion, that they result from the parent carbonatite magma and can move independently into upper layers of lithosphere forming carbonatite deposits. This conclusion seems to be incorrect for the following reasons: 1) these formations are small in size; 2) they possess an insignificant reserve of heat energy and cannot move far from the site of their origin, and are crystallized in several kilometers hence, do not demonstrate high contents of rare elements as they are not available in the mantle substance from which they were formed. A significant supply of these elements by plumes,

which gave rise to these carbonate drops, is hardly possible. It is more correct to term them as carbonates rather than carbonatites. To verify pure carbonatite nature of the primary magma some scientists give examples when carbonatites are not associated with silicate rocks. In our opinion such carbonatite veins and dykes are located far from silicate rocks which occur deeper and are not penetrated by the erosion or distracted by various geologic processes. The fact that they are not available at present doesn't mean they didn't exist in the past.

We describe the dynamics of forming the primary ultrabasic-alkaline carbonatite magma and its differentiation in the following way: a hot plume together with fluids (hydrocarbons, H, CN, etc. and possibly alkalis) following physical laws of transporting from hot to cold sites uplift to such PT conditions of the mantle where the mantle substance starts melting and reduced gases are oxidized under the influence of hotter plume, as compared with the mantle substance which is colder. . The positive factor for melting the mantle substratum is its preliminary metasomatic transformation by earlier geologic processes, in particular carbonitization and micatization. The reaction giving rise to primary carbonates but mainly melting of silicate magma can occur in these sites. The silicate magma is 500-1000 times higher in volume, than the carbonate melt (usual ratios of silicate rocks and carbonatites in alkaline complexes). This silicate melt absorbs the carbonate melt and is mixed with it. The main factor at melting of ultrabasic-alkaline magma is very low degree of selective melting of the mantle substance, lower than 1 %. Micas, garnet, ilmenite, chrome-diopside, enriched by rare elements as opposed to olivine and rhombic pyroxene, are most likely melted at first. Further this silicate magma with dissolved carbonates, overheated by plume heat starts to uplift through rift zones into the upper horizons of the earth's crust, until its inner pressure becomes balanced with lithostatic pressure of host rocks. A magmatic center is formed and early phenocrysts are crystallized. Depending on the magma's overheat degree and thermostatic properties of host rocks this magma can exists as liquid over a relatively long time span. When magma moved from the site of its origin to the magmatic center different elements were differentiated and particular compounds were formed. There was a redistribution of some rare elements between the silicate melt and carbonate liquid which is kept in the silicate magma by alkaline elements (i.e. complex compounds) and volatiles. The further tectonic movements around the magmatic center result in intruding of some portions of magma into upper horizons, which gave rise to massifs of alkaline rocks or lava flows on the surface. The crystallization of high-temperature minerals (olivine, diopside) gave rise to ultrabasic rocks of carbonatite complexes, while the residual melt is significantly enriched by alkalis, carbonate component and rare elements. The carbonate component, enriched by rare elements is separated as carbonatite salt melt-fluid from the silicate alkaline magma at different temperature, different stages of differentiation and crystallization of the alkaline-ultrabasic magma and depending on prevalence of different alkalis (sodium or potassium). As the potassium is a cation demonstrating

more alkaline features, as compared with sodium, it keeps alkaline-carbonate complexes from separation with the silicate melt for longer span of time and thus, in potassium complexes this separation takes place at later crystallization of the melt and at lower temperature, as compared with sodium complexes. It results in different ore potential of potassium and sodium rocks and associated carbonatites. Not pure carbonate components but the silicate carbonate which contains up to 20-40% of carbonate components is separated from the silicate melt during the first stage. Foskorites, kamaphorites, nelsonites and other rocks of the so-called ore complex are crystallized in sodium formation. Moreover, these rocks demonstrate high phosphorous content. When these rocks are crystallized the carbonate component of the second stage, which gave rise to carbonatites proper, is accumulated. The silicate-carbonate component is separated from the silicate magma in potassium complexes as well. At crystallization this silicate-carbonate component is divided into pyroxene-microcline, pure microcline in some cases silicate charoite (with Ba-Sr) and carbonate (carbonatite) components. If the carbonate fluid contained high Ba and Sr concentrations, it is separated into Ba-Sr benstonine, calcite and quartz-calcite components. The carbonate part of K-formation demonstrates low phosphorus contents, as it was separated as apatite during an early crystallization stage in biotite pyroxenites. However, [SO4] and F, which in the hydrothermal stage result in celestine-barite and fluorite veins, are frequently accumulated in K-carbonatites. Carbonatite salt melts demonstrate high alkalis concentration. They form complex compounds with these alkalis in the silicate magma. When carbonate minerals are crystallized in carbonatites these alkalis are separated as the solution and fenitize the host rocks. If alkaline carbonatite magma couldn't crystallized and instead of it erupted from a volcano (e.g. Oldoinyo Lengai), alkaline carbonates are crystallized. These carbonates are easily dissolved in water and thus are not preserved in nature.

As regard the time of carbonatite liquid separation and alkalinity type of primary silicate complexes three formation types of carbonatites are distinguished. We suggest to unite all carbonatite occurrences of unclear genesis as the fourth formation type.

The first formation type of carbonatites is less differentiated and related to the least differentiated K-ultrabasic kimberlite magmas. Such carbonatites were described by Kovalsky V.V. and Marshintsev V.K. in kimberlite province of the Eastern Anabar Region [12] . These carbonatites form veined bodies or breccias in diatreme structures with xenoliths from kimberlites. The primary kimberlite magma contains insignificant amount of the carbonate component as compared with other magmas and demonstrates higher inner pressure of CO2 that leads to magma explosion in the near-surface zone of the earth's crust. Moreover, the carbonate and silicate magmas are separated and both of them boil. The silicate component forms the kimberlite tuff-breccia, while the carbonate one forms gas CO_2 and H_2O (at hydrogen oxidation) and they carbonatize and serpentize the

kimberlite silicate part. The residual hydrothermal solution is crystallized as quartz-carbonate veins. In another case, if the magma doesn't explode the massive kimberlites are crystallized. In the Eastern Anabar Region they are termed as picrites. The carbonate component is separated as the salt melt and crystallized as dyke bodies. Such carbonatites are marked by the kimberlite association of rare elements (Cr, Ni, Co, Ba, Sr) and in cases Nb. Like kimberlites they contain xenogenic diamonds.

The second formation type of carbonatites is associated with ultrabasic-alkaline sodium complexes. It includes classical carbonatites of the Kola, Maimecha-Kotui, Sayan and other provinces. The carbonate-silicate component is separated at lower temperatures when pyroxenites and ijolite are crystallized. The silicate-carbonate phosphate liquid is separated at first. When it is crystallized foskorites, kamaphorites, nelsonites are formed. These rocks are associated with iron, apatite and phlogopite deposits. They demonstrate the increased Nb, Ta, U и Th concentrations. During the volcanic stage of Na complex origin the fluid-melt crystallized as tuff-explosive ore rocks of the Tomtor type demonstrating ore concentrations of Nb, Ta, TR, Y. During the crystallization of foskorite melts the essentially carbonate liquid is separated. This liquid gave rise to carbonatites (calcite, dolomite, ankerite and in cases siderite).

These carbonatites are more differentiated and contain the accumulated high-temperature rare-elements Nb and Ta. Silicate minerals of carbonatites are also high-temperature and contain [SiO4] radical. They include garnets, fortserites, clinohumite, etc.

The third formation type of carbonatites is related to alkaline potassium complexes. Earlier rocks include ultrabasic Bt-pyroxenites. The most vivid representative of this type is the Murun volcano-pluton on the Aldan shield, alkaline volcanics of Africa and Mongolia. We consider that carbonatites of Mauntain Pass USA, Bayun Obo China, Tamil Nadu India belong to this type. The silicate-carbonate component is separated at later magma differentiation stage, when granite and syenites are crystallized. When silicate-carbonate component is crystallized it is layered into 3 silicate melts (of microcline, pyroxene and charoite composition) and 2 carbonate melt-fluids (calcite and Ba-Sr – bensonite) (which can be exemplified by the Murun massif).

Silicate minerals in carbonatites include minerals with more silicate radicals – potassium feld spar, pyroxenes and micas. They rare contain Nb and Ta minerals, while deposits of rare earth elements (Ba-Sr, fluorite) are typical. In both cases we find gem stones (charoite and dianite).

The second and the third formation types were distinguished by [4] and we only supplemented them by new occurrences, like the Murun massif etc [19. 20].
Correlation between Sr and Nd isotope data and geodynamic setting of massifs and mantle type which gave rise to the magma of alkaline massifs

As known, the type of the primary mantle which gave rise to deep-seated rocks is determined by the ratio of Sr and Nd isotopes, considering the age of rock origin. Three major mantle types are distinguished: depleted mantle, enriched EM-1 and enriched EM-2

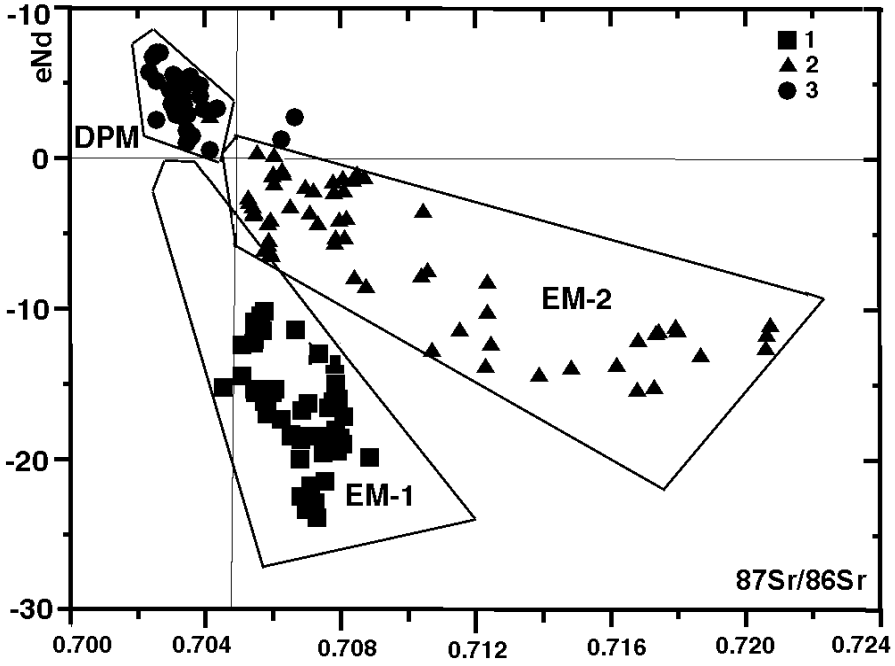

Fig.2. **Isotopes of Sr-epsilon Nd of alkaline, lamproite, carbonatite complexes and mantle rocks**. 1 – alkaline, lamproite, carbonatite complexes of rift zones between the Siberian Platform and Aldan shield as well as North-American Platform and Canadian shield; 2 –alkaline, lamproite, carbonatite complexes of folded areas; 3 – alkaline and carbonatite complexes of the Siberian platform surrounding. DPM-depleted mantle. Data for lamproites are taken from [2,13,17,27], and supplemented for carbonatites from [14,16].

Different mantle types show different isotopes values. So, depleted mantle is marked by positive values of epsilon Nd and values $^{87}Sr/^{86}Sr$ ranging from 0.702-0.705, the enriched EM-1 mantle demonstrates negative values of epsilon Nd and $^{87}Sr/^{86}Sr$ values varying from 0.705-0.709 and EM-2 mantle show negative values of epsilon Nd and $^{87}Sr/^{86}Sr$ values as 0.705-0.725. On the boundary of values three mantle types (EM-1, EM-2, depleted) there is a narrow intermediate area. Classification of rocks demonstrating Sr isotope values over 0.705 as mantle rocks raised doubts. However, mantle rocks such as lamproites of Spain and diamond-bearing lamproites of Australia 87Sr/86Sr values reach as high as 0.722.

We have for the first time obtained the data on geochemistry of **Nd** and **Sr** isotopes for a number of massifs of alkaline rocks and carbonatites of Siberia and Mongolia [26] and their classification resulted in interesting geodynamic conclusions.

Alkaline and carbonatite complexes are formed in different geodynamic settings from different mantle sources (EM-1, EM-2, depleted mantle). Isotope values of massifs located **in the surrounding of the Siberian Platform which**

experienced subduction of oceanic basalts lie in the field **of the depleted mantle**. They include massifs of the East-Sayan province (Bolshaya Zima, Srednya Zima, Tagnin and Zhidoi), Maimecha-Kotui province (Guli and Essei), Enisey Ridge (Kiya and Tatar) as well as East-Aldan and Sete-Davan provinces (Arbarastakh, Ingili and Gornoe Ozero).

Massifs **of folded belts** (areas of completed folding) **where the crustal substance subducted into the mantle through Benioff seismic zones lie in the field with isotope values of enriched EM-2 mantle**. They include carbonatite complexes of Mongolia (Mushugai-Khuduk, Ulugei Khid, Bayan-Khushu, Lugingol, Beltsin-Gol), Buryatiya (Khalyuta, Arhsan, Southern, Oshurkovo and Ermakovka), carbonatites of the North Tien Shan (Darai-Pioz), North Baikal Area (Burpala), as well as lamproites of Australia and Spain.

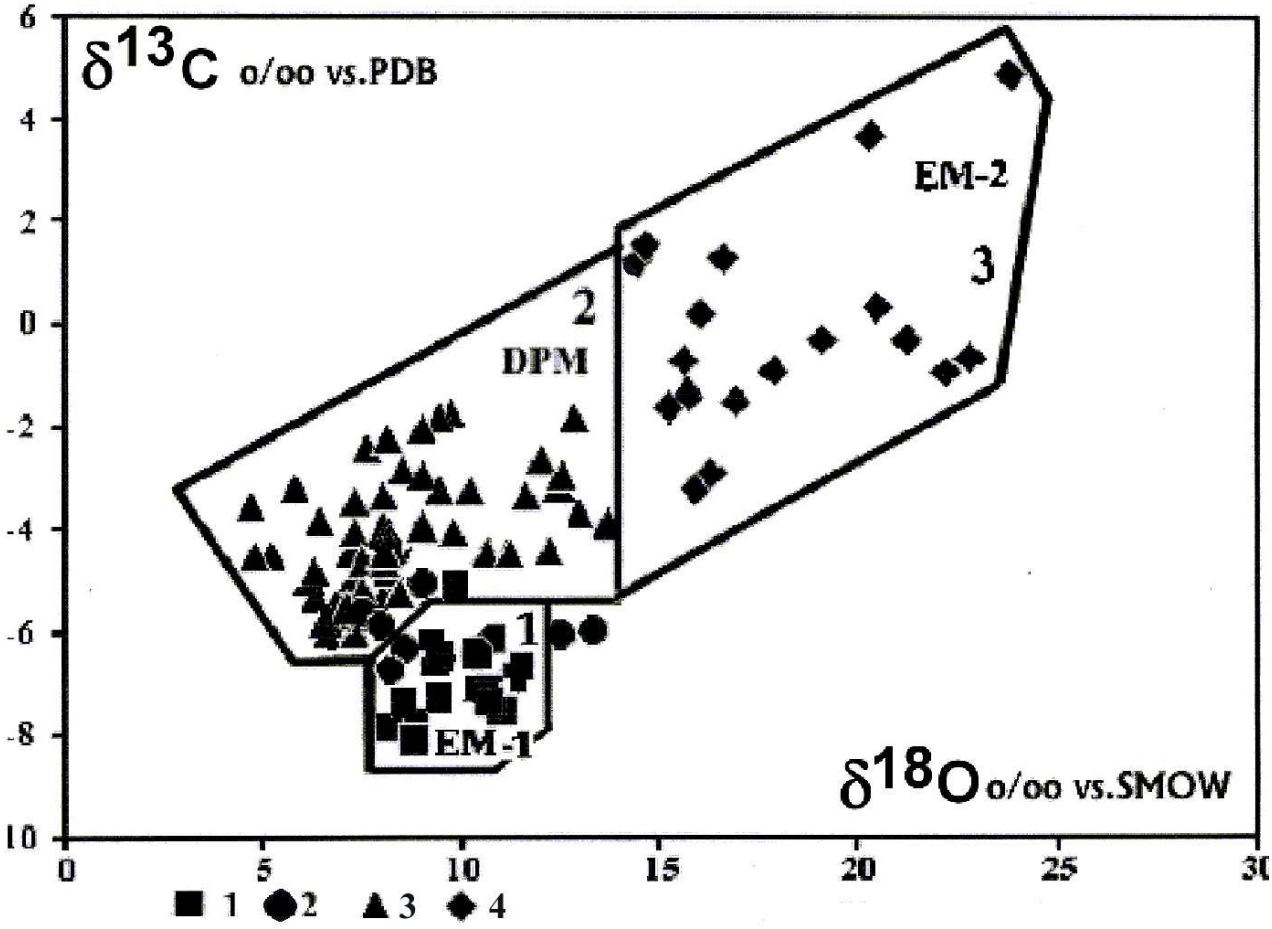

Fig. 3. **Correlation between f oxygen-carbon isotopes and mantle type**
Field 1 - EM-1 mantle, Field 2 – depleted mantle, Field 3 - EM-2 mantle. Dots of rocks of massifs: 1 - Murun, Khani, 2 - Bilibin, Ingili, Arbarastakh, 3 –massifs of the surrounding of the Siberian Platform, , 4 – massifs of folded areas.

The massifs **formed in midland rift zones** between the Siberian Platform and Aldan shield (as well as between the North American Platform and Canadian shield) which didn't experience **any subduction** lie in the field with isotope values

of the deepest **enriched EM-1 mantle**. These are the following massifs: Murun, Ryabinovyu, Yakokut, Bilibin, Khani and lamproites of Leucite Hills Wyoming, Smoky Butte and Preri Creek Montana (USA). Origin of these massifs is related to plume processes. However, the question arises how the depleted magma could give rise to such ore-bearing magmas of alkaline rocks. It can be explained by a low degree of selective melting of the mantle when magmas of alkaline rocks generated. Minerals enriched by rare elements (for example, garnet, ilmenite, mica) are generated.

As we analyzed both **Sr, Nd and C, O** isotopes in one and the same samples we made an attempt to use the data on the mantle type, obtained from Sr, Nd isotope (Fig. 6) for the diagram of carbon and oxygen isotopes [25]. We obtained a relatively compact pattern of massifs division by mantle type (Fig. 7).

Dots corresponding to isotope ratios from carbonatites of massifs of folded areas (Mongolia, Buryatiya, North Baikal area, South Tien Shan, etc.) **lie in Field 3.** Their primary magmas were formed **from enriched EM-2 mantle**. Isotope values in field 3 for carbonatites were earlier explained by capture of the atmospheric oxygen and surface water when carbonatites originated [1,16]. For the studied carbonatites this mechanism can operate, but as the secondary. When rocks from the folded areas were formed surface water was captured and those rocks showed increased values of heavy oxygen. When those rocks subsided along Benioff seismic zones to a significant depth in the mantle the crustal rocks were mixed with the mantle material and isotope carbon and oxygen values changed in that mixed mantle. When magmas of alkaline rocks melted from that mantle, they already had those isotope values. So, heavier oxygen for these alkaline magmas doesn't mean the contamination of these magmas by the crustal substance during magma intrusion and crystallization, as all elements but not only isotopes had to be mixed (that it is not observed in nature). Such high isotope oxygen values result from melting of magma of alkaline rocks **from the contaminated mantle**.

Dots of carbonatite massifs of the surrounding of the Siberian Platform lie in Field 2. The depleted mantle is typical of them.

The field 1 contains dots of carbonatite massifs, originated in rift zones between the Aldan shield and the Siberian platform or on the shield proper. Such characteristic of isotopes is common both to the Mesozoic ultrapotassium complexes of the Aldan shield (Murun massif, etc.) and to the Precambrian K-massifs (Khani massif). Melting of magma on these massifs is related to the plume processes, taking place on the Asian continent at that time. Isotope values of more ancient massifs of the Western Aldan (Arbarastakh, Ingili and Mountain Lake) are located on the boundary between fields 1 and 2. We suggest that such a location is either due to the lack of data concerning the geodynamic setting of these regions in the Precambrian or their proximity to margins of the platform with depleted type of mantle.

The above indicates that it is possible to use this diagram to define the type of the mantle for carbonatites at least for the Asian continent. As the analysis of

oxygen and carbon isotopes is much cheaper and easier than that of Sr and Nd isotopes, this application of diagram is most likely worthwhile. However, for new (recently discovered) carbonatite occurrences it is required to confirm the correctness of mantle type using the data on Sr and Nd isotopes.

Using the geochemical data of these isotopes we can infer that ore-bearing alkaline complexes could be melted from various types of mantle and its composition doesn't much influence on their ore potential. It is surprising, how the depleted mantle which produces barren basalts could give rise to ore-bearing alkaline complexes. **It is most likely that the main factors are small degree of selective melting of the mantle (less than 1 %) and fluid and alkaline components, brought by plumes, which stimulates this melting. A prolonged magma differentiation and layering of the substance under magma crystallization are of particular importance for accumulating of ore elements**.

The investigations were supported by the Russian Foundation for Basic Research (grants 06-05-64416, 08-05-90002).

REFERENCES

1. **Carbonatites: genesis and evolution** (edited by Keith Bell), London, 1989, 601p.
2. **DePaolo, B.J.,**. Neodymium isotope geochemistry // An Introduction. Springer-Verlag, New York. 1988.
3. **Egorov, L.S.** Ijiolite-carbonatite plutonism // Nedra. 1991, 260 pp.
4. **Ginsburg A.I., Samoilov V.S**. On carbonatite problem.//ZVMO, 1983, N 2, p.164-176
5. **Kogarko, L.N., Kononova, V.A., Orlova, M.P., Wooley, A.R.** Alkaline Rocks and Carbonatites of the World . London, Glasgow, New York, Melbourne, Madras. 1995.
6. **Kovalenko, V.I., Vladykin, N.V., et al.** The Lugingol massif of pseudoleucitic syenites in the MNR // Izvestia Akademii Nauk SSSR, seria geologicheskaia, 1974, N 8, p. 38-49.
7. **Kovalenko V.I., Vladykin N.V. et al.** Geochemical characteristics of rocks from near surface carbonatite kindred from Goby desert, Mongolia // Geochimia, 1977,№ 9, pp.1313-1326.
8. **Kovalenko V.I., Samoilov B.S., Vladykin N.V. et al.** Rare-metal carbonatites and apatite-magnetite rocks of Mongolia // Geology and magmatism of Mongolia, 1979, Nauka, v.30, p. 158-167.
9. **Kovalenko V.I., Yarmolyuk, V.V., Vladykin, N.V. et al.** Stages of formation, geodynamic setting and sources of rare-metal magmatism of central Asia // Petrology, 2002,v. 10, .№ 3, p. 227-253.
10. **Kovalenko V.I., Yarmolyuk V.V., Vladykin N.V., Kozlovsky A.M.** Problem of plumes and their bearing on sources of rare-metal magmatism in central Asia // Deep-seated magmatic sources and the problem of plumes Vladivostok, 2002,pp. 23-42.
11. **Kukharenko A.A., Orlova M.P., Bullakh A.G. et al.,** The Caledonian complex of ultrabasic-alkaline rocks and carbonatites of the Kola Peninsula and Northern Karelia , Nedra, 1965, 771pp.
12. **Marshintsev V.K.** Carbonatite formations of the eastern slope of the Anabar arched uplift . Yakutsk, 1974, 118pp.
13. **McCulloch M.T., Jaques A.L., Nelson D.R. and Lewis J.D.** Nd and Sr isotopes in kimberlites and lamproites from Western Australia: an enriched mantle origin // Nature 1983. vol. 302, 31 March, pp. 400-403.
14. **Nikiforov A.B. et al.** Chemical and isotope composition of carbonatites of Transbaikalia // Petrology, 2000, v.8, № 3, pp. 309-336.
15. **Pozharitskaya L.K., Samoilov V.S.** Petrology, mineralogy and geochemistry of carbonatites of the eastern Siberia, M. Nauka, 1972, 265pp.
16. **Pokrovsky, B.G.** Crustal contamination of mantle on evidence of isotope geochemistry. M, Nauka, 2000,228 p.
17. **Powell J.L. and Bell K**. Sr isotopic Studies of Alkaline Rocks: Localities from Australia, Span and Western United States // Contr. Mineral. And Petrol. 1970. 27. pp.1-10.
18. **Vladykin N.V.** Bilibin-massif K-alkali rocks // DAN,1996, v.349, N6, p. 972-975.
19. **Vladykin N.V.** Petrology and productivity of K-alkali rocks of Mongol-Okhotsk area of magmatism // The thesis in the of an scientific report, , Irkutsk, 1997. p.1-80.

20. **Vladykin N.V.** Malyi Murun Volcano-Plutonic Complex: An Example of differentiated Mantle Magmas of Lamproitic Type // Geochemistry International, 2000, v. 38, suppl. 1, pp. 573-583.
21. **Vladykin, N.V.** Ore potential of carbonatite tuffs of K-alkaline complexes of Siberia and Mongolia // 100-anniversary of studies of carbonatites of the Kola Peninsula, 2001. S-Peterburg, p. 49-51.
22. **Vladykin N.V.** The Aldan Province of K-alkaline rocks and carbonatites: problems of magmatism, genesis and deep sources // Alkaline magmatism and the problems of mantle sources. Irkutsk, 2001, pp. 16-40.
23. **Vladykin N.V., Tsaruk I.I.** Geology, chemistry and genesis of Ba-Sr-bearing ("benstonite") carbonatites of the Murun massif // Geology and Geophysics, 2003,v. 44, № 4, pp. 315-330.
24. **Vladykin N.V., Viladkar S.G., Miyazaki T., Mohan R.V.** Chemical composition of carbonatites of Tamil Nadu massif (South India) and problem of "benstonite" carbonatites // Plumes and problems of deep sources of alkaline magmatism. Khabarovsk, 2003, pp.130-154.
25. **Vladykin N.V., Morikiyo T., Miyazaki T.** Geochemistry of carbon and oxygen isotopes in carbonatites of Siberia and Mongolia and some geodynamic consequences // Deep seated magmatism it's sources and their relation to plum processes., Irkutsk– Ulan-Ude, 2004. pp. 96-112.
26. **Vladykin N.V., Morikiyo T. , Miyazaki T**. Sr and Nd isotopes geochemistry of alkaline and carbonatite complexes of Siberia and Mongolia and some geodynamic consequences.//Problems of sources of deep magmatism and plumes, Irkutsk, 2005, v.1, PP 19-37
27. **Volmer R., Mer R., Ogden P.,Schilling J.-G.,Kingsley R.H., Waggoner D.G.**
Nd and Sr isotopes in ultrapotassic volcanic rocks from the Leucite Hills, Wyoming //
Contr. Mineral. and Petrol. 1984, vol. 87, pp. 359-368

UDK 552.33+ 550.42

Mantle sources of highly reduced melts in peridotites from Sal Island, Cape Verde Archipelago

Ryabchikov I.D[1]., Kogarko L.N.[2], Brügmann G.E.[3]

[1]*Institute for Geology of Ore Deposits, Russian Academy of Sciences, Moscow, Russia.*
[2]Vernadsky Institute of Geochemistry, Russian Academy of Sciences, Moscow, Russia.

[3]*Max-Planck-InstituteFur Chemistry, Mainz, Germany.*

Sulphide globules with included Fe-Ni alloys and separate grains of metallic phases were found in intergranular glasses of Sal island [1, 2]. The presence of native metals and high temperatures of mineral equilibria in the lherzolites of Sal island [2] permit to suggest the contribution of lower mantle material into the ascending plume associated with the magmatism of Cape Verde. This hypothesis may be supported by experimental data, demonstrating that under the condition of lower mantle disproportionation of ferrous iron should take place with the formation of metallic phase (about 1%) and excess of ferric iron incorporated into Al-bearing silicate perovskite [3-5]. Equilibria with the participation of metallic phase are distinctly reflected in the behaviour of highly siderophile elements, which also include PGEs, and they significantly affect Re-Os isotope system, which serves as a sensitive monitor of the processes with the participation of sulphides and native metals [6]. We analysed a number mantle xenoliths from Sal island for PGEs and measured Os isotope composition in order to assess possible participation of lower mantle processes in the formation of composition of Cape Verde plume material.

Since both Os and Re are highly siderophile and chalcophile elements, they are mainly stored in mantle rocks in sulphide and metallic phases. The partitioning of these elements between immiscible silicate and sulphide melts during the partial melting of mantle peridotitesand also during the crystallization of sulphide-metallic melts results in the considerable shift in Re/Os ratios. During these processes Os is compatible and Re moderately incompatible element. By contrast, in other isotope systems used as petrogenetic indicators (Sm-Nd, Rb-Sr, Lu-Hf, U-Th-Pb) both parent and daughter elements are incompatible. Therefore, after sufficient time differences in Os isotope composition in various geological objects become much more noticeable than e.g. for Sr or Nd (the deviations of Nd isotope composition from chondrite standard are expressed in 10^{-4} units, whereas for Os 10^{-2} units, i.e. percent, are used). In particular, Re/Os ratios in basalts are several times higher than in mantle restite. Because of it after some time crustal Os

becomes highly radiogenic, whereas in mantle restite $^{187}Os/^{188}Os$ ratios evolve towards subchondritic values. These factors make Re-Os isotope system much more sensitive to the discrimination between crustal and mantle sources by comparison with other isotope systems with radiogenic isotopes.

Harzburgites, lherzolites and a few of pyroxenites are present among the mantle xenoliths of Sal island. Lherzolites are characterized by the maximal content of sulphide globules and grains of Fe-Ni alloys included into veinlets and pockets of glass situated between the grains of primary minerals of xenoliths (Fig. 1) We analyzed Ir,Os,Ru, Pt, Pd and Re, and measured Os and Re isotope composition for two samples of lherzolites (CV5 – close to primitive mantle with

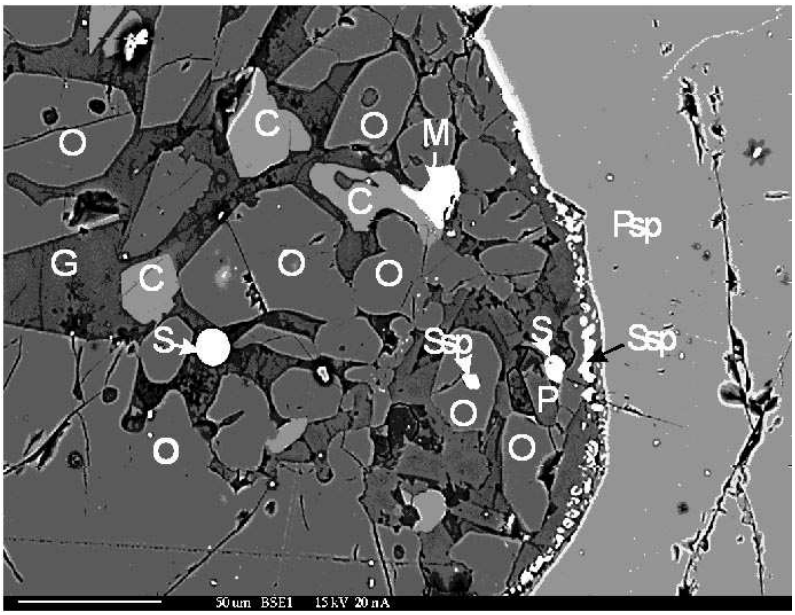

Fig. 1. **The pocket of glass (G) between the grains of primary olivine (O) and primary spinel (Psp). Microphenocrysts of olivine (O), clinopyroxene (C), secondary spinel (Ssp), grains of sulfide (S) and Fe-Ni alloy (M) are immersed in the glass. The zone of primary spinel surrounded by glass is characterized by very low concentrations of Fe^{3+}.**

respect to rock-forming oxides – 20% of Cpx, and CV55 – moderately depleted lherzolite – 14% of Cpx), one harzburgite (CV1), and one pyroxenite (CV37). The isotope composition of Os and Re was performed by Finnigan MAT 262 mass-spectrometerin Max-Planck Institute in Mainz. Concentrations of Pt, Pd, Ir and Ru were measured by isotope dilution. The results of analyses are shown in the Table.

Fig. 2 shows PGE and Re BSE normalized contents in the investigated samples [7]. This diagram demonstrates that PGE and Re contents in CV5 lherzolite is similar to BSE, they are somewhat lower in CV55 lherzolite, but with the exception of Pd maximum the ratios of elements are also similar to BSE, whereas CV1 harzburgite and CV37 pyroxenite are characterized by depletion of heavy PGEs in comparison with light PGEs.

A diagram in coordinates $^{187}Re/^{188}Os$ – $^{187}Os/^{188}Os$ is shown at Fig. 3. An attempt to interpret it in spite of significant scatter of points as isochrone yields age

of 64 Ma. However, the assumption of the closeness if isotope system in this case is completely unrealistic and it is clear that the prevailing part of PGEs and Re was introduced into the investigated rocks in the form of metallic and sulfide phases, which are transported by the infiltrating silicate melt. This process took place not long before the volcanic eruption, which transported the fragments of mantle rocks to the Earth's surface, as may be deduced from the zoning of spinel grains surrounded by glass bearing sulfides and native metals (Fig. 1). In this connection Fig. 3 should be viewed not as an isochrone but as a mixing line.

Table.

Concentrations of Re and PGEs (ppb) and isotope ratios in mantle xenoliths of Sal island.

Sample	Ir	Os	Ru	*Pt*	Pd	Re	$^{187}Re/^{188}Os$	$^{187}Os/^{188}Os$
CV-1	0,304	0,121	2,465	3,841	3,728	0,170	4,8771	0,1258
CV-37	0,334	0,443	0,547	5,455	11,184	0,449	4,1191	0,1273
CV-55	1,056	1,258	1,851	2,084	29,418	0,168	0,4589	0,1239
CV-5	2,243	2,786	7,256	5,071	5,353	0,266	0,3362	0,1202

Fig. 4 shows $^{187}Os/^{188}Os$ ratios from Os content in investigated samples. The observed inverse dependence suggests mixing of two components: in harzburgite and pyroxenite with the low contents of sulfide components more radiogenic Os isotope ratios, whereas in lherzolites, where sulfides and metals are present in substantially higher quantities, and they were introduced at much later time, Os is less radiogenic.

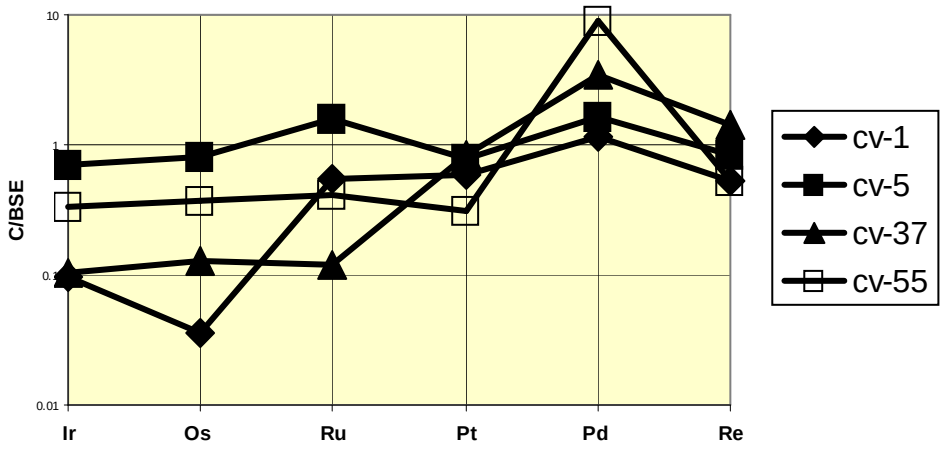

Fig. 2**. BSE normalized [7] PGE and Re contents in the investigated samples.**

The following sources of intergranular melts, transporting sulfides and metallic phases, may be suggested: (1) host volcanic rocks (melanephelinites), bringing xenoliths to surface, (2) partial melts produced in the lithosphere, (3) partial melts produced in asthenosphere (upper mantle), (4) partials melts formed from the material of lower mantle entrained into ascending plume.

The first of the above options is not consistent with a number of facts. Melanephelinites of Sal island contain a lot of titanomagnetite, and like the other lavas from intraplate oceanic islands [8, 9], they are characterized by elevated oxygen fugacities [2]. In contrast intergranular melts from the investigated lherzolites are characterized by anomalously reducing conditions, because they entrain grains of Fe-Ni alloys. Besides, lherzolites from Sal island have subchondritic $^{187}Os/^{188}Os$ ratios (0.1239, 0.1202), while alkaline basaltic rocks of interplate oceanic islands exhibit these ratios in excess of 0.13 [10]. Alkali basalts from Fogo island (southyern group of Cape Verde archipelago) also have high $^{187}Os/^{188}Os$ ratios: between 0.132 and 0.136 [11].

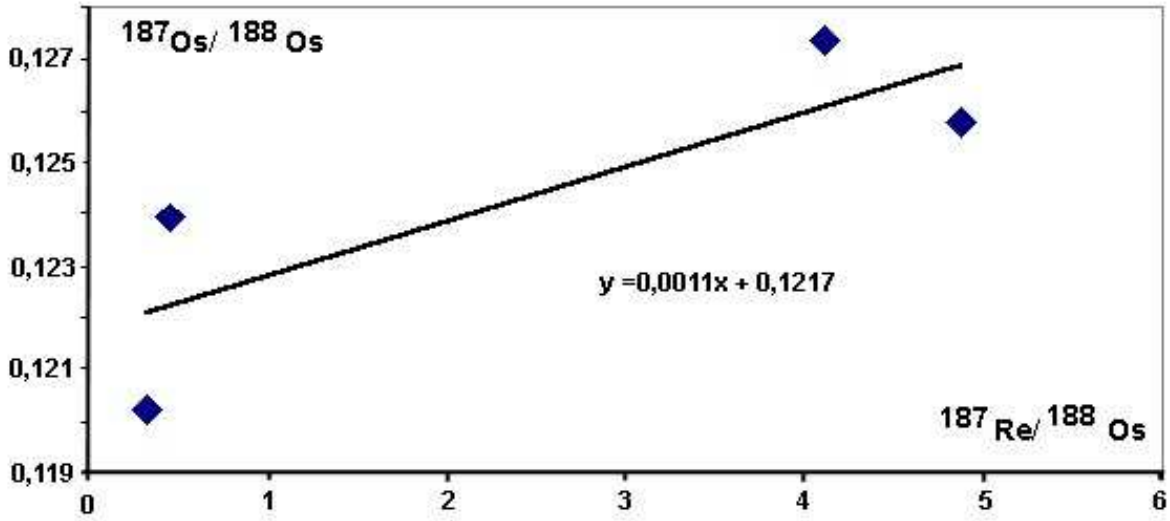

Fig. 3. **Diagram in coordinates $^{187}Re/^{188}Os$ – $^{187}Os/^{188}Os$ for mantle xenoliths from Sal island.**

As for the second of the above options, the presence of subcontinental African lithosphere under the Cape Verde islands was suggested on the basis of Os isotope composition in the lavas of Fogo island [11]. $^{187}Os/^{188}Os$ ratios in subcontinental lithosphere (average 0.1214) are close to Os isotope composition in the investigated lherzolites. A question, however, arises whether the formation of strongly reduced melts is possible during the partial melting of lithospheric material entrained by the rising plume. It was shown that the f_{O2}, characterising mantle xenoliths in kimberlites, drastically drops with the depth. This is caused by the stabilization of garnet and clinopyroxene components including Fe^{3+} (acmite, andradite, skiagite) with the increasing pressure [12]. At the depths around 200 km f_{O2} becomes 4 log units below the reference redox equilibrium quartz – magnetite – fayalite. Under these conditions Fe-Ni alloys are not stable, but sulphide melts present in mantle rocks may exhibit pronounced deficit of sulphur. Such sulphide phases with small grains of metallic alloys are sometimes found as inclusions in diamonds. The migration of S-deficient melts in the lower horizons of subcontinental lithosphere may result in the formation of blocks enriched in sulphides. Such material may retain its highly reduced character after

decompression. It may be possible, that partial melting of this material may cause the infiltration of melts transporting metallic grains into mantle xenoliths of Sal island.

Asthenospheric mantle (source of MORBs – option (3)) is characterized by higher $^{187}Os/^{188}Os$ ratios (0.125) by comparison with the investigated lherzolites. The estimated oxygen fugacities for asthenosphere [8] is also substantially higher than the level of the appearance of Fe-Ni pahses in mantle peridotites. At the same time, Os isotope composition in harzburgite and pyroxenite is similar to asthenospheric mantle and even to the bulk silicate Earth.

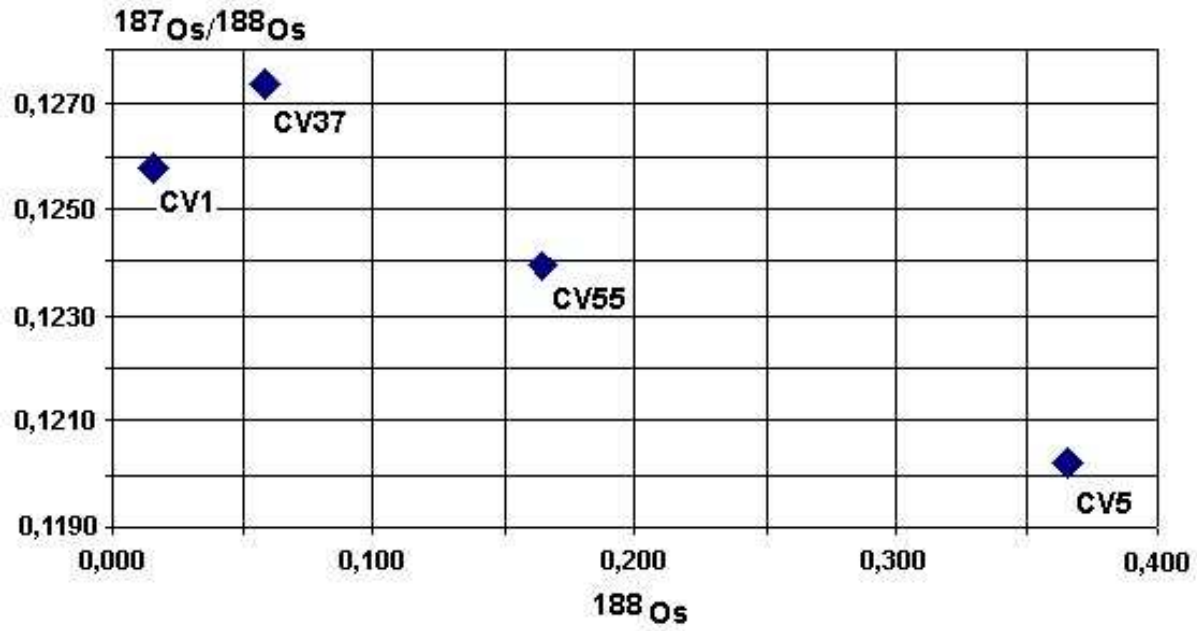

Fig. 4 **$^{187}Os/^{188}Os$ ratios as a function of ^{188}Os contents in mantle xenoliths from Sal island.**

Now we proceed to the option (4). A number of factors may afford intense redox differentiation and affect the behavior of siderophile elements in the lower mantle. These factors are the appearance of metallic phase due to the disproportionation of Fe^{2+} with the participation of Al-rich silicate perovskite [3-5], and also the possibility of the existence of sulfide-metallic melt in the system Fe-S-C at temperatures and pressures of lower mantle [13]. The migration of sulfide-metallic melt and precipitation of crystalline metallic and sulfide phases in certain blocks of lower mantle may result in the formation of the zones in lower mantle enriched and depleted in metals and sulfides. The ascend of the material, which lost substantial fraction of sulfides and metals entrained by rising mantle plumes, after the decrease in pressure and decomposition of silicate perovskite would result in the increase in oxygen fugacity, which is reflected in the relatively oxidized magmas of intraplate oceanic islands [8, 9]. In those rare cases when plume entrains material, enriched in metals and sulfides the highly reduced melts may appear, similar to intergranular melts with the grains of metals and sulfides present in the lherzolites of Sal island. In the course of the crystallization of metallic alloys

and sulfides they become enriched in Os relative to Re by comparison with the sulfide-metallic melt [14, 15]. As a result parts of the mantle enriched in metals and sulfides Re/Os ratio becomes reduced, and after certain period of time their $^{187}Os/^{188}Os$ ratios evolve towards the subchondritic values. It is possible that intergranular glasses rich in sulfides and metals in the lherzolites of Sal island, responsible for unradiogenic Os isotope composition were formed during the partial melting of material from lower mantle initially enriched in sulfides and metals due to the migration of sulfide-metallic melts at the levels of lower mantle.

In conclusion we may note, that Os isotope composition of mantle xenoliths from Sal island requires the participation of at least two components: one of them prevailing in harzburgites and pyroxenites is similar to Os of asthenospheric mantle (source of MORBs), whereas another component, which predominates in xenoliths of lherzolitic composition is characterized by less radiogenic Os. Intergranular glasses of lherzolites transporting substantial amounts of sulphides and metallic alloys with low-radiogenic Os , may correspond either to the partial melts from deep-seated material of the ancient subcontinental lithospheric mantle, or to the partial melts from the material of lower mantle, enriched in sulphides and metallic alloys, which originated during the crystallization of migrating sulphide/metallic melts. Much more intense disproportionation of Fe^{2+} with the formation of Fe0 under the pressures of lower mantle makes the second option more probable.

References

1. I.D. **Ryabchikov, L.N. Kogarko, T. Ntaflos and G. Kurat**, Металлические фазы в мантийных ксенолитах, Докл. АН 338, 95-98, 1994.
2. **I.D**. **Ryabchikov, T. Ntaflos, G. Kurat and L.N. Kogarko**, Glass-bearing xenoliths from Cape Verde: Evidence for a hot rising mantle jet, Mineralogy and Petrology 55(4), 217-237, 1995.
3. **D.J. Frost, C. Liebske, F. Langenhorst, C.A. McCammon, R.G. Trønnes and D.C. Rubie**, Experimental evidence for the existence of iron-rich metal in the Earth's lower mantle, Nature 428, 409-412, 2004.
4. **C. McCammon**, GEOCHEMISTRY: The Paradox of Mantle Redox, Science 308(5723), 807-808, 2005.
5. **F. Zhang and A.R. Oganov,** Valence state and spin transitions of iron in Earth's mantle silicates, Earth and Planetary Science Letters 249, 436-443, 2006.
6. **A.D. Brandon and R.J. Walker**, The debate over core-mantle interaction, Earth and Planetary Science Letters 232(3-4), 211-225, 2005.
7. **H. Palme and H.S.C. O'Neill**, Cosmochemical estimates of mantle composition, in: Treatise on Geochemistry, R.W. Carlson, ed. 2 (The Mantle and Core), pp. 1-38, Elsevier, Amsterdam, 2003.

8. **C. Ballhaus**, Redox states of lithospheric and asthenospheric upper mantle, Contributions to Mineralogy and Petrology 114, 341-348, 1993.
9. **I.D. Ryabchikov and L.N. Kogarko**, Redox equilibria in alkaline lavas from Trindade Island, Brasil, International Geol. Rev. 36, 173-183, 1994.
10. S.B. Shirey and R.J. Walker, The Re-Os isotope system in cosmochemistry and high-temperature geochemistry, Annu. Rev. Earth Planet. Sci. 26, 423-500, 1998.
11. **S. Escrig, R. Doucelance, M. Moreira and C.J. Allegre**, Os isotope systematics in Fogo Island: Evidence for lower continental crust fragments under the Cape Verde Southern Islands, Chemical Geology 219, 93-113, 2005.
12. **I.D. Ryabchikov**, Геохимическая эволюция мантии Земли, 37 pp., Наука, М., 1988.
13. **J. Li and R.W. Fei**, Experimental Constraints on Core Composition, in: Treatise on Geochemistry, R.W. Carlson, ed. 2 (The Mantle and Core), pp. 521-546, Elsevier, Amsterdam, 2003.
14. **C. Bockrath, C. Ballhaus and A. Holzheid**, Fractionation of the Platinum-Group Elements During Mantle Melting, Science 305(5692), 1951-1953, 2004.
15. **D. Walker**, Core participation in mantle geochemistry: Geochemical Society Ingerson Lecture, Geochimica et Cosmochimica Acta 64(17), 2897–2911, 2000.

UDK 552.33+ 550.42

Trace element partitioning between rhönite and silicate melt in Cape Verde volcanics

Kogarko L.N.[1], Hellebrand E.[2], Ryabchikov I.D.[3]

[1]*Institute for Geology of Ore Deposits, Russian Academy of Sciences, Moscow, Russia.*
[2]*Vernadsky Institute of Geochemistry, Russian Academy of Sciences, Moscow, Russia.*

[3]*Max-Planck-InstituteFur Chemistry, Mainz, Germany.*

ABSTRACT

Rhönite was found among phenocrysts of tephrite-phonolites from the islands of Bravo and Fogu, Cape Verde archipelago. Fresh volcanic glass and coexisting rhönite were analyzed by EMPA and SIMS methods in order to assess partition coefficients of trace elements between rhönite and magma. These partition coefficients reveal increase from light to heavy REE similar to K_d's of REE in clinopyroxenes, highly compatible behaviour of Ti, V, Cr, Fe^{3+} and elevated values by comparison with the elements of similar compatibility in basaltic magmatism for Zr, and Nb.

Introduction

Rhönite is a high-Ti mineral belonging to the aenigmatite group. It is usually considered to be a relatively rare constituent of alkaline magmatic rocks and veined mantle xenoliths [1, 2]. Recently, however, growing number of the discoveries of rhönite in alkaline effusives were reported, and therefore this mineral may play certain role in petrochemical and geochemical evolution of crystallizing magmas [3-6]. We have found rhönite among phenocrysts of tephrite-phonolites from the islands of Brava and Fogu, the Cape Verde archipelago. Because these rocks also contain fresh volcanic glass, we have analyzed coexisting phases by EMPA and SIMS methods in order to assess partition coefficients of trace elements between rhönite and magma.

Geological framework

Rhönite-bearing volcanics were found at the islands of Fogo and Brava. The island of Fogu represents a giant volcanic construction with the area of 576 km^2. This is the largest volcano on the African plate. In the valley Ribeira de Cabaliero the most ancient rocks of this island are outcropped. They are represented by a massif of intrusive carbonatite intersected by a dyke complex, consisting of nephelinites, ankaramites, carbonated basanites and phonolites.

The island of Brava is also a huge volcanic construction. It is built up from phonolites, phonolitic tuffs, tuff breccias, pumice and ash. The most ancient rocks of this island are intrusive carbonatites, blocks of olivine melanephelinites

included into agglomerates and tuffs of phonolitic composition. It is also likely, that boulders of coarsely crystalline carbonatites, found by our expedition 2.5 km to the east of the airport, also belong to this ancient complex.

At the western end of the island of Brava in the vicinity of the Pagea Bay numerous dykes occur, which cut a thick tuffaceous-sedimentary formation represented by tuffs and agglomerates of phonolitic composition. The younger rocks probably of the Quarternary age are represented by the flows of melanephelinites and numerous dykes, stocks and flows of phonolites.

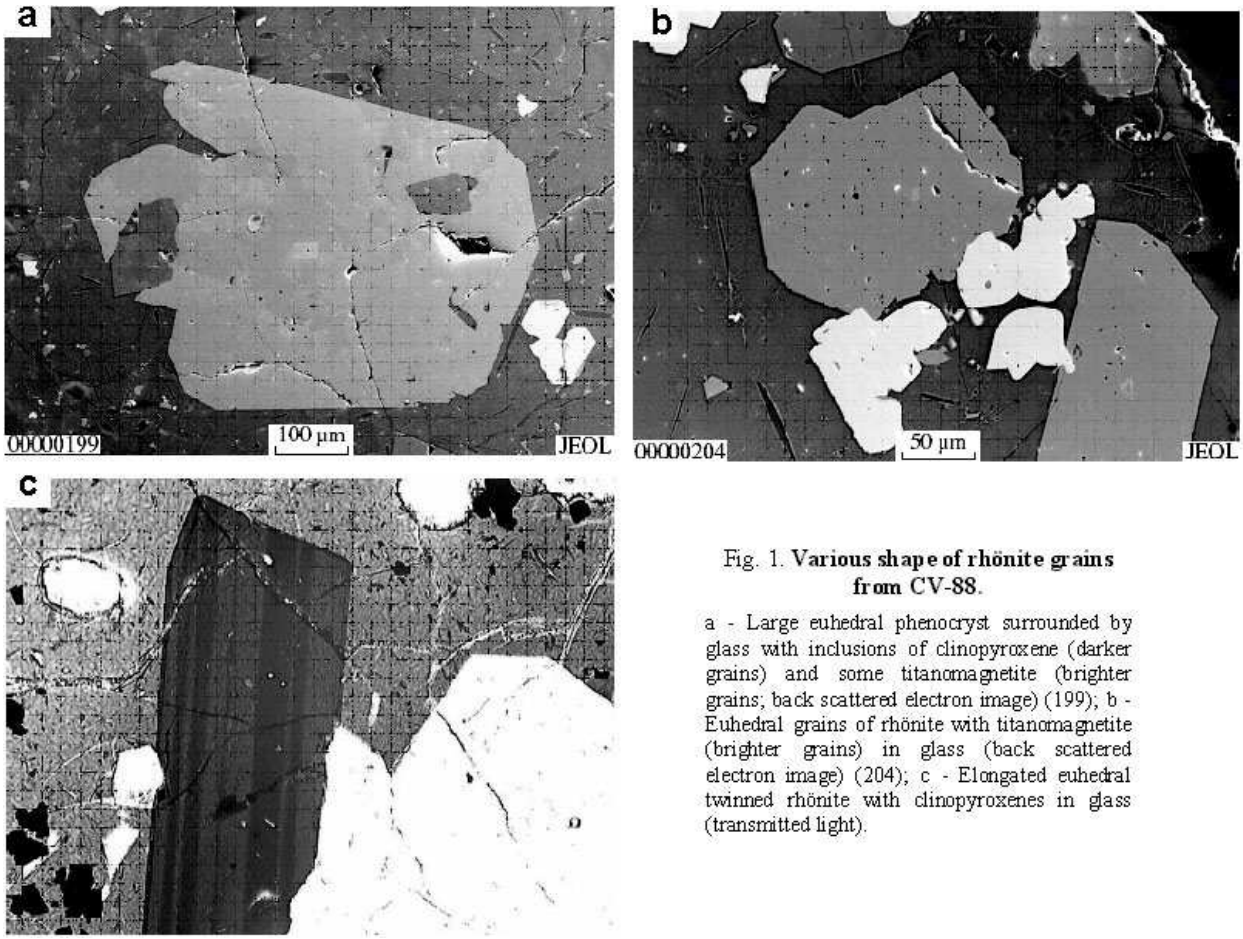

Fig. 1. **Various shape of rhönite grains from CV-88.**

a - Large euhedral phenocryst surrounded by glass with inclusions of clinopyroxene (darker grains) and some titanomagnetite (brighter grains; back scattered electron image) (199); b - Euhedral grains of rhönite with titanomagnetite (brighter grains) in glass (back scattered electron image) (204); c - Elongated euhedral twinned rhönite with clinopyroxenes in glass (transmitted light).

Thus the association of carbonatites and phonolites belongs to the most ancient complex, which is widely developed on the islands of the Cape Verde archipelago. In tephrite-phonolites dykes of the islands of Brava and Fogu associated with this ancient complex complex phenocrysts of rhönite are present. In these rocks the phenocrysts of pyroxene (titanoan fassaite), rhönite, titanomagnetite and apatite occur in a glassy groundmass, which contains rare microlites of aegirine. In some volcanics associated with ancient complex carbonate globules were discovered. They usually have oval or spherical shape, sharp meniscus and often exhibit coalescence of several adjacent globules.

Globules consist of almost pure calcite, and they include small amount of sphene, apatite, sodalite and clinopyroxene.

Phenocrysts of rhönite are represented by the grains of varying shape. Some of them are isometrical intergrowths of several euhedral grains up to 600 – 700 μm in diameter (Fig. 1A), others are elongated twinned laths (Fig. 1C).

Analytical methods

Glasses and minerals from the investigated rocks were analyzed on a JEOL RL-8900 electron microprobe at the Max-Planck-Institut für Chemie, Abteilung Geochemie, Mainz, Germany, at a 20 kV accelerating voltage and a 20 nA sample current. The standards for the calibration were natural and synthetic minerals.

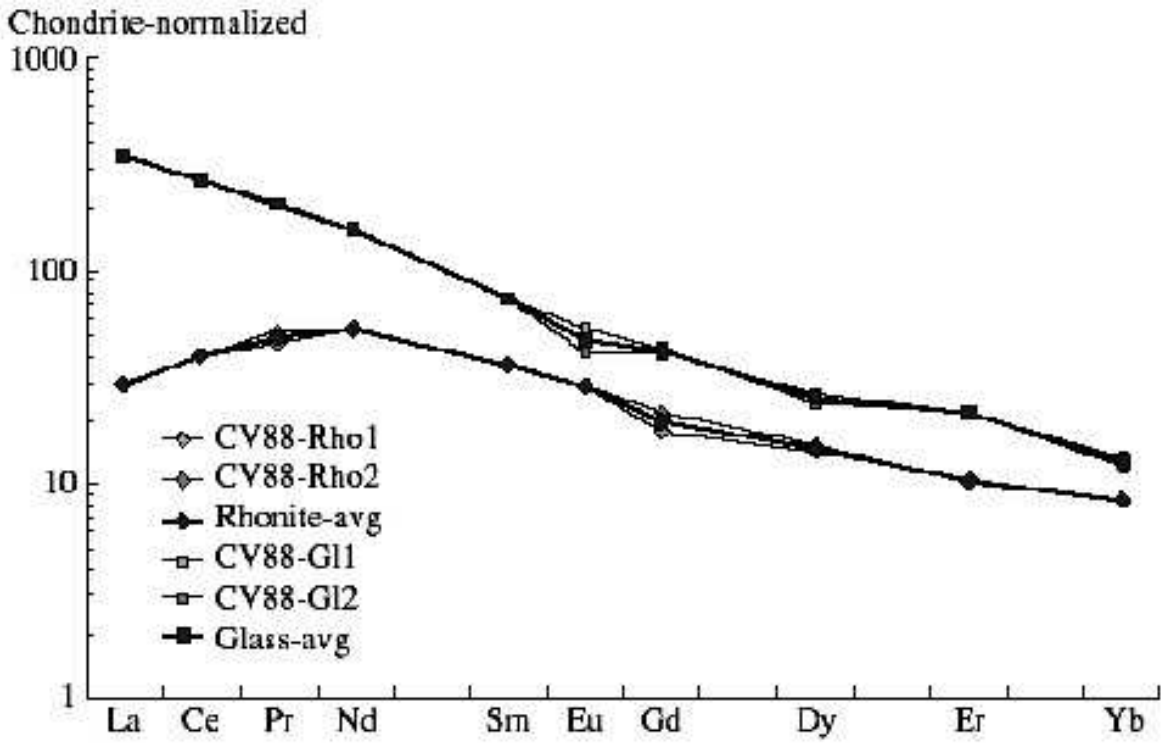

Fig. 2. **REE contents in rhönite (triangles) and glass (squares) normalized by CI chondrites [13].**

Trace elements in rhönite and glass were measured using the Cameca IMS-3f at the Max-Planck Institut für Chemie in Mainz following detailed petrographic and major element analyses. Trace element concentrations were determined by energy filtering techniques of Shimizu and Hart [7] using a 25eV energy window and a -80V energy offset from a 4500V secondary accelerating potential. Negative oxygen ions were used as a primary source with an accelerating potential of 12.5kV and a 6nA beam current, resulting in a spot size of <20μm. The overall accuracy and precision is better than 20 % for the REE and better than 12 % for the

other trace elements (2 sigma). More detailed analytical procedures are reported in Hellebrand et al. [8].

Results

Concentrations of major and trace elements in minerals and glasses of the investigated rock are shown in Tables 1 and 2. Table 2 also gives partition coefficients for trace elements for rhönite-melt pairs.

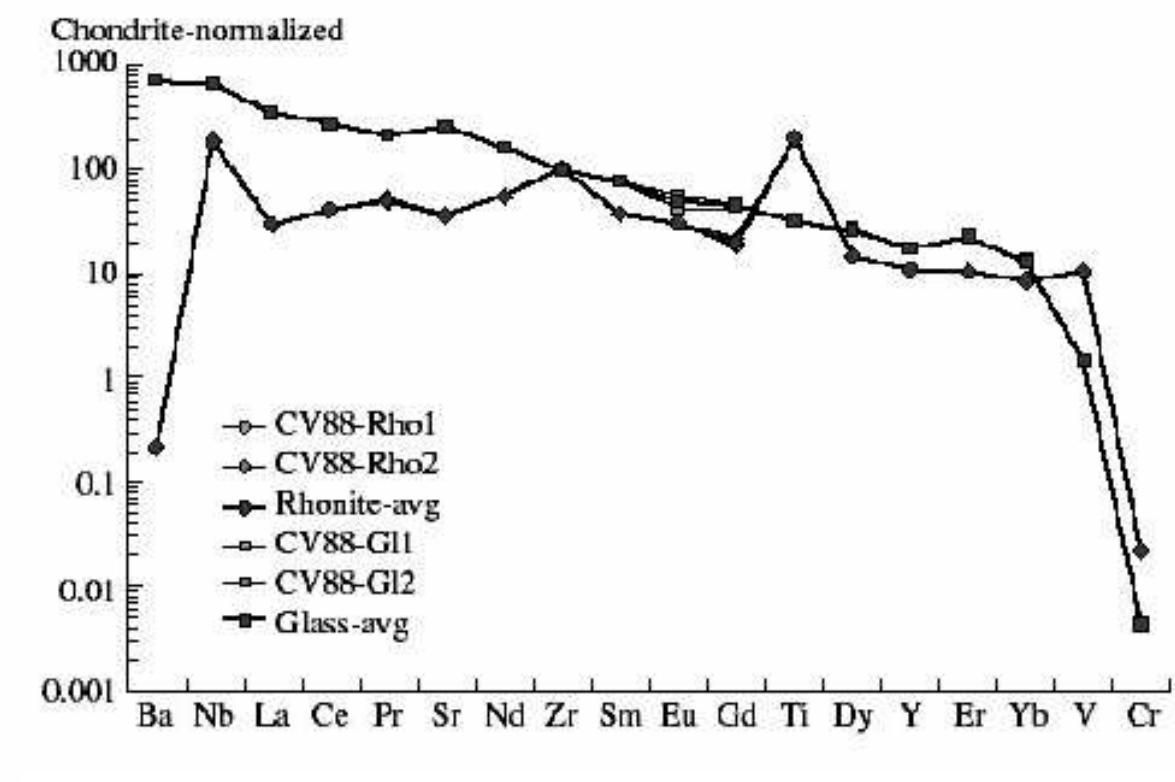

Fig. 3. **Spidergrams for rhönite (triangles) and glass (squares) with normalization by pyrolite [13].**

It can be seen from the comparison of Tables 1 and 2, that the measurements of titanium content in glasses by EPMA and SIMS yield very similar values (slightly above 2 wt % TiO_2), whereas for rhönites SIMS gives higher TiO_2 contents (around 14 wt %) by comparison with EPMA (10 – 11 wt % TiO_2). These discrepancies are probably due to the difficulties of working with very high concentrations on ion microprobe, and we, therefore, accepted EPMA data for Ti partition coefficient (around 5).

Chondrite-normalized REE diagram and primitive mantle normalized diagram for incompatible element contents in the investigated volcanic glasses (Figs 2 and 3) reveal increasing enrichment in highly incompatible elements typical for volcanic rocks from intraplate oceanic islands. There are no significant Nb or Eu

anomalies. This argues against the role of crustal contamination or plagioclase crystallization for the geochemical features of these rocks.

Partition coefficients of REE (Table 2 and fig 4) increase from La to Yb at approximately the same rate as for clinopyroxene in basaltic systems. K_d's for Ti,

Table 1.

Chemical composition of minerals and glass from CV-88 phonolite-tephrite determined by electron microprobe.

No.	1	2	3	4	5	6	7	8	9	10	11	12	13	14	15	16
SiO_2	24.96	24.10	24.39	23.96	24.09	22.68	24.17	24.78	24.10	47.78	49.56	49.54	49.42	50.15	42.72	45.17
TiO_2	11.04	10.84	10.83	10.99	10.63	11.84	10.71	10.84	9.94	2.20	2.33	2.21	2.25	2.12	4.09	3.48
Al_2O_3	15.90	16.48	16.75	16.83	16.29	15.95	16.61	16.41	16.87	19.42	19.59	19.66	19.67	19.91	10.45	7.78
Cr_2O_3	0.05	0.00	0.00	0.04	0.03	0.07	0.02	0.05	0.00	0.02	0.03	0.00	0.01	0.00	0.00	0.03
Fe_2O_3	7.33*	7.68*	8.16*	8.04*	7.70*	8.47*	8.82*	7.93*	7.73*	n.a.	n.a.	n.a.	n.a.	n.a.	3.96*	3.38*
FeO	15.06*	14.70*	14.69*	14.62*	14.52*	13.47*	13.91*	14.63*	14.70*	7.50**	7.60**	7.45**	7.74**	7.74**	3.82*	3.91*
MgO	11.97	11.66	11.96	11.83	11.87	11.72	12.21	12.24	11.09	2.51	2.62	2.57	2.72	2.49	10.40	11.86
CaO	11.57	11.72	12.03	11.84	11.67	11.69	11.63	11.54	11.66	6.46	6.65	6.80	6.48	6.32	22.45	22.65
Na_2O	1.23	1.12	1.05	1.06	1.05	1.09	1.14	1.20	1.14	2.19	4.35	4.75	4.81	4.80	0.74	0.61
K_2O	0.05	0.01	0.02	0.02	0.01	0.09	0.00	0.00	0.01	4.65	4.67	4.71	4.49	4.59	0.01	0.02
NiO	0.043	0.01	0	0.002	0	0	0	0	0	0.003	n.a.	n.a.	n.a.	n.a.	0	0
MnO	0.27	0.30	0.25	0.25	0.19	0.26	0.31	0.28	0.30	0.20	0.18	0.19	0.22	0.17	0.17	0.17
F	n.a.	n.a.	n.a.	n.a.	n.a.	n.a.	n.a.	n.a.	n.a.	0.237	0.215	0.178	0.195	0.182	n.a.	n.a.
Cl	n.a.	n.a.	n.a.	n.a.	n.a.	n.a.	n.a.	n.a.	n.a.	0.069	0.058	0.071	0.085	0.08	n.a.	n.a.
P_2O_5	n.a.	n.a.	n.a.	n.a.	n.a.	n.a.	n.a.	n.a.	n.a.	n.a.	1.116	1.149	1.059	1.096	n.a.	n.a.
S	n.a.	n.a.	n.a.	n.a.	n.a.	n.a.	n.a.	n.a.	n.a.	n.a.	n.a.	n.a.	n.a.	0.069	n.a.	n.a.
Total	99.47	98.61	100.13	99.49	98.05	97.33	99.52	99.90	97.54	93.24	98.97	99.27	99.14	99.64	98.80	99.06

No.	17	18	19	20	21	22	23	24	25	26	27	28	29	30	31
SiO_2	42.33	43.02	42.91	40.54	45.73	41.98	0.12	0.16	0.10	0.13	44.93	45.52	0.36	0.02	29.07
TiO_2	4.76	3.96	3.98	5.32	3.24	4.99	18.81	19.04	19.46	19.15	2.45	2.31	0.03	0.00	36.02
Al_2O_3	10.09	9.66	9.75	11.51	7.77	10.51	7.92	7.32	7.83	7.70	20.12	20.12	0.03	0.08	0.76
Cr_2O_3	0.01	0.00	0.01	0.01	0.02	0.02	0.01	0.051	0.06	0.00	0.01	0.04	0.00	0.01	0.50
Fe_2O_3	1.91*	2.73*	2.67*	2.98*	3.42*	3.52*	24.87*	25.33	25.55	24.50	n.a.	n.a.	n.a.	n.a.	n.a.
FeO	5.04*	4.54*	4.76*	4.67*	3.85*	3.95*	37.33*	36.76	37.31	38.46	7.64	7.41	0.27	0.05	1.35
MgO	10.51	10.58	10.51	9.72	12.06	10.69	7.16	7.46	7.61	6.55	2.24	2.47	0.21	1.08	0.01
CaO	22.04	21.86	22.00	21.79	22.26	22.26	0.05	0.044	0.03	0.02	6.43	6.40	52.88	56.90	26.92
Na_2O	0.59	0.73	0.65	0.68	0.76	0.65	0.01	0.064	0.11	0.06	2.90	2.92	0.05	0.00	0.11
K_2O	0.00	0.01	0.00	0.01	0.00	0.01	0.01	0.007	0.02	0.01	4.57	4.73	0.00	0.00	0.00
NiO	0	0.006	0.005	0	0	0	0.03	0.02	0	0	0.02	0.014	n.a.	n.a.	0
MnO	0.16	0.19	0.18	0.18	0.18	0.12	0.63	0.659	0.65	0.65	0.22	0.15	0.03	0.00	0.07
F	n.a.	n.a.	n.a.	n.a.	n.a.	n.a.	n.a.	n.a.	n.a.	n.a.	0.278	0.233	3.47	0.033	0.302
Cl	n.a.	n.a.	n.a.	n.a.	n.a.	n.a.	n.a.	n.a.	n.a.	n.a.	0.075	0.079	0.146	0	0.009
P_2O_5	n.a.	n.a.	n.a.	n.a.	n.a.	n.a.	n.a.	n.a.	n.a.	n.a.	n.a.	n.a.	41.39	0.156	n.a.
S	n.a.	n.a.	n.a.	n.a.	n.a.	n.a.	n.a.	n.a.	n.a.	n.a.	n.a.	n.a.	n.a.	n.a.	n.a.
Total	97.43	97.29	97.43	97.41	99.30	98.69	96.93	96.91	98.72	97.22	91.88	92.39	98.86	58.32	95.13

Note: * FeO and Fe_2O_3 calculated under the assumption of ideal stoichiometry of mineral. ** Total iron shown as FeO; n.a. - not analyzed; 1 – 9 rhönites; 10 – 14 volcanic glass; 15 – 22 clinopyroxenes; 23 – 26 titanomagnetites; 27 – 28 amphiboles; 29 apatite; 30 calcite from globule; 31 sphene.

V and Cr are high (5 – 7), but Nb remains incompatible (K_d = 0.27), although its K_d for rhönite is significantly higher by comparison with clinopyroxene.

On the whole, crystallization of rhönite is not likely to produce any significant anomalies in REE characteristics. However, significant rhönite crystallization will lead to negative Ti anomalies in the evolved melt (Ti-magnetite will do the same). To lesser extent, this will be seen in Zr and Nb as well, but since partition coefficient for Zr is around unity and for Nb is less than 1, strong anomalies will not develop, unless a lot of rhönite crystallized.

Discussion

Conditions of crystallization of rhönite

Experimental data for the melting relations in basanitic compositions show that simultaneous crystallization of rhönite and clinopyroxene starts at 1100 – 1150^{o}C [1]. We estimated oxygen fugacity for this temperature range from the compositions of coexisting titanomagnetite and melt in the investigated effusive.

Table 2.

Trace element contents (ppm) in rhönite phenocrysts and glass from CV-88 tephrite-phonolite determined by ion microprobe.

	Rhönite 1	Rhönite 2	Rhönite-average	Glass 1	Glass 2	Glass-average	D(Rh/L)
Ti	85742.1	83067.4	84404.8	13490.8	13498.4	13494.6	6.3
V	596.2	567.3	581.7	80.5	82.9	81.7	7.1
Cr	57.1	58.1	57.6	11.5	11.7	11.6	5.0
Sr	278.4	280.1	279.3	1985.6	1945.2	1965.4	0.14
Y	16.1	16.7	16.4	27.4	25.8	26.6	0.62
Zr	388.2	407.7	398.0	373.1	370.1	371.6	1.07
Nb	45.6	42.6	44.1	162.1	159.4	160.8	0.27
Ba	0.5	0.5	0.5	1684.1	1606.3	1645.2	0.0003
La	7.1	6.8	6.9	81.9	80.3	81.1	0.09
Ce	24.3	24.5	24.4	163.3	162.6	162.9	0.15
Pr	4.7	4.1	4.4	19.0	17.9	18.4	0.24
Nd	24.2	24.6	24.4	71.6	70.9	71.3	0.34
Sm	5.3	5.3	5.3	11.1	10.9	11.0	0.48
Eu	1.6	1.7	1.6	3.0	2.3	2.7	0.61
Gd	3.5	4.2	3.8	8.7	8.1	8.4	0.46
Dy	3.4	3.7	3.6	5.8	6.5	6.1	0.59
Er	1.7	1.6	1.6	3.4	3.4	3.4	0.48
Yb	1.3	1.4	1.4	2.2	2.0	2.1	0.66

First we estimated oxygen fugacity for equilibrium of phonolite-tephrite melt with metallic iron using formulae and parameters proposed by Borisov and Ariskin [9]. After it we calculated activity of Fe_3O_4 component for these very reducing conditions basing on the equilibrium constant of the following reaction taken from Robie et al [10]

$3\ Fe + 2\ O_2 = Fe_3O_4$

Then we recalculated f_{O2} to the actual value of Fe_3O_4 activity in the rock basing on the composition of titanomagnetite (using parameters from [11]) and taking into account decreasing activity of FeO in melt due to its partial oxidation (using method proposed by [12]). For this we used formula of the equilibrium constant of the following reaction

$6\ FeO + O_2 = 2\ Fe_3O_4$

These calculations yield f_{O2} close to quartz – magnetite – fayalite buffer ± 0.5 log unit for temperatures between 1050 and 1150°C. This level of oxygen fugacity is well within the range of f_{O2} values in which rhönite was synthesized in experiments with natural magmatic rocks [1].

Calculated Fe_2O_3 contents of phonolite-tephrite melt at QMF oxygen fugacity using the formulations of Kilinc et al [12] are close to 0.8 wt%. This together with Fe_2O_3 contents of the investigated rhönites (Table 1, NN 1 – 9) shows that partition coefficient of Fe_2O_3 between rhönite and melt is in the range of 9 and 11. Therefore, the crystallization of rhönite in a closed system will lead to the decrease in Fe^{3+}/Fe^{2+} ratio in the melt and as a consequence to the reduction of oxygen fugacity. Thus, crystallization of rhönite will affect redox characteristics of magmatic system in a similar way to the crystallization of titanomagnetite.

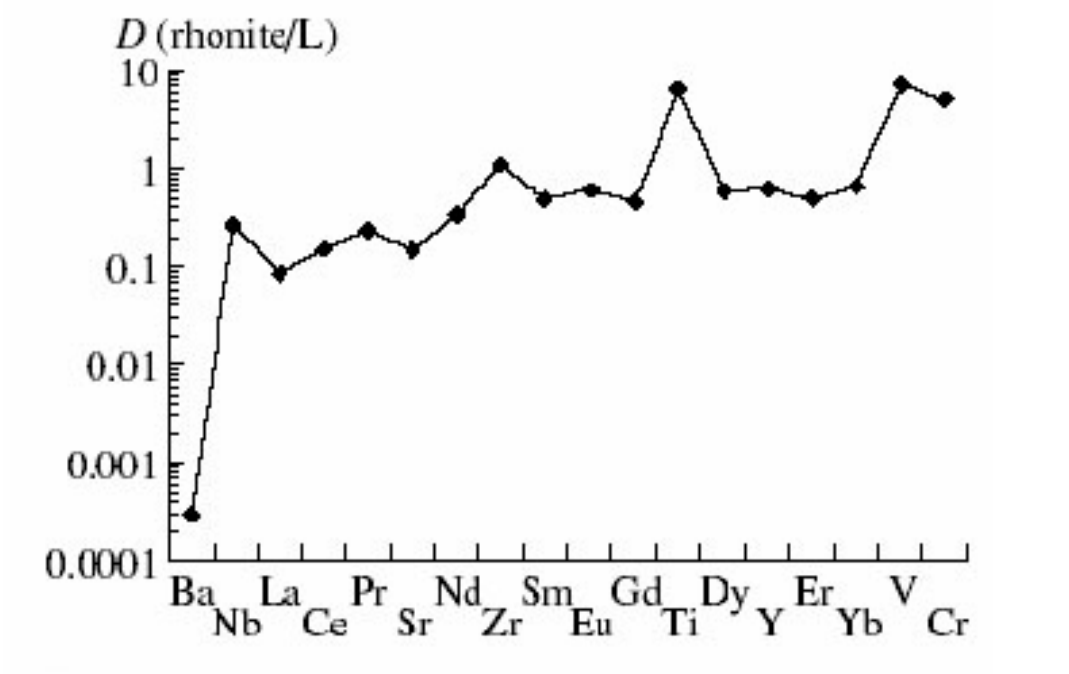

Fig. 4. **Partition coefficients for trace elements between rhönite and glass (Table 2).**

In order to find mineral assemblages favorable for the formation of rhönite we may consider the following simplified reaction among components of clinopyroxene and titanomagnetite

$Ca(Mg,Fe)Si_2O_6$(Cpx) + $CaAl_2SiO_6$(Cpx) + Fe_3O_4(Mt) + Fe_2TiO_4(Mt) = $Ca_2((Mg,Fe^{2+})_4Fe^{3+}Ti)(Si_3Al_2Fe^{3+})O_{20}$(Rhönite)

This reaction produces rhönite with crystallochemical formula similar to the average rhönite composition (Table 1) for the investigated rocks

$(Na_{0.29}Ca_{1.71})(Mg_{2.43}Fe^{2+}_{1.63}Mn_{0.03}Ti_{1.11}Fe^{3+}_{0.8})(Si_{3.3}Al_{2.7})O_{20}$

In this composition by comparison with the above simplified formula Ca is partly substituted by Na, and Fe^{3+} is partly substituted by Ti, Al and Si, but basically both formulae are very similar. It follows from the above reaction, that the formation of rhönite requires presence of clinopyroxene rich in Tschermak molecule and magnetite rich in ulvospinel. This is consistent with the fact that magnetites in the investigated rocks contain approximately 50 mol % of ulvospinel component, and clinopyroxenes include 20 – 25 mol % of Ca-Tschermak. Highly aluminous clinopyroxenes are also typical for other mineral assemblages, which include rhönite [1, 3].

CONCLUSIONS

1. The partition coefficients of trace elements estimated from the compositions of rhönite and volcanic glass in phonolite-tephrite from Cape Verde archipelago reveal increase from light to heavy REE similar to K_d's of REE in clinopyroxenes, highly compatible behaviour of Ti, V, Cr, Fe^{3+} and elevated values by comparison with the elements of similar compatibility in basaltic magmatism for Zr, and Nb.
2. Crystallization of rhönite is expected for the magmas, which also crystallize clinopyroxene with high content of Ca-Tschermak and magnetite with high content of ulvöspinel.
3. In some effusives rhönite is present among phenocrysts, and therefore its crystallization may significantly affect behavior of major and trace elements.

References

1. **Boivin P.** Donnees experimentales preliminaires sur la stabilite de la rhonite a 1 atmosphere. Application aux gisements naturels // Bull. Mineral., 1980, v. 103, p. 491-502.
2. **Kunzmann T.** The aenigmatite-rhonite mineral group // Eur. J. Miner., 1999, v. 11, p. 743-756.
3. **Fodor R.V., Hanan B.B.** Geochemical evidence for the Trindade hotspot trace: Columbia seamount ankaramite // Lithos, 2000, v. 293, p. 293-304.
4. **Golovin A.V., Sharygin V.V., Mal'kovets V.G.** Evolution of melt during the crystallization of the Bele pipe basanites (North Minusa depression) // Geol. geophis., 2000, v. 41, p. 1760-1782.
5. **Prestvik T., Torske T., Sundvoll B., Karlsson H.** Petrology of early Tertiary nephelinites off mid-Norway. Additional evidence for an enriched endmember of the ancestral Iceland plume // Lithos, 1999, v. 46, p. 317-330.
6. **Shaw C.S.J., Klugel A.** The pressure and temperature conditions and timing of glass formation in mantle-derived xenoliths from Baarley, West Eifel, Germany: the case for amphibole breakdown, lava infiltration and mineral-melt reaction // Miner. Petrol., 2002, v. 74, p. 163-187.
7. **Shimizu N., Semet M.P., Allegre J.C.** Geochemical applications of quantitative ion microprobe analysis // Geochim. et Cosmochim. Acta, 1978, v. 42, p. 1321-1334.

8. **Hellebrand E., Snow J.E., Hoppe P., Hofmann A.W.** Garnet-field melting and late-stage refertilization in 'residual' abyssal peridotites from the Central Indian Ridge // J. Petrol., 2002, v. 43, p. 2305-2338.
9. **Borisov A. Ariskin A.** Fe and Ni solubility in silicate melts equilibrated with metal // Lunar Planet. Sci. XXVII, 1996, p. 133-134.
10. **Robie R.A., Hemingway B.S., Fisher J.R.** Thermodynamic properties of minerals and related substances at 298.15 K and 1 bar (105 Pascal's) pressure and at higher temperatures. United States Government Printing Office, Washington D.C., 1978, 456 p.
11. **Wood B.J., Bryndzya L.T., Johnson K.E.** Mantle oxidation state and its relationship to tectonic environment and fluid speciation // Science, 1990, v. 248, p. 337-345.
12. **Kilinc A., Carmichael I.S.E., Rivers M.L., Sack R.O.** Ferric-ferrous ratio of natural silicate liquids equilibrated in air // Contrib. Mineral. Petrol., 1983, 83, p. 136-140.
13. **McDonough W.F., Sun S.-S.** The composition of the Earth // Chem. Geol., 1995, v. 120, p. 223-253.

УДК 551.22. (571)

PERMO-TRIASSIC SUPERPLUME AND ITS INFLUENCE TO THE SIBERIAN LITHOSPHERIC MANTLE

POKHILENKO N.P.

V.S. SOBOLEV INSTITUTE OF GEOLOGY AND MINERALOGY, SB RAS, 3 KOPTUGA AVENUE, NOVOSIBIRSK, 630090, RUSSIA, E-MAIL: DIRECTOR@IGM.NSC.RU

ABSTRACT

A complex study o xenogenic material of upper mantle origin from kimberlites of Middle Paleozoic and Mesozoic cycles of emplacement has demonstrated significant changes in thickness, structure and composition of the Siberian Platform lithospheric mantle. A comparative analysis of obtained petrological, mineralogical and geochemical results has shown that the thickness of lithosphere of North Eastern part of Siberian Platform was around 230 km at Middle Paleozoic time and was decreased to 140-150 km to Upper Jurassic time. This significant decrease of the lithosphere thickness was combined with drastic increase amount of garnet pyroxenites in the Mesozoic lithospheric upper mantle. These changes can be related with influence of Siberian Permo-Triassic Superplume on the deep-seated levels of the Siberian Platform lithospheric mantle.

INTRODUCTION

The flood basalt magmatism with the maximum intensity expressed 245-250 Ma ago [18] was the greatest event of the Siberian Platform Phanerozoic evolution. A territory of about 1.5 millions of km^2 was involved in this relatively short- term cycle of magmatic activity. As it is indicated by the results of deep drilling program, over 17 million km^3 of magmatic material where erupted and intruded on the Siberian Platform surface and into its Paleozoic sedimentary cover. This event was related with the superplume that reached the Siberian Platform lithosphere roots close to the end of Permian time [1].

Three maim cycles of kimberlite magmatism activity are known inside the Siberian Platform: Upper Devonian- Lower Carboniferous (370-345Ma), Triassic (245-215) Ma and Upper Jurassic (160-149Ma), and the last is significantly predominating in amounts of bodies [3, 4, 8]. Xenogenic material of the upper mantle origin from kimberlites of Mesozoic age provides some evidences of smaller thickness and secondary enriched in different scale lithospheric mantle at the time of kimberlite emplacement if compare with ones at Middle Paleozoic time [14, 20]. A comparative analysis of the composition variations of the garnets of upper mantle parageneses populations from the kimberlite bodies of Middle Paleozoic age existing in the area (fields of Middle- and Lower Oleneksky

kimberlite regions) suggests about significant variations of thickness and composition of the lithospheric mantle beneath the studied area at Middle Paleozoic time as well [15].

To understand the influence of this superplume event on the Siberian lithospheric mantle, composition of the suite of mantle xenoliths and garnet concentrate from kimberlites emplaced before superplume event where compared to that of kimberlites emplaced after this event.

SAMPLES AND METHODS

The compositions of over 19000 of pyrope grains from 111 kimberlite pipes in five kimberlite areas of the Yakutian diamondiferous province as well as near 1500 grains of the pyropes from the conglomerates of Lower Carboniferous age were studied with the use of the "Camebax-Micro" and JEOL JXA-8900 electron probes at V.S. Sobolev Institute of Geology and Mineralogy, Novosibirsk, Russia. The major and trace elements of xenoliths of metasomatized peridotites, Uv-4/76 and Uv-105/89, were studied at the Geophysical Laboratory of the Carnegie Institution, Washington, DC, USA, using the JEOL JXA-8900L microprobe and at the Department of Geology and Geophysics of the Oceanographic Institution, Woods Hole, USA, with the Cameca IMS 3f ion probe. The Ni and Zr contents for some pyropes from the kimberlites of the Yakutian diamondiferous province were measured by Dr. W.L.Griffin on the HIAF proton probe at the Department of Exploration and Mining, CSIRO, North Ryde, Australia.

We studied representative samples of pyropes (>100 grains from each pipe), the grain sizes being from +0.5 to 1.0 mm as recommended by [22]. The central part of the Yakutian diamondiferous province includes two kimberlite regions: the Malo-Botuobiya (Mirninsky field, pyropes from seven pipes were studied) and Daldyn-Alakit (Alakit-Markhinsky and Daldynsky fields (pyropes from 32 pipes were studied). The kimberlites of the Triassic cycle of emplacement were taken from the Anabar area (the studied pipes total to 34). There is evidence that post-Triassic kimberlites and related rocks intruded there in the range from 193 to 149 Ma [8]. Bodies of different ages are found within one field, and this is an example of polychronous kimberlites on local territory. Along with the majority of kimberlite pipes of the Anabar region, the kimberlites of the Kharamai field (pyropes from 12 pipes are studied), located near the southwestern margin of the Anabar Shield, belong to the Triassic cycle of emplacement. The available dating of the kimberlites of this field confirms this conclusion. The Upper Jurassic cycle of kimberlite magmatism in our study is represented by kimberlites of the Lower-Olenek district (the studied pipes total to 26).

Also, we studied pyropes liberated from some large samples (250-500 kg) of diamondiferous conglomerates of Lower Carboniferous age, found within the Kyutyungde graben and on its flanks. These conglomerates are located about 30 km east of the Beenchime field and about 40 km northeast of the Molodo field, which

were mentioned above to belong to the Upper Jurassic cycle of kimberlite magmatism.

To obtain objective and representative data on variations of garnet compositions from the upper mantle pyroxenites, we examined garnets from over 120 xenoliths of pyroxenites from a number of pipes, belonging to the Middle Paleozoic (Mir, Udachnaya,) and Upper Jurassic (Obnazhennaya) cycles of emplacement.

Special attention was given to a detailed mineralogical, petrological, and geochemical study of two unique xenoliths of metasomatized peridotites, Uv-4/76 and Uv-105/89, from the Udachnaya Pipe. The specific features of these xenoliths provide a possibility to study processes of transformation of initial depleted Cr-pyrope harzburgite-dunites of the root parts of lithosphere into enriched lherzolites and, probably, pyroxenites as a result of interaction with melts of asthenosphere origin.

RESULTS

The kimberlite fields of the Upper Devonian – Early carboniferous age are known for: a) central part of the Siberian Platform to the east of Tunguska area of Flood basalts, b) Northeast part of the Platform and c) there are evidences of the presence of Paleozoic kimberlites to the West of Tunguska flood basalts area. The evidences for the latter case are numerous findings of diamonds and kimberlite indicator minerals in the sediments of the Carboniferous age in this territory.

Kimberlites of Upper Jurassic age are mostly situated in the Northeast part of Siberian kimberlite province. However, several kimberlite bodies of that age have been found in the area to the west of Tunguska flood basalt province and the country rocks for these kimberlites are Lower Triassic basic tuffs and lavas. This locality is close to that of the proposed for unknown Paleozoic kimberlites, indicators of which were discovered in the Carboniferous sediments.

A detailed study of the composition, paragenesis and distribution peculiarities of the populations of upper mantle garnets from the different age Siberian kimberlites showed that:

1. The main compositional, paragenetic and distribution features of pyrope garnets and upper mantle xenolith in diamondiferous Paleozoic kimberlites of the central, Northeastern and Western parts of Siberian Platform are very similar. The P-T estimates using Ni-Cr in garnet geothermobarometry method [19] suggests, that the lithosphere thickness during the Middle Paleozoic time for all the studied areas of the platform was ~ 230-250 km, and heat flow was around 36-37 mWm^{-2} [10-15] (Fig. 1).
2. A comparative study of garnets and upper mantle xenolith from the Upper Jurassic kimberlites of the Northeast and West of Siberian platform demonstrated that the thickness of lithosphere was significantly decreased since

Middle Paleozoic to Jurassic time. The lithosphere thickness was decreased up to ~130-150 km and heat flow was increased up to the values of 40-41 mWm^{-2}.

3. A comparative analysis of distribution of upper mantle xenogenic material in kimberlites of different age inside the Siberian platform demonstrated the following changes in the cratonic mantle composition. First there is significant increase of the pyroxenites abundance (up to 10 times) in the mantle sampled by Jurassic kimberlites in comparison with that of mantle sampled by middle Paleozoic kimberlites (Table 1, Fig. 2). The second is very deep decrease in the amount of ultradepleted Gr-pyrope harzburgites and dunites in the thinned Jurassic lithospheric mantle of Siberian Platform.

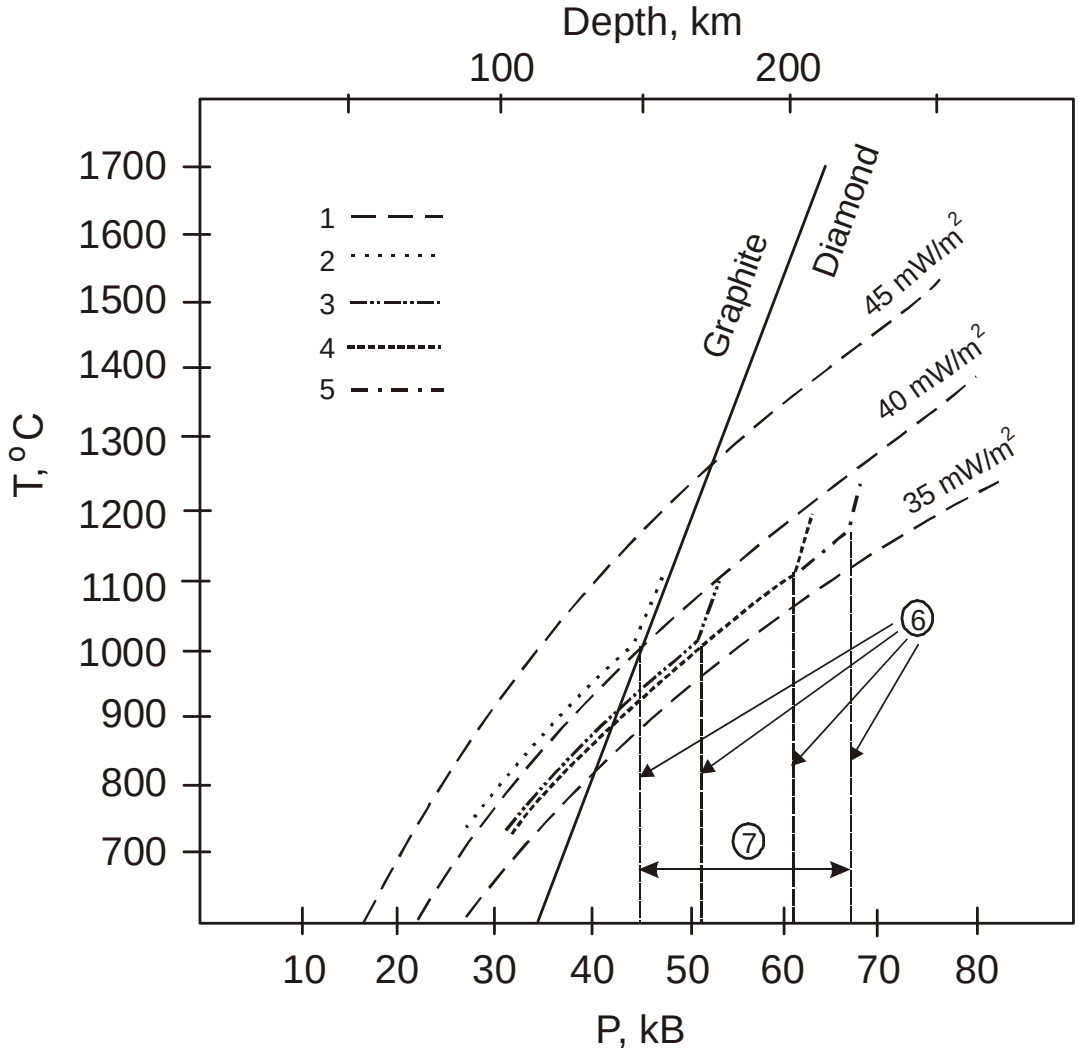

Fig. 1. **The estimations of lithosphere thickness and geotherm character for the North-Eastern marginal zone of the Siberian Platform at Middle Paleozoic and Jurassic time.**

1 – the geotherms calculated for the heat flows of various intensity; 2 – the geotherm for Lower Olenek region (Upper Jurassic time); 3 - the geothermfor the lithosphere under Ivushka pipe (Middle Paleozoic time); 4 - the geotherm of the South-Western board of Kyutungda graben (Middle Paleozoic time); 5 - the geotherm for the North-Estern board of Kyutungda graben (Middle Paleozoic time); 6 – the estimations of maximal pressures and depths of the root parts of lithosphere for areas 2-5 at various time; 7 – the maximal interval of lithosphere erosion of the region during the period between Lower Carboniferous and Upper Jurassic time.

A complex study of the mantle xenoliths from the kimberlites of the central regions have shown that in the Middle Paleozoic time the lithosphere in the region was about 250 km thick with a heat flow of 36 to 39 mWm^{-2}, beginning, at least, from depths of 200-210 km [2,10,11,15]. The mapping of the lithosphere of the Siberian Platform on the basis of Cr and Ni distribution in garnets and Zn distribution in Cr-spinels from kimberlite concentrates gave similar values of lithospheric thickness and heat flow in the central regions of the platform [6-7,19].

Table 1.

Peculiarities of pyrope garnet compositions from the Siberian kimberlites of different age of emplacement.

Kimberlite regions	N $\bar{n}$	CaO $\bar{x}$ / S	FeO $\bar{x}$ / S	Cr_2O_3 $\bar{x}$ / S	n_1,% diam.	n_2, (>5% Cr_2O_3)	n_3, (>7% Cr_2O_3)	n_4, (>10% Cr_2O_3)
1	7 3270	5.08 1.04	8.20 1.02	4.45 2.29	6.2	38.5	11.1	2.4
2	32 6726	4.89 1.25	8.06 1.07	4.20 2.34	7.6	35.8	15.2	3.2
3	34 4157	5.02 0.62	8.91 1.39	3.22 1.43	0.2	12.1	2.4	0.1
4	26 3834	4.23 0.59	9.44 1.62	2.75 1.26	0.1	4.8	2.1	0
5	12 1184	5.48 1.31	7.55 1.77	4.71 2.07	1.2	41.9	14.35	0.5
6	61	4.02	7.97	5.78	36.1	49.2	34.1	14.8
7	325	5.10	9.46	2.62	0	4.8	0	0

Note: Regions: 1 – Malo-Botuobonsky (D3); 2 – Daldyno-Alakitsky (D3); 3 – Anabarsky (T1); 4 – Lower-Oleneksky (J3); 5 – Kharamai kimberlite field (T1); 6 – Pyropes from Middle Paleozoic conglomerates of Kyutyungde graben area (C1); 7 – Pyropes from modern alluvials of Elietibiye River; N – number of studied pipes; n - number of studied pyropes.

As shown above, the garnets from the Upper Jurassic kimberlites in the northeast of the Siberian Platform have drastically different characteristics of distribution of compositions from those for the garnets from the Middle Paleozoic kimberlites in both central and northeastern parts of the Platform.

The main distinguishing features of the objects under comparison are:

1. A considerably reduced maximum Cr_2O_3 content for the garnets from the Upper Jurassic pipes (Table 1, Fig. 2).

2. A considerable increase in average content of FeO in the garnets from the Upper Jurassic pipes as compared with those for the garnets from the Middle Paleozoic pipes (Table 1).

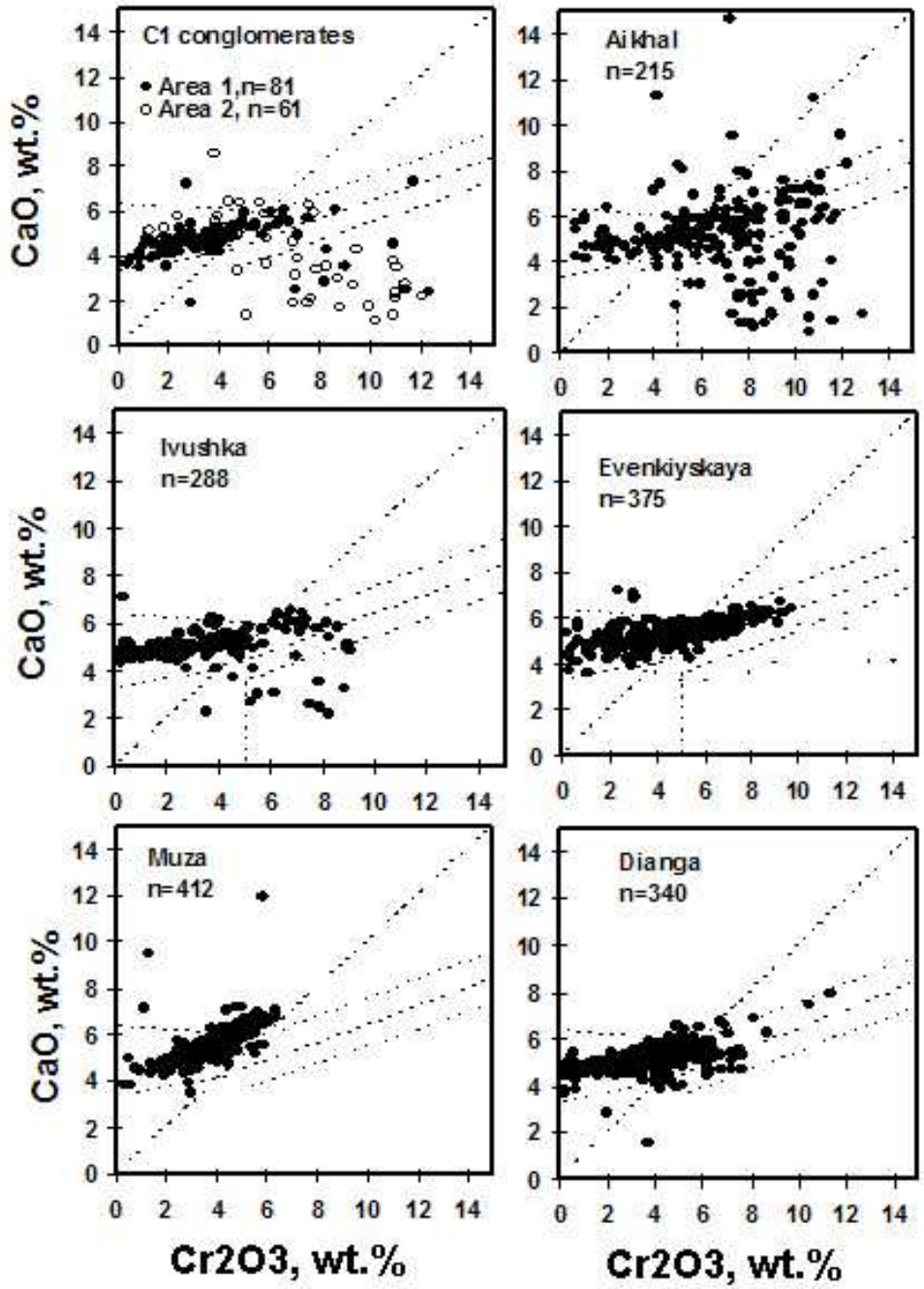

Fig. 2. **Cr2O3 vs CaO plot for peropes from: carboniferous conglomerates of Kyutyungde Graben area; high-grade Middle Paleozoic Aikhal Pipe; low grade Middle Paleozoic Ivushka Pipe, situated in Kyutyungde Graben area; Low Triassic Evenkiyskaya Pipe; Upper Jurassic Muza and Dianga Pipes.**

3. The presence, in variable amounts, of subcalcic Cr-pyropes of harzburgite-dunite paragenesis in the majority of kimberlites of Middle Paleozoic age, and their nearly complete absence from the Upper Jurassic kimberlites (Table 1, Fig. 2).

4. A many-fold increase in the share of garnets of pyroxenite paragenesis in the Upper Jurassic kimberlites as compared with those for the garnets from the Middle Paleozoic kimberlites throughout the platform.

A detailed study of a collection of mantle xenoliths from the Upper Jurassic Obnazhennaya pipe has shown that:

1. The share of pyroxenite xenoliths in it drastically increased as compared with the Middle Paleozoic pipes [15,19].
2. There are no harzburgite and dunite xenoliths containing subcalcic Cr-pyropes.
3. The maximum values of the parameters of equilibrium of upper-mantle rocks represented in the xenoliths do not exceed the values corresponding to depths of 120-130 km [14, 20, 22].
4. Results of study of distributions of garnet compositions from 26 pipes of Upper Jurassic age from the kimberlite fields of the northeastern margin of the Siberian Platform demonstrated the commonness of their main characteristics.

Comparison of the results obtained on studying garnets from heterochronous kimberlites of the Siberian Platform and their mantle xenoliths with the results of Cr-Ni thermobarometry [19] for a number of pipes permitted us to estimate the thickness of the lithosphere and values of heat flows in the central regions of the platform for the Middle Paleozoic and those in the northeastern regions - for the Middle Paleozoic and Mesozoic. These estimates for the northeastern part of the platform are compiled in Fig1, which shows that for the period from the Middle Paleozoic (D3) to the Upper Jurassic the lithosphere thickness in the region decreased by about 70 km; and the value of heat flow increased from 37 mWm^{-2} to 40-41 mWm^{-2}.

The most probable event which might be responsible for these significant changes in thickness of composition and structure of the lithosphere for this period is a paramount cycle of flood basalt magmatism expressed with different intensity over a total area about 1.5×10^6 km^2.

The process of thinning and modification of the Siberian lithospheric mantle was caused by an intensive interaction of the lithosphere roots with the huge amount of asthenospheric melt. The widespread melting, in turn, was initiated by the Siberian Superplume, which was located at the base of the Platform in Permo-Triassic time. This interaction added a significant amount of the basaltic component into the cratonic mantle of the Siberian Platform and nearly completely eliminated the most deep-seated layers of Pre-Permian cratonic mantle (Fig. 3). These eliminated layers were mostly composed by depleted dunites and harzburgites including the diamondiferous one and this is the main reason for the absence of diamonds in the Jurassic kimberlites.

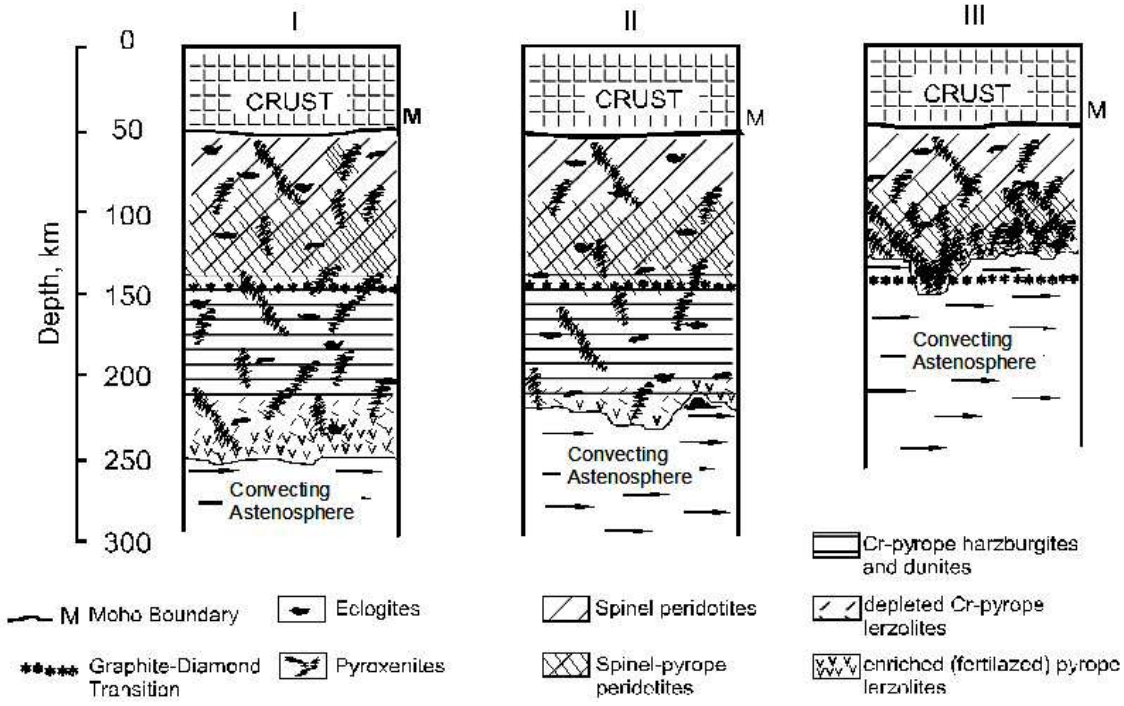

Fig. 3. **Schematic vertical sections of Siberian Platform Lithosphere: I – central regoin, Middle Paleozoic time; II – north-eastern region, Middle Paleozoic time; III – north-eastern region, Mesozoic (J3) time.**

The intermediate stage of transformation of the ultradepleted harzburgites into the enriched in pyroxene peridotites have been found in a rare kind of mantle xenoliths from Udachnaya pipe. Garnet grains in these xenoliths are zoned with the deep-purple core and red-orange rim. The core compositions and geochemical features belong to the subcalcic, Cr-rich pyropes, typical for extremely depleted harzburgites and dunites (Table 2) [16-17]. Whereas, rim composition is corresponds to lherzolite and even to pyroxenite paragenesis. The Cr_2O_3 content drops from 11.8 wt% in the core to 1wt % in the rim and CaO content significantly increased from core to rim. The calculations of REE content in garnet crystallized from basaltic melt indicate that this process can account for the heavy REE contents in garnet rim, but contain a less of middle REE`s and significantly less of LREE`s (Fig. 3). Therefore, the rims of the garnets not simply grow from the basic melt, but it formed by more complicated multistage process. It could be an interaction of existing Cr rich garnet with the basic melt as the combined composition of garnet core and that of calculated garnet are more similar to the rim composition, but still not account for LREE enrichment. The later metasomatic enrichment by kimberlite melt can add the necessary LREE`s to the rim [16-17].

Table 2.

Microprobe analyses of minerals of Uv-105/89 and Uv-4/76 metasomatized peridotite xenoliths, Udachnaya pipe, wt.%.

Uv-105/89										
	Zoned garnet									
	rim_1	rim_2	rim_3	rim_4	core	cpx_1	cpx_2	ilm_1	ilm_2	ilm_3
SiO_2	40.2	39.8	40.8	40.9	41.4	54.3	55.4	0.03	0.00	0.00
TiO_2	0.48	0.95	0.78	0.55	0.07	0.21	0.18	30.9	37.9	49.1
Al_2O_3	13.7	13.5	17.8	21.8	15.4	1.60	1.84	2.52	1.12	0.65
Cr_2O_3	11.5	10.2	5.17	1.05	11.8	0.80	0.36	15.9	9.66	1.17
FeO	10.5	11.5	12.4	11.8	6.93	4.31	4.49	42.2	42.9	37.8
MnO	0.58	0.55	0.48	0.45	0.51	0.08	0.10	0.29	0.18	0.21
MgO	16.8	15.0	16.7	18.1	22.4	16.9	17.4	7.05	6.20	10.4
CaO	6.58	8.81	6.95	5.32	2.49	19.5	19.5	0.03	0.06	0.02
Na_2O	0.08	0 .07	0.07	0.08	0.01	1.73	1.66			
NiO								0.22	0.12	0.11
Total	100.4	100.4	101.2	100.1	101.0	99.4	100.9	99.1	98.1	99.5
mg #	74.0	69.8	70.5	73.2	85.2	87.4	87.3	21.3	19.3	32.0

Uv - 4/76										
	Zoned garnet									
	rim_1	rim_2	core	ol_1	ol_2	cpx_1	cpx_2	enst	chr	phl
SiO_2	41.2	41.1	41.5	40.9	40.3	54.0	54.2	58.0	0.05	42.0
TiO_2	0.40	0.54	0.01	0.03	0.02	0.26	0.22	0.01	0.37	0.66
Al_2O_3	15.5	21.0	17.4	0.00	0.00	2.22	1.68	0.30	6.34	12.0
Cr_2O_3	8.68	1.64	8.61	0.00	0.00	3.57	1.07	0.30	61.1	0.52
FeO	7.52	11.1	6.77	8.27	12.8	2.40	3.58	4.10	19.2	3.32
MnO	0.52	0.52	0.43	0.11	0.10	0.09	0.09	0.08	0.54	0.01
MgO	20.2	17.5	22.6	50.3	46.8	15.8	16.44	36.9	12.6	26.2
CaO	5.66	6.79	2.71	0.00	0.03	17.9	20.5	0.19	0.01	0.06
Na_2O	0.07	0.06	0.03			3.20	1.86	0.05		0.08
K_2O										10.3
NiO				0.39	0.24	0.07		0.13		
Total	99.8	100.3	100.1	100	100.3	99.5	99.6	100.1	100.2	95.2
mg#	82.6	73.7	85.6	91.5	86.7	92.1	89.0	94.1	53.9	93.5

The same to described above processes, but in the much a bigger scale were responsible for the significant increase of pyroxenite abundance in Siberian lithospheric mantle during the Superplume event.

CONCLUSIONS

Comparative analysis of petrological and geochemical features of xenogenic material of lithospheric mantle from the Siberian Platform kimberlites of Pz (D3) and Mz (T2, J3) cycles of emplacement together with comparative analysis of geochemical peculiarities of these kimberlites allow us to conclude:

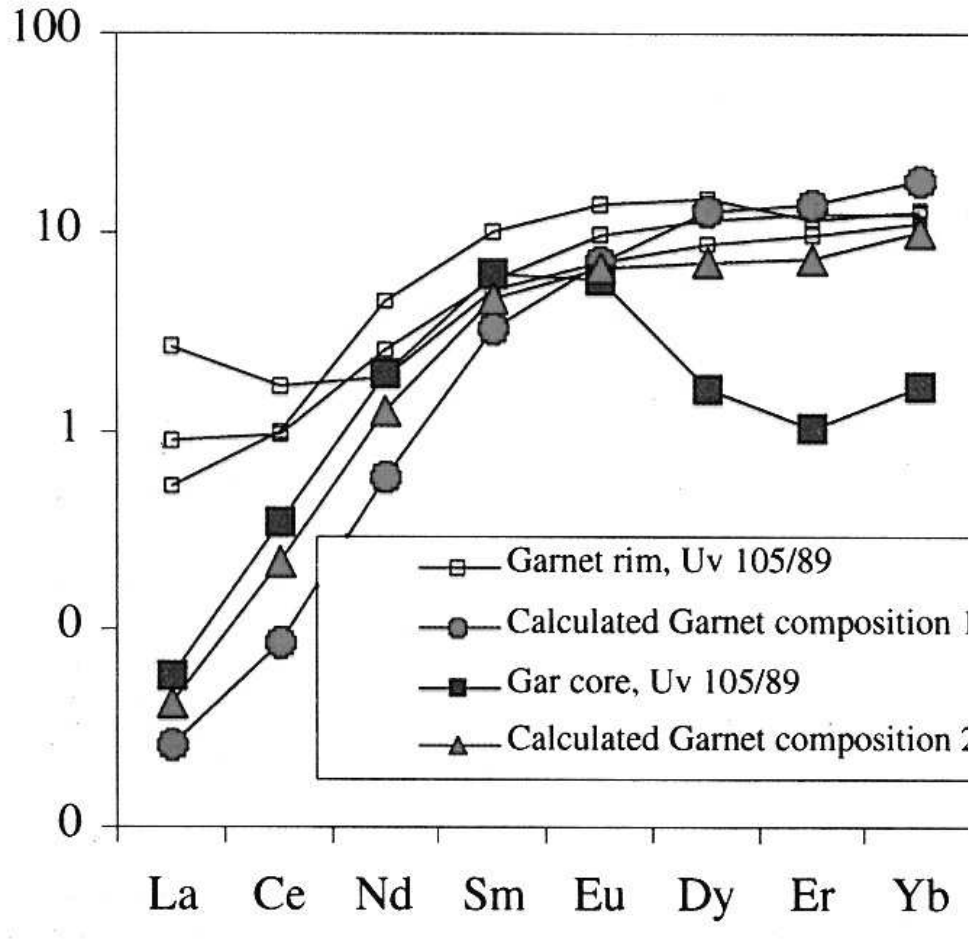

Fig. 4. **Primitive mantle normalized REE pattern of the calculated garnet composition compared to that of core and rim of the natural garnet from xenoluth Uv 105/89.**

1-is calculated composition of the garnet crystallized from the composition of tholeite from Siberian flood basalt province. 2-is calculated composition of garnet using the composition 1 and Uv-105/89 core composition in proportions of 50/50%. The tholeite composition is from Lighfoot et al, (1993). Distribution coefficients are from Halliday et al, (1995).

1. Maximal lithospheric mantle cross sections “sampled” by kimberlites of Pz age reached values of 220-250 km both in central part of the platform and its northeastern and southwestern margins.
2. Kimberlites of Mesozoic cycle (J3) of emplacement have “sampled” much thinner lithosphere (<150 km).
3. A significant basification of the lithospheric mantle matter took place in period between Pz (D3) and Mz (J3) cycles of kimberlite emplacement both beneath the northeastern and southwestern parts of Siberian Platform.
4. These large scale changes in structure and composition of the Siberian Platform lithospheric mantle can be connected with influence of Siberian superplume on the roots of lithospheric mantle between the Permian and Triassic periods. The same type of influence of Siberian Middle Paleozoic plume but in smaller scale took place for lithospheric mantle of central part of the platform as well.

REFERENCES

1. **Basu A.R., Poreda R.J., Renne F.T., Vasiliev Yu. R., Sobolev N.V., Turrin B.D.** High ^{3}He plume origin and temporal-spatial evolution of the Siberian flood basalts // Science, 1995, v. 269, p. 822-825.
2. **Boyd F.R., Pokhilenko N.P., Pearson D.G., Mertzman S.A., Sobolev N.V., Finger L.W.** Composition of the Siberian cratonic mantle: evidence from Udachnaya peridotite xenoliths // Contrib. Mineral. Petrol., 1997, v. 128, p. 228-246.
3. **Brakhfogel F.F.** The Age division of the kimberlitic and related magmatites in the North-East of the Siberian Platform (methods and results) // Extended Abstracts 6 IKC, Novosibirsk, 1995, p. 60-62.
4. **Davis G.L. Sobolev N.V., Kharkiv A.D.** New data on the age of Yakutian kimberlites obtained by U-Pb method by zircons // Dokl. Akad. Nauk SSSR, 1980, v. 254, p. 175-179 (in Russian).
5. **Halliday A.N., Lee D-C., Tommasini S., Davies G.R., Paslik C.R., Fitton J.G., and James D.E.**. Incompatible trace elements in OIB and MORB and source enrichment in the sub-oceanic mantle // EPSL, 1995, v. 133, p. 379-395.
6. **Griffin W.L., Ryan C.G., O'Reilly S.Y., Gurney J.J.** Lithosphere evolution beneath the Kaapvaal craton // Extended Abstracts 6 IKC, Novosibirsk, 1995, p. 203-204.
7. **Griffin W.L., Sobolev N.V., Ryan C.G., Pokhilenko N.P., Win T.T., Yefimova E.S.** Trace elements in garnets and chromites: diamond formation in the Siberian lithosphere // Lithos, 1993, v. 29, p. 235-256.
8. **Kinny P.D., Griffin B.J., Brakhfogel F.F.** SHRIMP U-Pb ages of perovskite from Yakutian kimberlites // Geologya i Geofizika, v. 38, p. 91-99. English translation: Russian Geology and Geophysics, 1997, v. 38, p. 97-105.
9. **Lighfoot P.C., Hawkesworth C.J., Hergt J.** Remobilization of the continental lithosphere by mantle plume: Major-, trace elements and Sr, Nd, and Pb isotope evidence from picritic and tholeitic lavas of the Noril'sk district, Siberian Trap, Russia // Contrib. Miner. Petrol, 1993, v 114, p. 171-188.
10. **Pokhilenko N.P., Pearson D.G., Boyd F.R., Sobolev N.V.** Megacrystalline dunites and peridotites: hosts for Siberian diamonds // Annual Report Dir. Geophys. Lab. Carn. Inst., Washington, 1991, p 11-18.
11. **Pokhilenko N.P., Sobolev N.V., Boyd F.R., Pearson D.G., Shimizu N.** Megacrystalline pyrope peridotites in the lithosphere of the Siberian platform: mineralogy, geochemical peculiarities and the problem of their origin // Geology and Geophysics, 1993, v. 34, p. 56-68.
12. **Pokhilenko N.P., Sobolev N.V., Safronov A.F. et al.** Magnesian garnets from kimberlites of the Northern part of the Siberian platform: Composition and processes of deep-seated zones of continental lithoshere // Extended Abst. Int. Symp., Novosibirsk, 1988, p. 75-77.
13. **Pokhilenko N.P., Sobolev N.V.** Mineralogical mapping of the North-East section of the Yakutian kimberlite province and it's main results // Extended Abstracts 6 IKC, Novosibirsk, 1995, p. 446-448.
14. **Pokhilenko N.P., Sobolev N.V.** Geology, peculiarities of distribution, methods of exploration of diamond deposits // Mirny, 1998, p. 65-68.
15. **Pokhilenko N.P., Sobolev N.V., Kuligin S.S. and Shimizu N.** Peculiarities of distribution of pyroxenite paragenesis garnets in Yakutian kimberlites and some aspects of the evolution of Siberian craton lithospheric mantle // Proceedings of 7th IKC, 1999, v. 2, p. 689-698.

16. **Shimizu N., Boyd F.R., Sobolev N.V., Pokhilenko N.P.** Chemical zoning of garnets in peridotites and diamonds // Miner. Mag. 1994, v. 58A, p. 831-832.
17. **Shimizu N., Pokhilenko N.P., Boyd F.R., Pearson D.G.** Geochemical characteristics of mantle xenoliths from Udachnaya kimberlite pipe // Russian Geology and Geophysic, 1997, v. 38, № 1, p. 194-205.
18. **Renne P.R., Basu A.R.** Rapid eruption of the Siberian Traps Flood Basalts at the Permo-Triassic Boundary // Science, 1991, v. 253, p. 176-179.
19. **Ryan C.G., Griffin W.L. and Pearson N.J.**. Garnet geotherms: Pressure -Temperature data from Cr-Pyrope garnet xenocrysts in volcanic rocks // J.Geoph. Res., 1996, v. 101, p. 5611-5625.
20. **Sobolev V.S., Sobolev N.V.** Doklady USSR Ac. Sc, 1964, v. 158, № 6, p. 108-111.
21. **Sobolev N.V., Lavrentiev Yu.G., Pokhilenko N.P., Usova L.V.** Chrome-rich garnets from the kimberlites of Yakutia and their parageneses // Contrib. Mineral. Petrol., 1973, v. 40, p. 39-52.
22. **Sobolev N.V., Lavrentiev Yu.G., Pokhilenko N.P., Usova L.V.** Chrome role in the kimberlite garnets: Problems of the Earth crust and upper mantle petrology // Nauka, Novosibirsk, 1978, p. 145-168 (in Russian).

УДК 549.211; 552.121

Multi-phase assemblages of nanometer-sized inclusion in cloudy Siberian diamonds: evidance from TEM

Logvinova A.M.[1], Wirth R.[2], Fedorova E.N.[1], Sobolev N.V.[1]

[1]*Institute of Geology and Mineralogy RAS SB, Koptyuga ave., 3, Novosibirsk, 630090, Russia.*
[2]*GeoForschungsZentrum, Potsdam, Experimental Geochemistry, Telegrafenberg, D-14482, Potsdam, Germany.*

ABSTRACT

Nanometer-sized isolated inclusions have been studied in four cloudy octahedral diamonds from the Internatsionalnaya and one from the Yubileynaya mines (Yakutia). Transmission electron microscopy (TEM) investigation of such microinclusions as electron diffraction, analytical electron microscopy (AEM), electron energy-loss spectroscopy (EELS) and high-resolution electron microscopy (HREM) were applied as well as line scan and elemental mapping of the samples. All crystals exhibit octahedral external habit with opaque central cuboid cores that contain numerous nano-inclusions. All nano-inclusions in the size range between 30 and 800 nm reflect the diamond habit and are considered primary, syngenetic to host diamond. They are composed of multi-phase assemblages, which include solid phases (silicates, oxides, carbonates), brines (halides), and fluid bubbles. These inclusions are relatively homogenous in composition and contain distinguishable crystalline and fluid phases. Al-bearing high–Mg silicate, dolomite, Ba-Sr carbonate, phlogopite, ilmenite, ferropericlase, apatite, magnetite, K-Fe sulfides (djerfisherite?) and kyanite have been identified as crystalline mineral phases by electron diffraction patterns, except the Ba–Sr carbonate. Several phases, including CaF2 and clinohumite-like phases, have never been reported as inclusions in diamond. The halide phase was KCl. Bubbles contained high K, Cl, O, P and less S, Ba, Si, Ti components. Carbonates were identified in TEM foils from all studied diamonds. They occur in all assemblages with silicates, oxides, sulfides and show a general enrichment in incompatible elements such as Sr and Ba. Some elemental variations may be explained by fractional crystallization of fluid/melt or mixing of fluids with different compositions (carbonatitic, hydrous-silicic, brines).

INTRODUCTION

Natural diamonds and their mineral and fluid inclusions are considered powerful geochemical indicators of the deep continental lithosphere exceeding depths of 120 – 150 km and sometimes even 300 km. Reliable reconstruction of the conditions of mineral formation at these depths based on an integrated study of diamonds and their inclusions is of principal importance for geosciences.

Providing a unique opportunity to study and improve our understanding of the evolution of this inaccessible portion of the Earth, diamond was long been recognized as an ideal container for preserving traces of the geochemical environment entrapped during its growth even when analytical possibilities were limited to only X-ray identification of mineral inclusions [11, 50]. The most important factor is that these inclusions were isolated from later mantle processes. Chemical composition of larger mineral inclusions [31, 39, 45] in the size range mainly between 50 and 200 micrometers have been readily determined both in micro and macrodiamonds worldwide [46]. Neutron activation analysis of gem quality diamonds containing no visible inclusions at all showed the presence of a number of elements which have been interpreted as constituents of minute drops of solidified melts from the diamond forming environment [8]. Some rare diamonds contain many hundreds of densely located monomineralic and polymineralic inclusions. One of such studied sample [27] represents a combination of a number of inclusions (5-50 micrometers in size) detectable by electron probe microanalysis (EPMA) and hundreds of considerably smaller mineral inclusions (less then 5 micrometers which are not detectable by EPMA but representing similar mineral phases (garnets and pyroxenes).

The mineral inclusions in diamonds were interpreted as remnants of two types of geochemical diamond forming environments: ultramafic (or peridotitic) – U/P type and eclogitic (E-type) as shown by systematic studies of inclusion bearing diamonds from numerous diamond mines worldwide [9, 12, 30, 45].

The presence of mica inclusions showing octahedral facets of negative diamond crystals and sometimes grown in with syngenetic diamond inclusions such as clinopyroxenes and chromites [39] testified their primary origin and significance of fluid containing H2O, F and Cl in the diamond forming medium.

As a result of many years of experimental and analytical studies on natural diamonds, most authors came to the conclusion that the mantle environment of diamond crystallization was represented by volatile-saturated melts or fluids [1, 33, 34, 35, 37, 38, 40, 47, 53, 61]. The carboniferous fluids and carbonates could be sources of carbon, which was saturated in the medium by redox reactions. Progress in research technology has made it possible to study micro- and nano-inclusions in diamonds from kimberlites and metamorphic rocks which often are surprisingly similar in diamonds from different rocks and to obtain new information on compositions of entrapped fluids [7, 13, 14, 23].

Combined with X-ray diffraction, modern analytical electron microscopy (AEM) allows phase identification, element mapping, and microanalysis of inclusions considerably less than one micrometer. This equipment “visualizes” every separate phase of a polymineralic nano-sized inclusion, determines its unit-cell parameters, and analyzes its chemical composition, thus providing positive identifications. Using focused ion beam techniques (FIB), we have prepared

superfine sections of inclusion-containing diamonds which beforehand were polished down to expose the inclusions [60]. The present work initiates systematic studies of the composition and paragenesis of mineral and fluid (melt) nanoinclusions in Siberian diamonds by the TEM method. We have studied more than 60 isolated inclusions in diamonds of octahedral and transitional habit from the Internatsionalnaya and Yubileinaya pipes (Yakutia), which are the highest grade (Internatsionalnaya) and largest (Yubileinaya) diamond mines. Such diamonds contain so-called cloudy parts, which consist of nanoinclusions dispersed zonally throughout cubic diamonds or filling the cuboid central zone in octahedrally faceted diamonds. Occurrence of cubic diamonds is rare in Siberian mines, octahedral stones are considered the most typical form [36].

In this paper we report data on the compositions of melt, fluid and near liquidus mineral assemblages located inside cloudy central parts of diamond crystals. Previous studies of similar dense cloudy inclusions in African, Canadian and Siberian diamonds have been reported by several authors [10, 16, 20, 21, 23, 62].

SAMPLE DESCRIPTION

Nanometer-sized isolated inclusions have been studied in four cloudy diamonds from the Internatsionalnaya (Im-201, Im-203, Im-204, Im-207) and one from the Yubileynaya (Ub-5) mines from two different kimberlite regions (Malo-Botuobiya and Daldyn-Alakit) respectively of the Siberian craton (Russia), all of which are of late Devonian age [6, 19]. The investigated diamonds were from 1.3 to 2.0 mm in size (Fig. 1), exhibiting octahedral and cubo-octahedral external habit with cloudy central cuboid cores which contain numerous nanoinclusions (see Fig.1). These cloudy cuboid cores are characterized by different density and abundance of inclusions as demonstrated by color differences in Fig.1, A and E. There were no cracks around the cloudy substance. The detected inclusions vary in size from 30 to 700 nm, and each consisted of several mineral and fluid phases.

METHODS AND ANALYTICAL TECHNIQUES

All of the diamonds were polished into 0.8-1.4 mm plates with two parallel surfaces for spectroscopic analysis. Polished thin sections have been examined in transmitted light at high magnification. The cathodoluminescence images of the diamond plates were obtained using a JSM-35 scanning electron microscope (I = 3nA, U = 20 kV) at the Institute of Geology and Mineralogy. Birefringence patterns of polished plates were observed with a polarized microscope.

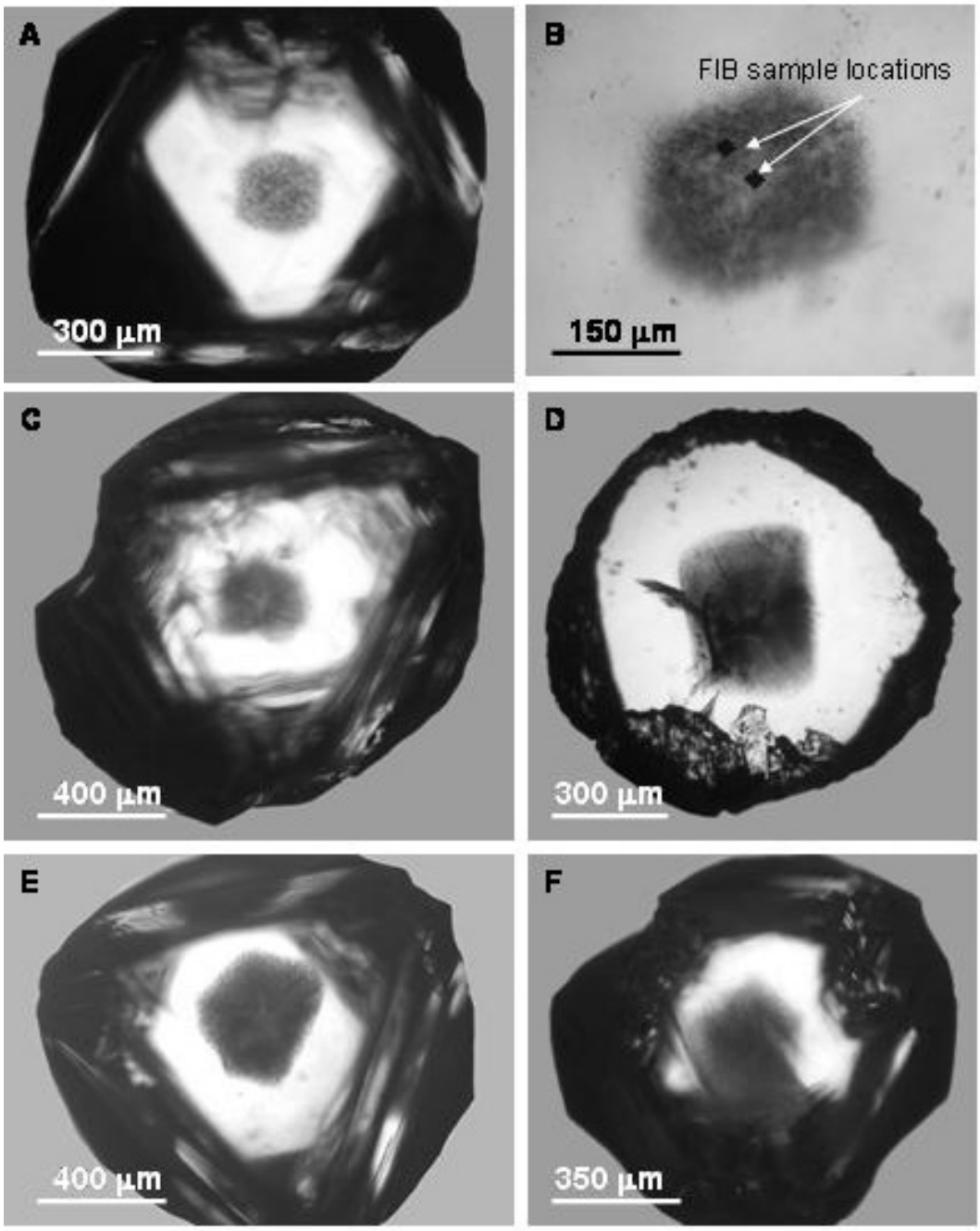

Fig. 1. **Optical micrographs of the five investigated cloudy diamonds from Internatsionalnaya and Yubileynaya pipes (Yakutia).**
(A) – Im- 204; (**B**) – the cloudy centre of the Im-204; (**C**) - Im-207; (**D**) -Ub-5; (**E**) – Im-203; (**F**) – Im-201. There are many nanoinclusions in the central cubic core. There are no visible cracks around the cloudy dense zone.

The impurity defects were initially characterized using Infrared (IR) spectroscopy. IR spectra were measured in the range 600 - 4500 cm-1 at a resolution

Table 1. **FTIR data for diamonds accoding growth zones.**

		Nitrogen				Hydrogen		Carbonate				Water	Molar
Sample	**Zone**	**N(A)ppm**	**N(B)ppm**	**N_{total} ppm**	**%B**	**α_{1405} cm^{-1}**	**α_{3107} cm^{-1}**	**ν_2**	**ν_3**	**$\alpha_{(860-880)}$ cm^{-1}**	**$\alpha_{(1430-1460)}$ cm^{-1}**	**$\alpha_{(1630-1650)}$ cm^{-1}**	**ratio***
Im-204	centre	761,2	125,85	887,0	14,2	8,6	28,0	880, sh875	880,sh1430, sh1457	9,1	25,2	0,1	0,24
	cloudy part	424,8	66,82	491,6	13,6	2,7	11,0	880	1450	0,3	0,5	-	
	interrim	776,0	52,32	828,3	6,3	-	-	-	1450	-	0,2	-	
	rim	591,9	19,97	611,8	3,3	-	-	-	-	-	-	-	
Im-207	centre	549,8	11,52	561,3	2,1	3,5	10,9	880	1450	10,5	22,6	0,2	0,22
	cloudy part	532,7	52,61	585,4	9,0	0,7	2,8	-	1450	-	0,1	-	
	interrim	564,9	83,54	648,4	12,9	-	-	-	-	-	-	-	
	rim	424,0	10,10	434,1	2,3	-	-	-	-	-	-	-	
Im-203	centre	686,4	15,87	702,3	2,26	3,6	15,1	879,sh 865	1448,sh1455, sh1435	4,2	12,6	0,3	0,21
	cloudy part	697,1	10,40	707,5	1,5	2,4	10,2	879,sh 865	1448,sh1455, sh1435	4,1	10,8	0,4	
	rim	816,4	10,50	826,9	1,3	-	0,1	-	-	-	-	-	
Im-201	centre	751	38,20	789,2	4,84	0,3	1,2	-	-	-	-	0,2	0,35
	cloudy part	637,7	65,50	703,3	9,32	0,7	3,1	879,sh876, sh865	1448,sh1455, sh1430	1,2	4,5	0,1	
	rim	755,8	11,50	767,3	1,4	-	0,1	-	-	-	-	-	
Ub-5	centre	699,4	583,60	1283	45,5	21,4	92,4	880, 865	1448, 1455	5,1	26	2,2	0,38
	cloudy part	594,2	417,30	1011,5	41,2	17,5	64,6	880, 865	1448, 1455	4,2	17,5	1,1	
	interrim	379,6	162,10	541,7	29,9	3,3	11,7	-	-	-	0,7	-	
	rim	264,5	19,10	283,7	6,75	0,1	0,6	-	-	-	-	-	

Note: * - Molar ratio $H_2O/(CO_2+H_2O)$ is calculated from the IR spectrum using molar absorption coefficient from (Navon et al., 1988)$\varepsilon(H_2O)$ = 80 (3400) and $\varepsilon(CO_2)$ =250 (1450).

of 1 cm-1 by means of a FTIR BRUKER VERTEX 70 spectrometer with the use of HYPERION 2000 microscope. The typical diameter of the aperture spot was 50 μm with 120 μm distance between analysis points. Nitrogen contents in A- and B-centers were calculated using the relations specified by Boyd [2]. The absorption coefficient was determined with correction for lattice modes in two-phonon region.

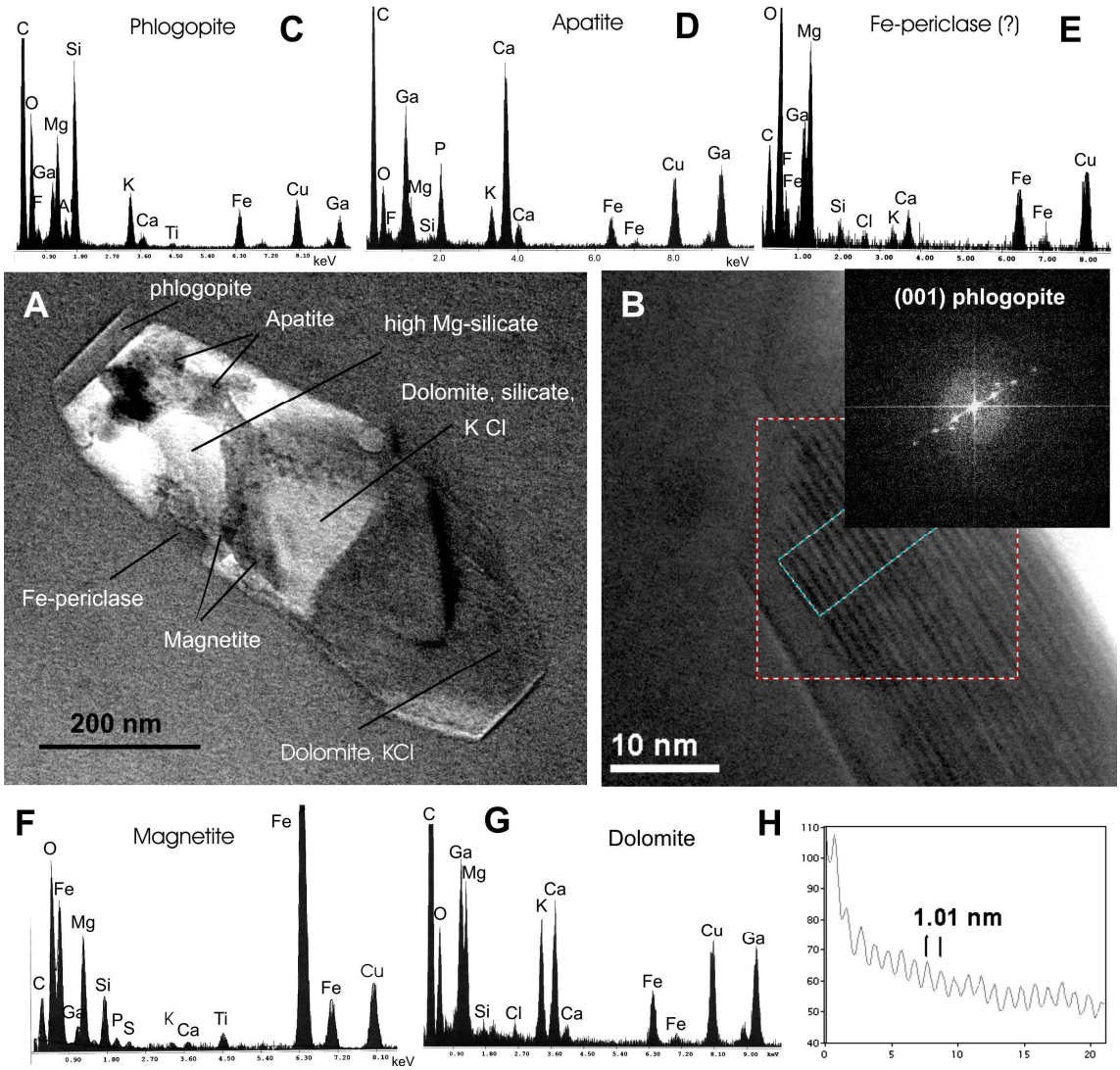

Fig. 2. **A) TEM image of nanometre-sized inclusion 1 in foil #860 (Diamond Im-201). (B, H) – Energy filtered TEM lattice fringe image of mica (diffraction pattern from fast Fourier transform FFT).The spacing between the fringes is used for phase identification.**

EDX spectra (C-G) from mineral phases within inclusion 1: (C)- phlogopite; (D) – apatite; (E) – Fe-periclase (?); (F) – magnetite; (G) – dolomite. Ga intensity in the spectra is due to implanted Ga during FIB sample preparation and Cu intensity comes from copper grid.

Electron transparent foils of the cloudy central part of the investigated diamonds were prepared for TEM investigation using the FIB technique [60]. The foils were 10-20 □m wide, 5-15 □m high and approximately 100 nm thick. The samples were coated with carbon before cutting the foil. The foils are suitable for TEM investigations such as conventional bright- and dark-field

imaging, electron diffraction, electron energy-loss spectroscopy (EELS), high-resolution electron microscopy (HREM) and AEM. TEM study was carried out using Philips CM200 electron microscope operated at 200 kV with a LaB6 electron source. EELS study was done using a Gatan imaging filter (GIF). Microstructure and compositions of minerals were studied using an AEM equipped with an energy dispersive X-ray (EDX) spectrometer with an ultra-thin window and a Si (Li) detector.

RESULTS

IR

Nitrogen is the most significant structural impurity in diamond. When diamond contains numerous inclusions of submicrometer size, it is worth studying nitrogen contents at different growth zones of the diamond. Prior to nitrogen analysis, the diamond plates were examined with CL. Our CL and IR spectroscopy data as well as analyses of similar samples by other authors [16, 62] suggest that the diamond crystals were refaceted.

IR spectra were obtained in different growth zones in all analyzed diamonds, and showed that studied diamonds from the Internatsionalnaya pipe were categorically different from the Yubileinaya diamond. All diamonds from two pipes analyzed in this work contain more nitrogen in the form A defects (peaks at 1282 cm-1) in central cubic zones of crystals varying from 424 to 756 ppm from Internatsionalnaya pipe and from 656 to 699 ppm from Yubileinaya pipe. Distribution of B defects (peaks at 1175 cm -1) is various. In the Im-207 and Im-201, the minimum N-content in the B- form has been recorded in the central cuboid site; in intermediate zone its content drastically increases and is apt to decrease over again, and very small B defects are observed at margin. For the Im-204, Im-203 and Ub-5 B –form nitrogen content are mach higher in the centre (Table 1). The degree of nitrogen aggregation (the percentage of nitrogen in B form) is considerably small in the crystals from Internatsionalnaya pipe than for the Yubileinaya diamonds (Table 1). For the first the predominant form of nitrogen is A-centre. It will be noted that the low degree of nitrogen aggregation (less 20% in B form) is characterized the Internatsionalnaya diamonds as a rule. In the Ub-5 diamond the nitrogen content drastically increases in core as compared with the margin of the crystal and the degree of nitrogen aggregation is 45,5% (Table1). IR has revealed that carbonates are present in micro-inclusions of the central cloudy part of investigated diamonds from two pipes . Typical spectra of dolomite (ν2 at 880, ν3 at 1448 ± 2 cm-1) are observed for the cuboid centre of the sample Im-207 (Table1). In addition to primary peak of dolomite (ν2 at 880) there are shoulders at 875 cm-1 (Im-204, Im-201) and at 865 cm-1 (Im-203, Im-201, Ub-5), which are probably related to ankerite- group and Ba-, Sr- carbonates respectively [41]. In the range of the vibration frequency ν3(CO32-) are observed favored dolomite peak (at 1448 ± 2 cm-1) for the most investigated diamonds and shoulders at 1430, 1455 cm-1 for some diamonds (Table1). The broad bands at 940 – 960, 1000 cm-1, 1050

(shoulder), 1095 and at 600 – 800 cm-1 (multiplet, week) were observed in all investigated diamonds. These bands may be attributed to mica [23].

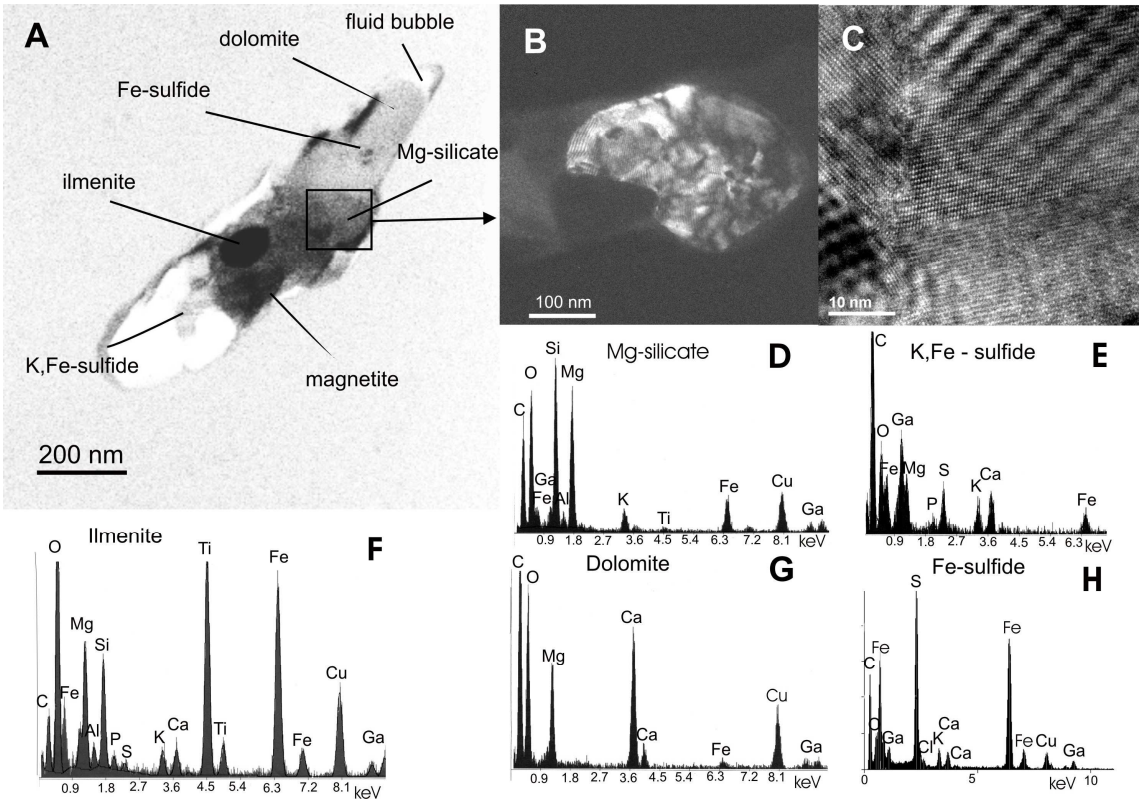

Fig. 3. **TEM bright field of nanometer-sized inclusion 3 in foil #852 (diamond Im-207). (B) – TEM bright field image from the high Mg-silicate phase.**

(C) – High-resolution image of Mg-phase super structure. EDX spectra (D-H) from mineral phases inside inclusion 3: (D) – Mg-silicate; (E) – dolomite; (F) – ilmenite; (G) – pyrrhotite; (H) – K,Fe-sulfide. Ga intensity in the spectra is due to implanted Ga during FIB sample preparation and Cu intensity comes from copper grid.

The present study shows that the presence of carbonates does not always imply the presence of hydrous phases, which are characterized by absorption bands in the region 1630 - 1660 cm -1 (ν (HOH)-bending vibration) and at 3200 - 3400 cm -1 (symmetric and asymmetric OH –stretching modes) in the IR spectra (Table 1). The central cuboid part of the samples from Internatsionalnaya and Yubileinaya pipes contains larger amounts of carbonates (absorption coefficients ν3 (CO32-) are 12 - 25 cm-1 and 26 cm-1 respectively) and small amount of water (absorption coefficients ν (HOH)-bending are 0.1 – 0.3 cm-1 and 2,2 cm-1 respectively). Our estimated H2O/ (CO2+H2O) molar ratios for the Internationalnaya pipe vary between 0.21 – 0.35. These results correlate well with data for diamonds from this pipe obtained by Zedgenizov [62]. For the Yubileynaya molar ratio is higher than for the Internatsionalnaya pipe and equal to 0.38 (see Table1).

The present data are revealed that the diamond-forming fluid to be rich in carbonate and hydrous- silicic endmembers [41]. The nanoinclusions in the cuboid cores of the investigated diamonds are mostly carbonatitic [62].

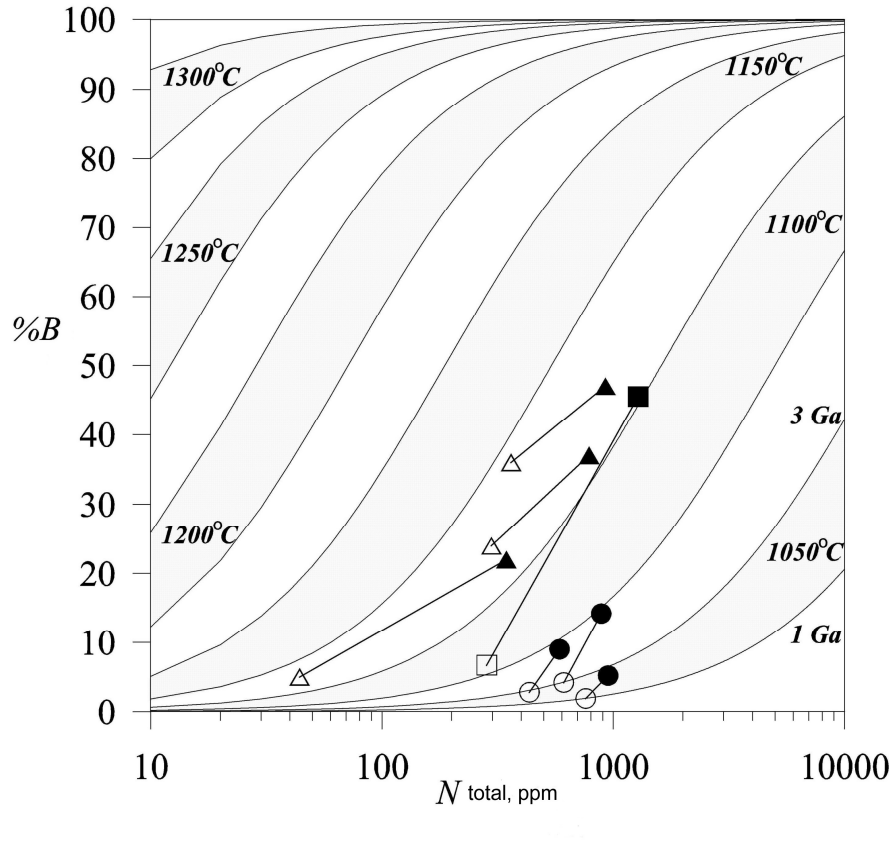

Fig. 4. **Nitrogen aggregation state (%B) plotted as function of nitrogen content (N_{ppm}) for individual diamonds from Internatsionalnaya and Yubileinaya pipes.**

Isotherms calculated for an assumed mantle residence of 1 and 3 billion years (Ga) for the temperature of 1050^0C to 1300^0C [55]. Thus the lines marked 1Ga and 3Ga at the bottom right are for the temperature of 1050^0C. There are Internatsionalnaya data (circle) and Yubileinaya (square) data from present study, data of the Internatsionalnaya (triangle), obtained by [62]. Note: solid symbol is related to the centre cloudy part (cuboid), open symbol is related to the rim of diamond (octahedral).

TEM

Cloudy aggregations in the core of the analyzed diamonds consist of nano-inclusions measuring 20 to 600 nm across. The nanoinclusions are considered primary, because they are faceted in the form of a diamond negative crystal for both monomineralic and polymineralic inclusions [45]. As a rule, the absolute majority of inclusions form polymineralic aggregates plus amorphous glassy matter and fluid bubbles.

Diamond Im-201. Foil #860 was cut from the inner cloudy part of the diamond crystal. Eleven nanoinclusions were detected. Dolomite was identified in all inclusions (Fig. 2-G). The inclusions are enriched in K and Cl. Using diffraction techniques (Fig. 2-B) and EPMA spectra (Fig. 2-C, D, phlogopite and apatite were

established in four cases, as well as ilmenite and magnetite in two cases. Figure 2-B shows the structure and electron diffraction pattern of phlogopite. The KCl phase is present everywhere. To determine the fluid phase composition, one of the bubbles was opened by electron beam and the composition was analyzed before and after opening. Moving contrast under the electron beam indicated the presence of a fluid. After opening the fluid bubble by the focused electron beam, the oxygen peak in the EDX spectrum decreased substantially, thus indicating that the fluid was composed mainly of KOH. Some fluid bubbles were decrepitated in the process of film slicing; the gas component is partially or completely released, with K (abundant in the diamond-generating melt) and partially P, S, Mg, and other constituents remaining on the walls.

Diamond Im-203. One foil (#853) was sliced off this sample, and six composite microinclusions were analyzed. All inclusions are uniform, composed of Ca, Mg, Fe-carbonates, Ba, Sr-carbonates, phlogopite, magnetite, KCl-rich phase, Fe-sulfide and quench product (K, Cl, P, S, Ba, Si, O. The noncrystallized residue contained K- impurity.

Diamond Im-207. Eight inclusions have been studied. All inclusions were uniform and contained, as a rule, up to six phases. The most representative inclusions are shown in Fig. 3. dolomite, apatite, magnetite. In three cases ilmenite and K,Fe-sulfide, most probably, djerfisherite (Fig. 3-H), were recorded. TEM bright field image and high-resolution image of high Mg-silicate phase superstructure (Fig. 3-B,C) allow this phase to be identified as a crystal with an interplanar distance of 7.4 Å. Despite the fact that precise identification of this phase has not been made yet, it is most similar to clinohumite (Table 2). However, such a phase has never been detected as a diamond inclusion. Bubbles of fluid contain a permanent impurity of F.. Inclusion 6 is a monomineralic inclusion of kyanite, which undoubtedly indicates the E-type paragenesis.

Diamond Im-204. Two foils (#861 and #863) were cut from the inner cloudy part of the diamond crystal (Fig.1-B). Foil #863 was cut from the centre of the crystal and contained seven nanoinclusions over 40 nm in size. Dolomite, magnetite, Al-bearing, high-Mg silicate, and K-rich phase were the main phases making up inclusions. Foil #861 was sliced from near the cloudy cuboid zone. It contained numerous nanoinclusions not exceeding 50 nm. We have also analyzed the three largest inclusions containing Mg, Si, Ca, P, K, Fe, and fluid bubbles enriched in K and O. Notably, Cl was not found in this system.

Table 2.

D-spacings for clinohumite (diamond Im-207 foil # 853).

dhkl	dhkl	hkl
observed	calculated from literature	
7,89 - 7,93	8,17	(011)
4,93 - 5,15	5,14	(020)
4,76	4,8	(021)
3,84	3,87	(111)
3,48	3,46	(121)

Diamond Ub-5 (foil #1079). Six inclusions have been studied. Their composition differs considerably from aforementioned inclusions. First, most space in the volume of the inclusion is occupied by glassy noncrystallized matter containing K, Cl, Ca, P, Ba, Sr, F, S, Cr, Fe, and O. All the phases supposedly identified as carbonates are amorphous noncrystallized substances. All of them were very sensitive to electron beam. Among the crystallized phases, we have identified Fe, Ni-sulfide, phlogopite, ilmenite. The composition of the sulfide phase and the presence of a noticeable amount of Cr in the residual melt imply that this group of inclusions belongs to the peridotite paragenesis. As inferred from the EDX spectrum, there is a silica- phase. Abundant fluorine content is also worthy of note. A phase was observed to contain Ca and F. All the analyzed inclusions contained a high-K phase, possibly KCl and/or KOH.

DISCUSSION AND CONCLUSIONS

The application of TEM imaging combined with FIB-milled foils opens new possibilities in observations of submicroscopic inclusions. Polymineralic inclusions which seem to be extremely rare in diamonds observed by routine techniques represented mostly by EPMA appear to be fairly common as nanoinclusions and are available for direct observation and identification. Moreover, nanoinclusions were composed not only of several mineral phases and quench products, but also of fluid bubbles which were sometimes preserved within superthin foils, but were mostly decomposed during sample preparation.

Establishing a link between micro mineral inclusions which undoubtedly belong either to ultramafic or peridotitic (U/P) or eclogitic (E-type) parageneses proved by studies of diamonds from all deposits worldwide [9, 12, 30, 45, 50] and polymineralic (touching) mineral nanoinclusions closely associated with fluid inclusions may provide the most definitive information on the realistic composition of a natural diamond forming medium. Some first steps in identifying coexisting mineral and fluid microinclusions in the same diamonds have been performed by Izraeli [17] and Tomlinson [57], and an important conclusion was drawn that fibrous diamonds grew in the same paragenetic environment as octahedral diamonds [57]. This conclusion confirmed the earlier statements on importance of carbonates, phlogopites and Ba-Sr-titanates as constituents of the diamond forming environment among inclusions in macrodiamonds [4, 39, 49, 59], which provide evidence for the metasomatic conditions of diamond growth. An additional evidence for such conditions is provided by the finding the clinohumite-like phase in present study [56].

Some important inclusions for paragenetic relations such as garnets, olivine, pyroxenes and chromites were not detected in our study. However, mica inclusions which are abundant in the studied diamonds may be classified either as phlogopites or biotites based upon their spectra and thus, related to proper parageneses. The same may relate to ilmenite typical both for U-type and E-type diamonds

depending on abundance of Mg (geikielite) component [48]. The most definitive evidence of E-type paragenesis may be present in Im-207 sample, containing an isolated kyanite nanoinclusion closely associated with K-Fe-sulfide (djerfisherite), pyrrhotite, apatite, dolomite, most probable clinohumite, magnetite, ilmenite.

The polymineralic inclusions including quench products and bubbles rich in K and Cl, were detected as multiple isolated formations in all studied diamonds. The morphology of the majority of them represents negative diamond crystals [45]. Earlier microRaman studies confirmed high internal pressure of similar inclusions within the diamonds [15, 63], which undoubtedly testify to their primary origin. All investigated inclusions demonstrate the significance of carbonates, especially, dolomite [51] and Ba, Sr carbonates, apatite (found earlier only once in a diamond coating [24], K, Cl, OH and sometimes, F -enriched fluids in kimberlitic diamonds formation. All of these phases, with the exception of those F-bearing, have been earlier detected in combination with silicates in cloudy and coated diamonds from Africa, Canada and Siberia [17, 23, 63].

The presence of primary brine inclusions in all studied diamonds confirms the significance of such fluids in diamond formation [16] and is consistent with identification of the significant role of mantle derived Cl in the groundmass of a uniquely fresh serpentine free Udachnaya kimberlite [18, 28, 32, 42]. Brine inclusions combined with different carbonate and OH-bearing inclusions mixed with silicates, sulfides and oxides of U-type and E-type parageneses represent the most realistic natural diamond forming medium with the range of bulk compositions between chlorides, carbonates and silicates. The carbonate and oxide were dominant part of the polymineralic nanoinclusions; the silicate part represented mostly by phlogopite were poorly identified.

Dolomites in nanoinclusions were surprisingly abundant; this is different from the macroinclusion data, where dolomite was not detected for a long time [12, 30] and found only recently [51]. The presence of magnesite in some diamonds described elsewhere [3] coupled with experimental data, indicates conditions about 6 GPa pressure, for a typical diamond formation temperature close to 1000-1100oC [5, 44]. The nitrogen content and aggregation characteristics can be used for the evaluation of time/ temperature mantle residence of diamond [29]. The plot of time/ temperature mantle residence of diamond, based on that of Taylor [55], is illustrated in Fig. 4. We have found that the values of time/ temperature determined by second- order kinetic equation suggest that the central cuboid zones are older than the octahedral rim for all investigated diamonds (Fig. 4). This conclusion is consistent with results obtained by Zedgenizov [62] for a mumber of similar Siberian diamonds. Following Sunagawa [52] we suggest that central core cuboid and surrounding octahedral outer part of investigated diamonds were formed in different stages and cuboid core after its formation elsewhere was transported to different conditions and environment and acted as seed crystal.

Ba and Sr enrichment of some carbonates detected in this study as nanoinclusions and found as typical inclusions in chromites in some Siberian

kimberlites [26], as well as Ba, Sr titanates discovered as inclusions in Siberian diamonds testify to the importance of metasomatic enrichment of diamond forming medium by these elements. The wide range of Sr abundance in subcalcic, Cr-pyropes included in Siberian diamonds [43] also confirms such a conclusion.

ACKNOWLEDGMENTS

We are grateful to Dave Mao, Anatoly Chepurov, Ofra Klein-BenDavid, John Valley and Ichiro Sunagawa for their critical reading of manuscript and useful comments which helped to improve the manuscript. This work was supported by Russian Foundation for Basic Research Grant 06-05-65021.

REFERENCES

1. **Anand, M., Taylor, L.A., Misra, K.C., Carlson, W.D., Sobolev, N.V.** (2004): Nature of diamonds in Yakutian eclogites: views from eclogite tomography and mineral inclusions in diamond. *Lithos*, 77, 333-348.
2. **Boyd, S.R., Kiflawi, I, Woods, G.S.** (1995): Infrared absorption by the B nitrogen aggregation in diamond. *Philos. Mag.*, 72, 351-361.
3. **Bulanova, G.P. (1995).** The formation of diamonds. *J. Geochem. Explor.*, 53, 1-23.
4. **Bulanova, G.P., Muchemva, E., Pearson, D.G., Griffin, B.J., Kelley, S.P., Klemme, S, Smith, C.B.** (2004). Syngenetic inclusions of yimengite in diamond from Sese kimberlite (Zimbabwe) – evidence for metasomatic conditions of growth. *Lithos*, 77, 181-192.
5. **Buob, A., Luth, R.W., Schmidt, M.W. and Ulmer, P.** (2006): Experiments on $CaCO_3$ – $MgCO_3$ solid solutions at high pressure and temperature. *Amer. Mineral.*, 91, 435-440.
6. **Davis, G.L., Sobolev, N.V., Kharkiv, A.D.** (1980): New data on the age of Yakutian kimberlites obtained by the U-Pb method on zircons. *Dokl. Acad. Nauk SSSR*, 254, 175-179.
7. **Dobrzhinetskaya, L.F., Wirth, R. and Green, H.W.** (2005). Direct observation and analysis of a trapped COH fluid growth medium in metamorphic diamond. *Terra Nova*, **17**, 472-477.
8. **Fesq, H.W., Bibby, D.M., Erasnus, C.S., Kable, E.J., Sellshop, J.P.** (1975): A comparative trace elements study of diamonds from Premier, Finsch and Jagersfontein mines, South Africa. Phys. Chem. Earth, IX, Ahrens, L. H. et al. (eds) Pergamon Press, 817-836.
9. **Gurney, J.J.** (1989). Diamonds. In: Kimberlites and related rocks. Geol. Soc. Austral. Spec. Publ. 14., v. 2, 935-965.
10. **Guthril, G.D., Veblen, D.R., Navon, O. and Rossman, G.R.** (1991). Submicrometer fluid

inclusions in turbid-diamond coats. Earth. Planet. Sci. Lett., 105, (1-3), 1-12.

11. **Harris, J.W.** (1968). The recognition of diamond inclusions: Part I: Syngenetic inclusions. Industr. Diamond Rev., 28, 402-410.
12. **Harris, J.W.** (1992): Diamond geology. In: Field J.E. (Ed). The Properties of Natural and Synthetic Diamonds, 345-393, Academic Press, London, 345-393.
13. **Hwang, S.L., Chu, H.T., Lui, T.F., Shen, P., Schertl, H-P., Liou, J.G., Sobolev, N.V.** (2006): Nanometer-size P/K-rich silica glass (former melt) inclusions in microdiamond from the gneisses of Kokchetav and Erzgebirge massifs: Diversified characteristics of the formation media of metamorphic microdiamond in UHP rocks due to host-rock buffering. Earth Planet. Sci. Lett., 243, 94-106.
14. **Hwang, S.L., Shen, P., Chu, H.T., Yui, T.F., Liou, J.G., Sobolev, N.V., Shatsky, V.S.** (2005): Crust-derived potassic fluid in metamorphic microdiamonds. Earth Planet. Sci. Lett., 231, 295-306.
15. **Izraeli, E.S., Harris, J.W., Navon, O.** (1999): Raman barometry of diamond formation. *Earth Planet. Sci. Lett*., **173**, 351-360.
16. **Izraeli, E.S., Harris, J.W., Navon, O.** (2001): Brine inclusions in diamonds: a new upper mantle fluid. Earth Plan. Sci. Lett., **187**, 323-332.
17. **Izraeli, E.S., Harris, J.W., Navon, O.** (2004): Fluid and mineral inclusions in cloudy diamonds from Koffifontein, South African. Geochim. Cosmochim. Acta, **68** (11), p.2561-2575.
18. **Kamenetsky, M.B., Sobolev, A.V., Kamenetsky, V.S., Maas R., Danyushevsky, L.V., Thomas R., Pokhilenko N.P., Sobolev N.V.** (2004): Kimberlite melts rich in alkali chlorides and carbonates: a potent metasomatic agent in the mantle. Geology, 32, 845-848.
19. **Kinny, P.D., Griffin, B.J., Heaman, L.M., Brakhfogel, F.F. and Z.V. Spetsius** (1997): Shrimp U-Pb ages of perovskite from Yakutian kimberlites. Geol. Geofiz., 38, 91-99. English Translation: Russ. Geol. Geophys., 38, 87-95.
20. **Klein-BenDavid, O., Izraeli, E., Hauri, E., Navon, O.** (2004): Mantle fluid evolution – a tale of one diamond. Lithos, 77, 243-253.
21. **Klein-BenDavid, O., Izraeli, E., Hauri, E. and Navon, O.** (2007): Fluid inclusions in diamonds from the Diavik mine, Canada and the evolution of diamond forming fluids. Geochim. Cosmochim. Acta., 71, 723-744.
22. **Klein-BenDavid, O., Logvinova, A.M., Izraeli, E.S., Sobolev, N.V., and Navon, O.** (2003b): Sulfide melt inclusions in Yubileinaya (Yakutia) diamonds. 8th International Kimberlite Conference, Extended abstracts, FLA _0111, 22-27 June 2003, Victoria,

Canada.

23. **Klein-BenDavid, O., Wirth, R., Navon, O.** (2006): TEM imaging and analysis of microinclusions in diamonds: a close look at diamond-growing fluids. Amer. Mineral., 91, 353-365.
24. **Lang, A.R. and Walmsley, J.C.** (1983): Apatite inclusions in natural diamond coat. Phys. Chem. Miner., 9, 6-8.
25. **Logvinova , A.M., Klein-BenDavid, O., Izraeli, E.S., Navon, O., Sobolev , N.V.** (2003a): Microinclusions in fibrous diamonds from Yubileynaya kimberlite pipe (Yakutia). 8th International Kimberlite Conference, Long Abstract, FLA_0025.
26. **Logvinova, A.M., Sobolev, N.V., Taylor, L.A.** (2003b). Chromite macrocrysts from kimberlites and lamproites as petrogenetic indicators: evidence from mineral inclusions. Suppl. Eos, Trans. AGU, v. 84 (46), p F1553.
27. **Logvinova, A.M., Zedgenizov, D.A., Sobolev, N.V.** (2001): Pyroxenite paragenesis of abundant mineral and probable fluid inclusions in a microdiamond from Mir kimberlite pipe. Dokl. Earth Sci., v. 380, p. 795-799.
28. **Maas, R., Kamenetsky, M.B., Sobolev, A.V., Kamenetsky, V.S., Sobolev, N.V.** (2005): Sr, Nd and Pb isotope evidence for a mantle origin of alkali chlorides and carbonates in the Udachnaya kimberlite, Siberia. Geology, 33, 549-552.
29. **Mendelssohn, M.J., Milledge, H.J.** (1995): Geologically significant information from routine analysis of the mid-infrared spectra of diamonds. Intern. Geol. Review, 37, 95-110.
30. **Meyer, H.O.A.** (1987): Inclusions in diamonds. In: Nixon, P.H. (Ed), Mantle xenoliths. John Wiley and Sons, Chichester, 501-522.
31. **Meyer, H.O.A., Boyd, F.R.** (1972). Composition and origin of crystalline inclusions in natural diamonds. Geochim. Cosmochim. Acta, 36, 1255-1273.
32. **Misra, K.C., Anand, M., Taylor, L.A., Sobolev, N.V.** (2004): Multistage metasomatism of diamondiferous eclogite xenoliths from the Udachnaya kimberlite pipe, Yakutia, Siberia. Contrib. Mineral. Petrol., 146, 696-714.
33. **Navon, O.** (1991): High internal-pressures in diamond fluid inclusions determined by infrared-absorbtion. Nature, 353, 746-748.
34. **Navon, O.** (1999): Formation of diamonds in the Earth's mantle. In J.Gurney, S. Richardson, and D.Bell, Eds., proceedings of the 7th International kimberlite Conference, p.584-604. Red Roof Designs, Cape Town.
35. **Navon, O., Hutcheon, I.D., Rossman, G.R., Wasserburg, G.J.** (1988): Mantle-derived fluids in diamond micro-inclusions. Nature 335, 784-789.

36. **Orlov, Yu. L.** (1977): The mineralogy of the diamond. New York, NY, Wiley, 235 p. (Translation of Mineralogiya almaza: Moscow, USSSR, Nauka press, 1973).
37. **Palyanov, Yu.N., Sokol, A.G. & Sobolev, N.V.** (2005): Experimental modeling of mantle diamond-forming processes. Russ. Geol. Geophys., 46, 1271–1284.
38. **Palyanov, Y.N., Shatsky, V.S., Sobolev, N.V., Sokol, A.G.** (2007): The role of mantle ultrapotassic fluids in diamond formation. Proc. Natl. Acad. Sci. USA, 104 (22), 9122-9127.
39. **Prinz, M., Manson, O.V., Hlava, P.F. and Keil, K** (1975): Inclusions in diamonds: garnet lherzolite and eclogite assemblages. Phys. Chem. Earth, 9, 797-815.
40. **Safonov, O.G., Perchuk, L.L. and Litvin, Yu.A.** (2007): melting relations in the chloride-carbonate-silicate systems at high pressure and the model for formation of alkalic diamond-forming liquids in the upper mantle. Earth Planet. Sci. Lett., 253, 112-128.
41. **Schrauder, M. and Navon, O.** (1994): Hydrous and carbonatitic mantle fluids in fibrous diamonds from Jwaneng, Botswana. Geochim. Cosmochim. Acta 58, 761-771.
42. **Sharygin, V.V., Golovin, A.V., Pokhilenko, N.P., Sobolev, N.V.** (2003): Djerfisherite in unaltered kimberlites of Udachnaya-East pipe, Yakutia. Dokl. Earth Sciences, 390, 554-557.
43. **Shimizu, N., Sobolev, N.V., Yefimova, E.S.** (1997): Chemical heterogeneities of inclusion garnets and juvenile character of peridotitic diamonds from Siberia. Geologiya I Geofizika, 38, 337-352.
44. **Shirasaka, M., Takahashi, E., Nishihara, Yu., Matsukage, K., Kikegawa, T.** (2002): In situ observation on the reaction dolomite = aragonite + magnesite at 900-1300 K. Amer. Mineral., 87, 922-930.
45. **Sobolev, N.V.** (1977): Deep-seated inclusions in kimberlites and the problem of Upper mantle the composition. F.R.Boyd, ed. American Geophysical Union, Washington DC. Translation from Russian, Moscow, Nauka Press, 1974.
46. **Sobolev, N.V., Logvinova, A.M., Zedgenizov, D.A., Yefimova, E.S., Seryotkin, Y.V., Floss, K., Taylor, L.A.** (2004): Mineral inclusions in microdiamonds and macrodiamonds from Yakutian kimberlites: a comparative study. Lithos, 77, 225-242.
47. **Sobolev, N.V., Shatsky, V.S.** (1990): Diamond inclusions in garnets from metamorphic rocks: a new environment for diamond formation. Nature, 343, 742-746.
48. **Sobolev, N.V., Sobolev, V.N., Snyder, G.A., Yefimova, E.S., Taylor, L.A.** (1999): Significance of Eclogitic and Related Parageneses of Natural Diamonds. Intern. Geol. Rev., 41, 129-140.

49. **Sobolev, N.V., Yefimova, E.S., Channer, D.M.DeR., Anderson, P.F.N. and Barron, K.M.** (1998) Unusual Upper Mantle beneath Guaniamo Guyana Shield: Evidence from diamond inclusions. Geology, 26, 971-974.
50. **Sobolev, V.S.** (1960): Conditions of formation of diamond deposits. Geologiya I Geofizika, (1), 7-22.
51. **Stachel, T., Harris, J.W., Brey, G.. P.** (1998): Rare and unusual mineral inclusions in diamonds from Mwadui, Tanzania. Contributions to Mineralogy and Petrology, 132, 34-47.
52. **Sunagawa, I, Yasuda, T. & Fukushima, H.** (1998): Fingerprinting of two diamonds cut from the same rough. Gems and Gemology. Winter Issue, 270-280.
53. **Taylor, L.A., Keller, R.A., Snyder, G.A., Wang, W.Y., Carlson, W.D., Hauri, E.H., McCandless, T., Kim, K.R., Sobolev, N.V., Bezborodov, S.M.** (2000): Diamonds and their mineral inclusions and what they tell us: A detailed "pull-apart" of a diamondiferous eclogite. Intern. Geol. Rev., 42, 959-983.
54. **Taylor, L.A., Logvinova, A.M., Wirth, R., Sobolev, N.V., Seryotkin, Yu.V., Yefimova, E.S. and Floss, C.**(2007): Eskolaite associated with diamond from Udachnaya kimberlite pipe, Yakutia, Russia. Amer. Mineral. (in press).
55. **Taylor, W.R., Canil, D., Milledge, H.J.** (1996): Kinetics of Ib to IaA nitrogen aggregation in diamond. Geochim. Cosmochim. Acta, v. 60, 23, 4725-4733.
56. **Ulmer, P. and Trommsdorff, V.** (1999): Phase relations of hydrous mantle subducting to 300 km. In: Fei Y. et al. (eds). The Geochemical Soc. Spec. Publ., 6, 259-281.
57. **Tomlinson, E.L., Jones, A.P., Harris, J.W.** (2006): Co-existing fluid and silicate inclusions in mantle diamond. Earth Planet. Sci. Lett., v. 250, p. 581-595.
58. **Walmsley, J.C., Lang, A.R.** (1992a): Oriented biotite inclusions in diamond coat. Mineral. Mag., 56, 108-111.
59. **Walmsley, J.C., Lang, A. R.** (1992b): On sub-micrometer inclusions in diamond coat – crystallography and composition of ankerites and related rombohedral carbonates. Mineral. Mag., 56, 533-543.
60. **Wirth, R.** (2004) Focused Ion Beam (FIB): a novel technology for advanced application of micro- and nanoanalysis in geosciences and applied mineralogy. Eur. J. Mineral., 16, 863-876.
61. **Wyllie, P.J. and Ryabchikov, I.D.**(2000): Volatile components, magmas, and critical fluids in upwelling mantle. Journal of Petrology, 41, 1195-1206.
62. **Zedgenizov, D.A., Harte, B., Shatsky, V.S., Politov, G.M., Rylov, G.M., Sobolev, N.V.** (2006). Directional chemical variations in diamonds showing octahedral following cuboid

growth. Contrib. Mineral. Petrol, 151 (1), 45-57.

63. **Zedgenizov, D.A., Kagi, H., Shatsky, V.S., Sobolev, N.V.** (2004) Carbonatitic melts in cuboid diamonds from Udachnaya kimberlite pipe (Yakutia): evidence from vibrational spectroscopy. Mineral. Mag., 68, 61-73.

UDK 553.81

Volcanic rocks of the Nyurbinskaya pipe: a portrayal of regional upper mantle evolution from the Riphean to the Carboniferous time, and its geodynamic relationships

Sablukov S.M. [1] , Sablukova L.I. [1] , Stegnitsky Yu.B. [2] , Karpenko M.A. [3], Spivakov S.V. [4]

[1] *"RUSGEO" Limited, Moscow;*
[2] *YaNIGP TsNIGRI, ALROSA Co. Ltd., Mirny;*
[3] *Nyurbinskaya Mine, ALROSA Co. Ltd., Mirny;*
[4] *Mirninskaya Expedition, ALROSA Co. Ltd., Mirny.*

ABSTRACT

Comprehensive examination of all the volcanic rock bodies incorporated in the Nyurbinskaya pipe (namely, pre-kimberlite mafic rocks, kimberlite rocks and post-kimberlite mafics) revealed that they differ drastically in intrusion time, type and model age of mantle source, and rock geochemistry. Nyurbinskaya pipe kimberlites are characterized by a significantly older age of intrusion (D_1em, 399.6∀4.6 Ma) and an older age of mantle source (T_{Nd}(DM) = 1100 Ma, εNd = +1.0, εSr = +25.2) as compared to older diamondiferous kimberlite rocks of the Yakutian province. According to K-Ar and Rb-Sr data, the pre-kimberlite dolerite of this pipe would be Late Riphean (703 Ma), whereas its post-kimberlite dolerite could be dated at the Early Carboniferous (328 Ma). For the pre-kimberlite dolerite, the role of melt source was played by some old enriched lithospheric mantle, probably with certain participation of some old lower crust matter (EM II, εNd = -12.2, εSr = +54.6; T_{Nd}(DM) = 2450 Ma). The post-kimberlite dolerite likely had its melt source in depleted mantle, probably with certain participation of some young upper crust matter (εNd = +4.7, εSr = +43.7; T_{Nd}(DM) = 770 Ma). The most prominent geochemical distinction between the petrologically similar Nyurbinskaya pipe dolerite rocks with differing age consists in that the post-kimberlite ("young") dolerite is characterized by significantly higher Fe, Ti, Nb, Ta, V, Mn, P, Y, Zr, Hf, REE, Th and U, contents and lower Al, Mg, Ni and Cr contents as compared to the pre-kimberlite ("old") dolerite. Geochemically, pre-kimberlite dolerite of this pipe is close to highly aluminous calc-alkali basalt common to volcanic arc in active continental margins and mature island arcs in subduction zones, while the post-kimberlite dolerite rocks are similar to sharply geochemically enriched high-Fe within-plate tholeiitic basalt. The set of volcanic rocks with differing age incorporated in the Nyurbinskaya pipe obviously portray the temporal evolution of the mantle sources of mafic and ultramafic magmatic melts from the Late Riphean to the Early Carboniferous time. The new compositional data Late Riphean basalt rocks with certain indicative isotopic-geochemical features related to a characteristic geodynamic situation could gain the definiteness in paleogeodynamic reconstruction of the formation and break-up of the Rodinia supercontinent (dated at the Neoproterozoic) and temporal evolution of the Siberian craton as one of its former constituents.

ITRODUCTION

Diamondiferous kimberlite rocks of the Nakyn field (discovered in 1994) stand apart from diamondiferous kimberlites occurring in other districts of Yakutia not only spatially but also in the majority of compositional characteristics. In particular, they are characterized by a predominance of pyrope and chrome spinel among their high-pressure minerals (along with almost complete absence of picroilmenite), an essentially phlogopite kimberlite rock matrix, and a peculiarly low concentration of all incompatible elements except K, Rb and P [3,6,8,12,13,26,32]. Another peculiar feature of the Nakyn field is that it abounds with diversified basaltic rock occurrences (dykes, stocks, chonoliths, etc.) [11,13,29,31]. The geological structure, age and various compositional characteristics of kimberlite and basaltic rocks occurring in the Nakyn field have already become a subject of quite voluminous literature (more than 30 articles and sections in monographs, however, some issues are still inadequately studied and/or disputable. Among the presently known Nakyn field kimberlite occurrences (the Botuobinskaya and Nyurbinskaya pipes, and Markhinskoye and Mayskoye rock bodies), the Nyurbinskaya pipe (under development since 2002) has received the most study. In addition to jointly present kimberlite rocks related to different intrusion phases, this pipe incorporates a comparatively old (prior to pipe intrusion, or "pre-pipe") dolerite intrusion (with its xenoliths occurring in kimberlite rocks of the same pipe) and a relatively young ("post-pipe") dolerite intrusion penetrating the pipe kimberlite rocks [11,29,31]. Undoubtedly, the compositional peculiarities of all these igneous rock bodies incorporated in the Nyurbinskaya pipe are worthy of detailed examination as this could help reveal the cause of the obvious peculiarity of Nakyn field kimberlite rocks and gain insight into the temporal evolution of the regional geodynamic situation and compositional characteristics of the regional upper mantle.

TARGETS OF STUDY AND ANALYTICAL METHODS

The program of comprehensive examination of the Nyurbinskaya pipe (August 2006 to June 2008) included geological description of drill core samples (32 core holes, about 3000 meters core samples), quarry and ore yard studies. We examined the geological structure of the pipe, the mineralogical, petrological and isotopic-geochemical characteristics of its kimberlite and basaltic rocks, the composition of the essential rock-forming and high-pressure minerals, and the petrological and mineralogical peculiarities of mantle rock xenoliths.

In all, 173 thin rock sections were studied, and six mineralogical analyses were carried out. The full silicate analysis (46 "wet chemistry" tests) was performed in the Analytical Centre of GIN RAS. The ICP-MS analysis (46 tests) was performed in the Laboratory of FSUE IMGRE MNR RF using an Elan-6100 DRC (Perkin Elmer) analyzer. The X-ray spectral microanalysis of minerals (912

analyses) was conducted in the Laboratory of GINTSVETMET using a Camebax Microbeam microanalyzer (U=20 kV, I=15-20 nA). Examination of mineral surface features (26 tests) was performed in the Laboratory of IGEM RAS using a S-2300 HITACHI scanning electron microscope (magn. up to x 5000). The X-ray phase analysis of rock samples (7 tests) was conducted in the Laboratory of FSUE VIMS MNR RF using a "X'Pert PRO" X-ray diffractometer (Phillips, Netherlands). K-Ar isotope characteristics of rock and mineral samples (10 tests) were examined in the Laboratory of Isotope Geochemistry and Geochronology, IGEM RAS. Sm-Nd and Rb-Sr isotopic dating of rock and mineral samples (Rb-Sr – 20 tests, Sm-Nd – 12 tests) was performed using a Finnigan MAT-261 mass spectrometer in the Laboratory of IGGD RAS, St. Petersburg.

GEOLOGICAL AND PETROLOGICAL PECULIARITIES OF NYURBINSKAYA PIPE KIMBERLITE ROCKS

The Nyurbinskaya kimberlite pipe is a complex volcanic structure formed as a result of multi-stage local volcanic activity. In addition to several igneous rock bodies related to different kimberlite intrusion phases, this structure incorporates a comparatively "old" intrusion of "pre-pipe" dolerite (with its rock xenoliths occurring in kimberlite of the same pipe), and a relatively "young", "post-pipe" dolerite intrusion penetrating the pipe kimberlite rocks [13,26,29,32].

The sharp, "cutting" shape of contact between the rock bodies related to the three main stages of volcanic activity (old mafics, kimberlite and young mafics) is evidence for a significant difference in their intrusion age (each preceding phase has had time to lithify and cool down before the next intrusion started). Along with this, separate intrusion phases within a common stage of volcanic activity either had a large time lag between each other (probably reflected in sharp, cutting contact appearance) or intruded nearly synchronously, such that two hot, unconsolidated (non-lithified) rock bodies contacted. Evidence for non-synchronous intrusion of rock bodies related to the three main stages of volcanic activity (intrusion phases) can be found primarily in the sharp, cutting appearance of contact between them (which means different ***relative age*** of these bodies) and in data on ***absolute age*** of these rock bodies.

According to data from a lot of studies [13,26], the Nyurbinskaya pipe has a two-phase internal structure. The early, intrusive phase is represented by porphyritic kimberlite occurring as a thin, NNE-oriented dyke traced at the NE and SW margins of the pipe, and also as small fragments and large xenolithic blocks (up to 10-20 m) in rocks related to the second intrusion phase. The second (and terminating), volcanic phase makes up the bulk of the type body, being represented by autolithic kimberlite breccia. The internal structure of the pipe is complicated by a dolerite intrusion (revealed by drilling at a depth of more than 300 m). Pipe kimberlites have a coarse porphyritic (magnophyric) texture, where olivine-1

macrocrystals, olivine-2 and (more rarely) phlogopite-2 phenocrysts are cemented in a carbonate-phlogopite matrix with rarely disseminated chrome spinel grains. The examinated kimberlite obviously underwent some intense post-magmatic (occasionally hypergenetic) transformation, which resulted in significant (occasionally complete) replacement by secondary minerals (up to 60-100%).

Our studies revealed that the Nyurbinskaya pipe is comprised of different structural and genetic rock varieties, all of them being derivates of magnophyric phlogopite kimberlite. Five subvertical internally homogeneous bodies (intrusion phases) can be distinguished in the pipe being studied, with varying degree of uncertainty, such that only phases ## 1 and 4 partially correspond to certain rock varieties described in literature (figure 1).

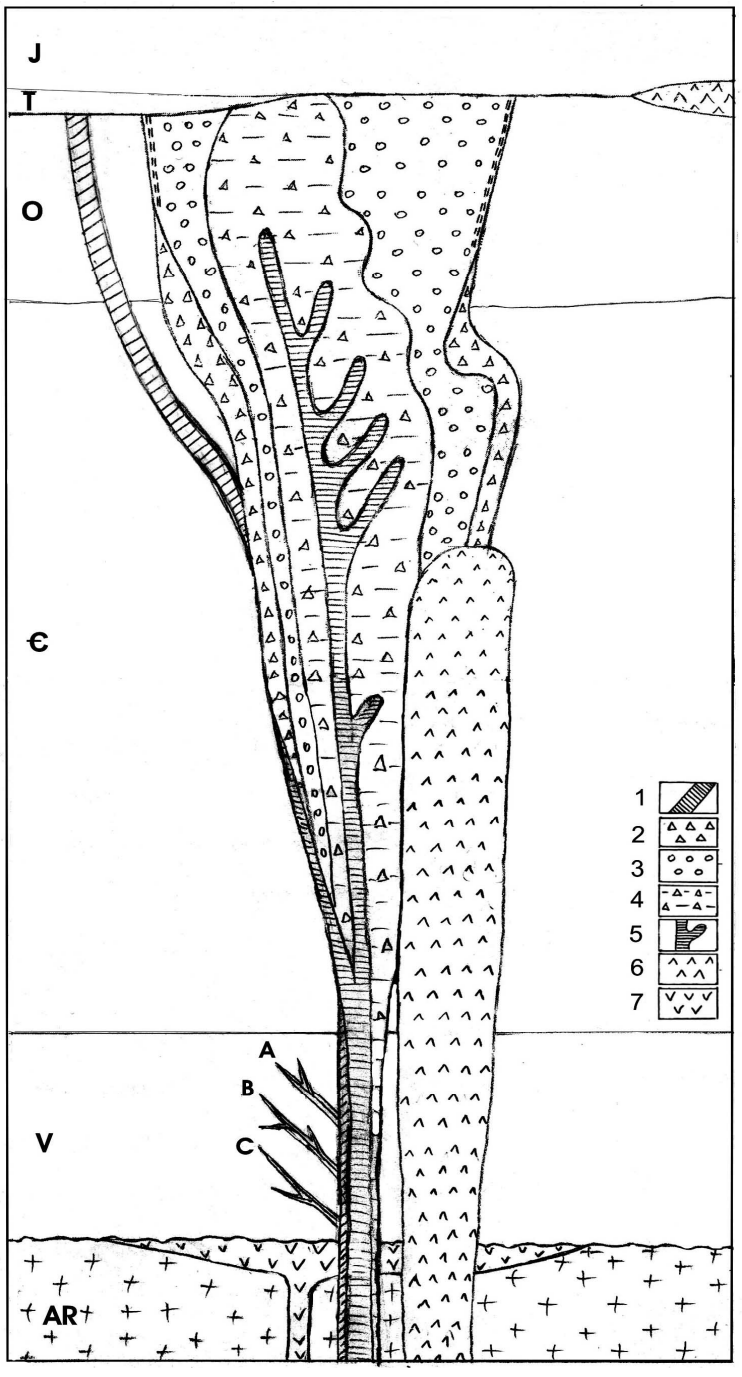

Fig. 1. **Model of structure of the Nyurbinskaya pipe (section).**
1 - Phase 1, "pre-ore" dyke of magnophyric kimberlite; 2 - Phase 2, kimberlite eruptive breccia; 3 - Phase 3, kimberlite tuffisite and xenotuffisite; 4 - Phase 4, kimberlite xenoclastic lava; 5 - Phase 5, magnophyric kimberlite; 6 – post-kimberlite basalts; 7 – pre-kimberlite basalts.

Phase 1: a thin (0.1-0.5 m) "pre-ore" dyke of strongly altered magnophyric kimberlite (or porphyritic kimberlite, after [17]).

Phase 2: intensely altered kimberlite eruptive breccia (xenotuff kimberlite breccia, after [17]) occurring as fragments of some rock body that was formed by the explosive phase of volcanic material intrusion, which "cleaned" the pipe-shaped channel from sedimentary rocks, having provided a relatively quiescent intrusion mode for subsequent volcanic activity phases.

Phase 3: moderately altered kimberlite tuffisite and

xenotuffisite (kimberlite tuff breccia, after [17]).

Phase 4: moderately altered kimberlite xenoclastic lava (autolithic eruptive kimberlite breccia, after [17]).

Phase 5: moderately altered magnophyric kimberlite lava and xenolava (or porphyritic kimberlite, after [17]). It is likely that large intervals of porphyritic kimberlite (up to 40 m thick as is visible) are comprised mostly of rock bodies related to certain separate intrusion phases rather than of penetrated rock xenoliths (as is stated in [13,26]). This suggestion is supported by the fact that the examined contact between the porphyritic kimberlite dyke (about 7 m thick) and tuffisite has a *"welded"* appearance, without any clear borderline, such that structural elements of rock remain unbroken on each side of the contact, even on the micrometric scale. The appearance of this contact suggests some simultaneous or nearly synchronous intrusion of two yet hot, not completely lithified ("loose") bodies, or some nearly synchronous injection of two portions of the same melt with inequal gas content.

It is not improbable that the rocks related to intrusion phases 3 and 4 (and, may be also to phase 5) may represent different facies of a common geological body with inequal gas content, or asynchronous portions of a common phase of magmatic material intrusion.

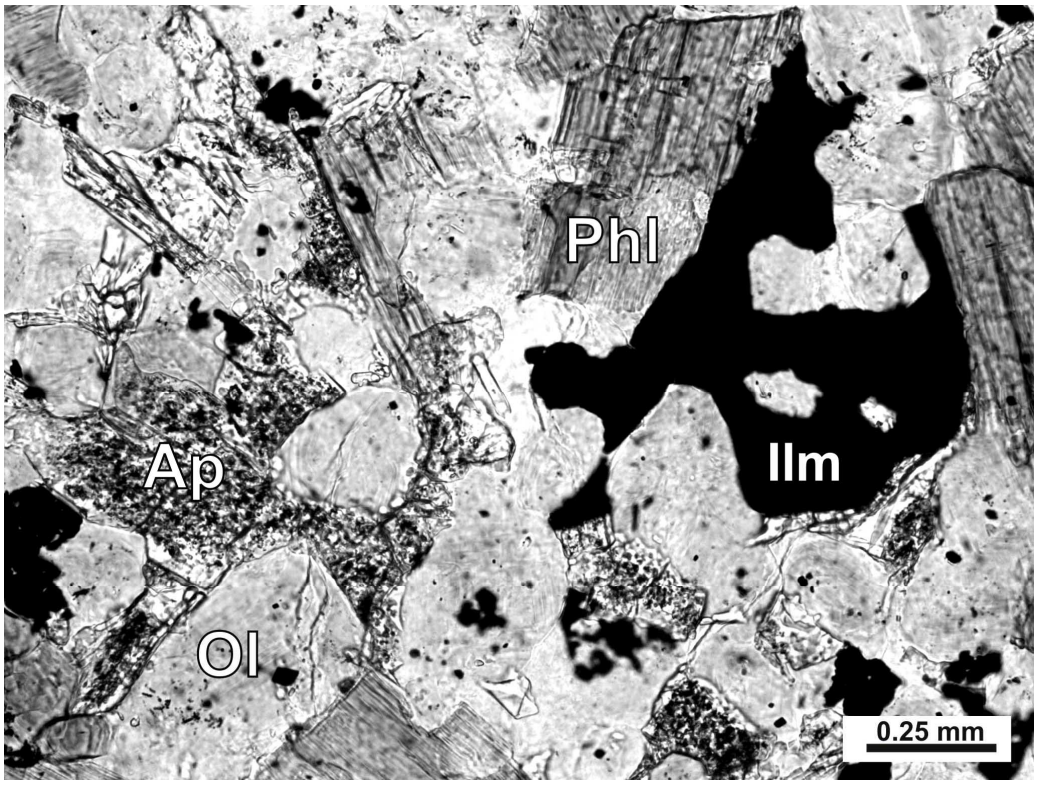

Fig. 2. **Phase B, xenolith of the apatite-ilmenite-olivine-phlogopite rocks (sample N-355): think section.** Polarized light. Ol – serpentinized olivine, Phl – phlogopite, Ap – apatite, Ilm – picroilmenite.

In addition to the above described "actual" rock bodies, which can be studied by drilling, also worthy of consideration are the "hypothetical" geological bodies of early kimberlitic or protokimberlitic rocks, which, although only show up as thin dykes, xenoliths and autoliths, still may bear important information on compositional and formation peculiarities of Nyurbinskaya pipe kimberlites. These "hypothetical" bodies (phases) are characterized by a completely crystalline (although microcrystalline) structure of rock matrix and "extreme" geochemical characteristics. In this study, we denoted them A, B and C (in contrast to "actual" rock bodies incorporated in the Nyurbinskaya pipe).

Phase A: a fluidal, aphyric (sporadophyric), microcrystalline ***apatite-olivine-carbonate-phlogopite kimberlite*** with some carbonatite elements. The structure of the rock is fluidal, with subparallel arrangement of carbonate, phlogopite and apatite laths.

Phase B : an aphyric (sporadophyric), microcrystalline ***apatite-picroilmenite-olivine-phlogopite kimberlite*** with some evidence of Fe-Ti-P metasomatism. The rock has a hypidiomorphic granular texture (with xenomorphic apatite and picroilmenite segregations filling the interstitial voids between idiomorphic olivine and phlogopite grains, see figure 2) and a foliated structure (owing to subparallel arrangement of phlogopite laths).

Phase C: a magnophyric *lamprophyre-type* ***olivine-phlogopite kimberlite*** with some evidence of K-metasomatism. The rock has a homogeneous, massive structure, with rare elements of banded structure (alternating porphyritic and almost monomineralic, microcrystalline phlogopite zones), and some inclusions showing a concentric zoned structure with magnophyric central zones and nearly aphyric margins (probably, analogues to "central-type autoliths" in kimberlite).

In addition, there appears to be evidence of another formation phase in the Nyurbinskaya pipe. This ***Phase # 6*** could be preliminarily (until better studied) identified as ***epiclastic rocks of crateral facies***. Truncation of the Nyurbinskaya pipe is approximately 480 m [9], this is why the crateral facies of the pipe could not survive ***in situ***. Nevertheless, the drill hole # 9/420 dissected at a depth of about 450 m a rock block, at least 8 m thick, with structural and textural features typical of crateral facies rocks. This block is composed of parallel layered volcanoclastic and volcanosedimentary rocks, very well sorted, with grainsize decreasing up the section as follows: tuff conglomerate – tuff gravelite – tuffstone, and the top of the section is represented by finely clastic limestone with trace amounts of tufogenic admixture. In other words, this rock block is characterized by ***a gradational lamination***, which is an indicative feature of crateral facies. About 20 m above this block and 20 m below it, zones of unsorted debris-clumpy host rock breccia with some admixture of kimberlitic material occur, which also may be related to crateral facies (colluvial formations); true, this relationship is not so obvious. Probably, the preserved block of crateral facies rocks traveled down the vent along a system of faults in the course of structural-tectonic transformation

of the pipe, which could be caused by invasion of a young post-kimberlitic mafic stock intrusion.

Geochemical peculiarities of different kimberlite

VARIETIES

Major and minor element contents of the examined kimberlite rocks are given in Tables 1 and 2. In general, chemical peculiarities of different kimberlite varieties are in line with their petrological characteristics and some variation in rock geochemistry for petrologically similar rocks are primarily due to inequal degree of secondary carbonatization and varying extent of phlogopite chloritization.

Table 1.

Chemical composition of the Nyurbinskaya pipe volcanic rocks (wt. %)

No	1	2	3	4	5	6	7	8	9	10	11	12	13
n	2	2	2	5	8	6	1	1	1	6	8	1	1
SiO_2	24,93	36,35	28,02	30,53	32,13	34,74	19,08	34,58	38,72	48,03	46,21	43,84	44,21
TiO_2	0,75	0,83	0,46	0,39	0,41	0,61	0,76	3,23	1,18	0,84	4,44	4,15	4,20
Al_2O_3	2,33	3,12	2,94	2,64	3,00	4,21	2,50	4,72	7,30	17,76	11,64	11,46	12,15
Fe_2O_3	3,02	4,06	5,69	4,38	5,62	5,80	4,57	4,89	3,68	2,38	3,97	1,90	5,34
FeO	2,14	2,19	0,77	2,49	1,97	2,01	1,97	4,60	3,59	4,65	12,39	9,25	6,83
MnO	0,10	0,07	0,08	0,09	0,09	0,10	0,05	0,16	0,06	0,05	0,19	0,15	0,05
MgO	5,77	21,52	17,80	26,80	28,32	26,37	17,95	28,30	26,03	8,56	5,88	9,23	10,12
CaO	31,49	11,55	16,94	10,09	8,10	6,37	25,17	4,59	3,92	5,17	7,59	13,00	2,84
Na_2O	0,09	0,24	0,37	0,16	0,16	0,29	0,12	0,17	0,22	1,55	1,79	0,99	0,88
K_2O	0,11	2,65	1,41	0,86	0,77	2,10	1,11	2,01	4,43	2,89	2,41	0,65	4,94
P_2O_5	1,12	0,98	0,41	0,42	0,46	0,62	1,78	1,70	0,23	0,12	0,74	0,73	0,58
L.O.I.	27,78	15,80	24,52	20,53	18,43	16,19	24,34	10,51	9,90	7,48	2,30	3,84	6,94
Total	99,61	99,35	99,39	99,38	99,46	99,40	99,40	99,46	99,26	99,46	99,54	99,19	99,08
$H2O^-$	0,73	2,30	3,89	3,03	2,27	2,84	0,72	2,01	2,01	4,38	0,77	1,44	1,83
$H2O^+$	2,58	2,36	2,84	7,58	9,38	7,36	4,64	7,08	4,62	2,56	1,16	2,41	3,85
CO_2	24,43	10,79	17,50	9,80	6,71	5,74	18,58	1,37	3,42	<0,2	<0,2	<0,2	0,90
Stot.	0,07	0,11	0,35	0,12	0,08	0,09	<0,1	<0,1	0,11	<0,1	<0,1	<0,1	0,92

Note: n – number of analysis; No: 1- Phase 1, “pre-ore” dyke magnophyric kimberlite; 2 - Phase 2, autolithe; 3 - Phase 2, kimberlite eruptive breccia; 4 - Phase 3, kimberlite tuffisite; 5 - Phase 4, kimberlite xenoclastic lava; 6 - Phase 5, magnophyric kimberlite; 7 - Phase A, microcrystalline apatite-olivine-carbonate-phlogopite kimberlite (sample 16/138-513); 8 - Phase B, microcrystalline apatite-picroilmenite-olivine-phlogopite kimberlite (sample N-355); 9 - Phase C, magnophyric lamprophyre-type olivine-phlogopite kimberlite (sample N-384); 10 - pre-kimberlite basalts (dolerite xenoliths); 11 - post-kimberlite basalts (dolerite); 12 - post-kimberlite basalts (glass); 13 - near pipe basalt (sample 4/660-65).

Table 2.

Minor element composition of the Nyurbinskaya pipe volcanic rocks (ppm)

No	1	2	3	4	5	6	7	8	9	10	11	12	13
n	2	2	2	5	8	6	1	1	1	6	8	1	1
Be	3,37	3,00	2,56	2,48	2,69	3,60	6,32	1,98	1,76	1,20	2,15	4,10	1,30
Sc	13,92	13,0	7,49	7,69	8,07	11,82	20,2	35,27	18,80	41,2	34,4	33,5	24,3
V	79	102	67	61	61	65	194	92	44	241	381	320	317
Cr	1248	1876	549	660	699	1143	1234	1010	2008	398	26	21	52
Mn	411	564	566	615	516	570	359	730	389	234	1280	734	262
Co	65,2	74,1	36,8	51,5	51,5	60,3	24,1	55,4	124,2	38,8	40,1	34,4	55,7
Ni	590	985	643	969	850	901	499	865	1277	280	53	104	76
Cu	36,0	65,9	24,2	15,9	9,7	8,8	5,5	14,8	33,7	69,7	264,0	130,2	118,9
Zn	2246	41	32	36	31	39	19	74	45	33	126	125	107
Ga	10,8	8,0	6,1	5,2	4,9	6,4	4,5	11,5	13,3	14,4	25,4	22,8	21,1
Rb	4,2	93,1	45,3	26,1	20,2	50,3	34,0	65,8	148,6	29,0	43,4	11,3	36,9
Sr	184	381	299	343	415	502	207	242	82	543	767	624	419
Y	11,5	10,2	9,9	8,0	7,5	7,0	22,0	9,0	2,4	8,7	56,9	57,2	19,3
Zr	85,3	106,9	80,4	60,1	59,6	63,0	215,7	149,2	32,0	76,3	465,1	456,6	266,6
Nb	31,8	51,1	20,8	20,9	20,2	24,0	90,3	39,1	7,6	4,9	51,6	53,9	34,8
Mo	0,69	1,33	2,25	1,02	1,54	1,14	0,69	1,16	0,77	2,79	3,01	1,23	1,98
Cd	0,16	0,19	0,14	0,18	0,20	0,28	0,15	0,18	0,06	0,13	0,41	0,33	0,21
Cs	0,37	0,71	1,22	0,54	0,37	0,66	0,47	1,66	1,03	0,43	0,59	0,42	0,15
Ba	77	714	377	301	272	554	141	292	736	705	359	262	673
La	14,0	13,9	13,0	9,8	8,54	12,0	34,5	21,9	6,1	9,5	45,7	54,6	29,7
Ce	28,7	31,2	27,0	21,4	19,0	25,4	89,0	43,2	11,2	17,8	102,0	118,0	66,9
Pr	4,0	4,3	3,5	2,9	2,7	3,6	12,9	6,2	1,5	2,2	14,3	16,0	9,4
Nd	17,9	18,9	14,8	12,8	11,9	15,3	53,9	27,3	5,8	8,6	61,5	66,8	39,7
Sm	3,98	3,90	3,01	2,70	2,65	3,08	10,65	5,89	1,13	1,69	14,04	14,80	7,94
Eu	1,07	1,21	0,71	0,78	0,77	0,88	2,77	1,51	0,31	0,66	3,76	5,05	2,40
Gd	3,61	3,18	2,58	2,27	2,33	2,53	8,19	4,75	0,91	1,70	13,75	14,13	6,26
Tb	0,47	0,40	0,34	0,31	0,32	0,33	1,03	0,56	0,12	0,27	2,13	2,14	0,88
Dy	2,35	1,94	1,83	1,60	1,63	1,64	5,26	2,62	0,60	1,67	12,46	12,37	4,73
Ho	0,41	0,33	0,34	0,29	0,30	0,29	0,90	0,42	0,10	0,35	2,41	2,39	0,86
Er	0,95	0,76	0,90	0,72	0,73	0,69	2,06	0,87	0,25	0,96	6,29	6,19	2,14
Tm	0,12	0,10	0,13	0,10	0,10	0,09	0,26	0,10	0,04	0,14	0,86	0,83	0,29
Yb	0,67	0,51	0,78	0,57	0,57	0,51	1,45	0,56	0,24	0,88	5,17	5,02	1,71
Lu	0,09	0,07	0,11	0,08	0,08	0,07	0,20	0,07	0,04	0,13	0,73	0,71	0,24
Hf	1,91	1,97	1,73	1,29	1,39	1,54	4,16	5,79	1,09	1,99	11,27	10,85	6,58
Ta	1,76	1,98	0,77	0,84	0,93	1,38	3,09	6,33	0,81	0,31	3,66	3,58	2,52
W	1,00	3,29	3,74	0,80	10,13	5,64	-	-	-	-	-	-	-
Pb	4,55	2,59	2,05	1,85	1,90	2,28	1,61	6,53	5,79	7,39	2,18	1,87	4,57
Th	1,23	1,07	1,93	1,22	1,09	1,10	7,01	1,40	0,32	1,61	5,11	5,37	4,08
U	1,85	0,54	1,00	0,49	0,44	0,33	1,55	0,47	0,86	0,30	1,47	1,98	1,06

Note: see table 1

The very strongly altered (carbonatized, chloritized and silicified) or contaminated (with limestone and siltstone xenoliths) kimberlite rocks (respectively, magnophyric "pre-ore" dyke kimberlite related to ***Phase 1*** and eruptive kimberlite breccia related to ***Phase 2***) reflect the initial kimberlite composition only very approximately, just with respect to some of the least mobile elements. In general, "pre-ore" dyke rocks are similar in distribution of the main elements of low mobility to porphyritic kimberlite related to ***Phase 5***, but their higher than average P_2O_5 content (0.8-1.44 wt. %) makes them closer to lamprophyre-type porphyritic kimberlite rocks related to the "early kimberlitic" stage, denoted here as ***Phases A*** and ***B***. The distribution of major and minor elements in ***Phase 2*** rocks agrees well with the "hybrid" nature of eruptive breccia abounding with xenogenic carbonate material and fragments of porphyritic kimberlite related to early intrusion phases.

The initial kimberlite composition in most adequately reflected in moderately altered kimberlite tuffisite (***Phase 3***), kimberlite xenoclastic lava (***Phase 4***) and magnophyric kimberlite lava and xenolava (***Phase 5***). The rocks related to ***Phases 3*** and ***4*** are characterized by a very high Mg index (24.6-31. wt. 5% MgO, with magnesian index Kmg = 84.0-90.1), medium K_2O (0.4-1.29 wt. %), Al_2O_3 (1.85-4.2 wt. %), $FeO_{tot.}$ (5.88-8.87 wt. %) contents, and a lower than average TiO_2 content (0.36-0.46 wt. %). ***Phase 5*** rocks differ from ***Phase 3*** and ***Phase 4*** tuffisite and xenoclastic lava (which are similar to them in Mg index) by their higher TiO_2 (0.49-0.69 wt. %), K_2O (1.18-2.54 wt. %), P_2O_5 (0.51-0.85 wt. %), and Cr (1060-1400 ppm) contents. In rocks with very high proportion of phlogopite, Al_2O_3 content ranges up to 6.62 wt. %.

The examined kimberlite rocks are characterized by heterogeneously distributed but generally low to medium (for kimberlite series rocks) incompatible element contents. The concentration of *large-ion lithophilic elements* (LILE) in these rocks is moderate, close to average for kimberlitic series rocks, in particular, their K_2O (0.5-2.54 wt. %), Rb (14.8-96.0 ppm, Cs (0.23-1.32 ppm); Sr (162-768 ppm (up 944 ppm)) and Ba (199-730 ppm). Along with this, the rocks are characterized by very low HFSE: Zr (46-73 ppm, up to 117 ppm), Hf (0.98-1.78 ppm), Nb (17.9-55.0 ppm), Ta (0.81-2.04 ppm), TiO_2 (0.36-0.69 wt. %, up to 0.88 wt. %), Th (0.92-2.23 ppm), U (0.36-2.16 ppm), ΣREE (45-80 ppm, up to 90 ppm). Tuffisite and xenoclastic lavas related to intrusion ***Phases 3*** and ***4*** are nearly identical in incompatible element distribution. Rocks with lava appearance (porphyritic kimberlite rocks related to different intrusion phases) differ from volcanoclastic rocks (tuffisite, xenoclastic lava) by having higher concentrations of almost all incompatible elements.

In general, our geochemical data obtained for the main kimberlite rock varieties in the Nyurbinskaya pipe are close to previously published data [8,13,26,32]. Along with this, it is important to emphasize that inclusions of kimberlite rocks related to the early kimberlite formation stage stand apart from the

rest of Nyurbinskaya pipe kimberlite rocks by their "extreme" (extremely high and low) concentrations of the essential elements, primarily of the incompatible ones.

The aphyric microcrystalline ***Phase A apatite-olivine-carbonate-phlogopite kimberlite*** (sample 16/138-513) differs from typical pipe kimberlite rocks by its higher than average CaO, CO_2 , K_2O (1.11 wt. %) contents and, what is most important, has the highest (among the Nyurbinskaya pipe kimberlites), P_2O_5 (1,78 wt. %), V (194 ppm), Be (6,32 ppm), Y (22 ppm), Zr (215 ppm), Hf (4.16 ppm), ΣREE (223 ppm) and Th (7 ppm) contents, and the second highest Nb (90.2 ppm) and Ta (3.09 ppm) contents, with a rather high Nb/Ta ratio (29.2). This distribution of minor elements, along with the essentially carbonate rock composition, may point to the relationship of this rock to some carbonatite process or KREEP-type metasomatism.

The aphyric microcrystalline ***Phase B apatite-picroilmenite-olivine-phlogopite kimberlite*** (sample N-355), having a very high MgO content (28.3 wt. %), is characterized by also high K_2O (2.01 wt. %), Al_2O_3 (4.72 wt. %) and P_2O_5 (1.70 wt. %) contents and, what is most important, very high TiO_2 (3.23 wt. %), Sc

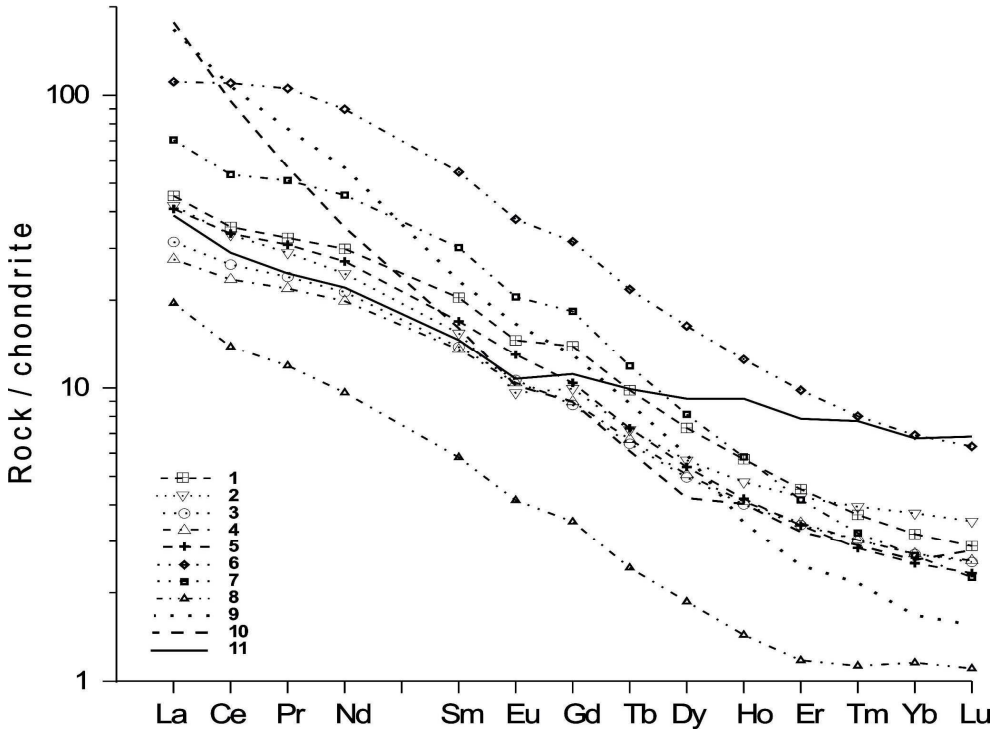

Fig. 3**. Chondrite normalized [4] REE distribution patterns for kimberlite rocks of the Nyurbinskaya pipe**

1 - Phase 1, "pre-ore" dyke of magnophyric kimberlite; 2 - Phase 2, kimberlite eruptive breccia; 3 - Phase 3, kimberlite tuffisite and xenotuffisite; 4 - Phase 4, kimberlite xenoclastic lava; 5 - Phase 5, magnophyric kimberlite; 6 – Phase A, microcrystalline apatite-olivine-carbonate-phlogopite kimberlite; 7 – Phase B, microcrystalline apatite-picroilmenite-olivine-phlogopite kimberlite; 8 - Phase C, magnophyric lamprophyre-type olivine-phlogopite kimberlite; 9 – Fe-Ti series kimberlite (group 1); 10- Al-series kimberlite (group 2); 11 – Al-series olivine melilitite of the Arkhangelsk province.

(35.2 ppm) and Ta (6.33 ppm) contents, which is characteristic of Fe-Ti series kimberlites [20] or Group 1 kimberlites [24], along with a very low Nb/Ta ratio

(6.2). These geochemical features might point to the relationship of this rock to the proto-kimberlitic melt [18] and be evidence of Fe-Ti-P metasomatism.

The magnophyric ***Phase C olivine-phlogopite lamprophyre-type kimberlite*** (sample N-384), having a very high MgO content (26.03 wt. %) and a higher than average TiO_2 content (1.18 wt. %), is characterized by the highest (among the analyzed rocks) concentrations of Ni (1277 ppm), Co (124 ppm), Cr (2008 ppm), Al_2O_3 (7.30 wt. %), K_2O (4.43 wt. %) and Rb (148 ppm). Along with this, this Phase C rock has the lowest (among the examined rocks) P_2O_5 (0.23 wt. %), Sr (82 ppm), Y (2.4 ppm), Zr (32 ppm), Hf (1.1 ppm), Nb (7.6 ppm), Th (0.32 ppm), and ΣREE (28 ppm) contents, with a very low Nb/Ta ratio (9.3). These geochemical features agree well with the essentially phlogopite composition of this rock, which probably formed under the action of Rb-K mantle metasomatism.

Of particular interest is the REE distribution in different kimberlite varieties, with generally low REE content of all these kimberlite rocks (ΣREE = 45.0-81.4 ppm; up to 90.1 ppm). The appearance of lanthanide distribution curves (normalized to chondrite) is quite peculiar but nearly the same for all the examined kimberlite rocks (with certain difference just is absolute REE content values), which is evidence for their consanguinity (figure 3). These curves have a “flexure bend”, with a gentle positive slope in heavy and light lanthanide ranges (with $(La/Yb)_N$ = 9 – 20) and a somewhat steeper positive slope in the medium lanthanide range. Whereas in the heavy lanthanide range distribution curves of the examined rocks are similar to that of *Al-series* Zimni Bereg kimberlites, in the light lanthanide range the distribution curves of the Nyurbinskaya pipe rocks fit to the distribution curve of extremely geochemically depleted Al-series olivine melilitite. (Note that distributions of some other elements, in particular, Ta and Sc, in the examined pipe rocks are also somewhat “intermediate” between those typical of diamondiferous kimberlite and olivine melilitite of Al-series). Maximum lanthanide content is found in microcrystalline ***Phase A apatite-olivine-carbonate-phlogopite kimberlite*** (with some carbonatite features), while minimum lanthanide concentrations are characteristic of the magnophyric ***Phase C olivine-phlogopite lamprophyre-type kimberlite*** (almost purely alkaline, Rb-K mantle metasomatism product).

In general, it can be said (taking into account the possibility of redistribution of different elements in various metasomatic and hypergenetic processes) that the examined rocks of the Nyurbinskaya pipe are similar in geochemistry to South African Group 2 kimberlites and Al-series kimberlites of the Arkhangelsk diamond province, primarily, to crystalloclastic tuffisite in kimberlite pipes of the Zolotitsky cluster (which has been also mentioned in previous studies [8,12]); moreover, they are even closer to extremely geochemically depleted Al-series olivine melilitite [20], being characterized by very low TiO_2, Ta, Sc, Th, U, and LREE contents. Along with this, inclusions of rocks related to the early kimberlite formation stage stand apart from the rest of Nyurbinskaya pipe kimberlite rocks by their extremely high and low concentrations of many elements, which highlights the prominent

role of alkaline (Rb-K), Fe-Ti-P and KREEP metasomatism and carbonatite process elements in pipe formation. The ***Phase B apatite-picroilmenite-olivine-phlogopite kimberlite*** is similar in composition to differentiated Fe-Ti-series Zimni Bereg kimberlite rocks [20] and/or Group 1 kimberlites [24].

Geological and petrological peculiarities of old (PRE-KIMBERLITE) MAFIC ROCKS

In order to examine the characteristic compositional features of reliably pre- and post-kimberlite mafic rocks, it was necessary to sample igneous mafic rock bodies showing direct (explicit) geological evidence of their intrusion time with respect to Nyurbinskaya pipe kimberlite rocks, i.e., those mafic rock bodies for which the nature of their contact with kimberlite can be identified unambiguously.

Having analyzed drill core samples from 32 drill holes, in no case did we encounter any evidence of pre-pipe rocks like those described in [11,29,31]. Along with this, many researchers report the presence of "moderately alkaline dolerite" xenoliths [11] or "angular trap fragments" [29] in Nyurbinskaya pipe kimberlite rocks, naturally recognizing the pre-kimberlite age of these dolerite rocks.

Table 3.

Chemical composition of the pre-kimberlite and post-kimberlite basalt minerals (wt. %)

No	Mine-rale	SiO_2	TiO_2	Al_2O_3	Cr_2O_3	FeO	MnO	MgO	CaO	Na_2O	K_2O	BaO	SrO	Total
1	ilm	-	50,55	0,00	0,05	47,56	1,09	0,14	-	-	-	-	-	99,39
2		-	49,12	0,39	0,07	48,96	0,75	0,27	-	-	-	-	-	99,56
3		-	50,02	0,08	0,02	48,20	0,48	0,25	-	-	-	-	-	99,05
6	plag	52,56	0,04	28,55	0,02	0,55	0,00	0,08	11,56	3,93	1,00	0,32	0,00	98,61
7		50,32	0,01	30,32	0,00	0,53	0,00	0,06	13,92	3,52	0,27	0,06	0,00	99,01
8		53,93	0,07	27,59	0,00	0,72	0,01	0,11	10,76	5,06	0,60	0,02	0,09	98,96
9	Ti-mgt	-	12,65	1,69	0,09	79,33	0,21	0,12	-	-	-	-	-	94,09
10		-	14,21	0,36	0,10	79,89	0,30	0,13	-	-	-	-	-	94,99
11		-	16,51	1,77	0,10	76,80	0,33	0,19	-	-	-	-	-	95,70
12	cpx	49,24	1,37	2,31	0,09	11,33	0,31	14,09	18,66	0,23	0,00	-	-	97,63
13		49,03	1,29	2,18	0,01	13,74	0,32	13,99	16,79	0,26	0,02	-	-	97,63
14		49,11	0,99	1,80	0,00	14,10	0,39	13,11	18,15	0,33	0,00	-	-	97,98
15	ilm	-	50,90	0,12	0,03	46,74	0,61	0,82	-	-	-	-	-	99,22
16		-	50,45	0,03	0,03	47,50	0,58	0,55	-	-	-	-	-	99,14
17		-	50,17	0,05	0,03	48,09	0,57	0,46	-	-	-	-	-	99,37
18	plag	54,44	0,07	27,83	0,00	0,54	0,00	0,08	10,94	5,09	0,38	0,00	0,00	99,37
19		53,41	0,14	28,22	0,02	0,63	0,00	0,14	11,79	4,42	0,34	0,00	0,05	99,16
20		53,73	0,10	27,94	0,00	0,75	0,05	0,10	11,67	4,49	0,28	0,07	0,17	99,35

Note: 1-11 (sample N-329) – pre-kimberlite basalt; 12-20 (sample 22/380-231,5) – post-kimberlite basalt

Reasoning from the aforesaid, we decided that there would be no other way to identify reliably pre-kimberlite mafic rock bodies in the Nyurbinskaya pipe than through searching for mafic rock xenoliths in kimberlite rocks of this pipe. As a

result of quarry and ore yard studies, we collected a set of 11 dolerite xenoliths for through examination (it is notable that these xenoliths were very similar in appearance to post-pipe dolerite).

Pre-pipe dolerite xenoliths occur in Nyurbinskaya pipe kimberlitic tuffisite and xenoclastic lava ("autolithic breccia") quite commonly. Varying in size between 6 and 20 cm, they have generally ovalized, sometimes geometrically regular shapes. Secondary alteration rims of these xenoliths are not thick (mostly 3 to 6 mm), and the internal zones of the samples have a quite fresh appearance. Some of the xenoliths demonstrate concentric elements of globular to shell-like cleavage. The rocks have a homogeneous dark grey coloration.

All the analyzed xenoliths are similar in rock texture. Most of them are massive, equigranular, microcrystalline dolerite with prevailing grainsize of 1.0-1.5 mm (more rarely, 0.7-1.0 mm), except for two samples (N-275 and N-412) having a porphyritic texture (with glomeroporphyritic clinopyroxene and plagioclase phenocrysts varying in size from 1.0 to 1.5 mm) and showing a microcrystalline doleritic texture of rock matrix (with grainsize of 0.2-0.3 mm). The structure of the rocks is homogeneous and massive, without any amygdaloidal inclusions. The rocks show a varying degree of alteration: clinopyroxene (40-50% of the rock volume) is completely replaced by secondary minerals (single olivine grains are also replaced), but tabular plagioclase crystals (40-50% of the rock volume) have in some samples surprisingly fresh appearance. Plagioclase generally corresponds to An_{62} (with compositional variation between An_{46} and An_{83} – see table 3). Opaque minerals (3-5% of the rock volume) are represented by small (generally 0.1-0.3 mm rarely up to 0.5 mm), xenomorphic (interstitial) or idiomorphic segregations of titanomagnetite and Mn-ilmenite (table 3). In addition, a single grain of medium-Cr magnesian chrome spinel has been identified.

GEOLOGICAL AND PETROLOGICAL PECULIARITIES OF YOUNG (POST-KIMBERLITE) MAFIC ROCKS

All the researches of the Nyurbinskaya pipe agree about the post-kimberlitic origin of the within-pipe mafic rock body, taking into account its well defined cross-cutting contact with kimberlite and marked alteration features, both endocontact (chilling zones in mafic rocks) and exocontact (some skarn-like features in kimberlite) [26,29]. Along with this, some researches believe that the dyke (or stock) of mafic rock that has been discovered by drilling in the Nyurbinskaya pipe is made up of both pre-kimberlite and post-kimberlite mafics (!!!) [11].

We have analyzed post-kimberlite mafics of the Nyurbinskaya pipe in drill core samples from four drill holes (32/265, 16/400, 22/420 and 22/380) and in the zone of mafics-kimberlite contact. In addition, we examined a core sample from

drill hole # 4/660, which dissected some basalt body of unclear age and morphology 200 m SE of the pipe being studied.

Core samples from all four drill holes bear information on a contact between a mafic rock body and pipe kimberlite. This contact points unambiguously to post-kimberlitic origin of this mafic intrusion, therewith being rather difficult to examine by itself, with peculiar and disputable features encountered in core samples from each of the four drill holes.

Drill hole # 22/380 dissected a mafic rock body at its contact with metasomatized kimberlite tuffisite at a depth of 217 m. Large "drops" of magmatic melts, which intruded here into kimberlite, occur lithified as "prominences", or apophyses, of basalt glass, 1.0-1.5 cm thick and 15-20 cm long, with a solid, homogeneous structure. Somewhat lower (deeper), there is a complexely structured, zoned contact between the main mafic rock body and pipe kimberlite.

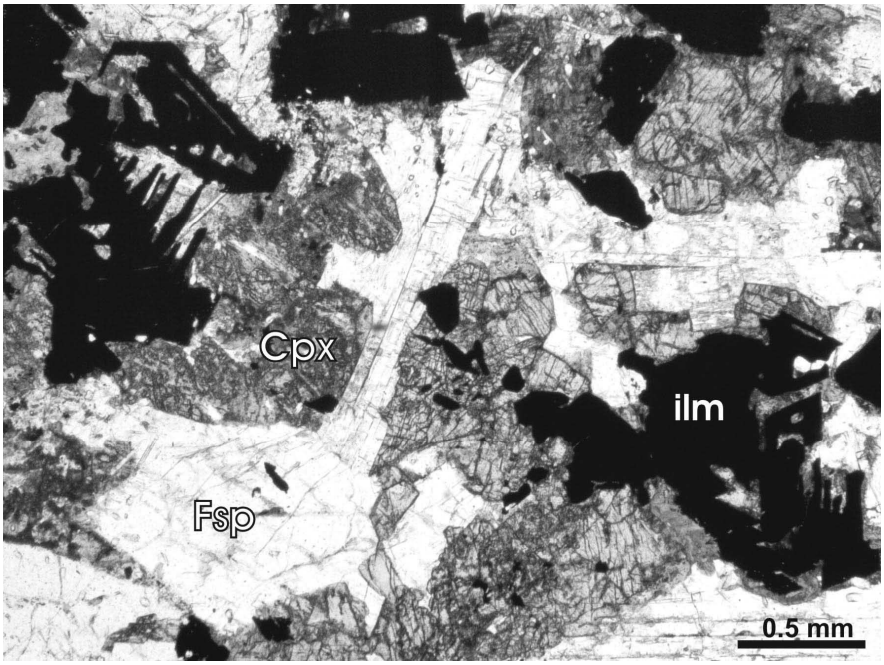

Fig. 4. **Post-kimberlite dolerite (sample 32/265-500), think section: plane light.**
Cpx – clinopyroxene, Fsp – feldspar, Ilm – ilmenite.

Along the very kimberlite contact, the rock consists of basalt glass, but this glassy zone (in contrast to the above described apophyses) is only 1-3 mm thick. The next zone is made up of miniphyric basalt (2 m thick). It has a heterogeneous structure, which shows itself both in a sharp change of rock texture (however, without any break in continuity) and in the presence of vein-like basalt segregations (all with the same geochemistry), which suggests repeated basaltic melt injections. The basalt zone sharply grades into a zone of microcrystalline dolerite with rare amygdaloidal inclusions and, further, into medium-grained crystalline dolerite with characteristic skeleton crystals of ilmenite (figure 4). Mineral chemistry of rock from this drill core sample is similar to that from drill

hole # 32/265 (table 3). Almost throughout the whole examined depth interval (214-233 m), and even within the zone of immediate mafic-kimberlite contact, the rocks have an unexpectedly “fresh” appearance, with solid structure free of joints and gangue, which is very favourable for geochemical examination.

To summarize, the structural features of the post-kimberlite mafic rocks and the appearance of their contact with kimberlite (especially the apophyses of chilling basalt glass) suggest that the basaltic melt intruded into pipe kimberlite when this latter was already cold, which may be indirect evidence for large temporal lag between the kimberlite and basalt intrusion events. Rock samples with the most fresh appearance were picked from core samples from drill holes ## 32/265 and 22/382 for isotope geochemistry tests.

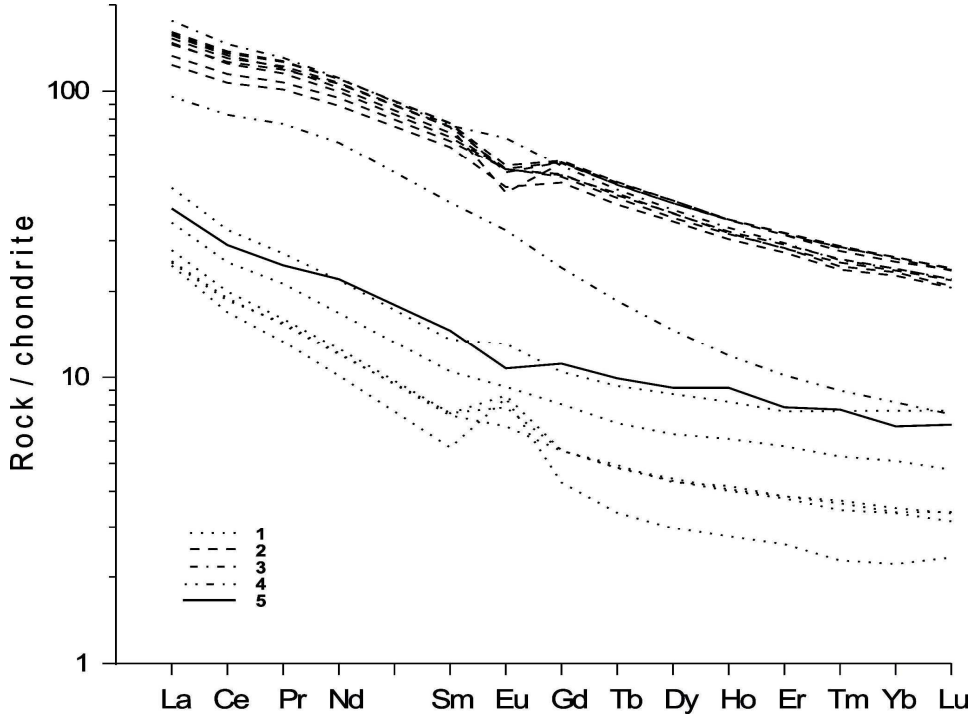

Fig. 5. **Chondrite normalized REE distribution pat-terns for basite rocks of the Nyur-binskaya pipe (Boynton, 1984).**

1 – pre-kimberlite basite; 2-4 – post-kimberlite basite: 2 – dolerite, 3 – basalt glass, 4 - a body of basalts in 200 m to the east from Nyurbin-skaya pipe (sample 4/660-65); 5 - Al-series olivine melili-tite of the Arkhan-gelsk province.

In general, the pre- and post-kimberlite dolerite rocks of the Nyurbinskaya pipe are petrologically similar to each other. However, post-kimberlite dolerite is characterized by somewhat more fresh appearance (with preserved clinopyroxene as augite), with a less basic plagioclase composition (An_{54} against An_{62} in pre-kimberlite dolerite), and a significantly (20to 4 times) higher proportion of opaque minerals represented mostly by ilmenite (rather than titanomagnetite as is the case in pre-kimberlite dolerite).

GEOCHEMICAL PECULIARITIES OF "OLD" AND "YOUNG" MAFIC ROCKS IN THE NYURBINSKAYA PIPE

In order to obtain statistically representative geochemical characteristics of mafic rock bodies in the Nyurbinskaya pipe, we examined six samples of pre-

kimberlite mafics (picked for their minimum extent of secondary alteration) and nine fresh samples of different structural varieties of post-kimberlite mafic rocks (tables 1 and 2).

Analysis of the obtained numerical data and geochemical diagrams plotted based on it reveals that the petrologically similar mafic rock bodies with differing age (separated by the kimberlite intrusion stage) ***differ drastically in rock geochemistry***.

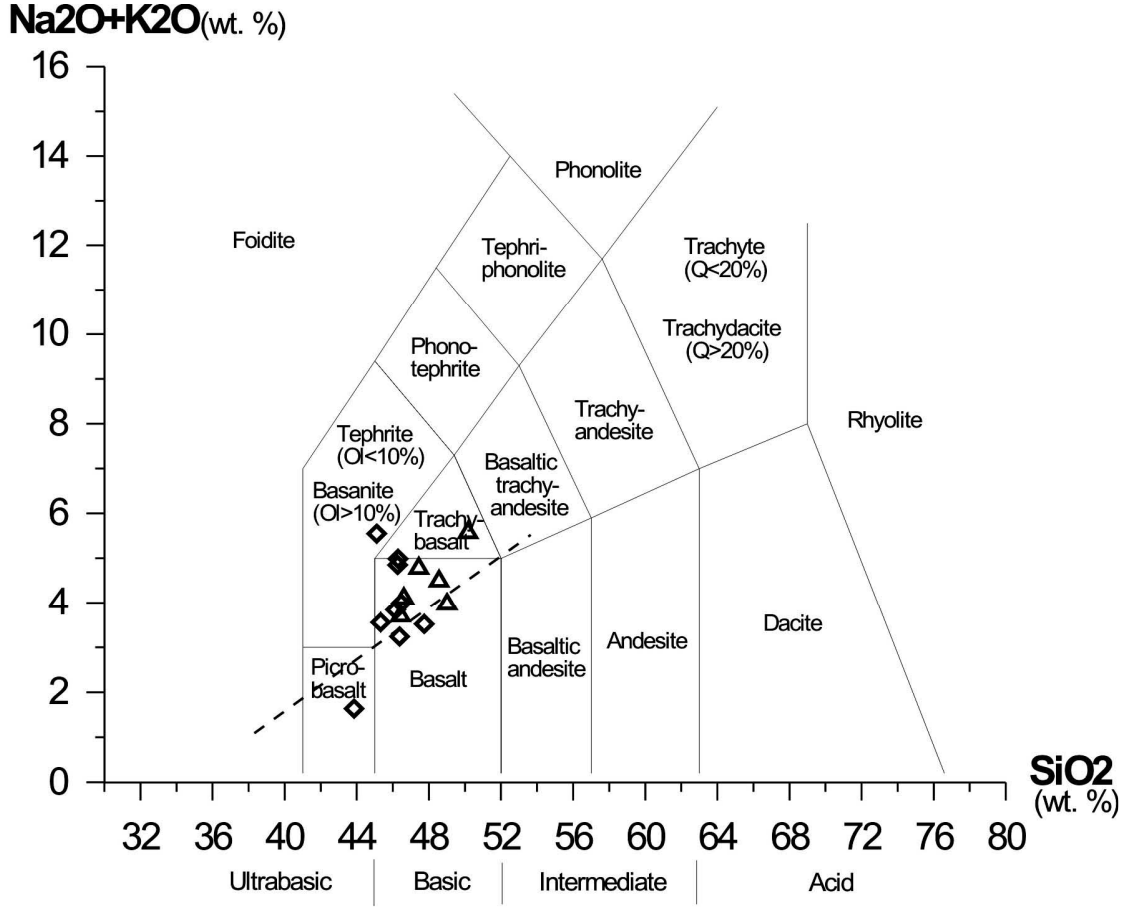

Fig. 6. **Chemical composition of basite rocks from the Nyurbinskaya pipe (diagram after [14]).**

Triangles - xenoliths of the pre-kimberlite basites; a rhombus - post-kimberlite basites.

Only SiO_2, Na_2O, K_2O and Co contents of pre- and post-kimberlite mafic rocks of the Nyurbinskaya pipe are nearly the same. As regards other geochemical characteristics, the pre-kimberlite mafic are 1.5 times higher in Al_2O_3 and MgO, two to three times higher in Ba and Pb five times higher in Ni and 15 times higher

in Cr as compared to the post-kimberlite mafic rocks. Along with this, the "young" (post-kimberlite) mafics are sharply enriched in the overwhelming majority of elements as compared to the pre-kimberlite("old") mafics, being 1.5-2.5 times higher in $FeO_{tot.}$, CaO, Be, V, Ga, Rb, Cs and Sr, about three to six times higher in TiO_2, MnO, P_2O_5, Cu, Zn, Y, Zr, Hf, REE, Th and U, and ten times higher in Nb and Ta! The most prominent geochemical features of pre-kimberlite ("old") mafic rocks of the pipe being studied are their very low TiO_2 and $FeO_{tot.}$ contents and high Al_2O_3 contents as compared to the post-kimberlite ("young") mafics. Of particular interest is REE distribution in mafic rocks of the Nyurbinskaya pipe (figure 5). The appearance of lanthanide distribution curve (normalized to chondrite) is generally the same for pre- and post-kimberlite mafic rocks. However, the post-kimberlite mafics are approximately five times richer in REE as compared to pre-kimberlite ones, therewith featuring a well defined negative Eu

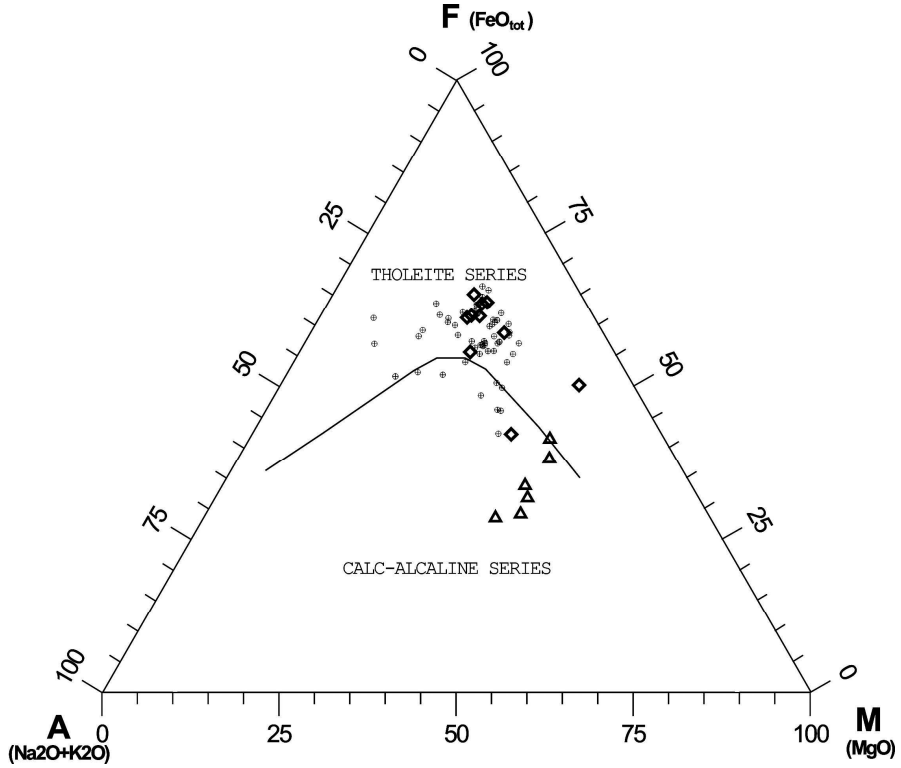

Fig. 7. **Chemical composition of basite rocks from the Nyurbinskaya pipe (AFM diagram after [19]).**

Triangles - xenoliths of the pre-kimberlite basites; a rhombus - post-kimberlite basites; circles – Nakyn field basites on data's of the previous study [11,26,31].

peak, whereas the pre-kimberlite rocks show a pronounced positive Eu peak. Geochemically, the analyzed pre-kimberlite dolerite would be related to some geochemically depleted source, and the post-kimberlite ones to some sharply geochemically enriched source. The pre-kimberlite mafic rocks of the Nyurbinskaya pipe are most similar in geochemistry and in Nd-Sr isotope

characteristics to Al-series olivine melilitite of the Arkhangelsk diamond province [20].

To typify the mafic rocks present in the Nyurbinskaya pipe, we resorted to geochemical classification diagrams. Analysis revealed that in the SiO_2 – Na_2O+K_2O diagram (figure 6) both pre- and post-kimberlite mafics occupy quite similar positions in the field of subalkaline and, to a lesser extent, tholeiitic series. However, many researches (see above) reported a clearly secondary, i.e., metasomatic nature of high alkalinity shown by these rocks. According to our data, in samples from the post-kimberlite mafic rock body, when passing away from the kimberlite contact, certain change is observed not only in the structure of this mafic rock (from basalt glass to nearly gabbro-dolerite) but also in the behaviour of alkalies. Namely, alkali content and ratios are close to initial in the basalt glass zone and in gabbro-dolerite located as far as 15 m away from the contact, whereas the nearer the kimberlite contact, the higher the alkali (primarly, K_2O) content of the mafic rocks (table.1). Therefore, there is no point in trying to identify and typify these rocks based on their alkali content. It would rather make sense to use the AFM and Al – Fe+Ti – Mg classification diagrams (figures 7,8), from which is evident that the pre-pipe mafics fall into the field of calc-alkaline series, whereas the post-pipe mafic rocks are related to the tholeiitic series.

Of course, these extremely sharp geochemical distinctions suggests absolutely different structural settings for the forming conditions of pre- and post-pipe mafic rocks. Geochemically, pre-kimberlite mafics correspond to highly aluminous calc-alkali basalt of volcanic arc in active continental margins and mature island arcs in subduction zones [15], and the post-kimberlite ones to sharply geochemically enriched high-Fe within-plate tholeiitic basalt (figure 11).

The mafic rock body that has been dissected 200 m SE of the pipe (sample 4/660-65) is very similar (while not identical) in geochemistry to post-kimberlite mafic rocks of the Nyurbinskaya pipe. It is likely that this body formed at the same stage of magmatic activity.

Analysis of published data (see above) reveals that geochemical characteristics of pre- and post-kimberlite mafic rocks of the Nakyn field are very similar; indeed, in the classification diagrams, the figurative points of both mafics fall into the same compositional fields (figures 7,8). It is likely that the authors of all these reports examined just post-kimberlite mafics and no other, and subdivision of these rocks into tholeiitic and alkaline varieties appears somewhat incorrect because of being based on the distribution of highly mobile alkalies only, without regard for other classification criteria, same of which are much more stable and reliable. As regards published analytical data on all mafic rocks examined in the studies just cited, all of them fall in the classification diagrams into the tholeiitic basalt field.

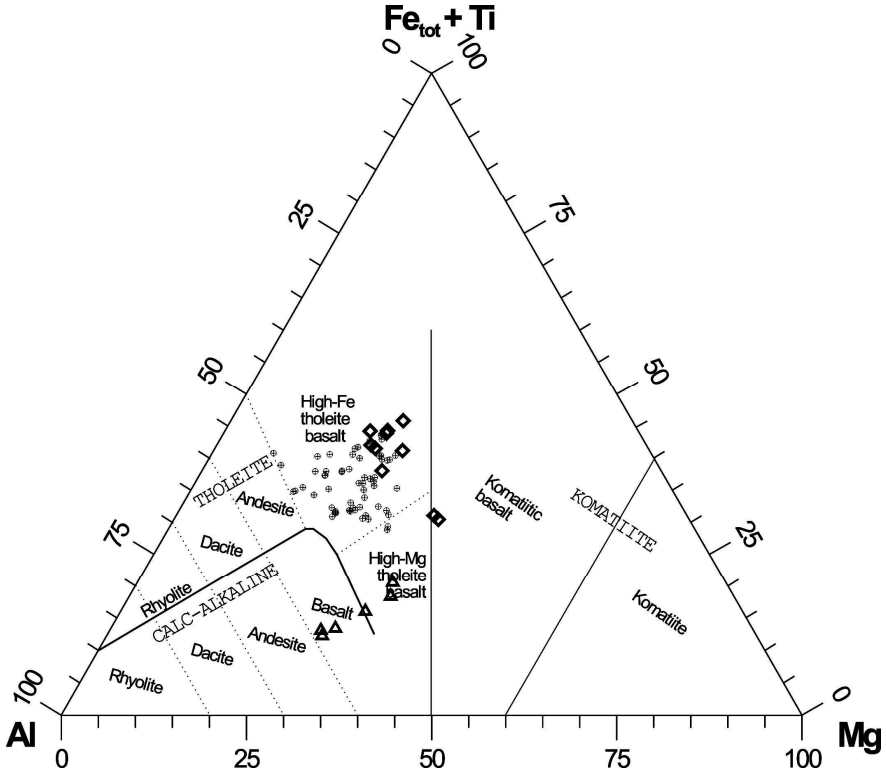

Fig. 8. **Chemical composition of basite rocks from the Nyurbinskaya pipe (A-FT-M diagram after [19]).**

Triangles - xenoliths of the pre-kimberlite basites; a rhombus - post-kimberlite basites; circles – Nakyn field basites on data's of the previous study [11,26,31].

As was mentioned above, extremely sharp distinctions in rock geochemistry suggest very dissimilar structural settings for forming conditions of the pre- and post-pipe mafic rocks and, probably, very different formation age and isotope characteristics for these mafics.

THE AGE OF KIMBERLITE, "OLD' AND "YOUNG" MAFICS

The Nyurbinskaya pipe penetrates Lower Ordovician strata and is overlain by Lower Jurassic deposits. If only this geological data is considered, the uncertainty of pipe intrusion age would be about 280 million years. In this connection, many researches repeatedly tried to determine the age of the Nyurbinskaya pipe (usually together with the Botuobinskaya pipe of the same Nakyn district) more precisely. Although high-precession isotope dating methods were used in these studies (Ar-Ar and/or Rb-Sr dating), a wide scatter of radiogeochronological data is evident. According to different reports, the age of the Nyurbinskaya pipe is assessed at 450 Ma to 332 Ma [1,2,13,23,30].

In 2006, we subjected Nyurbinskaya pipe rocks to K-Ar and Rb-Sr dating within the framework of a common comprehensive study. Based on the obtained results, we determined the intrusion age of the Nyurbinskaya pipe as **399.6∀4.6** Ma, i.e., Early Devonian, Emsian to Pragian (D_1ems-prg)[21]. In order to determine more precisely the age of Nyurbinskaya pipe kimberlite rocks, we

performed additional Rb-Sr isotope dating of the concentrically zoned magnophyric ***lamprophyre-type Phase C olivine-phlogopite kimberlite*** (sample N-384). Tests were made with bulk rock and essentially phlogopite rock matrix samples. Results of Rb-Sr analysis of these samples shown in figure 9. As is seen from this figure, the Rb-Sr isochrone age calculated for Nyurbinskaya pipe rocks (seven points, including five Rb-Sr analyses made in 2006) is **394.2∀6.2** Ma (MSWD=1.6), which, in general, is not contradictory to absolute age value determined in our previous studies by Rb-Sr dating (**399.6∀4.6** Ma) and by K-Ar dating (**399.8∀8** Ma).

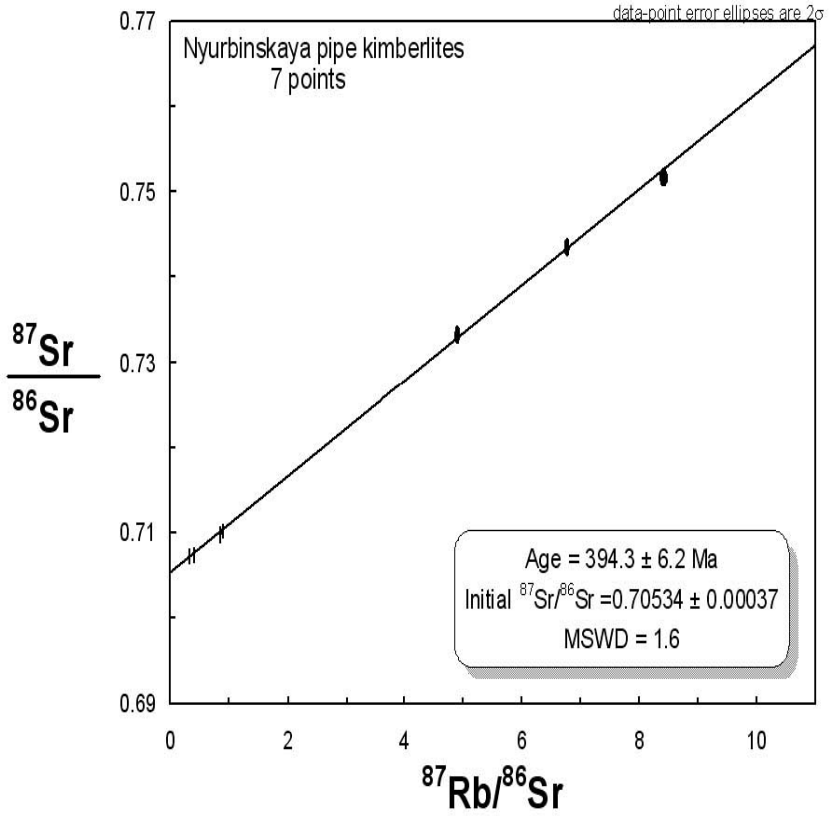

Fig. 9. **Rb-Sr isochron diagram for Nyurbinskaya pipe kimberlites.**

To summarize, additional analyses confirmed the previously determined kimberlite intrusion age for the Nyurbinskaya pipe: **399.6∀4.6** Ma, i.e., Early Devonian, Emsian to Pragian (D_1ems-prg), or Early Devonian, early Emsian (D_1ems^1).

In order to determine the age of pre-pipe mafic rocks of the Nyurbinskaya pipe, were collected a set of samples from the least altered central zones of large dolerite xenoliths. For Rb-Sr dating, we prepared bulk samples of two rock varieties and separated the nonmagnetic fraction of -0.5+0.25 mm, size fraction of

the rock, which proved to consist of feldspar (table 4). The most consistent isochrone dating result was obtained with bulk rock samples N-329 and N-332 and nonmagnetic fraction of sample N-329. The Rb-Sr isochrone age of these rocks (calculated for three points) is 703∀82 Ma (N=3, initial $^{87}Sr/^{86}Sr$ = 0,70750∀0.00015; MSWD=1.9), which is Late Riphean.

For K-Ar analysis, we prepared three bulk rock samples (size fraction -0.5+0.25 mm). One of the samples showed a Late Riphean age, whereas another two samples gave an Early Carboniferous age. It is not improbable that xenolithic rocks could have been rejuvenated as a result of K ingress (the "youngest" samples are very rich in K).

To summarize, the most probable intrusion age for Nyurbinskaya pipe pre-kimberlite dolerite would be **703∀82** Ma, which is Late Riphean. This old age aggress well with the peculiar geochemical characteristics of pre-kimberlite mafics.

To determine the age of post-pipe mafics, we collected a set of samples from different most fresh-looking rocks incorporated in the mafic intrusion penetrating the pipe. For Rb-Sr dating, we prepared bulk samples of three rock varieties (22/380-217 – basalt glass, 32/265-475.3 – microcrystalline dolerite, 32/265-497.7 – coarse-grained crystalline dolerite), electromagnetic fraction I-III from sample 32/265/497.7-GM, and -0.5+0.25 mm nonmagnetic fraction represented by feldspar grains from samples -32/265-475.3-P and 32/265-497.7-P. According to results of this dating, the Rb-Sr system of this mafic rock body appears disrupted. The most consistent isochrone dating result was obtained using two bulk rock samples (22/380-217 and 32/265-475.3) and the nonmagnetic fraction of sample 32/265-475.3, i.e., rocks with pronounced evidence of fast solidification and, consequently, weak differentiation. The Rb-Sr age of these rocks as calculated for three points is 269∀20 Ma (N=3, initial $^{87}Sr/^{86}Sr$ = 0.708070∀0.00040; MSWD=0.36), i.e., Early Permian; this is unlikely to be true.

For Sm-Nd analysis, we prepared three fractions of coarse-grained crystalline dolerite sample 32/265-497.7: bulk sample, electromagnetic fraction I-III, and nonmagnetic fraction. The Sm-Nd isochrone age of this rock, as calculated for three points, is 325∀140 Ma (N=3, initial $^{87}Sr/^{86}Sr$ = 0.51248∀0.00013; MSWD=1.9), i.e., Early Carboniferous, which is more realistic than the Rb-Sr dating result (see above), but its determination error appears to be too large.

For K-Ar analysis, we prepared three bulk samples of rocks from the mafic intrusion penetrating the pipe, and one sample taken from the basalt body dissected by drilling 200 m SE of the pipe (sample4/660-65). Dating results proved to be close to each other. The age of the chilling phase of the mafic body, i.e., basalt glass (sample 22/380-217), determined as 328∀4 Ma (Early Carboniferous) appears to be the most realistic. It coincides with the Sm-Nd isochrone age (although determined with rather large error) and agrees with date on the age of post-kimberlite mafic rocks reported in previous studies of different researches [11,26,31].

The most probable intrusion age of post-kimberlite dolerite in the Nyurbinskaya pipe would be **328∀4** Ma, i.e., Early Carboniferous. This age corresponds to the terminating stage of Middle Paleozoic tectono-magmatic activization.

To summarize, the three main stages of volcanic activity in the Nyurbinskaya pipe are largely separated in time: ***Stage 1, "old" mafics*** – Late Riphean, **703∀82** Ma; ***Stage 2, kimberlite*** – Early Devonian, **399.6∀4.6** Ma; ***Stage 3, "young" mafics*** - Early Carboniferous **328∀4** Ma.

ISOTOPIC CHARACTERISTICS OF KIMBERLITE ROCKS, "OLD" AND "YOUNG" MAFIC ROCKS

All the examined kimberlite samples are characterized by higher than average εSr values (+17.1 to +39.5), which may be related to post-magmatic rock alteration. Along with this, εNd values determined for the examined rocks (-0.7 to +2.1) are characteristic of mantle sources like BSE or weakly depleted mantle, which makes the Nyurbinskaya pipe kimberlite rocks close to Group 1 South African kimberlites [24] and to Fe-Ti series Zimni Bereg kimberlite rocks of the

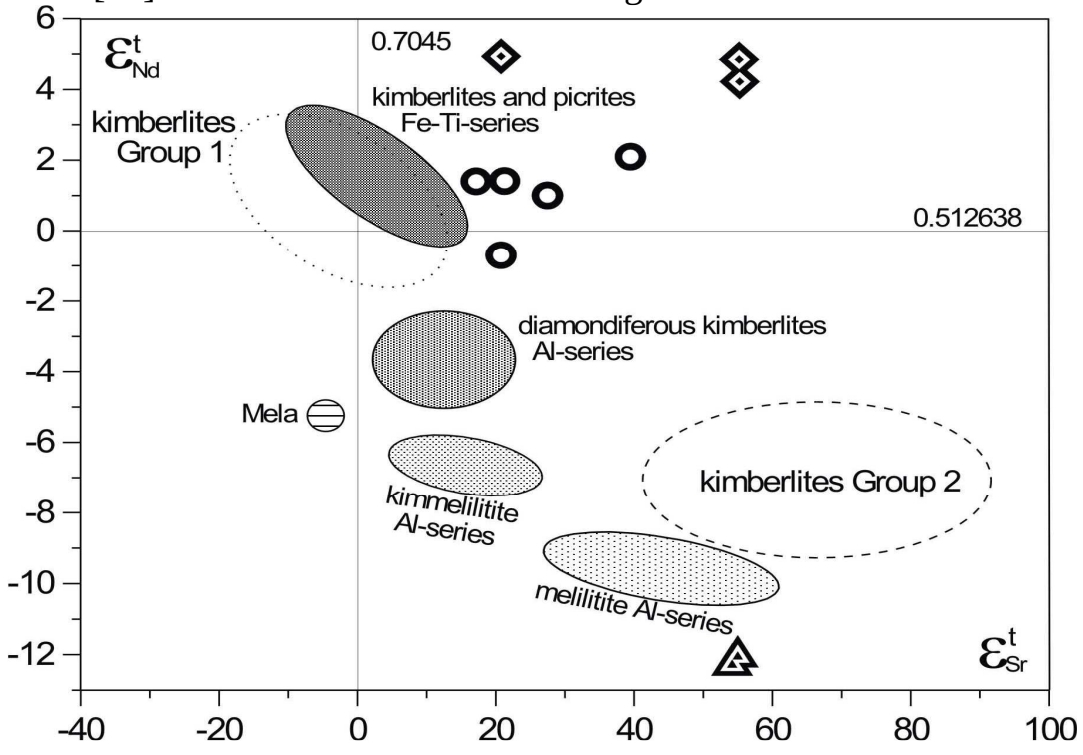

Fig. 10. **Sr and Nd isotope composition of the volcanic rocks from the Nyurbinskaya pipe in comparison by volcanic rocks of Zimni Bereg (Arkhangelsk province) [22].**

Circles – kimberlites of different types; a triangles – xenoliths of the pre-pipe dolerites; rhombus - post-pipe basites.

Arkhangelsk diamond province. In general, Nyurbinskaya pipe kimberlite rocks are characterized by εNd = +1.0 and εSr = +25.2. The model age of mantle

source for Nyurbinskaya pipe kimberlite rocks as determined with respect to depleted mantle (T_{Nd}(DM)) for five examinated samples is 1110 Ma, which agrees perfectly with the age of kimberlite mantle source determined for the Nyurbinskaya pipe in previous studies [8,12]. Along with this, model age of diamondiferous kimberlite rocks from other Yakutian kimberlite fields is much younger: T_{Nd}(DM) = 0.6-0.7 Ga [3].

In order to determine the type of mantle source for pre-pipe mafic rocks, we analyzed Nd-Sr isotope characteristics of two rock samples from the Nyurbinskaya pipe (table 4). Analysis revealed that the role of melt source for pre-kimberlite dolerite rocks was played by old, enriched lithospheric mantle (EM II, εNd = -12.2, εSr = +54.6), with a model age of T_{Nd}(DM) = 2450 Ma, probably with some participation of old lower crust matter of subduction origin (figure 10). This old model age of mantle source, much like the old age of dolerite intrusion itself, agrees well with prominent geochemical peculiarity of pre-kimberlite mafic rocks. The examined pre-kimberlite mafics are similar in model age and geochemistry to Al-series olivine melilitite of the Arkhangelsk diamond province.

Table 4.

Isotope characteristics of the Nyurbinskaya pipe volcanic rocks

Volcanic bodies	Age, Ma	εSt	εNt	T_{Nd}(DM), Ga
Kimberlites of the *Malo-Botuobinsky, Daldyn-Alakitsky and Verkhne-Munsky district* [3,5]	320-370	-5	+3	0,6-0,7
Nyurbinskaya pipe: 3. post-kimberlite basalts 2. kimberlites 1. pre-kimberlite basalts				
	328+/-4	+43,7	+ 4,7	0,770
	399,6+/-4,6	+25,2	+ 1,0	1,110
	703+/-82	+54,6	-12,2	2,450

In order to determine the type of mantle source for post-pipe mafic rocks of the Nyurbinskaya pipe, we examined Nd-Sr isotope characteristics for three rock samples (table 4). Analysis of the obtained data revealed that the role of melt source for post-kimberlite dolerite was played by moderately depleted mantle (εNd = +4.7 , εSr = +43.7) with model age T_{Nd}(DM) = 770 Ma, probably with some participation of young upper crust matter (figure 10).

Our study did not confirm the previously determined absolutely identical model age for all mafic and kimberlite rocks of the Nakyn field T_{Nd}(DM) = 1100 Ma [31]. The pre-kimberlite mafic rocks (T_{Nd}(DM) = 2450 Ma) differ drastically in model age not only from post-kimberlite mafics (T_{Nd}(DM) = 770 Ma) but also from pipe kimberlite (T_{Nd}(DM) = 1100 Ma).

To summarize, post-kimberlite dolerite is very similar in model age of mantle source to diamondiferous kimberlite rocks from the Malo-Botuobinsky and

Daldyn-Alakitsky districts (T_{Nd}(DM)=0.6-0.7 Ga, [3]), being also similar to kimberlite rocks from these regions in intrusion age and essential geochemical peculiarities. Along with this, pre-kimberlite mafics and kimberlite rocks of the Nyurbinskaya pipe differ drastically in all these parameters both from post-kimberlite mafics and from diamondiferous kimberlite rocks from other Yakutian districts (table 4).

FORMATION AFFILIATION OF KIMBERLITE, "OLD" AND "YOUNG" MAFIC ROCKS

The Nyurbinskaya kimberlite pipe is a complex volcanic structure incorporating different kimberlite intrusion phases together with an older intrusion of pre-pipe mafic rocks (xenoliths of which occur in kimberlite rocks) and a post-pipe mafic intrusion penetrating the pipe kimberlite.

Nyurbinskaya pipe kimberlite rocks show a peculiar combination of compositional features typical of Group 1 and Group 2 kimberlites. They are not similar to "isotopically transitional" kimberlite rocks, such as kimberlites of the Lomonosov deposit, Guaniamo sills (Venezuela) and some Brazilian kimberlite varieties.

In general, based on a set of compositional characteristics, Nyurbinskaya pipe kimberlite rocks appear to represent a peculiar kimberlite variety, being most similar to typical Yakutian kimberlites and Group 1 kimberlites in the character of mantle source and set of mantle xenoliths [22]. They also bear evidence of asthenospheric effect on mantle substrate, but this effect is somewhat reduced, only showing itself as intense K metasomatism, whereas the effect of Fe-Ti metasomatism (which is the most characteristic feature of Group 1 kimberlites) is not so evident. Geochemical characteristics of Nyurbinskaya pipe rocks (very high ultramaficity and, particularly, very low concentrations of incompatible elements) suggest that they are related to a geochemically depleted mantle source which experienced some enrichment from superimposed mantle metasomatism.

Our detailed studies revealed that the mafic rock bodies with differing age incorporated in the Nyurbinskaya pipe are not related to a common Middle Paleozoic activization stage of the Siberian platform. Quite the reverse, the pre-pipe and post-pipe mafics formed in different time and dissimilar tectono-magmatic situations, which caused the drastic difference in their geochemical and isotope characteristics.

The pre-kimberlite mafic rocks of the Nyurbinskaya pipe are sharply depleted in almost all incompatible elements, being in all respects similar to *highly aluminous calc-alkali basalts of volcanic arcs in active continental margins and mature island arcs in subduction zones* [15], such that they could be considered as a ***petrotype*** of volcanic rocks related to this geodynamic situation in the Siberian craton. Isotopic characteristics of these pre-kimberlite mafic rocks also completely correspond to this geodynamic situation as they undoubtedly reflect the important

role of subduction processes in the formation of mantle source of these rocks. Mafic rock occurrences with similar age, composition and tectonic setting occur, in particular, in the Sharyzhalgay nose of the Siberian platform [7]. However, in the pre-pipe mafic rocks of the Nyurbinskaya pipe the typomorphic geochemical characteristics are much better pronounced.

It is interesting that the "young", Early Carboniferous post-kimberlite mafic rocks are sharply enriched as compared to the "old" pre-kimberlite mafic rocks in the overwhelming majority of elements: $FeO_{общ.}$, CaO, Be, V, Ga, Rb, Cs and Sr, (1.5-2.5 times), TiO_2, MnO, P_2O_5, Cu, Zn, Y, Zr, Hf, REE, Th, U, (3 to 6 times), and Nb and Ta (more than 10 times!). The post-kimberlite mafic rocks correspond in their geochemical and isotope characteristics to *sharply geochemically enriched low-Al, high-Fe and high-Ti within-plate tholeiitic basalts of riftogenic series* characteristic of riftogene mode of development of active continental margins [15].

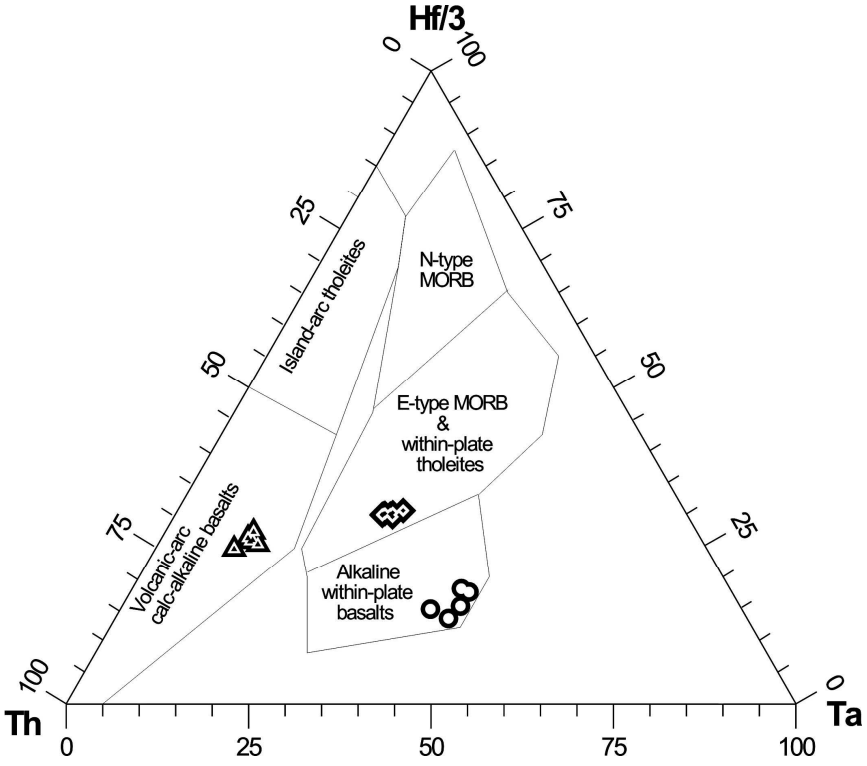

Fig. 11. **Chemical composition of volcanic rocks from the Nyurbinskaya pipe (diagram after [27]).**

Circles – kimberlites of different types; a triangles – xenoliths of the pre-pipe dolerites; rhombus - post-pipe basites.

Geochemically, pre-kimberlite mafic rocks correspond to a geochemically depleted source, and the post-kimberlite mafics to a sharply geochemically enriched source.

In rare element distribution features evident from the classification diagram [27], pre-kimberlite mafic rocks of the Nyurbinskaya pipe correspond to calc-alkali basalts of volcanic arc, pipe kimberlite rocks to within-plate alkali basalt, and post-kimberlite mafic rocks to within-plate tholeiitic basalts (figure 11).

INDICATIONS OF PRE-PLUME AND POST-PLUME MANTLE CONDITION

Geological bodies related to the three different stage of magmatic activity in the Nyurbinskaya pipe differ drastically both in intrusion age and in almost all geochemical and isotopic characteristics. The most prominent geochemical features of pre-kimberlite ("old") mafic rocks in the Nyurbinskaya pipe are their significantly lower TiO_2 and $FeO_{tot.}$ contents and higher Al_2O_3 content as compared to the post-kimberlite ("young") mafics in the same pipe (figure 12). It is noteworthy that the essential petrochemical difference between the relatively old, Early Devonian kimberlite rocks of the Nakyn field and comparatively young, Late Devonian and Mesozoic kimberlites of other Yakutian kimberlite fields also consists in relatively low TiO_2 and $FeO_{tot.}$ contents and high Al_2O_3 contents shown by the "old", i.e., Nakyn field kimberlite rocks (figure 12). In addition, the petrological model age of the "young", Fe- and Ti-enriched post-kimberlite dolerite rocks of the Nyurbinskaya pipe (T_{Nd}(DM) = 770 Ma) is generally the same

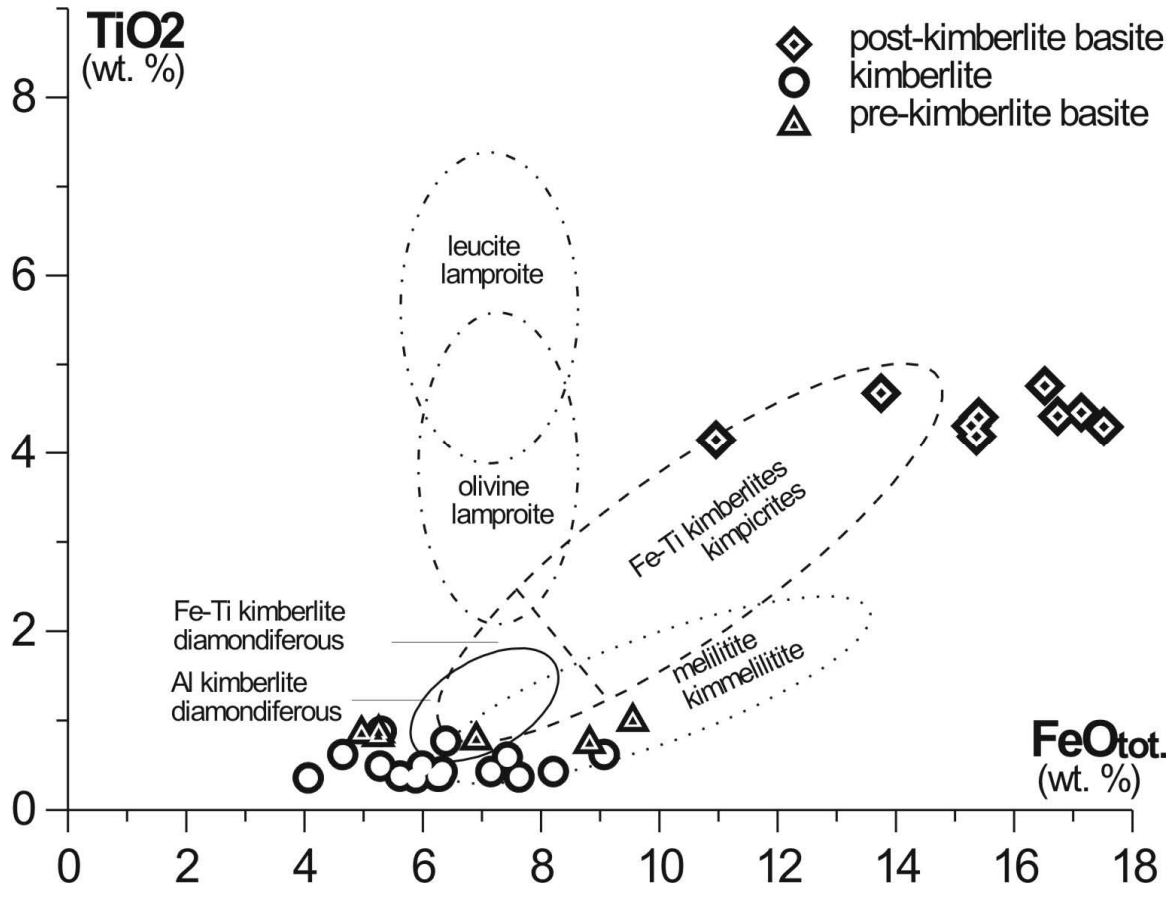

Fig. 12**. Chemical composition of volcanic rocks from the Nyurbinskaya pipe in coordinates: FeO_{tot} - TiO_2**

as that of the relatively young (as compared to the Nyurbinskaya pipe kimberlite) Fe- and Ti-rich kimberlite rocks in other Yakutian kimberlite fields (T_{Nd}(DM) = 0.7-0.6 Ga)[3].

It is not improbable that these prominent and consistent geochemical distinctions between the “old” and “young” mafics in the Nyurbinskaya pipe and very similar, also prominent geochemical distinctions between the relatively old kimberlite rocks of the Nyurbinskaya pipe and relatively young kimberlites in other Yakutian regions are related to some common geological processes, which obviously exerted similar effect on respective upper mantle zones, i.e., zones of magma generation for both mafic and kimberlite rocks.

The role of a global geological process that could have caused such sharp changes in (at least) geochemical characteristics of the upper mantle and given rise to intense Fe-Ti mantle metasomatism could have been played by some asthenospheric diapir (intrusion) or, in other words, mantle plume. The relatively old geological bodies (both mafic and kimberlite) that intruded prior to the plume might reflect the composition of old, geochemically depleted lithospheric mantle, whereas the relatively young mafic and kimberlite bodies, which intruded after the plume event, might reflect the latest composition of the upper mantle with varying extent of metasomatic transformation and geochemical enrichment due to the plume effect. Evidence in favour of this assumption can be found not only in geochemical peculiarities of respective rocks with differing age but also in characteristic features of essentially mantle rock fragments, i.e., dept-derived inclusions, which may reflect particular characteristics of the mantle specific to different stages and periods of its evolution (before and after the plume intrusion).

The relatively old (“pre-plume”) magmatic rocks, i.e., Early Devonian Nyurbinskaya pipe kimberlites and the mafic rocks penetrated by the pipe, are all characterized by low Fe and Ti contents and by the absence of picroilmenite in kimberlite (rare mantle rock xenoliths occurring here do contain some picroilmenite, but its composition is atypical of kimberlite). Along with this, the relatively young (“post-plume”) magmatic rocks, among which are not only the mafic rocks penetrating the pipe kimberlite but also the Late Devonian and Mesozoic kimberlite rocks in other Yakutian kimberlite fields, are characterized by comparatively high Fe and Ti contents and by the presence (and/or very high concentration) of picroilmenite in kimberlite rocks (the composition of picroilmenite in kimberlites and mantle rock xenoliths is here typical “kimberlitic”).

The post-plume, metasomatized upper mantle condition is characteristic of the majority of Yakutian kimberlite fields, while evidence of probably pre-plume (“relict”) condition of geochemically depleted upper mantle has yet only been found in some Nakyn field kimberlite rocks. This is why direct examination of mantle rock fragments from Nakyn field kimberlites is of interest as one can deal here with relict rocks bearing information on those upper mantle zones that do not exist any more, having reworked by latest geological processes.

TECTONIC RELATIONSHIP OF MAFIC AND KIMBERLITE MAGMATISM

Taking into account the Late Riphean age of reliably identified "pre-kimberlite" mafic rocks, it should be realized that the existing conceptions on the confinement of kimberlite, pre-kimberlite and post-kimberlite mafic rocks to a common Middle Paleozoic epoch and to common structural elements and magma-controlling structures call for additional corroboration or correction [26]. In particular, the issues of possible presence of Devonian pre-kimberlite mafics in the Nakyn field and probable kimberlite intrusion through fracture zones in pre-kimberlite mafic rocks (which could be considered as a structural indicator for exploration) appear disputable. It is not improbable that *post-kimberlite mafic melts* intruded through fracture zones in kimberlite rather than kimberlite melts through fracture zones in *pre-kimberlite mafic rocks*. Moreover, as is evident from Figure 2.62 [9] and Figure 1 [10], the patterns of magma-controlling faults are very different for kimberlite and mafic rock occurrences. Therefore, the inferred relationship of structural control systems for Nakyn kimberlite and mafic rocks is far from obvious.

EVIDENCE OF SUBDUCTION IN "OLD" MAFIC AND KIMBERLITE ROCKS. BREAK-UP OF RODINIA

Identification of the previously unknown in the Middle Markha region basaltic magmatism variety, i.e., Late Riphean high-Al calc-alkali basalt rocks typical of volcanic arcs in active continental margins and mature island arcs in subduction zones, brought additional evidence for the significant effect of subduction processes on regional lithospheric mantle. Probably it is precisely these subduction processes that are responsible not only for the peculiar oxygen isotope ratio values shown by diamondiferous eclogite xenoliths in the Nyurbinskaya pipe [25], but also for uncommon structure and mineral chemistry of mantle rock xenoliths analyzed in our previous study [22]. It is also not improbable that subduction processes contributed to compositional peculiarity of Nakyn field kimberlite rocks.

The Late Riphean time of formation, determined for the pre-pipe dolerite rocks as **703+/-82** Ma, falls into the period of fundamental tectonic transformation of Northern Asia. "Among the Late Riphean tectonic structures of Northern Asia are the Siberian craton, microcontinents with predominantly Riphean crust, and ***Late Riphean island arcs***. These structures formed approximately 700 million years ago, when the supercontinent Rodinia, which included the Siberian craton, and its framing shelf, fragments of which now exist as microcontinents, were involved in riftogenic processes. The break-up of Rodinia, inferredly caused by the

effect the Pacific mantle superplume on its lithosphere, was accompanied by within-plate magmatic events distributed over a vast area" [28].

As was noted in [16]: "Opening of a basin between Siberia and Laurentia … proceeded gradually, like in the present-day Red Sea rift, however, with a significant shift component. This geodynamic situation could be promoted by the formation of a subduction zone in the Taimyr margin of Siberia, where island arc volcanic activity dates back to *960 million years ago"*. Our studies revealed that a subduction zone with volcanism typical of active continental margins and mature island arcs, existed in the Late Riphean (700 Ma) not only in the northern, Taimyr marginal area of Siberia (Central Taimyr island arc [16]), but also in the eastern marginal zones of Siberia, in particular, in the area of the present-day Nakyn kimberlite field (the Nakyn segment of an active continental margin – figure 13).

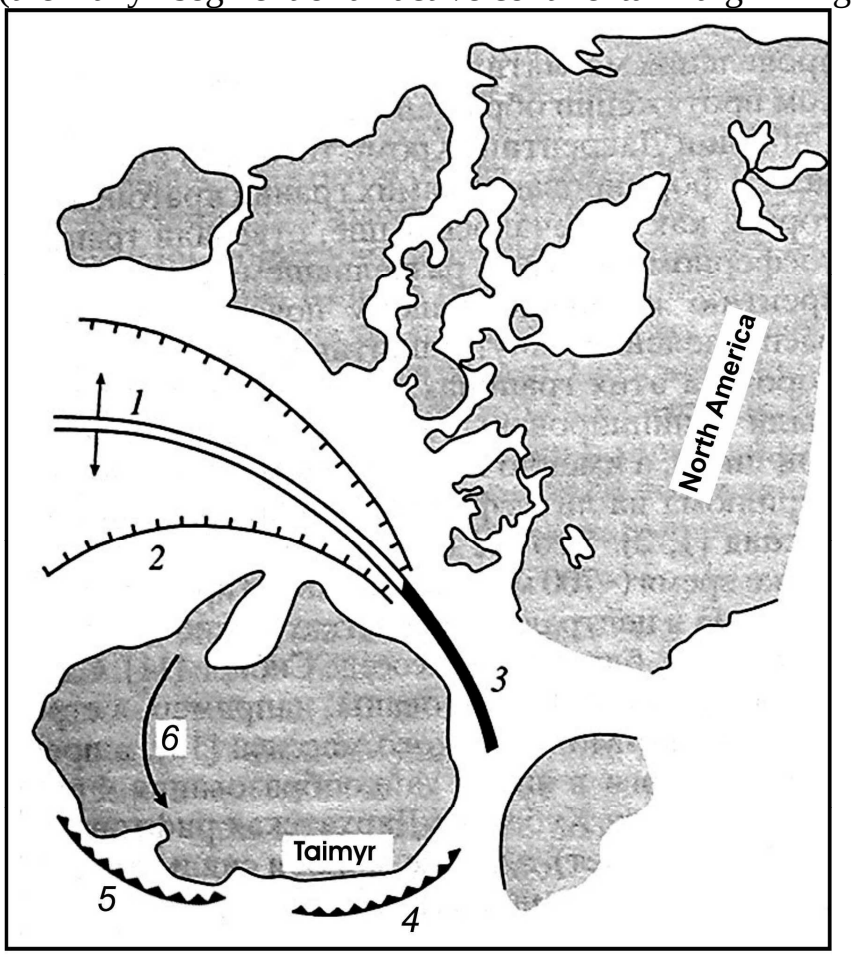

6

Fig. 13. **A scheme of formation Late Riphean-Vendian break-up between Siberia and Laurentia for age about 600 Ma (after [16] with our additions).**

1- axis of break-up (spreading) and a direction of growth of the oceanic basin generated in an interval 750-600 Ma; 2 - boards of oceanic basin; 3 - an axis of the break-up formed in an interval 600-550 Ma; 4, 5 - zones of Late Riphean-Vendian accretion and subduction (4 – the Taimyr segment, 5 – the Nakyn segment); 6 - a direction of craton rotations, given by break-up with Laurentia.

The newly obtained data on the composition of Late Riphean pre-kimberlite basalt rocks with typomorphic isotope-geochemical features unambiguously related to a characteristic geodynamic situation must gain definiteness in paleogeodynamic reconstructions of the formation and Neoproterozoic break-up of the supercontinent Rodinia and temporal evolution of one of its former constituents, namely, the Siberian craton.

CONCLUSIONS

Comprehensive examination of all the volcanic rock bodies incorporated in the Nyurbinskaya pipe (pre-kimberlite mafics, kimberlite and post-kimberlite mafic rocks) revealed that they differ drastically in time of intrusion, type and model age of mantle source, and geochemical characteristics. Geochemically, pre-kimberlite dolerite rocks correspond to high-Al calc-alkali basalt rocks of volcanic arcs in active continental margins and mature island arcs in subduction zones, and the post-kimberlite dolerite rocks are similar to sharply geochemically enriched high-Fe and high-Ti within-plate tholeiitic basalt rocks related to the riftogenic mode of regional structural evolution. The volcanic rocks with differing age incorporated in the Nyurbinskaya pipe present a record of temporal evolution of mantle sources of basic and ultrabasic magmatic melts from the Late Riphean time to the Early Carboniferous. Identification of the previously unknown in the Middle Markha region basaltic magmatism variety, showing itself in Late Riphean high-Al calc-alkali basalt rocks, brought additional evidence for the significant effect of subduction processes on regional lithospheric mantle. It is not improbable that it is precisely these subduction processes that are responsible for substantial compositional peculiarity of Nakyn field kimberlite rocks.

ACKNOWLEDGEMENTS

The authors are grateful to all the geologists and engineers affiliated in the Nyurbinsky Mine, Mirninskaya expedition and YaNIGP TsNIGRI, ALROSA Co. Ltd., who not only presented us with a possibility of examining the quarry walls, ore yard stockpiles and drill core samples but also rendered us the utmost help and assistance in our field work.

REFERENCES

1. **Agashev A.M., Fomin A.S., Watanabe T., Pokhilenko N.P.** (1998) Preliminary age determination of recently discovered kimberlites of the Siberian kimberlite province.// 7-th IKC. Cape Town. Extended Abstracts. P. 9-10.

2. **Agashev A.M., Pohilenko N.P., Tolstov A.V., Poljanichko V.V., Mal'kovets V.G., Sobolev N.V** (2004) New data on age of the kimberlites from the Yakutia diamond province. // Doklady RAS. Volume 399. N 1. pp. 95-99.
3. **Bogatikov O.A., Kononova E.A., Golubeva Yu.Yu. et al.** (2004). Petrogeochemical and isotope variation of the kimberlite Yakutia compositions and their reason. // Geochemy. N 9. p. 915-939
4. **Boynton W.V**. (1984) Geochemistry of the rare earth elements: meteorite studies. In: Henderson P. (ed.) Rare earth element geochemistry. Elsevier, pp. 63-114.
5. **Brahfogel' F.F.** (1984) Geological aspects of the kimberlite magmatism of Northeast of the Siberian platform. Yakutsk. 128 p.
6. **Cherny S.D., Fomin A.S., Yanygin Yu.T., Banzeruk V.I , Kornilova V.P.** (1998) Geology and composition of the Nakyn field kimberlite pipes and diamond properties (Yakutia) // 7-th IKC. Cape Town. Extended Abstracts. P. 9-10.
7. **Gladkochub D.P., Sklyarov E.V., Masukabsov A.M. et al.** (2000). Neoproterozoic dyke swarms of the Sharyzhalgay ledges - indicators of disclosing of Paleoaziatsky ocean //Dokl. RAS. T 375. N 4. p. 504-508.
8. **Golubeva Yu.Yu., Pervov, V.A., Kononova V.A.** (2006) Low-titanium diamondiferous kimberlites – a new petrogeohemical type. Comparison Nakyn (Yakutia) and Zolotitsa (the Arkhangelsk area) versions // Regional geology and metallogeny.-2006.- V. 27.-pp. 15-25.
9. **Grakhanov S.A., Shatalov V.I., Shtyrov V.R et al.** (2007) Diamond looses of the Russia. Novosibirsk. 457 p.
10. **Ignatov P.A., Bushkov K.I., Tolstov A.V., Yanygin Yu.T.** (2008). Mapping of hidden displacements of kimberlite-controlling structures in Nakyn kimberlite field. // in: "Problems of kimberlite and diamond formation, platform magmatism evolution – new opinions and facts. Yakutsk. Pp. 325-331.
11. **Kiselev A.I., Yarmolyuk V.V., Egorov K.N et al.** (2006) Middle Paleozoic basite magmatism of the NW parts Vilyuy rift: composition, sources, geodynamic. // Petrology, T. 14. No 6. pp. 626-648.
12. **Kononova V.A., Golubeva Yu.Yu., Bogatikov O.A., Nosova A.A., Levskij L.K., Ovchinnikova G.V.** (2005) Geochemical (ICP-MS geochemistry, isotopy Sr, Nd, Pb) heterogeneity kimberlites from Yakutia: questions of genesis and diamond potential. // Petrology. Volume 13. N 3. pp 227-252.
13. **Kornilova V.P., Fomin A.S., Zajtsev A.I.** (2001) New type diamondiferous kimberlites on the Siberian platform. // Regional geology and metallogeny. V. 13-14.- pp. 105-117.
14. **Le Maitre R.W., Bateman P., Dudek A. et al.,** 1989. A classification of igneous rocks and glossary of terms. Blackwell, Oxford.
15. **Martynov Yu.A.** (1999) Geochemistry of basalts of active continental margins and mature island arcs (North-West Pacific). Vladivostok. Dalnauka. 218 p.

16. **Metelkin D.V., Vernikovsky V.A., Kazansky A.Yu.** (2007) Neoproterozoic stage of Rodinia evolution based on new paleomagnetic data from the western margin of the Siberian craton. //Geology and Geophysic. T. 48. N. 1. p. 42-59.
17. **Milashev V.A**. (1963). Term "kimberlite" and classification of the kimberlitic rocks. // Geology and Geophysic. N 4. pp. 42-52.
18. **Pohilenko N.P., Sobolev N.V., Zinchuk N.N.** (2001) Anomaly kimberlites the Siberian platform and Slave craton, Canada, their major features in connection with a problem of forecasting and searches. // Diamonds and diamond potential of the Timan-Ural region. Materials of the All-Russia meeting. Syktyvkar. Pp. 19-21.
19. **Rickwood P.C.** (1989) Boundary lines within petrologic diagrams which use oxides of major and minor elements. Lithos, 22. 247-263.
20. **Sablukov, S.M.,** 1990. Petrochemical series of the kimberlite rocks. Dokl. Akad. Nauk SSSR 313 (4), pp. 935-939.
21. **Sablukov S.M., Banzeruk V.I., Sablukova L.I., Stegnitskij J.B., Bogomolov E.S., Lebedev V.A.** (2007) Ancient age of the Nakyn field kimberlites (Yakutia) - one of the reasons of an originality of their material structure // VIII International conference «New ideas in sciences about the Earth». Moscow. Reports. T. 5. pp. 209-212.
22. **Sablukov S.M., Sablukova L.I., Stegnitskij J.B., Banzeruk V.I.** (2007) Lithospheric mantle characteristics of the Nakyn field in Yakutia from data's on mantle xenoliths and basalts in the Nyurbinskaya pipe/ Works of VII International Seminar «Alkaline magmatism, its sources and plumes». Irkutsk-Napoli pp. 140-156.
23. **Shamshina E.A., Zaitsev A.I.** (1998) New age of Yakutian kimberlites. // 7-th IKC. Cape Town. Extended Abstracts. p.783-784.
24. **Smith, C.B., Gurney, J.J., Skinner, E.M.W., Clement, C.R., Ebrahim, N.,** (1985). Geochemical character of Southern African kimberlites. A new approach based on isotopic contents. Trans. Geol. Soc. S. Afr. 88, 267-280
25. **Spetsius Z.V., Teylor L.A, Valley J.V. et al.** (2006) Garnets of oxygen isotope composition in diamondiferous xenoliths (Nyurbinskaya pipe, Yakutia). // Works of VI International Seminar «Deep magmatism, its sources and plume». Mirny-Irkutsk. pp. 59-78.
26. **Tomshin M.D., Fomin A.S., Janygin Ya.T. etc.** (1998) Features of magmatic formations Nakyn kimberlite fields of the Yakutia province // Geology and geophysics. T.39, N 12. pp. 1693-1703.
27. **Wood D.A.** (1980). The application of the Th-Hf-Ta diagram to problems of tectonomagmatic classification and to estabilishing the nature of crustal contamination of basaltic lavas of the British Tertiary volcanic province. Eart Planet. Sci. Lett. 50. 11-30.
28. **Yarmolyuk V.V., Kovalenko V.I.** (2001). A Late Riphean break-up of Siberia and Laurentia in displays within-plate magmatism. / Dokl. RAS. T. 379. N. 1 .P. 94-98.

29. **Zankovich N.S., Zinchuk N.N.** (2001) Petrographical and mineralogical characteristics of the kimberlite pipes of different phases of Nakyn fields. // Problems of diamond geology and some ways of their decision. Voronezh. Pp. 54-72/
30. **Zaytsev A.I., Kornilova V.P.,Fomin A.S., Tomshin M.D**. (2001). About age of the kimberlites from Nakyn field (Yakutia). // Geology of diamond - the present and the future. Voronezh. Pp. 47-53.
31. **Zemnuhov A.L., Zajtsev A.I., Kopylova A.G., Tomshin M.D., Janygin Yu.T.** (2005) Basaltic magmatism Khannja-Nakyn district. // Geology of diamond - the present and the future. Voronezh. Pp. 482-494.
32. **Zinchuk N.N., Aljabjev T.E., Banzeruk V.I., Stegnitsky Yu.B., Rotman A.Ya., Egorov K.N., Koptil' V.I.** (2005) Geology, material structure and diamond potential of the kimberlites from the Nakyn kimberlite fields of Yakutia (on an example of Nyurbinskaya pipe). // Geology of diamond - the present and the future. Voronezh. Pp. 807-824.

UDK 551.22+552.11

Plume interaction and evolution of the continental mantle lithosphere.

Ashchepkov I.V. [1], Pokhilenko N.P. [1], Vladykin N.V. [2], Logvinova A.M. [1], Rotman A.Y. [3], Afanasiev V.P. [1], Pokhilenko L.N. [1], Kuligin S.S. [1], Malygina L.V. [1], Alymova N.V. [2], Stegnitsky Y.B. [3], Khmelnikova O.S [1].

[1] Institute of Geology and Mineralogy, SD RAS Novosibirsk 630090, Russia;

[2] Institute of Geochemistry SD RAS, Favorsky str. 1a, Irkutsk, 66403;

[3] Central Science and Research Geology And Prospecting Institute Of The Stock Company "ALROSA", Chernyshevsky Str,7, Mirny, 678170 Russia

ABSTRACT

Monomineral thermobarometry (MTB) of EPMA data for heavy monomineral separates (HMS) for>Yakutian kimberlite pipes compile mantle SSE-NNW traverse. Orthopyroxene (Opx) MBT for mantle beneath Udachnaya give three PT paths: low temperature (LT) conductive branch [9] estimated with [25, 42, etc.] thermometers and two more HT- PT paths referred to values of Fe#Ol (0.07, 0.085 and 0.11) correspondently. PT estimates for garnets, pyroxenes reflect mantle layering, for ilmenite reflect conditions of the polybaric mantle protokimberlite systems where Cr-rich ilmenites trace the PT paths of the metasomatites.

MTB for Udachnaya, Ybileynaya Nyurbinskaya and nearest pipes of kimberlites xenoliths and xenocrystsshow colder PT path using HMS analyses. Polymineral TB [9, 10, 37, 42] produces more smooth geotherms. Monomineral TB give wider range PT points of compositions reflecting heating near the magmatic channels. Regularities of mantle sections and layering in Daldyn field are recognized on the PT and P-X diagrams. Thermal conditions of the lower part of mantle sections were heated by the protokimberlite melts created megacrystalline associations. PT values of subcalsic garnets are correlating with those of picroilmenites. Large pipes like Udachnaya reveal complex layering consisting from 12-13 units correlating with the peaks of Re/Os ages [14]. Pyroxenites and 'hot' eclogites are found within ~55-65, ~40 and ~50 kbars. Mantle in Alakite field is subjected to pervasive multistage metasomatism, Fe-enriched Cr-diopsides, Ti- rich- low-Ca garnets locate near the melt feeders marked by ilmenites. Ilmenite PT trends were formed by rising (accompanied by AFC) protokimberlites. Stepped 10–12 layering is marked by periodic Fe#-rise, Ca-decrease in garnet is correlating with Cr- rise of clinopyroxenes. In Nakyn field rhythmic layering found for peridotites in lower part (P>40kbar), fertilization by Fe-Cpx (40-50 kbar) follow the Ilm- forming system ~55-60 kbar correlating with depleted (low-Ca) peridotites occurrence. In Anabar fields highly depleted mantle > 40 kbars is subjected to Fe- metasomatism and includes the relics of LT peridotites and pervasive metasomatism accompanied protokimberlite feeders marked by Cr-low ilmenites accompanied by fertilization. In upper section abundant Gar-CPx rocks are typical.

Evolution of the protokimberlite systems reconstructed comparing the different kimberlites phases show the gradual rise of the level of ilmenites associations, Fe#

enrichment and degree of the melt interaction. Diamond growth possibly occurs in the zones of influence of protokimberlite systems and is accompany the heating of mantle columns.

INTRODUCTION

Recent developing success of the Earth Sciences including isotopy of mantle rocks and magmas and their geochemistry and experimental petrology dating of mantle processes [11, 43] bring to the combining of the plate tectonics and plume dynamics and appearance of the theory which allow to receive explain the influence of the deep seated geodynamics with the relatively shallow tectonic processes, accounting the developing of different types of magmatism in the various geodynamic settings and decode the cycles of tectonic and mantle activity [3, 36]). Mantle magmas which bring to the surface the samples from the depth appear in the different setting as a result of the plume mantle activity of different types. The hot spots which carry the xenoliths in oceanic environments contain not only the xenoliths from the shallow mantle just near the upper magmatic chamber or source but sometimes more deep materials which suppose presence of kimberlitic types of melts within the conduit connecting the shallow and deep mantle [62]. The wet finger plums [62] which are developing in the relatively young continental plates and especially in the continental margins like in Circum Pacific in the back ark and environment like in Mediterranean [33]. The finger plums occurred within the continental mantle like in East Africa [34] trace the rift zones and the junction and the convergent boundaries including the margins of the paleoarks like in Transbaikal and Mongolia [7]. The source of the wet plums is likely located near the 410 km boundary where the hydrous modifications of Mg2SiO4 like wadsleites can produce the wet plums due to the peridotite melting [60]. The water can be transported to the depth by subduction processes [29]. But there are some isotopic and geochemical evidences about the precens of eclogite components in the hot spot and even in komatiite magmas [53].

PLUMES AND CONTINENTAL PLATE MAGMATISM

Long time kimberlites was sought to be the special type of melt produced by special plums. But in the 90^{th} it was shown that Mesozoic kimberlites are result of the hot spots and their tracks are the traces of the pate migration like in South America [13] and in North America [20]. Nevertheless in Siberia and in Baltic shield, Zimny Bereg [35] most of kimberlites are erupted in the lat Devonian time. In this period Fennoscandia and Baltica and Siberia compile close group of continents (Fig.1). And magmatic activity appeared at first as the basaltic magmatism then within short 350-360 ma period produced kimberlites in Siberian platform in the great lineal NNE zone crossed the paleo continent from Low Lena to the Southern part in Biryusa basin. The chain of the separate fields are located in the different distance which is more dense in the northern part, despite in the

similarity with the hot spot track they are likely resulted from the deep seated superplum. The next line which connect Nakyn an Malo- Botuobinsky fields probably trace the next permeable subparallel zone (fig.1).

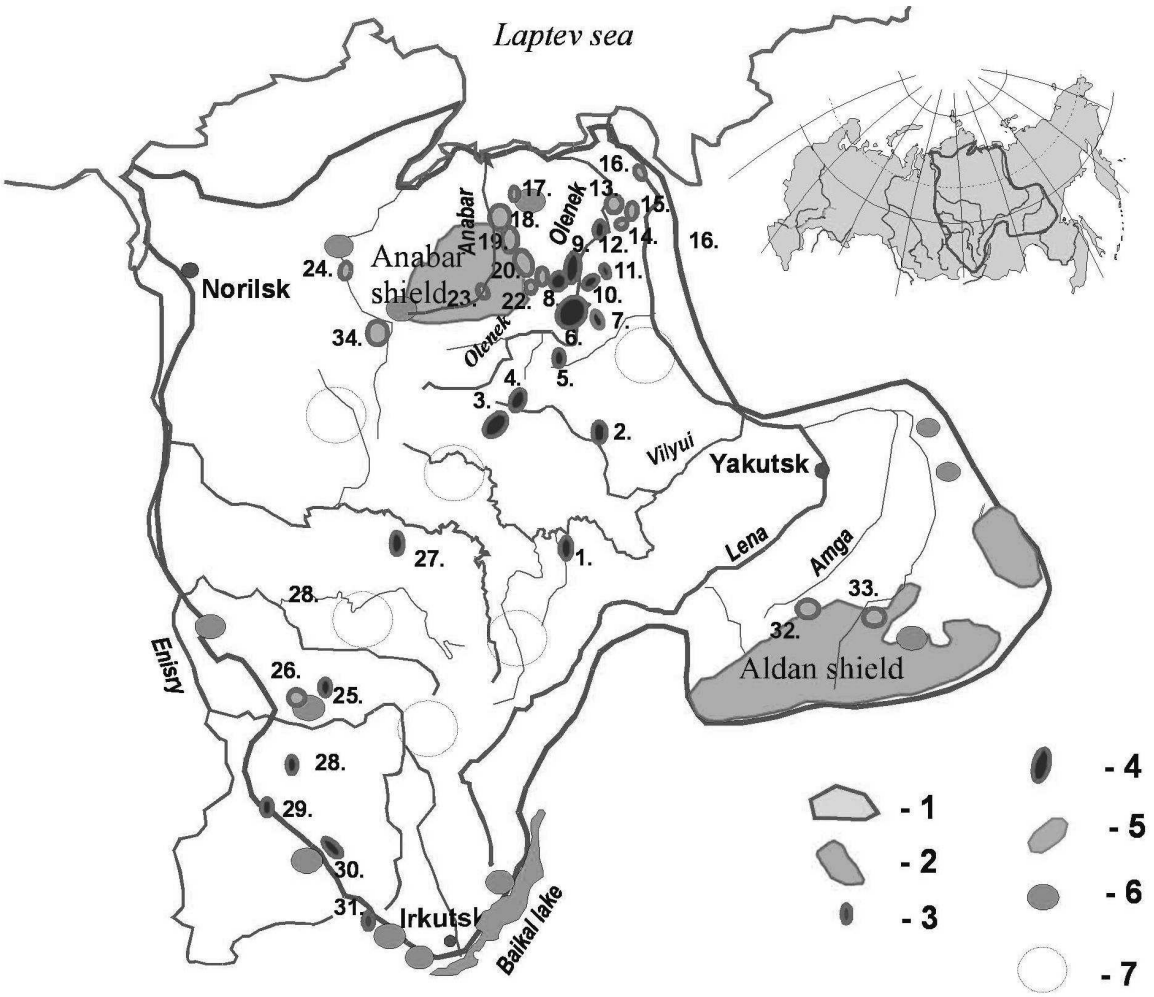

Fig.1. **Scheme of the location fo kimberlite and karbonatite fields in Siberian platform.**

Modified after [24]: 1. Siberian platform. 2. Shields. 3. Precambrian kimberlites. 4.Paleozoic kimberlites. 5. Mesozoic kimberlites. 6. Carbonatits massifs. 7. Probable regions of kimberlite location.

Fields: 1. Malo-Botuobinskoe, 2. Nakyn, 3. -Alakit-Markha, 4- Daldyn, 5 - Upper Muna, 6 — Chomurdakh, 7 - Severnei, 8 - West Ukukit, 9 - East Ukukit, 10 - Ust-Seligir, 11. Upper Motorchun, 12. Merchimden, 13. Kuoika, 14 - Upper Molodo, 15. Toluop, 16. Khorbusuonka, 17. Ebelyakh, 18. Staraya Rechka, 19. Ary-Mastakh, 20. Dyuken, 21. Luchakan, 22. Kuranakh, 23. Middle Kopnamka, 24. Middle Kotui, 25. Chadobets, 26. Taichikun-Nemba, 27. Tychan, 28. Muro-Kova, 29. Tumanshet, 30. Belaya Zima, 31. Ingashi, 32.- Chompolin, 33.Tobuk-Khatystyr, 34. Kharamai.

Internal structure of Alakite and Daldyn kimberlite fields shows regular distribution of pipes (fig. 2). Large pipes under exploration or having perspective for diamonds are located in a nearly equal distance one from another in the elliptic lines. Such a structure is typical for Cenozoic volcanic fields [7, 21] may result from the rotation of the plume head created periodically rising blobs of melts. In

Daldyn field the ellipsoidal trajectory is not closed. Location of the kimberlite fields is also controlled by the permeable zones in lithosphere. Relatively large pipes are located in the line Udachnaya - Zarnitsa. Such a model of the plume rotation plum within a fracture was described mathematically and then experimentally. The dense grouping in the Northern part fin Daldyn field and around Sytykanskaya pipe probably is the projection of the plume conduit which due to buoyancy may rise like diapir.

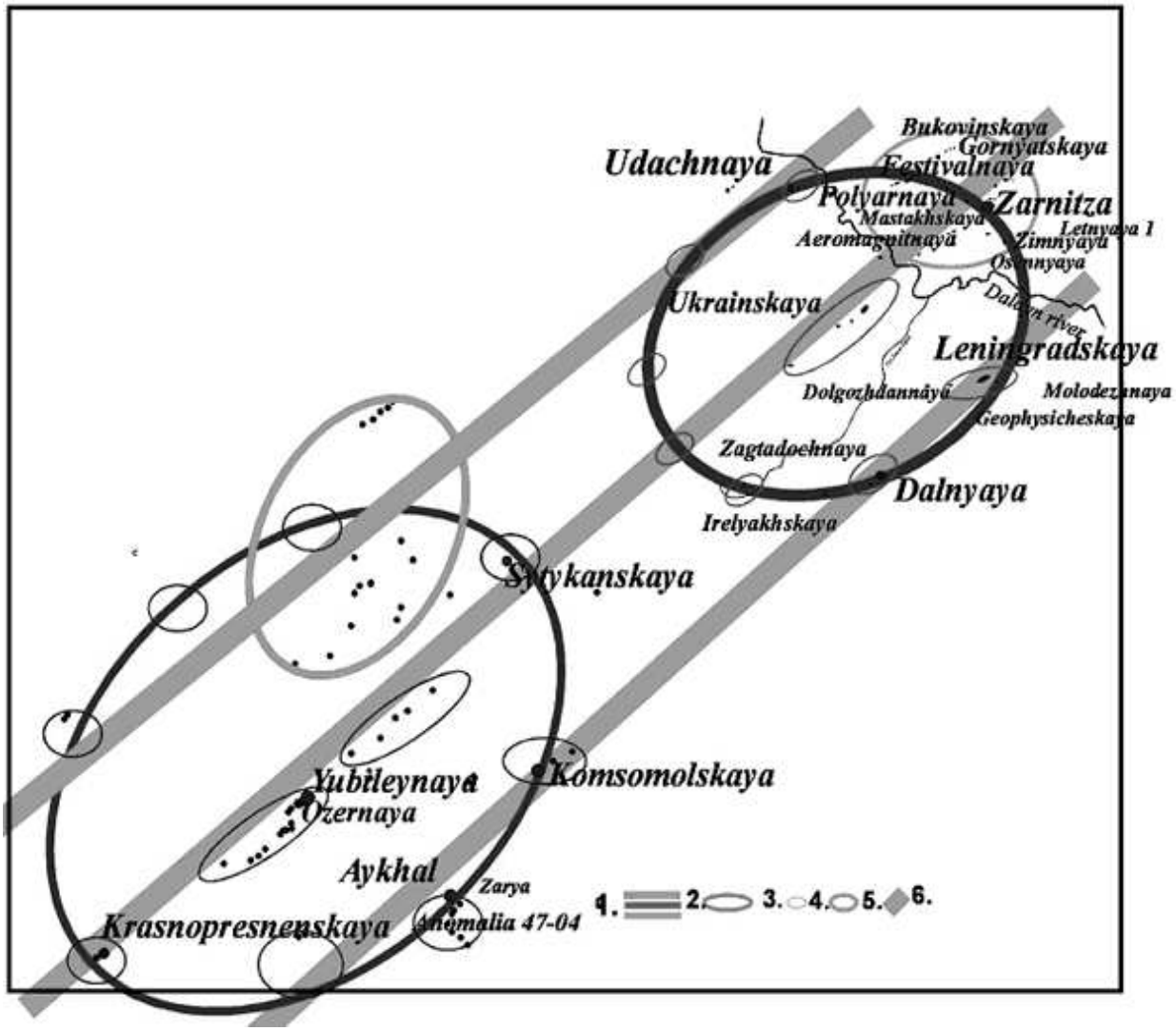

Fig. 2. **Location of kimberlite pipes in Daldyn and Alakite fields.**

1. Kimberlite pipes. 2. Lateral (permeable) zones of pipe location. 3. Trajectories of hypothetical hot stream migration. 4. Probable zones of PT location. 5. The area of scattered kimberlite location. 6. Triple NNE lines of the kimberlite pipe location.

Concentric structure for Daldyn filed was suggested to be the result of mantle diapirism but concentration of large pipes in the peripheral pipes suggest the highest melt concentration what is not typical for mantle diapirs.

CONTINENTAL KEEL GROWTH AND LAYERING

Recent studied proved layered mantle structure of the lithospheric mantle [8, 14, 15, 18, 19, 23, 26-28, 50, 51]. It is divided into 3-7 major units according to garnet thermobarometry, but combination of several methods [6] give more detail layering consisting from 9-13 units [6] for mantle beneath Udachanaya and other large pipes like Mir. The common model for continental mantle lithosphere (SCML) growth is the underplating of oceanic and probably continental lithosphere beneath the continental keel of craton which according to Re/Os ages of the sulfides was created in Achaean time and prevail in Siberia and Northern groups of continents [8, 14, 19, 23, 28, 43, 46, 50]. Recent data show more extending time of creation referring to Proterozoic and Phanerozoic time [46] and a complex structure modified by melt percolation. According to these models only the cores of the cratons were created in Archean [18, 43] and the outer parts were formed in the Proterozoic and later time.

Detail studies of the mantle columns reveal that mantle consist from the contrast layers of different nature [46] having quite different modal composition and geochemistry of mantle rocks. Mantle keel is more refractory then convective mantle and have positive buoyancy due to the olivine-melt density inversion near 80-85 kbar [1] in peridotite and basaltic systems. It represents the thermal and chemical boundary layer simultaneously [27]. Primary the mantle keel can be produced in the early stage by the compaction of the olivine mush flotation in early magmatic ocean or more likely due to mantle diapirism with high melting degree [26]. Another reason of growth is underplating of the oceanic mantle slices or back ark mantle wedge [23, 46]. Subduction with the eclogitization in wide scale work before 2.7 ma [64]. In Daldyn region average mantle compositions is similar to oceanic abyssal harzburgites and eclogites to oceanic basalts representing underplating of subducted slabs [46, 47, 55-57]. The subduction of back ark mantle wedge may be supposed for such mantle blocks as Alakite region with the broad developing of the high degree metasomatism with the formation of alkaline pyroxenes and high general depletion continental material. Relatively fertile and metasomatized mantle compositions similar to the xenoliths from orogenic massifs occurs only in shallow mantle level mainly in Mesozoic pipes [13] or as upper most spinel lherzolites in several regions. Thus underplating of continental mantle together with continental keel [23] like in Himalaii it is difficult to suggest, though high Al- eclogites which occurs are more close to the continental crust then to basaltic.

Correlation of the superplume events with growth of crust [11] due to subduction [12, 36] and growth of continental keel have the same time intervals and close reasons. Age histogram for the crust [11] and He isotopy [44] and the Re/Os age histogram for Udachnaya pipe [14] as well as for whole cratons [44] are very similar.

As it was shown 10-13 layer structure if mantle keel is pronounced in the large territories and should be formed nearly simultaneously during superplume

events. They were accompanied by the appearance of the relatively thick and hot melt lenses beneath the continents which should prevent transformation of basaltic crust to eclogites and possibly their submelting. This may explain relative rarity of eclogites in the mantle structure. Melted crust material produced more acid melts intruded the lower crust and erupted to surface. The residual peridotite part of slabs was moved beneath continent similar to low angle subduction what was accompanied by the fast convection in the low viscous asthenosphere. After melt removal and freezing it was joined to the continental keel. According to this model the thickness of continental keel can't exceed 300 km being restricted by melt solid inversion boundary [1]. This is correct in general for mantle keel in Gondwana continental group [23, 26, 27]. But northern Lawrasian group which mowed slower in plate motion sometimes reveal the signs of more thick cold lithosphere [23].

DETECTION OF THE LAYERING

In most of mantle sections in Siberia amount of units is close to 10-13 [6] which agree with amount of superplume events in the Precambrian history of the Earth [11, 43] and seems to be the attribute of the mantle lithosphere not only in Siberia.

General division of the mantle column in to two units at 40 kbars is a common feature of the mantle column [6]. At first this was found by the inflection of the garnet Cr_2O_3-CaO trends near 4-5% Cr_2O_3 [57]. Many pyroxenite and eclogites xenoliths found in Udachnaya and other pipes [51] belong to the interval near 40 kbar. Usually Cr-low pyrope garnets from the upper mantle part reveal the variations in CaO and TiO_2 showing pyroxenitic affinity. Upper part often is heated up to 1200^{o}C what is typical for the xenoliths from alkaline basalts [7, 8, 26]. This should result from the plum melts influence at the depth of the upper asthenospheric lens 20-30 kbars. In the interval 40-20 kbar at least 2-3 inflection of garnet PT trend [6] is recognized everywhere [Fig. 3-9]. No evidences found if this a result of the melt concentration determined by the physic- chemical boundaries [61]and features of melt and fluids or layering produced by slab underplating [51]. Eclogites according to thermobarometry are found not only in lower [55, 56,] but in upper part also [46].

Layering is emphasized by the trend of increasing or complex inflections Fe# or for the garnets in each horizon (Fig. 3). Very often there are several subparallel lines of P-Fe# likely due to the melt percolation. Several horizons are traced by the Cr-bearing ilmenites or by the clinopyroxene clots.

General tendency of the mantle columns from 40 to 65 kbar is the continuous growth of depletion [43] to the bottom in 3-4 horizons detected for Udachnaya and other pipes due to loss of CaO in garnets with the depth. Enriched in the bottom layer near 60-55 kbars exist in the most of the studied pipes. Usually the calculated pressure interval for ilmenites coincide with the appearance of sub –calsic garnets. This may be interpreted as melt percolation of ilmenite – forming melts within

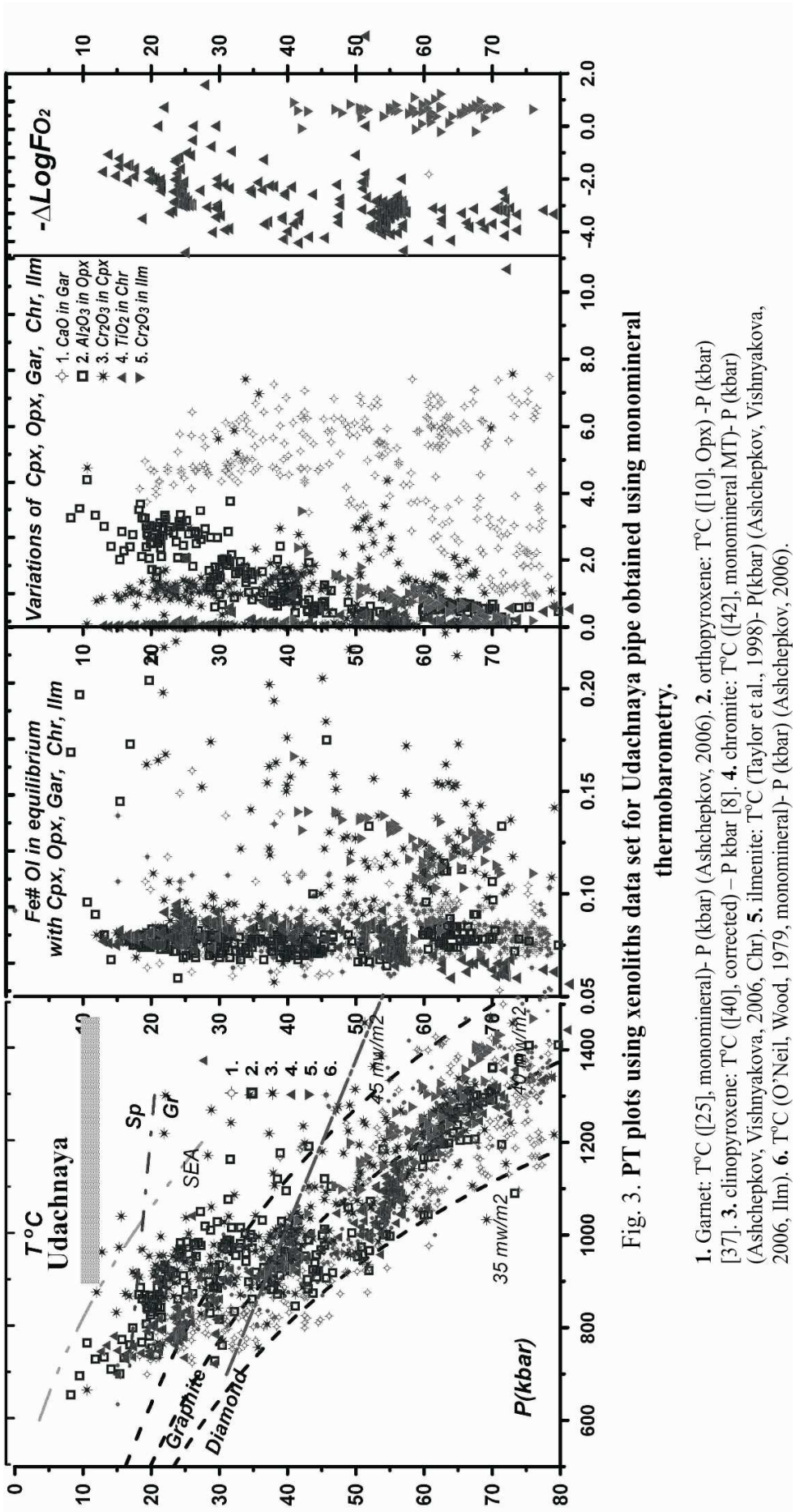

Fig. 3. **PT plots using xenoliths data set for Udachnaya pipe obtained using monomineral thermobarometry.**

1. Garnet: T°C ([25], monomineral)- P (kbar) (Ashchepkov, 2006). **2.** orthopyroxene: T°C ([10], Opx) -P (kbar) [37]. **3.** clinopyroxene: T°C ([40], corrected) – P kbar [8]. **4.** chromite: T°C ([42], monomineral MT)- P (kbar) (Ashchepkov, Vishnyakova, 2006, Chr). **5.** ilmenite: T°C (Taylor et al., 1998)- P(kbar) (Ashchepkov, Vishnyakova, 2006, Ilm). **6.** T°C (O'Neil, Wood, 1979, monomineral)- P (kbar) (Ashchepkov, 2006).

dunite conduites. The time of partial melting is unknown, for Ti-rich knoringites typical in many pipes it may coincide with the developing of magma feeders.

Deformed peridotites found in 70-60 kbar interval represent the peridotites material that was fertilized by plum melts but the structure of shearing may result from the hydraulic fracturing. Similar layer may be formed due to tectonic sharing in upper mantle part also [45-47]. It may be the reason of repeated steps in PT trend for in the lower part of mantle column.

Low Cr- diopsides which are typical for many mantle columns in Daldyn region represent possibly the precipitates from the plum melt portions hybridized with the peridotites. They very often accompany it PT diagram the PT estimates for ilmenites and their parental malts are close in mg'.

Large amount of polymineral associations with pyroxenes refer to diamond window- 45-60 kbars, but the rocks without pyroxenes should be higher in pressure. Lower horizons which are judging from the diamond inclusions are mainly megacrystalline dunites with pyropes [49, 55] and chromites, harzburgites, eclogites and pyroxenites [48, 55, 57]. They likely represent the relics of subducted slabs, channels of the melt and fluid movements and lenses of the pyroxenites leaved by plume melts. This is the transitional part from the lithosphere to asthenosphere where according to the most megacrystaline rocks are occurring [41]. Sharp layering determined by the pyroxene thermobarometry for mantle column beneath the Udachnaya [6] suppose that common subduction model for the mantle layering beneath Siberia at least for Daldyn kimberlite field. Zircons ages from eclogites and lower crust suggest the plume events to be recorded during underplating of melts beneath the crust till the kimberlite eruptions [11] what probably affect also the peridotites in the mantle column.

The numerous multistage modification events are detected in the xenoliths due to zonation in minor and major components [55]. They are correlating with the superplume events [11, 14, 19, 36].

Lateral and vertical variations of the mantle structure of Siberian platform [6, 9, 15](show the increasing depletion of the lower part of the mantle lithosphere northward. Geochemical features show the vertical zonation of trace elements and using the CARP division on clusters [17] and the distributions of groups in different pressure intervals. Despite on the good correlation of Al_2O_3 with the modal compositions of peridotites and with the Cr and Y content [19, 43] of garnet this method leaves many questions concerning the agreement with the general polybaric thermobarometry and with modal composition for Siberian peridotites. In general the depth of melting determine the modal compositions which refer to position of cotectics [22]. Many very depleted xenoliths according to modal and whole rock composition often reveal enriched compositions of pyroxenes and garnets in mantle xenoliths from Alakite and other regions. Simple correlation of the time of the rock formation with the geochemical features with the division in Archon, Proton and Tecton [19, 43] may be corrected because the Re/Os ages are

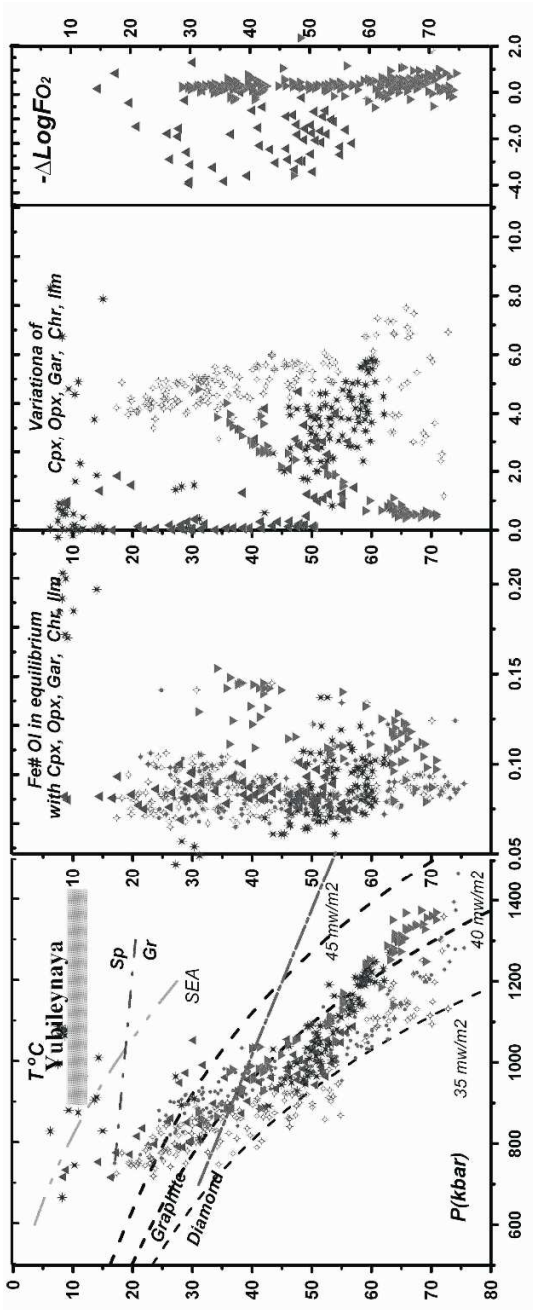

Fig. 4. PT plots using xenoliths data set for Yubileinaya pipe obtained using monomineral thermobarometry.Signs are the same

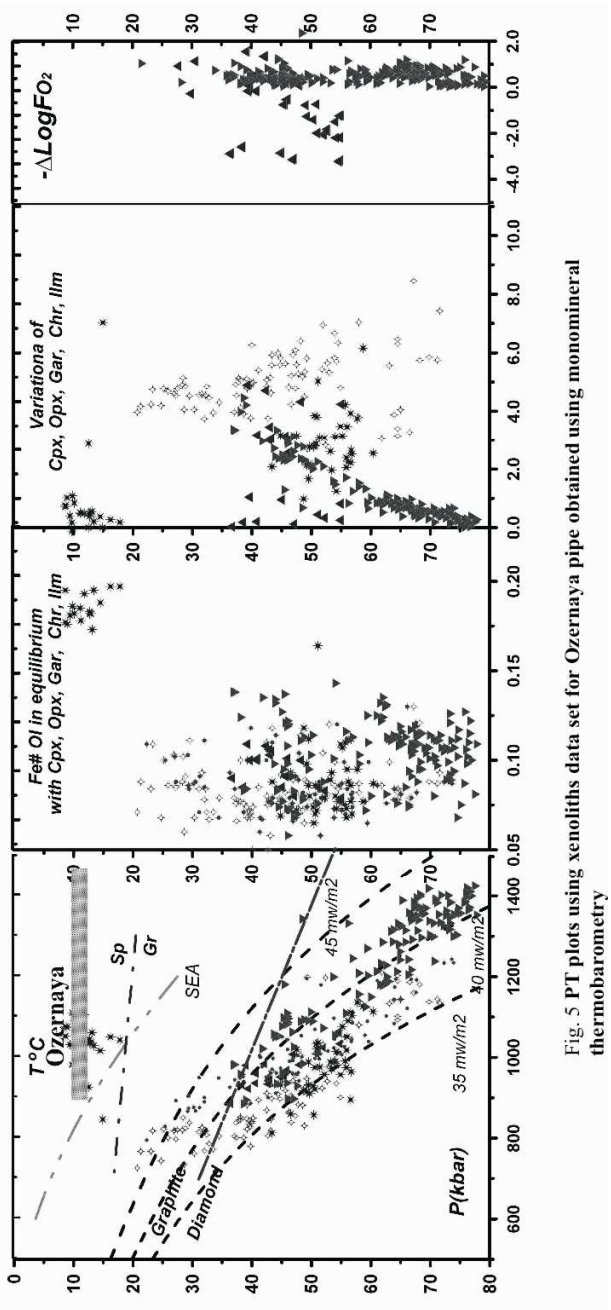

Fig. 5 PT plots using xenoliths data set for Ozernaya pipe obtained using monomineral thermobarometry

very conservative often do not correspond to the events of the melting and modification [58].

General sketches of mantle columns receive with garnet thermobarometry [16, 52] are detailed by the complex of five or more methods of monomineral thermobarometry [6] and compared with the results of geochemistry which very often show the disequilibrium of the minerals in the mantle xenoliths [2].

Universal barometric equation [8] for clinopyroxenes allow to work with peridotites and eclogites. Original barometric equations for five minerals [6] were modified to reach better agreement allow obtaining PT diagrams for mantle columns beneath kimberlite pipes using heavy mineral separates. It's gave possibility to compare and reconstruct not only the structure, petrography and composition of the rocks in the mantle column in the different levels more comprehensive then garnet thermobarometry [15] combined with garnet geochemistry [16] Original data base of LAM ICP MS minerals from the xenoliths and xenocrysts > 800 TRE analyses allowed to compare in general the compositions of peridotites in the different levels of mantle columns and lateral variation from for different kimberlite fields. This data will be discussed in another paper.

1. Developing of feeder and vein systems.

Evolution of the magmatic sources were estimated comparing ilmenite compositional trends and temperature and pressure (TP) estimates for the three phases from Yubileynaya pipe. Ilmenite thermobarometry produce TP estimates close to the clinopyroxene TP conditions in middle part mantle columns [6]. The higher values (55-70 kbar) refer to feeders and HT metasomatites at the base lithosphere of large pipes. Metasomatites riches the the garnet spinel boundaries like in mantle beneath the Mir pipe but mostly upper metasomatic level is close to 40 kbar coinciding with the pyroxenite lens. Picroilmenites from kimberlites of Siberian platform are mainly formed during the polybaric AFC fractionation of protokimberlite melts at the stage of feeder systems creation and produced a long compositional trends. Inflections in trend are due to mantle layering and pulsing intrusion, several levels of Cr – enrichment results from the contamination of parental ilmenite magma in wall rock peridotites and branching in the finishing stage due to the crystallizing in veins and veinlets.

DISCUSSION

2. Evolution of the magmatic sources.

Ilmenite TP values determined for the mantle columns matching three stages of kimberlite activity beneath the Yubileynaya pipe (fig. 4-6) show the evolution of thermal conditions. The pipe is composed from several bodies which have there own names: Ozernaya cutting the NW part and Ottorzhenets locating very close to the north in the same quarry. Heavy fractions ilmenites from autholithic kimberlite expose the most deep (~70 kbars) and relatively high temperature conditions show

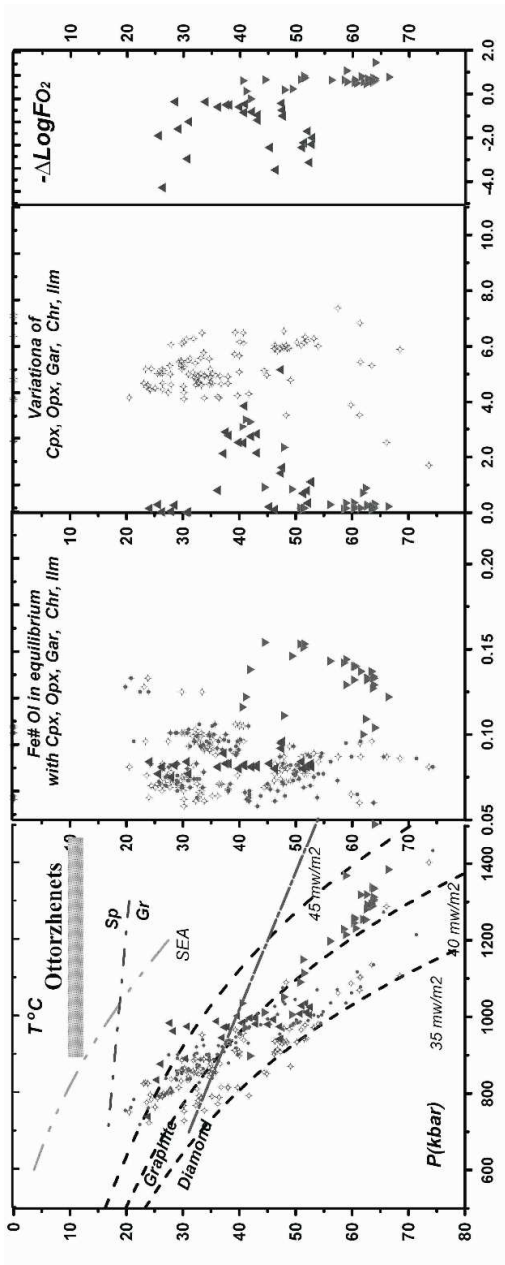

Fig. 6 **PT plots using xenoliths data set for Ottorzhenets pipe obtained using monomineral thermobarometry.** Signs are the same.

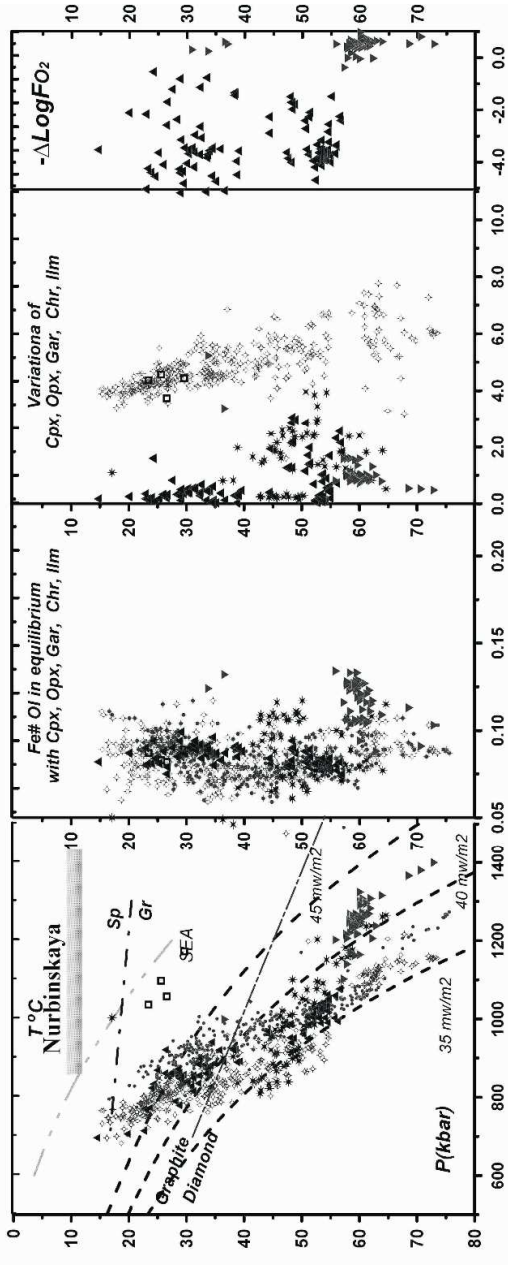

Fig. 7. **PT plots using xenoliths data set for Nyurbinskaya pipe obtained using monomineral thermobarometry.**

Signs are the same.

the HT PT path with the inflection at 40-30 kbar. Ilmenite plot widely disperse at the base of the mantle column forming scattering between 42 to 33mwm-2 geotherms. TP estimates for Ozernaya mantle columns reveal also the base of lithosphere from 70 kbar. The dispersion of TP estimates is higher. Geotherms or TP path reflecting TP path of ilmenite parental melt represent more high temperature conditions then in previous stage. Array of TP values for the ilmenites from the Ottorzhenets (crater boundary phase) trace the 40 mwm-2 geotherm forming 4 separate groups from 65 to 40 kbar coinciding with those determined for garnets. Hence TP conditions determined for three stages show the difference of TP conditions with heating and increasing the degree of scattering also marked by clinopyroxene TP estimates. Comparing the Fe# for the coexisting olivines it is clear that the develoing of magmatism was accompanied by increase of the Fe# especially in the upper pert of mantle column. The late phases contained the differentiation of the mantle column to enriched high-ca compositions and depleted varieties.The example from the Yubileinaya and nearest pipes may be supported by the material from Nakyn filed where the material from the main phase in Nyurbinskaya pipe contain very low fraction of ilmenite which is mainly correspondent the feeders and accompanied deep seated metasomatites with the high Fe#. In mantle column of Botuobinskaya pipe the location in the base is similar but there are some. The materials from the placer show that within the Nakyn field the phase which reflect the more evolved magmatic source exist (Fig. 7-9). The Ilmenite create the polybaric trend in 5 levels which is accompanied by the Fe# increase for clinopyroxenes.

3. Refertilization – depletion events.

Common model of the mantle column based on the Re/Os and other isotopic system suppose a very ancient creation of the lithospheric structure beneath the continents. But these are model ages which reflect the events of rock creation but not a resent magmatic modification events, because the Re/Os is very conservative system. In general the inflection in Cr_2O_3- CaO- trends and increase in Fe# coincides with the clots of TP points for ilmenites. Cr- less ilmenites which are close in isotopy to kimberlites [41] reflect the most clean derivates from the protokimberlite mater together with the Cr- low pyroxenes and Cr- less pyrope garnets. The reaction phases which are commonly Ti – enriched create metasomatic associations constituting the contact zones of the magmatic systems and probably the roofs of the relatively large magmatic sources (chambers). In many xenoliths zones of the of the enrichments are correspondent to the increasing of Fe, which is more typical for the sheared peridotites in the lithosphere base [56] but also is found in the different levels in mantle column including spinel facies. In general this fertilization event corresponds to the evolving of the protokimberlite system and direct contacts with the [38] with the megacrystalline associations support this conclusion. The more ancient enrichment in silica [9] are the attribute

of the subduction – related processes. Possible that hydrous metasomatism

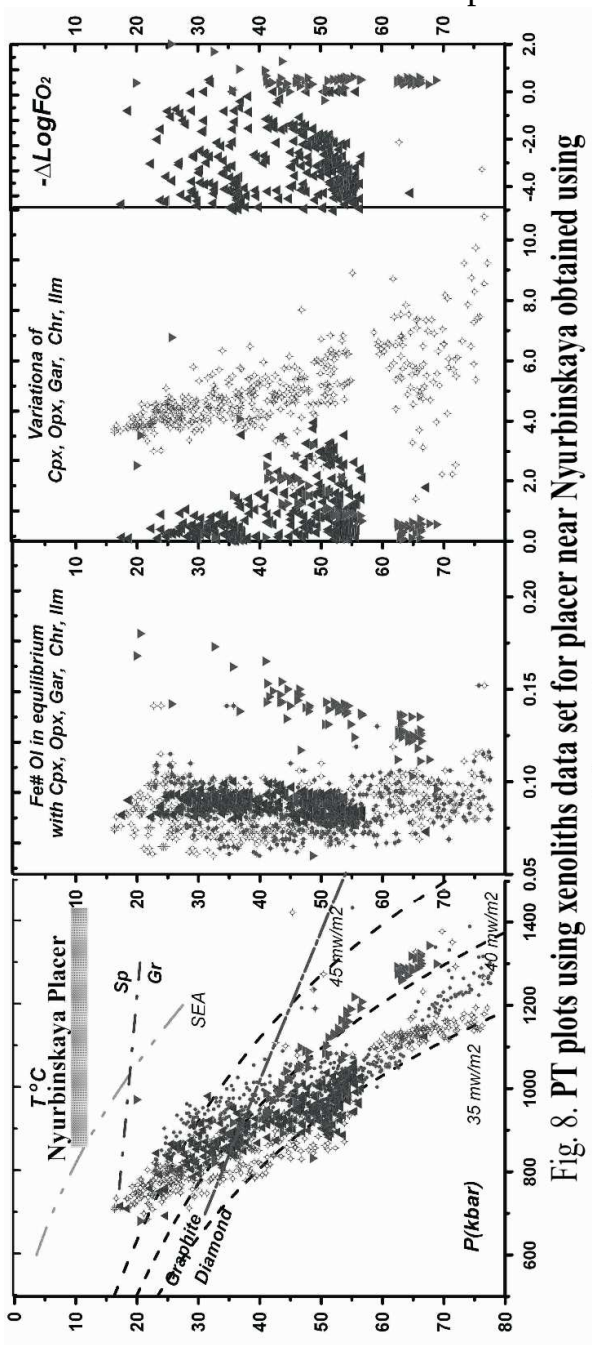

Fig. 8. PT plots using xenoliths data set for placer near Nyurbinskaya obtained using monomineral thermobarometry. Signs are the same.

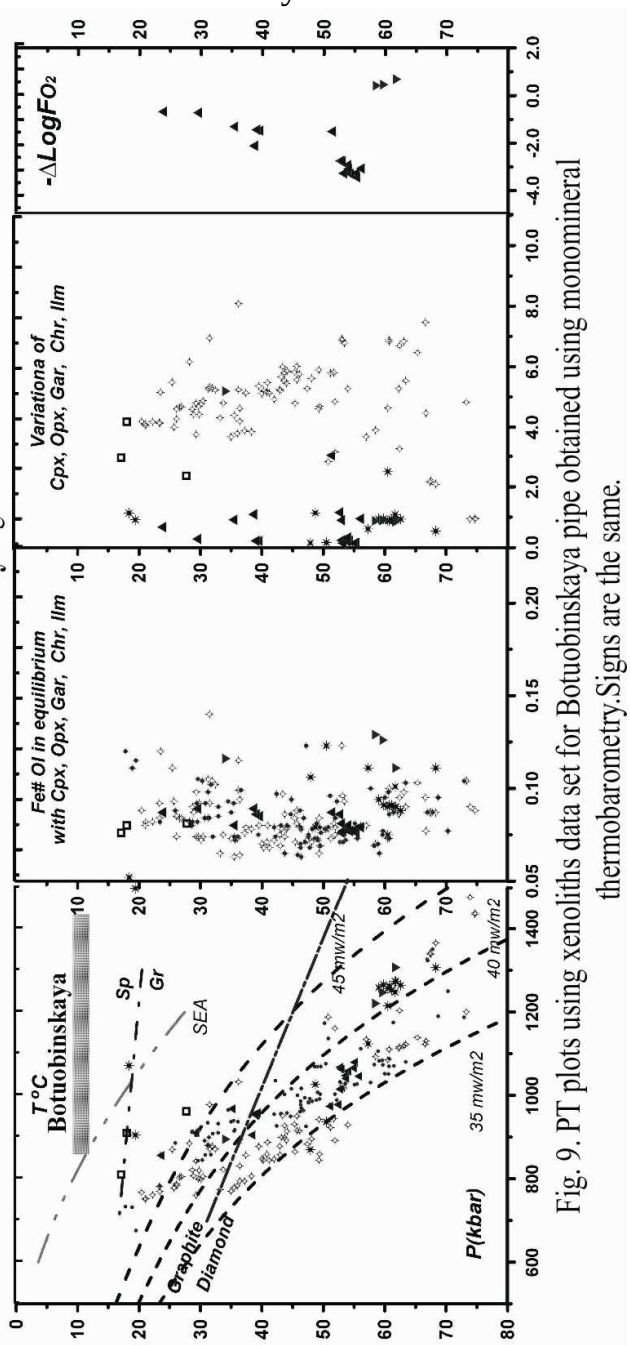

Fig. 9. PT plots using xenoliths data set for Botuobinskaya pipe obtained using monomineral thermobarometry. Signs are the same.

and carbonatitic reflect the other stages of the continental keel modification [60] but it may also accompany the separate pulses of the deeply evolved protokimberlite melts. Geochemical features show that Cr-less ilmenites from megacrysts have the TRE patterns that corresponds to the garnet – free associations, probably dunite veins. The S- type patterns are created by the chromatography due to melt percolation. Mg-Cr rich chromites which never were found in the mantle harzburgites and lherzolites correpogs to the dunites which also are the melt – fluid conduits. They in some lithospheric columns in kimberlite regions Ti rich chromites compile with olivine dunite veins instead for ilmenites

like in Upper Muna. It is likely that some knoringite garnets with the S- type REE patterns are also fragments of the megacrystalline dunite [48] specific veins also.

4. Interaction with the protokimberlites and the problems of the diamond growths.

The thermobarometry of peridotites and mantle inclusions from kimberlites show that clinopyroxenes marks in general not only the low–temperature conductive gradient typical for ancient associations reveling subduction origin but also mark relatively high temperature associations [31] which are close to the TP estimates from ilmenites and other megacrystalline associations. Even the diamond bearing eclogites [45, 54] which show the signs of heating repeat practically TP path of the ilmenite megacrystalls in mantle columns beneath the Udachnaya pipe. The ilmenite bearing associations and multiplied inclusions from the cloudy and other types of diamonds are result of crystallization near the evolving protokimberlite systems. The pulsing character of the melt filtration possibly is the reason of the multistage zonation of the diamonds. The polymict mantle inclusions are possibly a result of the growth in the magmatic breccia surrounding the channels of the melt movement.

CONCLUSIONS

1. Monomineral thermobarometry evidences for the multistage melt percolation events of the protokimberlites within the mantle columns beneath the kimberlite pipes.
2. The heating and fertilization processes as well as the depletion to dunites within the zones of melt movement are accompanied the melt percolation.
3. The productivity of kimberlite pipes possibly is highly influenced by the processes take place not long before the eruption.

REFERENCES

1. **Agee C.B.** Crystal-liquid density inversions in terrestrial and lunar magmas // Physics of the Earth and Planetary Interiors, 1998, v.107, p. 63–74.
2. **Agranier A., Lee C.-T.A.** Quantifying trace element disequilibria in mantle xenoliths and abyssal peridotites // Earth Planet. Sci. Lett., 2007, v. 257, p. 290-298.
3. **Anderson Don L.** New Theory of the Earth, Press. 2006.
4. **Artemieva I.M., Mooney W.D.** On the relations between cratonic lithosphere thickness, plate motions, and basal drag // Tectonophysics, 2002, v. 358, p. 211-231.
5. **Ashchepkov I.V., Andre L.** Pyroxenite xenoliths in picrite basalts (Vitim plateau): origin and differentiation of mantle melts // Russian Geol. Geophys, 2002, v. 43, p. 343-363.
6. **Ashchepkov I.V., Pokhilenko N.P., Vladykin N.V., Rotman A.Y., Afanasiev V.P., Logvinova A.M., Kostrovitsky S.I., Pokhilenko L.N., Karpenko M.A., Kuligin S.S., Malygina E.V., Stegnitsky Y.B., Alymova N.A. Khmelnikova O.S.** Reconstruction of mantle sections beneath Yakutian kimberlite pipes using monomineral thermobarometry // Geol. Soc London, Sp. Pub., 2008, v. 293, p. 335-352.

7. **Ashchepkov I.V., Travin A.V., Saprykin A.I., Andre L., Gerasimov P.A., Khmelnikova O.S.** About the ages of xenoliths bearing basalts in Baikal rift zone // Russsian Geology and Geophysics, 2003, v. 44, № 11, p. 1162-1190.
8. **Ashchepkov I.V.** More precise equation of the Jd-Di barometer // Herald of Earth Sciences department Russian Academy of Sciences, 2003, № 1 (21).
9. **Boyd F.R., Pokhilenko N.P., Pearson D.G., Mertzman S.A., Sobolev N.V., Finger L.W.** Composition of the Siberian cratonic mantle: evidence from Udachnaya peridotite xenoliths // Contrib. Mineral. Petrol., 1997, v. 128, p. 228-246.
10. **Brey G.P., Kohler T.** Geothermobarometry in four-phase lherzolites. II. New thermobarometers, and practical assessment of existing thermobarometers // Journal of Petrology, 1990, v. 31, p. 1353-1378.
11. **Condie K.C.** Continental growth during a 1.9-Ga superplume event // Journal of Geodynamics, 2002, v. 34, p.249 –264.
12. **Garfunkel Z.** Formation of continental flood volcanism — The perspective of setting of melting // Lithos, 2008, v. 100, p. 49–65.
13. **Gibson S.A., Thompson R.N., Leonardos O.H., Dickin A.P., Mitchell J.G.** The late Cretaceous impact of the Trindade mantle plume: evidence from large-volume, mafic, potassic magmatism in SE Brazil // J. Petrol., 1995, v. 36, p. 189–229.
14. **Griffin W.L., Spetsius Z.V., Pearson N.J., O'Reilly S.Y.** In situ Re–Os analysis of sulfide inclusions in kimberlitic olivine: New constraints on depletion events in the Siberian lithosphere // Geochem. Geophys. Geosyst., 2002, v. 3, p. 1069, doi:10.1029/2001GC000287.
15. **Griffin W.L., Ryan C.G., Kaminsky F.V., O'Reilly S.Y., Natapov L.M., Win T.T., Kinny P.D., Ilupin I.P.** The Siberian lithosphere traverse: Mantle terranes and the assembly of the Siberian Craton // Tectonophysics. 1999a, v. 310, p. 1–35.
16. **Griffin W.L., Cousens D.R., Ryan C.G., Sie S.H., Suter G.F.** Ni in chrome pyrope garnets: a new thermometer // Contrib. Mineral. Petrol., 1989, v. 103, p. 199–203.
17. **Griffin W.L., Fisher N.I., Friedman J., Ryan C.G., O'Reilly S.Y.** Cr–pyrope garnets in the lithospheric mantle. I. Compositional systematics and relations to tectonic setting // J. Petrol. 1999b, v. 40, p. 679–704.
18. **Griffin W.L., Natapov L.M., O'Reilly S.Y., van Achterbergh E., Cherenkov A.F., Cherenkov V.G.** The Kharamai kimberlite field, Siberia: Modification of the lithospheric mantle by the Siberian Trap event // Lithos, 2005, v. 8, № 1, p. 167– 187.
19. **Griffin W.L., O'Reilly S.Y., Abe N., Aulbach S., Davies R.M., Pearson N.J., Doyle B.J., Kivi K.** The origin and evolution of the Archaean lithospheric mantle // Precambrian Research, 2003, v. 127, p. 19–41.
20. **Heaman L.M., Kjarsgaard B.A., Creaser R. A.** The temporal evolution of North American kimberlites // Lithos, 2004 , v. 76, p. 377– 397.
21. **Humphreys E.D., Dueker K.G, Schutt D.L., Smith R.B.** Beneath Yellowstone: Evaluating plume and nonplume models using teleseismic images of the upper mantle // GSA Today, 2000, p. 123, 1-7.
22. **Ionov D.A., Hofmann A.W.** Depth of formation of subcontinental off-craton peridotites // Earth Planet. Sci. Lett., 2007, v. 261, p. 620–634.
23. **King S.D.** Archean cratons and mantle dynamics // Earth Planet. Sci. Lett., 2005, v. 234, p. 1-14.
24. **Kostrovitsky S.I., Morikiyo T., Serov I.V., Yakovlev D.A., Amirzhanov A.A.** Isotope-geochemical systematics of kimberlites and related rocks from the Siberian Platform // Russian Geol. Geophys., 2007, v. 48, № 3, p. 272-290.
25. **Krogh E.J.** The garnet-clinopyroxene Fe-Mg geothermometer - a reinterpretation of existing experimental data // Contrib. Mineral. Petrol., 1988, v. 99, p. 44-48.

26. **Lee C.-T., Rudnick R.L.** Compositionally stratified cratonic lithosphere and geochemistry of peridotitic xenoliths from the Labait volcano Tanzania // Proceedings of the VII international Kimberlite Conference. The P.H. Nixon volume, 1999, p. 728-735.
27. **Lee C.-T.A., Lenardic A., Cooper F., Niu C.M., Levander A.** The role of chemical boundary layers in regulating the thickness of continental and oceanic thermal boundary layers // Earth Planet. Sci. Lett., 2005, v. 230, p. 379-395.
28. **Lehtonen M.L., O'Brien H.E., Peltonen P., Johanson B.S., Pakkanen L.K.** Layered mantle at the Karelian Craton margin: P-T of mantle xenocrysts and xenoliths from the Kaavi-Kuopio kimberlites, Finland // Lithos, 2004, v. 77., p. 593-608.
29. **Litasov K.D., Kagi H., Shatskiy A, Ohtani E., Lakshtanov D.L., Bass J. D., Ito E.** High hydrogen solubility in Al-rich stishovite and water transport in the lower mantle // Earth Plan. Sci. Lett., 2007, v. 262, № 3-4, p. 620-634.
30. **Litasov K.D., Ohtani E., Ghosh S., Nishihara Y., Suzuki A., Funakoshi K.** Thermal equation of state of superhydrous phase B to 27GPa and 1373K // Physics of the Earth and Planetary Interiors, 2007, v. 164, № 3, p. 142-160.
31. **Logvinova A.M., Ashchepkov I.V.** Thermobarometry of diamond inclusions in Yakutian kimberlites // Geochim. Cosmochim Acta, Sp. Suppl., 2008, (in press).
32. **Logvinova A.M., Taylor L.A., Floss C., Sobolev N.V.** Geochemistry of multiple diamond inclusions of harzburgitic garnets as examined in situ // Int. Geol Rev., 2005, v. 47, p. 1223-1233.
33. **Lustrino M., Wilson M.** The Circum-Mediterranean anorogenic Cenozoic igneous province // Earth Science Reviews, 2007, v. 81, p. 1-65.
34. **Macdonald R., Rogers N.W, Fitton J.G., Black S., Smith M.** Plume-lithosphere interactions in the generation of the basalts of the Kenya Rift, East Africa // Journal of Petrology, 2001, v. 42, № 5, p. 877-900.
35. **Mahotkin I.L., Gibson S.A., Thompson R.N., Zhuravlev D.Z., Zherdev P.U.** Late Devonian Diamondiferous Kimberlite and alkaline picrite (proto-kimberlite) magmatism in the Archangelsk region, NW Russia // Journal of Petrology, v. 41, p. 201-212.
36. **Maruyama S., Santosh M., Zhao D.** Superplume, supercontinent, and post-perovskite: Mantle dynamics and anti-plate tectonics on the Core–Mantle Boundary // Gondwana Research, 2007, v. 11, p. 7–37.
37. **McGregor I.D.** The system MgO- SiO_2- Al_2O_3: solubility of Al_2O_3 in enstatite for spinel and garnet peridotite compositions // Amer. Mineral., 1974, v. 59, p. 110-119.
38. **Moore A.E., Lock N.P.** The origin of mantle-derived megacrysts and sheared peridotites-evidence from kimberlites in the northern Lesotho Orange Free State (South Africa) and Botswana pipe clusters // S. Afr. J. Geol., 2001, v. 104, № 1, p. 23-38.
39. **Moore R.O., Griffin W.L., Gurney J.J., Ryan C.G., Cousens D.R., Sie S.H., Suter G.F.** Trace element geochemistry of ilmenite megacrysts from the Monastery kimberlite, South Africa // Lithos, 1992, v. 29, p. 1-1 8.
40. **Nimis P., Taylor W.** Single clinopyroxene thermobarometry for garnet peridotites. Part I. Calibration and testing of a Cr-in-Cpx barometer and an enstatite-in-Cpx thermometer // Contrib. Mineral. Petrol., 2000, v. 139, № 5, p. 541-554.
41. **Nowell G.M., Pearson D.G., Bell D.R., Carlson R.W., Smith C.B., Kempton P.D., Noble S.R.** Hf Isotope Systematics of Kimberlites and their Megacrysts: New Constraints on their Source Regions // J. Petrology, 2004, v. 45, p. 1583-1612.
42. **O'Neill H.St., Wall V.J.** The olivine orthopyroxene-spinel oxygen geobarometer, the nickel precipitation curve, and the oxygen fugacity of the Earth's upper mantle // Journal of Petrology, 1987, v. 28, p. 1169-1191.

43. **O'Reilly S.Y., Griffin W.L.** Imaging global chemical and thermal heterogeneity in thein the subcontinental lithospheric mantle with garnets and xenoliths: Geophysical implications // Tectonophysics, 2006, v. 416, p. 289–309.
44. **Parman S.W.** Helium isotopic evidence for episodic mantle melting and crustal growth // Nature, 2007, v. 446, p. 900-903.
45. **Pasyanos M.E., Nyblade A.A.** A top to bottom lithospheric study of Africa and Arabia // Tectonophysics, 2007, v. 444, p. 27-44.
46. **Pearson D.G., Snyder G.A., Shirey S.B., Taylor L.A., Carlson R.W., Sobolev N.V.** Archaean Re-Os age for Siberian eclogites and constraints on Archaean tectonics // Nature, 1995, v. 374, p. 711-713.
47. **Pearson D.G.** The age of continental roots // Lithos, 1999, v. 48, p. 171-194.
48. **Pokhilenko N.P., Sobolev N.V., Kuligin, S.S., Shimizu N.** Peculiarities of distribution of pyroxenite paragenesis garnets in Yakutian kimberlites and some aspects of the evolution of the Siberian craton lithospheric mantle // Proceedings of the VII International Kimberlite Conference, 2000, the P.H. Nixon volume, p. 690-707.
49. **Pokhilenko N.P., Pearson D.G., Boyd F.R., Sobolev N.V.** Megacrystalline dunites: sources of Siberian diamonds / Carnegie Inst. Wash. 1991, yearb. 90: p. 11-18.
50. **Rudnick R.L., Nyblade A.A.** The thickness and heat production of Archean lithosphere: Constraints from xenolith thermobarometry and surface heat flow, in Mantle Petrology: Field Observations and High Pressure Experimentation: A Tribute to Francis R.(Joe) Boyd, edited by Y. Fei, C. Bertka, and B.O. Mysen // Geochem. Soc., 1999, p. 3-12.
51. **Rudnick R.L., McDonough W.F., O'Connell R.J.** Thermal structure, thickness and composition of continental lithosphere // Chem. Geol. 1998, v. 145, p. 395–411.
52. **Ryan C.G., Griffin W.L., Pearson N.J.** Garnet geotherms: Pressure-temperature data from Cr-pyrope garnet xenocrysts in volcanic rocks // J. Geophys. Res. B., 1996, v. 101, № 3, p. 5611-5625.
53. **Sobolev A.V., Hofmann A.W., Sobolev S.V., Nikogosian, I.K.** An olivine-free mantle source of Hawaiian shield basalts // Nature, 2005, v. 434, p. 590-597.
54. **Sobolev N.V., Logvinova A.M., Zedgenizov D.A., Seryotkin Y.V., Yefimova E.S., Floss C., Taylor L.A.** Mineral inclusions in microdiamonds and macrodiamonds from kimberlites of Yakutia: a comparative study // Lithos, 2004, v. 77, iss. 1-4, p. 225-242.
55. **Sobolev V.N., Taylor L.A., Snyder G.A., Sobolev N.V.** Diamondiferous eclogites from the Udachnaya pipe, Yakutia // International Geology Review, 1994, v. 36, № 1, p. 42-64.
56. **Sobolev N.V.** Deep-Seated Inclusions in Kimberlites and the Problem of the Composition of the Upper Mantle. Am. Geophys. Union, Washington, D.C. 1977.
57. **Solov'eva L.V., Lavrent'ev Yu.G., Egorov K.N., Kostrovitskii S.I., Korolyuk V.N., Suvorova L.F.** The genetic relationship of the deformed peridotites and garnet megacrysts from kimberlites with asthenospheric melts // Russian Geology and Geophysics, 2008, v. 49, № 4, p. 207-204.
58. **Spetsius Z.V., Belousova E.A., Griffin W.L., O'Reilly S.Y., Pearson N.J.** Archean sulfide inclusions in Paleozoic zircon megacrysts from the Mir kimberlite, Yakutia: implications for the dating of diamonds // Earth Planet Sci. Lett., 2002, v. 199, № 1-2, p. 111-126.
59. **Suzuki A., Ohtani E., Morishima H., Kubo T., Kanbe Y., Kondo T., Okada T., Terasaki H., Kato T., Kikegawa T.** In situ determination of the phase boundary between wadsleyite and ringwoodite in Mg_2SiO_4 // Geophys. Res. Lett., 2000, v. 27, p.803–806.
60. **Tappe S., Foley S.F., Stracke A., Romer R.L., Kjarsgaard B.A., Heaman L.M., Joyce N.** Craton reactivation on the Labrador Sea margins: $^{40}Ar/^{39}Ar$ age and Sr-Nd-Hf-

Pb isotope constraints from alkaline and carbonatite intrusives // Earth Planet. Sci. Lett., 2007, v. 256, p. 433-454.
61. **Wilson M., Downes H.** Tertiary-Quaternary intra-plate magmatism in Europe and its relationship to mantle dynamics / In: Gee, D. & Stephenson, R. (eds.) Geological Society, London, 2006, Memoirs 32, p. 147-166.
62. **Wirth R., Rocholl A.** Nanocrystalline diamond from the Earth's mantle underneath Hawaii // Earth Planet. Sci. Lett., 2003, v. 211, № 3, p. 357-369.
63. **Wyman D.A., Ayer J.A., Conceição R.V., Sage R.P.** Mantle processes in an Archean orogen: Evidence from 2.67 Ga diamond-bearing lamprophyres and xenoliths // Lithos, 2006, v. 89, iss. 3-4, p. 300-328.

УДК 549.0; 552.3

Fluid regime peculiarities of the lithosphere mantle of the Siberian platform

Pokhilenko L.N., Pokhilenko N.P., Fedorov I.I., Tomilenko A.A., Usova L.V., Fomina L.N.

Sobolev Institute of Geology and Mineralogy SB RAS, Russia, e-mail: lu@uiggm.nsc.ru

ABSTRACT

Xenoliths of different genesis from diamondiferous kimberlite pipes of Yakutia (Udachnaya, Mir) and nondiamondiferous kimberlite pipe Obnazhennaya have been studied. The microprobe analysis of their components has been made with the use of a CAMEBAX-MICRO X-ray microprobe (CAMECA, France) and the P-T conditions of equilibrium of these rocks have been determined using the programs TEMPEST and TERRA. The volatiles from the minerals of mantle xenoliths have been analyzed on a setup, assembled from three standard gas chromatographs LXM-80 and equipped with original device for thermic extraction of gases. This setup makes it possible to determine simultaneously all gases of interest (CO_2, H_2O, CH_4, H_2, N_2, CO, O_2, C_2-C_n) from the same sample. The chromatographic data have been recalculated into the P-T conditions of equilibrium of our rocks. The calculations have been made for C-O-H system in the presence of solid carbon using the HCh code, which employs the minimization of Gibbs's free energy method. Basing on the results of calculation we can conclude that the main mantle fluid components of the studied xenoliths are H_2O and CO_2 or CH_4. The oxygen fugacity fields of the studied rocks are situated near the buffer equilibrium WM. Redox characteristics of xenoliths are discussed with consideration for their position in vertical cross section of the upper mantle, where the general trend has been toward the elevation of the samples recovery as their origin depth increases. The action of metasomatism on the oxidation of rocks is observed.

INTRODUCTION

The results of petrologic, geochemical and isotope-geochemical studies of the deep-seated rock xenoliths in kimberlites obtained in the last decades demonstrated both a variety of their types [28, 7, 31, 21, 22, 29, 10], and complicated multi-stage character of the lithosphere mantle substrate evolution [27, 20]. The data on diamond inclusions [17, 4, 30, 24, 9, 15, 8, 14] and a bare handful of mantle rocks in kimberlites and alkaline basalts however limit information on the composition of volatile components and the upper mantle redox conditions [11, 1, 6, 12, 13, 26]. We have studied 160 xenoliths of different paragenetic types from the diamondiferous kimberlite pipes Udachnaya (133 samples), Mir (11 samples) and diamond-free Obnazhennaya pipe (16 samples) to create a real (objective) model of the fluid regime in the profile of the Siberian platform lithosphere mantle. An effort has been made to construct a mantle profile with regard to fO_2 of rocks.

EXPERIMENTAL TECHNIQUES

CAMEBAX-MICRO microprobe analyzer of French company CAMECA was used to analyze chemical composition of mineral phases of rocks. Natural minerals of the compositions, which most closely resemble the compositions of the expected phases, were used as standards. P-T parameters of xenoliths formation were calculated from the microprobe data. The calculations were carried out by TEMPEST program of A.A. Finnerti which later improved by T.M. Blinchik and by TERRA program designed by I.V. Aschepkov [2, 3].

The composition of volatiles from the mantle rock xenoliths was analyzed by gas chromatography on the unique setup, which admits of determination of all gases (CO_2, H_2O, CH_4, H_2, N_2, CO, O_2, C_2-C_n,) from one probe of powder-like

materials simultaneously. The setup and analytical procedure are detailed in Osorgin [18]. Chromatographic setup calibration made by the introduction of certain amounts of pure gases made it possible to determine the following error: CO_2, C_2-C_n, N_2, CO, CH_4 – 2 rel.%; H_2, H_2O – 10 rel.%. The charge (300mg) was inserted into the V-like quartz tube, blown by helium and heated up to 200°C. The released gases were removed to avoid the affect of the surface-adsorbed gases on the results of analyses. The sample was subsequently quenched in two stages: 10 min. at 600°C and 10 min. after 1 min. break at 1000°C. Gas phase, released at each stage, was analyzed in chromatograph.

Table 1a.

Representative microprobe analyses (wt.%) of garnet from the xenoliths of the studied rocks of the Udachnaya (UV), Mir (M), Obnazhennaya (O) pipes.

sample	Para-genesis	SiO_2	TiO_2	Al_2O_3	Cr_2O_3	FeO	MnO	MgO	CaO	Na_2O	Total
UV574/89	d	41.8	0.02	17.1	8.72	7.14	0.45	21.97	2.6	0.004	99.85
UV39/89	d	41.7	0.01	15.12	11.16	7.1	0.46	22.77	1.2	0.02	99.57
UV17/91	h	42.1	0.017	17.77	7.61	7.08	0.36	23.07	1.39	0.038	99.42
UV467/89	gsl	41.6	0	20.19	4.1	7.64	0.42	19.16	6.06	0.058	99.16
UV531/89	gl	41.5	0	19.27	5.38	8.11	0.44	18.38	6.18	0	99.21
M120/72	gl	42.5	0.126	22.02	1.96	7.29	0.31	20.59	4.82	0.062	99.72
UV79/89	dp	41.2		17.23	9.01	7.19		19.21	6.17		100
UV448/89	dp	42.2	0.572	17.72	6.38	6.8	0.29	20.82	4.73	0.092	99.61
UV-13/91	dp	42.1	0.72	20.32	0.99	13.03		17.93	4.69	0.05	99.83
UV464/86	ecl	39	0.458	20.97	0.051	22.7	0.46	6.89	9.26	0.158	99.95
O/283	ecl	41.8	0.04	23.9	0.17	13	0.37	13.7	7.22	0.05	100.3
M1/88	ecl	41.8	0.16	22.88	0.05	11.85	0.3	18.43	3.98	0.09	99.54
O/407	pyrox	42.6	0.11	23.22	0.6	8.46	0.33	20.93	4.18	0.033	100.5
M31/01	pyrox	42	0.14	22.21	1.41	9.63	0.61	19.08	4.41	0.062	99.51
UV11/99	pyrox	41.1	0.61	21.28	0.357	14.61	0.34	16.48	4.44	0.107	99.37

Note: Paragenesis: d - dunite, h - harzburgite, gsl – garnet-spinel lherzolite, gl – garnet lherzolite, dp – deformed peridotite, ecl – eclogite, pyrox – pyroxenite.

Data were obtained using CAMEBAX-MICRO x-ray microprobe analyzer of French company CAMECA in Laboratory of x-ray microprobe analysis of Institute Geology and Mineralogy SB RAS (operator L.V. Usova).

Table 1 b.

Representative microprobe analyses (wt.%) of pyroxene from the xenoliths of the studied rocks of the Udachnaya (UV), Mir (M), Obnazhennaya (O) pipes

sample	Para-genesis	mineral	SiO_2	TiO_2	Al_2O_3	Cr_2O_3	FeO	MnO	MgO	CaO	Na_2O	K_2O	Total
UV17/91	h	Opx	57.99	0.007	0.351	0.22	4.36	0.087	36.54	0.094	0.037		99.68
UV562/89	sl	Opx	56.51	0.025	2.73	0.573	4.89	0.113	35.53	0.34	0.043		100.75
UV536/89	sl	Opx	56.54	0.014	2.51	0.475	4.86		35.22	0.32	0.008		99.95
UV467/89	gsl	Opx	58.03	0.057	0.86	0.349	4.43		35.63	0.45	0.06		99.85
UV531/89	gl	Opx	57.96	0	0.93	0.369	4.84	0.152	34.8	0.45	0.051		99.54
M120/72	gl	Opx	57.3	0.069	1.29	0.386	4.31	0.06	36.21	0.208	0.043	0.004	99.87
UV79/89	dp	Opx	57.77	0.169	0.56	0.438	5.32		34.42	0.89	0.235		99.797
UV448/89	dp	Opx	57.79	0.069	0.64	0.368	5.02	0.131	34.01	0.9	0.271	0.049	99.25
O/407	pyrox	Opx	58.29	0.11	1.11	0.15	4.41	0.07	35.31	0.24	0.04		99.73
UV562/89	sl	Cpx	53.76	0.061	3.36	1.42	1.49	0.07	15.87	21.89	1.48		99.401
UV536/89	sl	Cpx	53.8	0.003	2.45	0.841	1.6		17.23	23.1	0.455		99.48
UV467/89	gsl	Cpx	55.31	0.108	1.61	1.28	1.09		16.99	22.45	1.15		99.99
UV531/89	gl	Cpx	54.82	0.034	1.65	1.45	1.45	0.108	16.41	22.11	1.13		99.24
M120/72	gl	Cpx	54.22	0.562	5.71	1.4	1.47	0.047	13.8	19.56	2.9	0.006	99.68
UV79/89	dp	Cpx	55.03	0.292	1.34	1.63	3.3		18.45	17.57	1.63		99.242
UV448/89	dp	Cpx	55.17	0.39	2.05	1.75	3.3	0.134	18.19	16.39	2.08	0.021	99.47
UV-13/91	dp	Cpx	55.04	0.236	1.78	0.322	4.76		17.03	19.3	1.6		100.06
UV464/86	ecl	Cpx	54.65	0.502	6.38	0.406	7.64	0.069	10.12	16.21	4.23	0.035	100.242
O/283	ecl	Cpx	53.2	0.19	8.72	0.16	2.55	0.03	11.5	19.1	3.51		98.96
M1/88	ecl	Cpx	56.85	0.46	8.51	0.05	2.26	0.04	11.13	15.05	5.58	0.01	99.95
O/407	pyrox	Cpx	55.04	0.45	8.08	0.62	1.9	0.03	12.85	18.2	3.46		100.61
M31/01	pyrox	Cpx	55.23	0.12	2.04	0.89	2.41	0.07	16.17	20.98	1.8	0.002	99.71
UV11/99	pyrox	Cpx	55.45	0.262	2.98	0.178	5.09	0.099	15.39	17.65	2.52	0.032	99.65

Note: Paragenesis: h - harzburgite, sl – spinel lherzolite, gsl – garnet-spinel lherzolite, gl – garnet lherzolite, dp – deformed peridotite, ecl – eclogite, pyrox – pyroxenite.

Data were obtained using CAMEBAX -MICRO x -ray microprobe analyzer of French company CAMECA in Laboratory of x -ray microprobe analysis of Institute Geology and Mineralogy SB RAS (operator L.V. Usova).

Equilibrium molecular composition of fluids at P-T parameters of xenoliths formation was calculated from chromatographic data by minimization of the system free energy according to HCh program designed by Yu.V. Shvarov (MSU, Geological department). The values of Gibbs free energy and oxygen fugacity for iron-wustite (IW), wustite-magnetite (WM), graphite-CO-CO2(CCO) buffer equilibriums were taken from Chepurov et al. [5]. Oxygen fugacity of the rocks was calculated from the obtained data by $fO_2=P*X_{O2}*\gamma$, where P – total pressure, X_{O2} – oxygen mole fraction, γ – oxygen fugacity coefficient. Calculations of fluid

Table 1c.

Representative microprobe analyses (wt.%) of olivine, spinel and picroilmenite from the xenoliths of the studied rocks of the Udachnaya (UV) and Mir (M) pipes.

sample	Para-genesis	mineral	SiO_2	TiO_2	Al_2O_3	Cr_2O_3	FeO	MnO	MgO	CaO	Na_2O	NiO	Total
UV574/89	d	Ol	41.51			0.032	7.18	0.089	51.03	0.01		0.343	100.19
UV39/89	d	Ol	41.46			0.017	6.96	0.1	51.37	0		0.337	100.24
UV17/91	h	Ol	41.26			0.027	7.4	0.082	50.81	0.007		0.339	99.92
UV562/89	sl	Ol	41.41			0.008	7.68	0.104	50.19	0.01		0.383	99.78
UV536/89	sl	Ol	40.95			0	7.66	0.097	50.55	0.01		0.344	99.62
UV467/89	gsl	Ol	41.45			0.01	7.33	0.089	50.63	0.01		0.421	99.93
UV531/89	gl	Ol	41.61			0	7.5	0.097	50.46	0.01		0.347	100.02
M120/72	gl	Ol	40.91	0	0	0.009	7.64	0.105	50.38	0.006	0	0.403	99.46
UV79/89	dp	Ol	41.02			0.05	8.93	0.112	49.34	0.04		0.349	99.84
UV448/89	dp	Ol	41.47			0.053	7.89	0.118	50.03	0.04	0.043	0.32	99.92
UV-13/91	dp	Ol	39.59			0.001	14.15	0.159	45.65	0.032		0.141	99.72
UV39/89	d	Sp		0.063	4.95	63.73	18.77		12.01				99.52
UV562/89	sl	Sp		0.07	34.47	33.29	16.68	0.21	14.79			0.12	99.63
UV536/89	sl	Sp		0.011	38.11	30.46	13.95		17.23				99.76
UV467/89	gsl	Sp		0.893	7.85	59.45	18.79		12.58				99.55
UV-13/91	dp	Picro		50.97	0.35	0.58	36.6	0.2	10.78			0.07	99.55
UV11/99	pyrox	Picro	0	49.18	0.646	1.02	39.34	0.228	9.6	0	0		100.15

Note: Ol - olivine, Sp - spinel, Picro – picroilmenite. Paragenesis: d – dunite, h - harzburgite, sl – spinel lherzolite, gsl – garnet-spinel lherzolite, gl – garnet lherzolite, dp – deformed peridotite, pyrox – pyroxenite.

Data were obtained using CAMEBAX-MICRO x-ray microprobe analyzer of French company CAMECA in Laboratory of x-ray microprobe analysis of Institute of Geology and Mineralogy SB RAS (operator L.V. Usova).

components start from assumption that the systems are closed and hence H/(OH) ratios do not change in any reactions between the system components during temperature and pressure drop, as rocks are exposed at the surface. An excess-free carbon fluid equilibrium was the second important event, which occurred in the lithosphere of cratons during their stabilization according to D. Pearson and coauthors [19].

RESULTS

Table 1 (a, b, c) demonstrates the most representative microprobe analyses of minerals from the xenoliths of the studied rocks of ultrabasic (harzburgite-dunites,

spinel and garnet peridotites, deformed (sheared) peridotites) and basic (eclogites, pyroxenites) parageneses. Chromatographic analyses of monomineral fractions of typical representatives of all groups of xenoliths under study and calculated H/(O+H) values, which characterize redox conditions of the rocks formation, are given in Table 2. Table 3 shows the calculated fluid component composition in equilibrium with the studied rocks. H/(O+H) ratios of the mantle rocks fall in most cases within 0.60-0.68 and rarely decrease up to 0.53-0.58. In three sheared peridotites (UV-448/89, UV-495/89, UV-242/89) this ratio is 0.3-0.4 (Table 2),

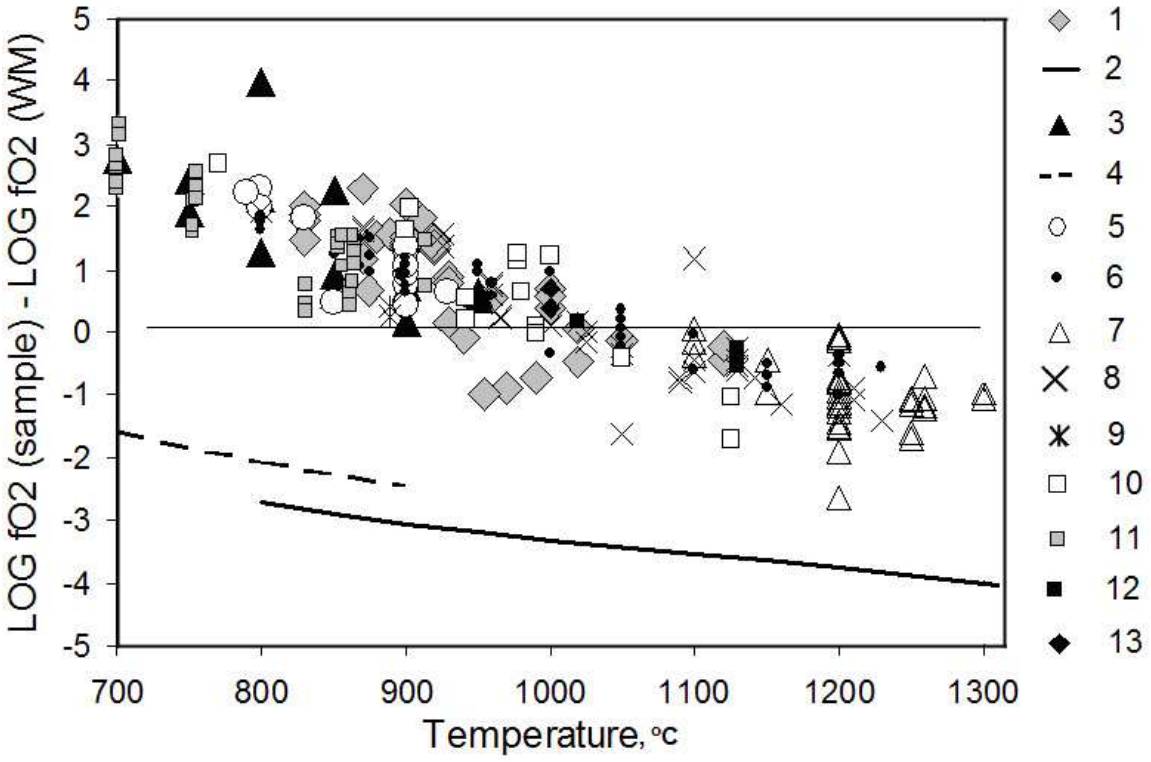

Fig. 1. **Temperature dependence of oxygen fugacity for the xenoliths of harzburgite-dunites, deformed (sheared) peridotites of the Udachnaya pipe, eclogites and pyroxenites of the Udachnaya, Mir and Obnazhennaya pipes, garnet peridotites of the Udachnaya and Mir pipes (assigned to the standard buffer WM).**

1 - harzburgite-dunites of Udachnaya pipe; 2 - buffer WM (P=5G Pa); 3 - spinel peridotites of Udachnaya pipe; 4 - buffer WM (P=2G Pa); 5 - garnet-spinel peridotites of Udachnaya pipe; 6 - garnet peridotites of Udachnaya, Mir pipes; 7 - deformed (sheared) peridotites of Udachnaya pipe; 8 - eclogite of Udachnaya pipe; 9 - eclogites of Obnazhennaya pipe; 10 - piroxenites of Udachnaya, Mir pipes; 11 - piroxenites of Obnazhennaya pipe; 12 - diamondiferous eclogites; 13 - diamondiferous dunite.

that is indicative of a high oxidation of the samples and consequently the calculations show abnormally high content of carbon dioxide in the equilibrium fluid (Table 3). H/(O+H) = 0.78 (Table 2) in sheared peridotite UV-79/89, i.e. it was formed under reduction conditions and methane content in the fluid is higher than carbon dioxide and only water content is lower (Table 3). By and large among the ultrabasic paragenesis of xenoliths from the kimberlite pipes of the Siberian

platform the highest average value H/(O+H) 0.65 is characteristic of harzburgite-dunites, 0.64 of the grained peridotites, 0.63 of sheared peridotites and 0.65 of the basic parageneses of the Yakutian pipes.

Mole fractions of the main fluid components were calculated for all minerals of xenoliths in hand. As for harzburgite-dunites, we had olivine and sometimes garnet. Calculations for spinel and garnet-spinel lherzolites were made only for olivine. Pyroxenes were added to the calculations for garnet lherzolites and sheared peridotites. The compositions of fluid systems of nearly half of eclogites and vast majority of pyroxenites were calculated from chromatographic analysis of garnet and pyroxene. In most cases the calculated values of oxygen fugacity and fluid component composition coincide for the coexisting minerals.

Fig. 1 shows fO_2 of all the xenoliths calculated from chromatographic analysis for P-T conditions of rocks equilibrium and assigned to the standard buffer WM. Oxygen fugacities of the majority of samples are similar to the buffer WM and differ at most by two log units. Spinel lherzolites are the most oxidized of the studied ultrabasic rocks. Their field falls above the WM buffer like the field of garnet-spinel lherzolites. The field of the deepest complex of mantle xenoliths – deformed peridotites falls below zero-point (WM). Harzburgite-dunites are intermediate between the fields of the garnet-spinel lherzolites and deformed peridotites. The field of gannet peridotites with broad temperature range are both above and below the WM buffer. It completely overlaps with the fields of sheared peridotites, harzburgite-dunites and the most part of spinel lherzolites. Eclogites and pyroxenites of the diamond-free pipe Obnazhennay are the most oxidized rocks of basic parageneses, their fields completely fall above the WM buffer. Fugacity values of diamondiferous eclogites from Udachnaya and Mir pipes are in the area of WM buffer equilibrium. Diamondiferous dunite from the Udachnaya pipe is spaced close to them but in more oxidized area.

DISCUSSION

Pokhilenko and coauthors [23] presented a model of the mantle profile of the center of Siberian platform in the Paleozoic time (Fig.2-I) and the northeastern part in the Mesozoic time (Fig. 3-I). By this model spinel lherzolites with only a few of garnet pyroxenites and rare eclogites are dominant in the central regions (middle-Paleozoic time) immediately under the Moho boundary, which is the crust-mantle transitional zone. Garnitization of peridotites begins from the depths of 65-70 km (P=1,7-2,0 GPa) initiating the formation of pyrope-spinel peridotites, which coexist with highly depleted chromite-containing peridotites. Alternating associations of chromite-pyrope and pyrope peridotites are dominant in the lithosphere mantle from the depths of 80-100 km. Chrome-pyrope harzburgites and dunites dominate in the mantle section from 120 to approximately 180 km. Harzburgite-dunites become less depleted from a depth of 180 km and depleted lherzolites appear. The root parts of lithosphere mantle from 200-210 km to the

lithosphere - convecting asthenosphere transitional zone are represented by deformed (sheared) peridotites with petrochemical and geochemical signs of secondary enrichment due to metasomatic effect of fluids and melts of asthenospheric origin [23, 25].

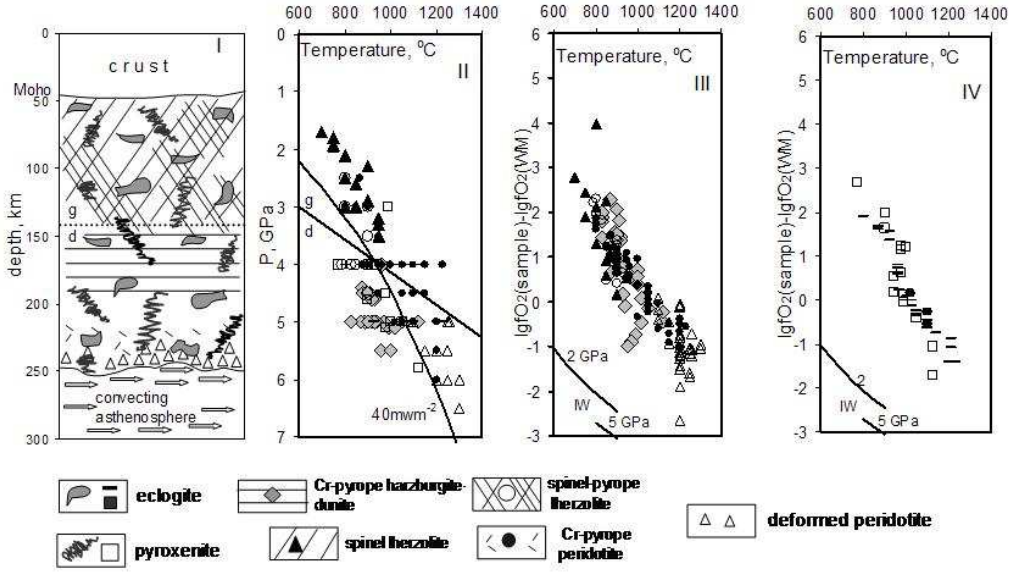

Fig. 2. **Vertical cross sections: I – mantle profile of the center of Siberian platform in the Paleozoic time [27], II – P-T parameters of the equilibrium of the mantle rocks, III – oxygen fugacity for the xenoliths of ultrabasic paragenesis of the Udachnaya and Mir pipes, IV – oxygen fugacity for the xenoliths of basic paragenesis of the Udachnaya and Mir pipes.**

Fig. 2 also demonstrates our determinations of P-T parameters of the equilibrium of the mantle rocks from the Udachnaya and Mir pipes of the same regions (Fig.2-II) and a diagram of temperature dependence of oxygen fugacity for the xenoliths of both ultrabasic (Fig. 2-III) and basic (Fig. 2-IV) paragenesis of the Udachnaya and Mir pipes. The diagram of P-T parameters of rocks equilibrium and $\Delta \lg fO_2$–T,C diagrams are patterned parallel to the mantle cross section to correlate pressure with depth and oxygen fugacity field of the rocks – with their position in the cross section. Similar diagrams for the rocks of the northeastern margin of the Siberian platform in the Mesozoic era are given in Fig. 3.

The deepest rocks - sheared peridotites show greater variations in $\Delta \lg fO_2$, than expected having regard to their position in the mantle cross section (Fig. 2-III). This can be explained by the different degree of metasomatic effect on the rock group. Deep astenospheric fluids, which penetrated along the cracks of weak zones, interacted with a part of the deformed sheared peridotites. The fluids oxidize them to such a degree that CO_2 amount compared favorably to the amount of H_2O (UV-448/89, UV-495/89, UV-242/89). Free of metasomatism deformed

sheared peridotites yet show high degree of reduction of coexisting fluid. CH_4 (UV-79/89) was of great importance in the process. Oxygen fugacity also varies widely in harzburgite-dunites which are located above in the lithosphere mantle and occupy a larger area of depths. Originally these rocks, extremely depleted in fusible components, have been probably more reduced as evidenced by the highest H/(O+H) ratio among the studied rocks (average for hezburgite-dunites 0,65). Further they also suffered multistage metasomatism [20], but of different type than sheared peridotites. More likely partial carbonization with the active CO_2 fluids,

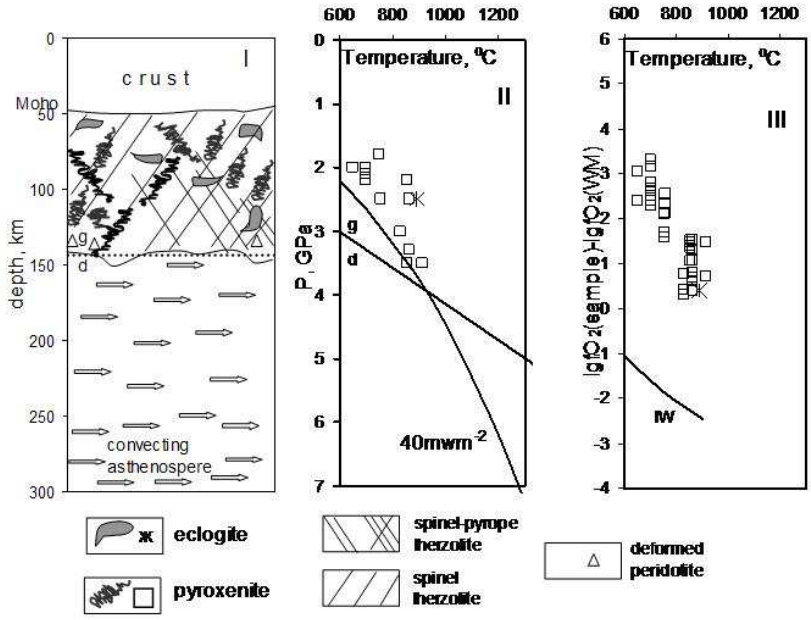

Fig. 3. **Vertical cross sections: I – mantle profile of the northeastern part of Siberian platform in the Mesozoic time [27], II – P-T parameters of the equilibrium of the mantle rocks, III – oxygen fugacity for the xenoliths of basic paragenesis of the Obnazhennaya pipe.**

which interacted with harzburgite-dunites and were entrapped by their minerals like inclusions (UV-386/86, UV-574/89, UV-39/89 UV-409/86, UV-305/89), occurred [23, 25, 16]. The samples representing the mantle areas, which did not participate in the processes and preserved earlier fluid characteristics, shows that CH_4 dominates CO_2 along with high values of water mole fraction (UV-49/76, UV-15/93, UV-278/89). Less depleted spinel lherzoliths from the upper part of the lithosphere mantle cross section, which avoided secondary enrichment, were

Table 2.

Chromatographic analyses (mg/kg) of monomineral fractions of typical representatives of all groups of xenoliths from Udachnaya (UV), Mir (M, MB), Obnazhennaya pipes

sample	paragenesis	mineral	H/(O+H)	CO_2	H_2O	H_2	N_2	CO	CH_4	C_2H_2	C_2H_4	C_3H_8	C_4H_{10}	C_5H_{12}
UV-47/76	d	Ol	0.6511	29	527	0	0	27	1.5	-	-	-	-	-
UV-15/93	d	Ol	0.671	150	1100	20	0	97	5	6	1	4	4	1
UV-574/89	d	Ol	0.6162	59	140	0	0	26	3	4	1	4	4	1
UV-409/86	d	Ol	0.6393	210	720	7	0	40	5	5	1	4	4	1
UV-278/89	d	Ol	0.6775	7	101	1	0	0	0.5	0	0.5	0	0	0.5
UV-386/86	d	Ol	0.6337	58	360	0	0	31	2	2	0	1	1	0.5
		Ga	0.6522	130	1700	0	0	10	0	0	0	0	0	0
UV-17/91	h	Ol	0.6424	130	900	0	0	20	2	2	0.5	2	2	2
		Ga	0.6601	270	5050	8	0	50	4.5	3	1	4	5	2
UV-39/89	d	Ol	0.626	190	940	0	0	90	5	3	1	3	3	1
UV-305/89	d	Ol	0.6219	460	1560	2	0	10	4	4	0	2	2	1
UV-446/89	sl	Ol	0.6437	230	1180	6	0	30	3	3	4	0.5	2	1
UV-1467/89	sl	Ol	0.6724	20	420	7	0	75	3	2	0	1	2	1
UV-562/89	sl	Ol	0.6197	13	53	0	0	4	0.5	0	0	0	0	0
UV-536/89	sl	Ol	0.5652	160	220	0	0	15	2	3	0	2	2	1
UV-467/89	gsl	Ol	0.6597	89	430	9.9	0	92	4	3	0.5	3	5	1.5
UV-126/93	gsl	Ol	0.63	117	537	0	0	76	6	6.5	0.5	6	6.5	3
UV-315/89	gl	Ol	0.6652	87	423	12	0	117	6	4.5	1	4	4.5	2
UV-442/89	gl	Ol	0.6075	80	380	сл.	16	90	2	1	0	1	2	0.5
UV-531/89	gl	Ol	0.5355	92	197	0	0	108	0	-	-	-	-	-
M-120/72	gl	Ga	0.6431	330	1630	10	0	29	2	1.5	0	1	1	1
		Cpx	0.6698	620	7960	70	0	40	5	2	0.5	2.5	3	2
M-126/72	gl	Ga	0.6511	90	1170	0	0	30	1.5	1	0	1	2	1
		Cpx	0.6541	1550	22500	0	0	110	10	3	0.5	4.5	6	4

Note: Ga – garnet, Ol – olivine, Cpx - clinopyroxene, Opx – ortopyroxene, Picro – picroilmenite. Paragenesis: d – dunite, h - harzburgite, sl – spinel lherzolite, gsl – garnet-spinel lherzolite, gl – garnet lherzolite, dp – deformed peridotite, ecl – eclogite, pyrox – pyroxenite.

Table 2 (continuation).

sample	paragenesis	mineral	H/(O+H)	CO_2	H_2O	H_2	N_2	CO	CH_4	C_2H_2	C_2H_4	C_3H_8	C_4H_{10}	C_5H_{12}
UV-525/89	dp	Ga	0.6011	12	33	0	0	2	0	0	0	0	0	0
UV-13/91	dp	Ga	0.6533	440	4260	18	0	160	4	3	2	4	6	4
		Cpx	0.6533	1170	10500	50	0	310	4	5	4	9	8	3
		Picro	0.6432	900	5800	10	0	42	3	2	1	4	6	2
		Ol	0.6242	610	2020	9	0	80	3.5	4	1	4	8	4
UV-79/89	dp	Ga	0.7766	68	131	36	0	121	2	-	-	-	-	-
UV-242/89	dp	Ga	0.4508	132	166	0	0	203	0	-	-	-	-	-
UV-448/89	dp	Ga	0.4074	69	73	0	0	129	0	-	-	-	-	-
UV-495/89	dp	Ga	0.3437	49	40	0	0	113	0	-	-	-	-	-
UV-522/89	dp	Ga	0.67	50	94	12	0	110	3	-	-	-	-	-
UV-149/84	ecl	Ga	0.6655	64	1879	5	0	5	0	0	0	0	0	0
UV-464/86	ecl	Ga	0.6552	1370	10900	56	0	127	18	13	5	9	11	4
UV-1/91	ecl	Ga	0.6549	300	3910	3	0	40	4	4	1	4	6	2
O-283	ecl	Ga	0.6661	200	1670	20	0	50	3	1.5	0	1	2	1
		Cpx	0.6755	600	8600	100	0	130	6	3	1	6	10	10
M-1/88	ecl	Ga	0.6435	380	1930	10	0	20	1.5	0	0	1	4	2
		Cpx	0.6445	2880	18400	50	0	120	6	2	0	3	8	3.5
MB-1	ecl	Ga	0.6482	49	583	0	0	15	0	-	-	-	-	-
M75	ecl	Ga	0.6575	67	560	6	0	38	0	-	-	-	-	-
UV-11/99	pyrox	Ga	0.6967	60	1360	30	0	27	1.5	1	0	1	2	1
UV-10/79	pyrox	Ga	0.5852	4	36	0	0	18.3	0	0	0	0	0	0
UV-181/89	pyrox	Ga	0.6619	150	4270	3	0	20	3	2	0.5	2	2	1
O-1091	pyrox	Ga	0.5814	310	590	0	0	26	1.5	1.5	0	1	1	1
		Opx	0.6523	1010	4290	60	0	120	6	3	0.5	4	8.5	7
O-407	pyrox	Ga	0.6463	320	1860	10	0	40	3	1.5	0.5	1	2	0.5
		Cpx	0.6506	1320	12200	20	0	80	6	2	0	4.5	6.5	4
		Opx	0.6629	580	9000	40	0	180	13	4	0.5	8.5	10	12
M-31/01	pyrox	Ga	0.6571	140	2610	0	0	13	1.5	0.5	0	1	2	1
		Cpx	0.546	1940	2350	0	0	30	3	1	0	2	10	2

Note: Data were obtained using gas chromatography on the unique setup in Laboratory of termobarogeochemistry of Institute of Geology and Mineralogy SB RAS (operator L.N. Fomina).

Table 3.

Calculated fluid component composition in equilibrium with the studied rocks from Udachnaya (UV), Mir (M, MB), Obnazhennaya (O) pipes.

sample	paragenesis	mineral	T, °C	P, GP a	H_2O	O_2	H_2	CO	CO_2	CH_4
UV -47/76	d	Ol	1000	5	0.9634	6.35E -18	0.0005	0.0003	0.0352	0.0005
UV -15/93	d	Ol	960	4	0.9788	1.28E -19	0.002	0.0001	0.0052	0.014
UV -574/89	d	Ol	900	5	0.8894	5.28E -19	0.0003	0.0003	0.1097	0.0004
UV -409/86	d	Ol	900	5	0.9374	4.14E -19	0.0004	0.0002	0.0612	0.0008
UV -278/89	d	Ol	950	5	0.9725	4.77E -20	0.0033	0	0.0006	0.0235
UV -39/89	d	Ol	900	4.5	0.9099	2.14E -19	0.0003	0.0002	0.0892	0.0004
UV -305/89	d	Ol	900	4.5	0.9021	2.64E -18	0.0002	0.0002	0.0975	0
UV -386/86	d	Ol	850	5	0.8537	9.83E -19	0.0002	0.0003	0.1455	0.0003
		Ga	850	5	0.9647	8.03E -20	0.0005	0.0001	0.0335	0.0012
UV -17/91	h	Ga	1000	5	0.9828	6.44E -19	0.0006	0.0001	0.0157	0.0008
		Ol	1000	5	0.9454	2.21E -18	0.0003	0.0003	0.0538	0.0002
UV -446/89	sl	Ol	800	2	0.9364	4.44E -22	0.0012	0.0003	0.0567	0.0055
UV -1467/89	sl	Ol	950	3.5	0.9351	4.29E -19	0.0061	0.0008	0.0239	0.0342
UV -562/89	sl	Ol	900	2.5	0.8836	1.20E -20	0.0009	0.0005	0.1135	0.0015
UV -536/89	sl	Ol	850	3	0.7798	6.26E -19	0.0014	0.0014	0.2146	0.0028
UV -467/89	gsl	Ol	900	3.5	0.9632	1.04E -19	0.0019	0.0003	0.0255	0.0092
UV -126/93	gsl	Ol	900	3.5	0.9131	3.38E -19	0.001	0.0054	0.082 9	0.0025
UV -315/89	gl	Ol	900	4	0.9665	7.17E -20	0.0022	0.0002	0.0176	0.0134
UV -442/89	gl	Ol	1050	4.5	0.8595	5.06E -17	0.0024	0.0021	0.1318	0.0044
UV -531/89	gl	Ol	1000	4	0.7267	2.56E -17	0.0011	0.0024	0.2687	0.0012
M -110/72	gl	Ga	875	4	0.9435	9.67E -20	0.00 08	0.0002	0.053	0.0024
		Cpx	875	4	0.9664	5.00E -20	0.0011	0.0002	0.0274	0.0049
		Opx	875	4	0.9742	2.76E -20	0.0015	0.0001	0.0151	0.0091
M -126/72	gl	Ga	900	4	0.952	1.55E -19	0.0014	0.0004	0.0407	0.0055

Note: Minerals: Ga – garnet, Ol – olivine, Cpx - cl inopyroxene, Opx – ortopyroxene, Picro – picroilmenite.
Paragenesis: d – dunite, h - harzburgite, sl – spinel lherzolite, gsl – garnet -spinel lherzolite, gl – garnet lherzolite, dp – deformed peridotite, ecl – eclogite, pyrox – pyroxenite.

Table 3 (continuation).

sample	paragenesis	mineral	T,°C	P, GPa	H_2O	O_2	H_2	CO	CO_2	CH_4
UV-79/89	dp	Ga	1200	5.5	0.7191	2.37E-17	0.024	0.0003	0.0011	0.2554
UV-242/89	dp	Ga	1200	5.5	0.5782	8.66E-15	0.001	0.0054	0.415	0.0005
UV-448/89	dp	Ga	1200	5.5	0.5087	1.01E-14	0.0008	0.0058	0.4843	0.0003
UV-495/89	dp	Ga	1200	5.5	0.4127	1.21E-14	0.0006	0.0064	0.5801	0.0002
UV-522/89	dp	Ga	1200	5.5	0.9463	4.24E-16	0.0075	0.0012	0.0203	0.0247
UV-525/89	dp	Ga	1250	5.5	0.8487	2.98E-15	0.0025	0.0032	0.1427	0.0028
UV-13/91	dp	Ga	1100	5	0.9644	7.87E-17	0.0015	0.0007	0.0318	0.0017
		Cpx	1100	5	0.9644	7.87E-17	0.0015	0.0007	0.0318	0.0017
		Picro	1100	5	0.9441	1.31E-16	0.0011	0.0008	0.0529	0.001
		Ol	1100	5	0.9047	2.30E-16	0.0008	0.0011	0.0929	0.0005
MB-1	ecl	Ga	1100	5	0.9558	1.06E-16	0.001	0.0005	0.0418	0.001
M-75	ecl	Ga	1100	4	0.9227	6.48E-17	0.0071	0.0022	0.0454	0.0226
M-1/88	ecl	Ga	950	4	0.934	1.92E-18	0.0018	0.0006	0.0577	0.0059
UV-464/86	ecl	Ga	1000	5	0.9714	8.43E-18	0.0007	0.0003	0.0267	0.0009
UV-1/91	ecl	Ga	800	4	0.9678	3.05E-21	0.0006	0.0001	0.029	0.0025
O-283	ecl	Ga	900	2.5	0.9382	6.21E-20	0.0043	0.0005	0.0301	0.0269
UV-10/79	pyrox	Ga	900	4	0.8241	7.07E-19	0.0006	0.0008	0.1735	0.001
UV-181/89	pyrox	Ga	1000	4.5	0.9858	3.73E-18	0.0013	0.0001	0.012	0.0008
UV-403/84	pyrox	Ga	1000	3	0.9246	2.94E-18	0.0052	0.0013	0.0483	0.0206
		Cpx	1000	3	0.9291	2.07E-18	0.0063	0.0011	0.034	0.0295
UV-11/99	pyrox	Ga	1100	6	0.9196	1.39E-17	0.01	0.0003	0.0031	0.067
		px	1100	6	0.9642	6.21E-17	0.0049	0.0006	0.0137	0.0165
O-1091	pyrox	Ga	650	2	0.8167	2.75E-24	0.0003	0.0002	0.1815	0.0012
		Opx	650	2	0.952	6.01E-25	0.0009	0.0001	0.0397	0.0073
O-407	pyrox	Ga	850	2.5	0.9273	4.69E-20	0.0026	0.0006	0.0577	0.0117
		Cpx	850	2.5	0.9327	4.09E-20	0.0028	0.0006	0.0503	0.0136
		Opx	850	2.5	0.9422	2.59E-20	0.0036	0.0005	0.0319	0.0219
M31/01	pyrox	Ga	900	4.5	0.9779	1.28E-18	0.0004	0.0001	0.0216	0.0001
		Cpx	900	4.5	0.7508	1.48E-17	0.0001	0.0002	0.2489	0

initially more oxidized and CO_2 plays an important part in the component composition of the coexisting fluid (UV-562/89, UV-536/89).

Fluid characteristics of eclogites and pyroxenites correlate well with their position in the lithosphere mantle cross section (Fig. 2-IV). Eclogite of the Obnazhennaya pipe (Fig. 3-III) showed greater reduction of the coexisting fluid than the P-T parameters of equilibrium proposed. Pyroxenites of this pipe have demonstrated good agreement between their position in the mantle cross section and the degree of oxidation of the fluid extracted from their minerals.

CONCLUSION

The obtained results have shown that: 1) Redox formation conditions of all studied xenoliths are similar to the buffer equilibrium WM, usually the difference does not exceed two log units of fO_2. Water prevailed in the composition of the mantle fluid, the second was carbon dioxide and rare – methane. CO and H_2 contents were generally one order of magnitude lower. 2) The general trend has been toward the elevation of the samples reduction with the depth of their formation though the post crystallization metasomatic effect distorts this trend. For example, the deformed peridotite with abnormally high CO_2 content in three samples occurred due to that effect. 3) Spinel peridotites of the lithosphere mantle under the Udachnaya pipe are the most oxidized among the studied ultrabasic rocks, fresh harzburgite-dunites and deformed peridotites of the root parts of mantle under the pipe are the most reduced rocks. 4) Eclogites and pyroxenites of the lithosphere mantle under the diamond free Obnazhennaya pipe are the most oxidized among the studied basic rocks. Eclogites and pyroxenites of the diamondiferous pipes Udachnaya and Mir demonstrate a wide range of redox equilibrium conditions. 5) $lgfO_2$ values of diamondiferous eclogites from Udachnaya and Mir pipes and diamondiferous dunite from Udachnaya pipe lie nearly along the line of the buffer equilibrium WM, demonstrating the average level of redox conditions of formation of parent diamondiferous rocks.

REFERENCES

1. **Andersen T., O'Reilly S.Y., and Griffin W.L.** The trapped fluid phase in upper mantle xenoliths from Victoria, Australia: implications for mantle metasomatism // Contrib. Mineral. Petrol., 1984,v. 88, p. 72-85.
2. **Ashchepkov I.V.** Clinopyroxene Jd barometer for mantle peridotites and eclogites and thermal conditions of the lithospheric keels of cratons and surroundings // A Geo Odyssey. GSA Annual meeting. Boston, 2001, ID 11658.
3. **Ashchepkov I.V., Pokhilenko N.P., Vladykin N.V., Kuligin S.S., Malygina E.V., Pokhilenko L.N., Ovchinnikov Y.I.** Using of Jd-Di clinopyroxene thermobarometry for the mantle reconstraction // "Experiment in GeoSciences", 2001, v. 10, № 1.
4. **Bulanova G.P., Spetsius Z.V., Leskova N.V.** Sulfides in diamonds and xenoliths from kimberlite pipes of Yakutia. Novosibirsk, Nauka, 1990, 119 p. (in Russian).
5. **Chepurov A.I., Fedorov I.I., Sonin V.M.** Experimental modeling of the processes of diamond formation. Novosibirsk, SB RAS Sci.C UIGGM, 1997 (in Russian).
6. **Daniels L.R.M., Gurney J.J.** Oxygen fugacity constraints on the Southern African lithosphere // Contrib. Mineral. Petrol., 1991, v. 108, p. 154-161.
7. **Dawson J.B.** Kimberlites and their xenolites. Moscow: Mir, 1983, 300 p. (in Russian).

8. **Eggler D.H., Lorand J.P., Meyer H.O.A.** Sulfides, diamonds, mantle fO2 and recycling // Fifth international kimberlite conference, extended abstracts, Araxa, June 1991. Proceedings-of-the-International-Kimberlite-Conference, 1991, v. 5, p. 88-91.
9. **Izraeli E.S., Harris J.W., Navon O.** Brine inclusions in diamonds: a new upper mantle fluid // Earth Plan. Scien. Lett., 2001, v. 5807, p. 1-10.
10. **Jaques A.L., O'Neill H.S., Smith C.B., Moon J., Chappell B.W.** Diamondiferous peridotite xenoliths from the Argyle (AK) lamproite pipe, Western Australia // Contrib. Mineral. Petrol., 1990, v. 104, p. 255-276.
11. **Kadik A.A.** Effect of redox state of planetary substance on the formation of carbon-saturated fluids in the Earth's upper mantle. Institute of Geochemistry and Analytical Chemistry, RAS, Moscow, Vestnic OGGGGN RAS, 1999, №4 (10) (in Russian).
12. **Kadik, A.A., Sobolev, N.V., Zharkova, Ye.V., Pokhilenko, N.P.** Redox conditions of formation of diamond-bearing peridotite xenoliths in the Udachnaya kimberlite pipe, Yakutia // Geochem. Int., 1990, v. 27 (3), p. 41-53.
13. **Kadik A.A., Zharkova E.V., Spetsius Z.V.** Redox formation conditions of diamond-containing kyanite eclogite in the kimberlite pipe Udachnaya, Yakutia // Doklady ANR, 1993a, p. 217-221 (in Russian).
14. **Kadik A.A., Zharkova E.V., Yafimova E.S., Sobolev N.V.** Electrochemical determinations of proper oxygen volatility of diamond crystals // Doklady ANR, 1993b, v. 328(3), p. 386-389 (in Russian).
15. **Klien-BenDavid O., Izraeli E.S., Hauri E.H., Navon O.** Mantle fluid evolution – a tale of one diamond // Lithos, 2004, v. 77, p. 243-253.
16. **Kogarko L.N.** Role of deep-seated fluids in genesis of mantle heterogeneities and alkaline magmatism // Geol. And Geoph., 2005, v. 46, № 12, p. 1234-1245 (in Russian).
17. **Melton C.E., Giardini A.A.** The composition and significance of gas released from natural diamonds from Africa and Brazil // Amer. Mineral., 1974, v. 59, p. 775-782.
18. **Osorgin N.Yu.** Chromatographic analysis of gas phase in minerals (procedure, apparatus, metrology). Novosibirsk, IGG SB AS USSR, 1990 (in Russian).
19. **Pearson D.G., Boyd F.R., Haggerty S.E., Pasters J.D., Field S.W., Nixon P.H., Pokhilenko N.P.** The characterization and origin of graphite in cratonic lithospheric mantle: a petrological carbon isotope and Raman spectroscopic study // Contrib. Mineral. Petrol., 1994, v. 115, p. 449-466.
20. **Pearson D.G., Shirey S.B., Carlson R.W., Boyd F.R., Pokhilenko N.P., Shimizu N.** Re-Os, Sm-Nd, and Rb-Sr isotope evidence for thick Archaean lithospheric mantle beneath the Siberian craton modified by multistage metasomatism // Geochim. et Cosmochim. Acta, 1995, v. 59, № 5, p. 959-977.
21. **Pokhilenko N.P.** Mantle paragenesis in kimberlites, their origin and prospecting significance // Ph.D. thesis, manuscript. SB AS USSR, Institute of Geology and Geophysics, Novosibirsk, 1990 (in Russian).
22. **Pokhilenko N.P., Sobolev N.V., Boyd F.R., Pirson G.D., Shimizu N.** Megacrystalline pyrope peridotites in the lithosphere of the Siberian platform: mineralogy, geochemical peculiarities and origin // Geol. and Geophys., 1993, v. 34, № 1, p. 71-84 (in Russian).
23. **Pokhilenko N.P., Sobolev N.V., Kuligin S.S., Shimizu N.** Peculiarities of Distribution of Pyroxenite Paragenesis Garnets in Yakutian Kimberlites and Some Aspects of the Evolution of the Siberian Craton Lithospheric Mantle // Proceedings of the VIIth International Kimberlite Conference, University of Cape Town, South Africa, April 11-17, 1998,v. II. Cape Town, 1999, p. 689-698.
24. **Schrauder M. and Navon O.** Hydrous and carbonatitic mantle fluids in fibrous diamonds from Jwaneng, Botswana // Geochim. et Cosmochim. Acta, 1994,v. 58, № 2, p. 761-771.
25. **Shimizu N., Pokhilenko N.P., Boyd F.R., Pearson D.G.** Trace Element Characteristics of Garnet Dunites/Harzburgites, Host Rocks for Siberian Peridotitic Diamonds // Proceedings of the VIIth International Kimberlite Conference, University of Cape Town, South Africa, April 11-17, 1998, v. II. Cape Town, 1999, p. 773-782.
26. **Simakov S.K.** Redox state of eclogites and peridotites from sub-cratonic upper mantle and connections with diamond genesis // Contrib. Mineral. Petrol., 2006, v. 151, № 3, p. 282-296.
27. Smith D., Boyd F.R. Compositional heterogeneities in phases in sheared lherzolite inclusions from African kimberlites // Proc. 4-th Kimb. Conf., 1989, v. 2, № 14, p. 709-724.
28. **Sobolev N.V.** Deep-seated inclusions in kimberlites and the problem of the upper mantle composition. Nauka. SB Novosibirsk, 1974 (in Russian).
29. **Solov'eva L.V.** Composition and evolution of the upper mantle under the Siberian platform and the problem of diamond formation. Ph.D. thesis, Irkutsk, 1998 (in Russian).
30. **Tal'nikova S.B., Barashkov Yu.P., Svoren I.N.** Composition and gas content in diamonds of eclogite and ultrabasic paragenesis from kimberlite pipes of Yakutia // Dokl. AN SSSR, 1991, v. 321, № 1, p. 194-197 (in Russian).
31. **Ukhanov A.V., Ryabchikov I.D., Kharkiv A.D.** Lithosphere mantle of the Yakutian kimberlite province. M.: Nauka, 1988 (in Russian).

UDK 552.122.086

Pecularities of mineralogy and petrography of the upper-muna field kimberlites: application to the lithospheric mantle composition

Spetsius Z.V., Zezekalo M.Yu., Tarskhix O.V.

YANIGP CNIGRI, AK "ALROSA" (ZAO), Mirny, Russia;

Abstract

The broughted results of the studies kimberlite rocks from Zapolyarnaya, Deymos, Poiskovaya, Novinka and Komsomolskaya-Magnitnaya pipes (Verhne-Muna field). It is established that all diatremes are executed by two structure types of kimberlites: porphiric kimberlites and kimberlitesыми brecchias, presenting independent introduding phases. The temporary relations porphiric kimberlites and kimberlite brecchias are installed on single samples. The results of their study, as well as presence of xenoliths of porphiric kimberlites in autolithic brecchia allow drawing a conclusion that their consolidation passed before formation of kimberlite brecchias. High amount of fresh olivines is noted in all pipes of Verhne-Muna field. Between indicator minerals leader place belongs to the garnet. Comparatively to diatremes from the other fields, kimberllites of Verhne-Muna field are characterized by low contents of sedimentary rocks debris, wide-spread distribution of ultrmafic mantle rocks. The particularity of all pipes is nearly full absence, both eclogite and garnet websterite xenoliths. This evidence is confirmed also by the composition of the assotiations of indicator minerals that is indicative of essential difference of lithosperic mantle given field in contrast with nearby kimberlitic fields.

INTRODUCTION

Enormous actual material is received in process of more than 50 years studiing on chemical composition, petrography and mineralogy of different kimberlite pipes of Yakutia. In spite of undoubted resemblance in formation kimberlites in the whole each pipe and each field have inherent their own individual particularities, on which they differ from kimberlites from the other fields [2, 7]. The detailed study of kimberlite rocks, nature their secondary transformation and clarification their minerallogy is of great importance for decision of the practical problems, in accordance with dividing of the intruding phases, nature their three-dementional distribution in diatremes, specificity postmagmatic transformations, that are determine their geologycal-technological particularities.

RESULTS

Verhne-Muna kimberlitesoe field is located in upper current of river Muna and is presented by 16 pipes and 4 dikes [3, 4, 9]. The typical particularity of this field is a close location of kimberlite bodies and their small sizes. Probably this has

served the reason that kimberllites explored us pipes much gangplank between itself. There were organized the detail studies of kimberlite rocks on saparate levels of upper parts of main pipes: Zapolyarnaya, Deymos, Poiskovaya, Novinka and Komsomolskaya-Magnitnaya of this field (528 samples). It was used complex metohds of petrographic studies, in which entered macro- and micro-srructure of kimberlite rocks, chemical analysis of the varieties kimberlites, X-ray analysis of the kimberlitic ground mass, determination of the heavy minerals, study of the composition of indicator minerals.

In spite of row separate difference, all pipes Upper-Muna field have a general line, conditioned presence two types kimberlites (with the exclusion of pipes Novinka) and vicinity of the mineral composition. All diatremes built by two structural types of kimberlites: porphiric kimberlites (PK) and kimberlites brecchias (KB), being derived independent phases of the intruding. The structural types differ on olivine disribution in different shaving classes, contents of debris of sedimentary rocks, presence "autolithes" formation, contents of indicator minerals, in particular garnet (Table 1).

Table 1.

Modal Composition of Kimberlites from Uppermuna Field

Pipe	Type of rocks	Number. of samples	Xenoliths of sedimentary rocks,vol.%	Xenoliths of ultramatic rocks,vol.%	Autholiths, vol.%	Average content of olivine, kg/t
Zapolyarnaya	PK	74	4,06	1,36	0,16	2,29
Deymos	PK	7	3,44	1,65	0	5,36
Poiskovaya	PK	50	2,47	0,29	0,08	9,07
Novinka	PK	110	4,14	1,91	0,32	10,62
Komsomol'skaya-Magnitnaya	PK	72	4,44	1,61	0,21	13,86
Zapolyarnaya	KB	87	14,92	1,01	2,63	3,03
Deymos	KB	17	11,75	0,97	0,14	18,33
Poiskovaya	KB	9	20,96	0,65	2,18	13,00
Komsomol'skaya-Magnitnaya	KB	52	14,76	0,93	1,39	7,76

Unlike the other pipe, where come to light the multiple temporary contacts between kimberlites of the different consolidation phases, in kimerlites Upper-Muna field sharp contacts reveal itself seldom. They are characterized with gradual transition and mutual mix petrographic sign. Inwardly of the each petrographic type possible to select to varieties, conditioned by correlation porphiric and clastic structural elements, for instance, amongst PK: mega-, media-, miniphorphiric and etc. Amongst kimberlite brecchias: small-, media- and coarse debris.

Porphiric kimberllites in all pipes have approximately alike composition and structural signs. The small differences are conditioned by correlation of

dimensionality porphiric separations and the intensity of secondary mineralisation development. These rocks are grey, light-gray of the colour, sometimes with pale-blu, or brown tones. Small lightning of rocks is noted most often near contact with strong calcitisation. Brown tone is conditioned by broad development of pyraurite, less heicite and separation of ferric gidrooxydes in some areas. Olivine psevdomorphoses are mainly oval form and built basically by the serpentine sometimes with carbonate. Moreover the serpentine always dominates in composition pseudomorphoses. Big amount of fresh olivine is noted in all pipes of Upper-Muna field. Usually olivine is saved in the manner of relicts in rather large grains, partly substituted by serpentine. On place some grains are noted emptinesses and cavities serpentine solvent, in the manner of geodes or rims on some grains своеобразных. The most intensive this process is shown in upper levels parts of pipes. As a whole the structure of the rocks is porrphyric and texture - massive.

The autolithes contents in brecchias can reach up to 10-20%. Quite often small autolithes are shells of early kimberlite phases, surrounding xenoliths of sidimantary or crustal rocks or grains of deep xenocrystic minerals - basically olivines and pyropes. The autolithes texture can be as massive, so and concentrically-fluidal. In the first case they can contain pseudomorphoses on olivine of first generations. As a whole kimberlite brecchias of Upper-Muna field are characterized by low contents of sedimentary rocks debris (average 12%), comparatively to diatremes from the other kimberlites.

The study of modal composition of big amount of kimberlite samples rocks from the Upper-Muna pipes shows that contents olivine pseudomorphoses (size more than 4-5 mm in diameter) in porphiric kimerlites vary from 10 to 13% and in kimberlite brecchias 4-8% (practically in 2 times less). The content olivine xenocrysts (size > 8 mms) decreases nearly on order. For porphiric kimberlites content of pseudomorphoses (class 1-2 mm) is not more than 50%, for kimberlite брекч brecchias this factor varies from 50 to 60% moreover KB contains the big amount pseudomorphoses on olivine II generation. The distribution of olivine grains of different classes is one of stable that is tracked in all studied by us pipes. This content and correlation can serve the priority criterion at typisation of kimberlite rocks [8].

The spectrum of mineral composition of the ground mass of kimberlite rocks of Muna pipes it is enough close, however their contents broadly vary, both on kimberlite types, and in separate samples. As judged by the X-ray data test (the indicator panel. 2), both in PK, and in KB dominating mineral are серпентин and calcite, in most cases are present the mica and chlorite. In ground mass all pipes, in that or other correlation, counter montichillite and perovskite, amount last quite often is up 10%. Usually, perovskite is present in the manner of little grains heap in serpentine-carbonate mass, as well as in composition reactionary rims around olivinea. It is around the world noted its zonal nature moreover, probably, not only in respect of major, but also trace elements [10]. Montichellite meets in the manner

of isometric and round form, sometimes resorbed, smoll crystalls; quite often he also has a zonal construction. The contents its in different types and separate sample of the bore holes, as judged by given microscopic study, uneven. Follows to note, presence perovskite, montichillitea and titanomagnetite in composition of the ground mass kimberlites this field is indicative of hightemperature nature of kimberlitic melt, but development titanomagnetite on final stage of the shaping kimberlite pipe points to increasing oxygen redox conditions [1]. The progressive enrichment by the ferric and titanium oxides of kimberlitic magmas on the final stage of the crystallisation process is noted as well as in a result of studies zonality of olivines [1]. Necessary to note that hightemperature nature of kimberlitic magmas and increasing of oxygen situations on final stage of the crystallizations is emphasized broad development powerful kelyphitic rims on garnet megacrysts from these pipes. This in turn well agreed with intensive manifestation of the dissolution and corrosions of diamonds from these pipes that, as likely as not, is and one of the reasons low diamond grade of kimberlites Muna field.

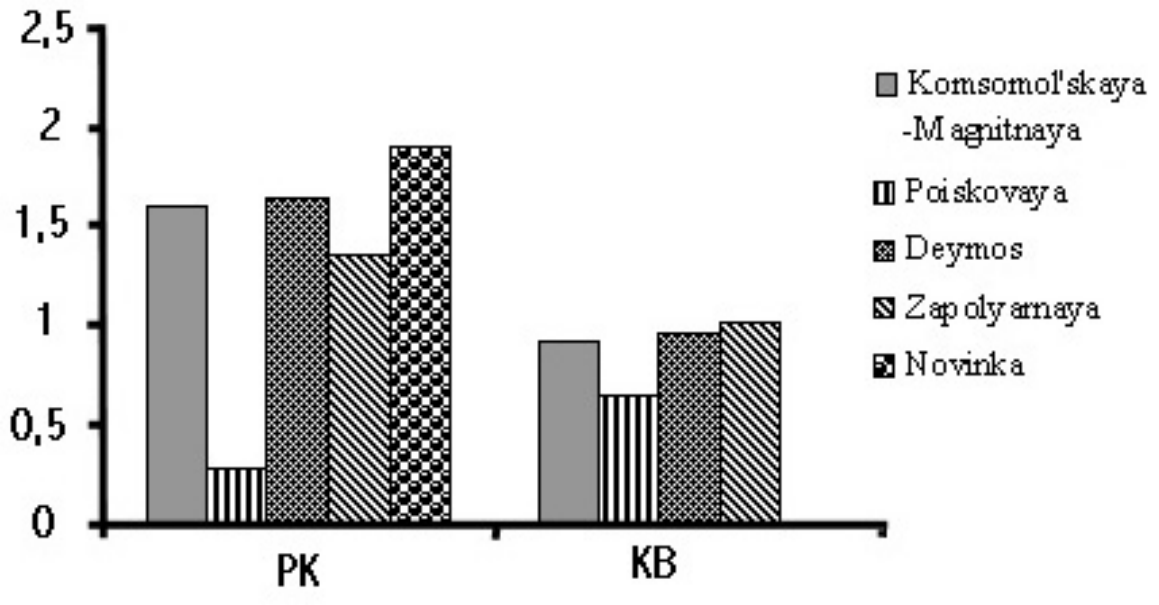

Fig. 1. **Distribution of ultramafic xenoliths in kimberlites of the Upper Muna field.**

The temporary relations porphiric kimberlites and kimberlite brecchias are installed on single samples. From studied currently collections only several samples from pipe Zapolyarnaya and pipes Komsomolskaya-Magnitnaya demonstrate the well-marked contacts between porphiric kimberlites and brecchias. The results of their study, as well as fact of the frequent presence single sample porphiric kimberlites in the manner of xenoliths in brecchias allows to draw a conclusion that their consolidation passed before formation of kimberlitic brecchias.

Distribution of mantle xenoliths in investigation pipes is far unlevel (Fig. 1).

The most their amount and a spectrual variety are fixed in pipe Zapolyarnaya, Novinka and Komsomolskaya-Magnitnaya. In pipe Deymos they are meet less;

else less in pipe Poiskovaya. At count modal composition 814 xenoliths of the deep rocks were noted in kimerlites Upper-Muna field. Basically, these are dunites and olivinites, garnet lherzolithes and garnet-spinel harzburgites. Practically all of these in one or another degree are subject of serpentinisation, So, a part of them is presented by serpentinites of menshened rock types. The intensity of the processes of secondary development of ultramafic rock xenoliths is found in full correspondence to with degree of the transformation of kimberlite rocks, in which they were noted.

The form of deep xenoliths is most often oval; their surfaces are smooth. Their sizes (in samples) small: from 1-2 to 1-3 mms refer to on long axis, in single samples up to 20 mm. In all pipe garnetbearing varieties prevail over samples without garnet.

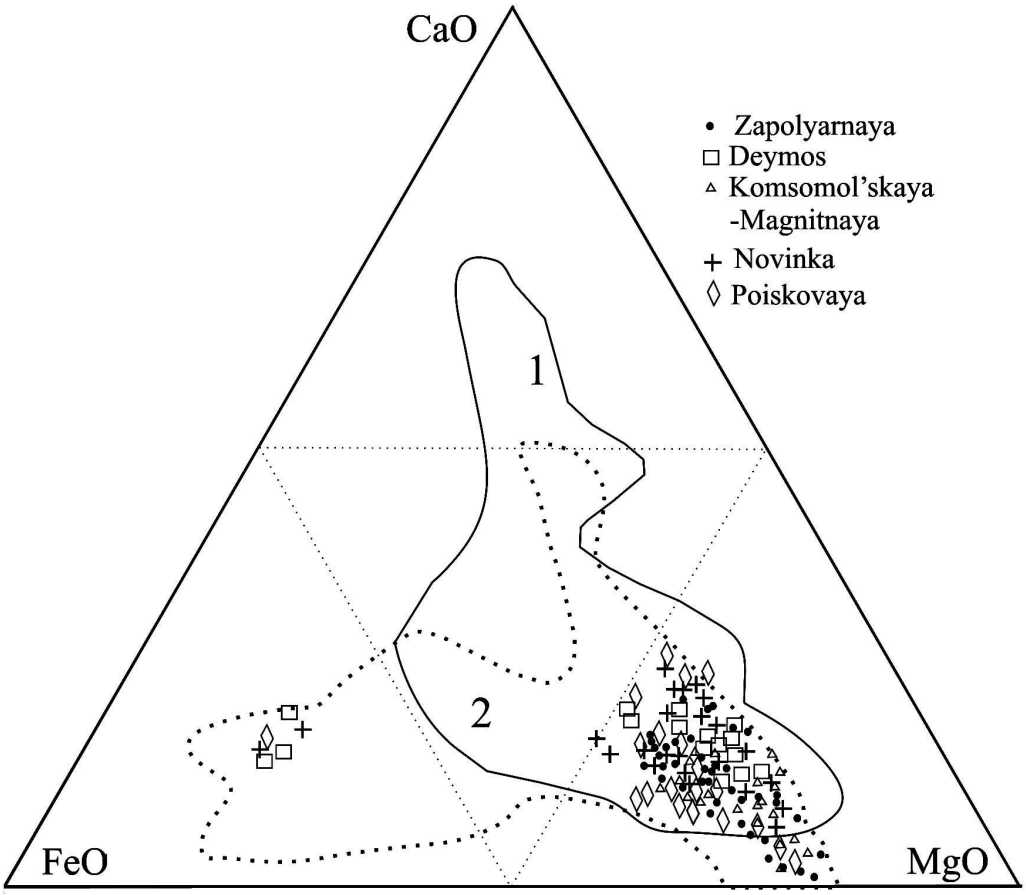

Fig.2. **Garnets composition from kimberlites of the Upper Muna.**

The contents garnet and cromspinels in xenoliths of the deep rocks vary from 2 to 10-15 %, in small nodules (size 3-5 mms) up to 30-50 %. Chomshpinel in xenoliths is presented xenomorphic grains by size from 0,05 to 0,5-0,7 mm. In kimerlites of the Komsomolskaya-Magnitnaya pipe are installed enriched by phlogopite deep rocks of olivine-phlogopite xenoliths. The rocks are small- and medium-grained and consist mainly of orange-red phlogopite (80-85 mod. %). Amphibole and clinopyroxene are present in the manner of admixture.

In pipe Zapolyarnaya noted single samples of eclogites. As a whole amount xenoliths deep assotiation in porphiric kimerlites nearly in two times exceeds such in kimberlite brecchias.

In smaller amount, than mantle, are noted xenoliths of the crustal metamorphic rocks. They wide-spread practically in all pipes of Upper-Muna field, only in the pipe Poiskovaya noted only single samples. They are presented basically by debris of biotite-garnet and amphibole-garnet gneiss, less crystalline schist. The crustal metamorpic rocks are subject to same secondary change, as accomodating kimberlite. The separate samples show intensive serpentinisation, to a lesser extent is carbonatised. The typical for crustal xenoliths is a presence of the quartz in many assotiations. As contrasted with deep xenoliths debris of crustal rocks comparatively biger in size. Dominate xenoliths size 1-5 refers to on long axis, less up to 7-10 mm. Distribution of mantle minerals in composing their kimerlites, as well as deep xenoliths, unevenly. Leader place in both petrographic types, certainly, occupies the garnet. The most its amount is noted in pipe Zapolyarnaya (the average contents 0,67 - 0,56 %). Distribution of garnet is uneven, is noted its greater contents in porphiric kimerlites. From comparative

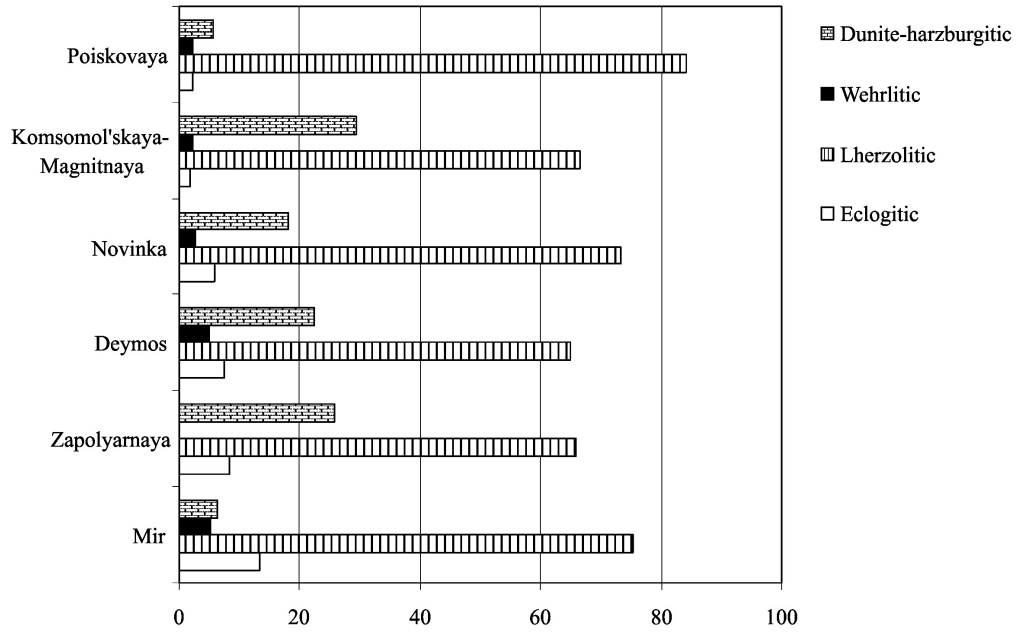

Fig.3. **Relationship of garnet megacrysts of different paragenesis in kimberlite pipes of the Upper Muna field.**

diagram of the garnet compositions in different pipes (Fig. 2) wholly obviously their resemblance on contents main component Ca, Mg and Fe. As judged by microprobe data garnets from studied pipes are close in variations of Cr also, Ti and Mn. The comparison of garnet compositions from Muna field pipes with garnet populations from kimberlites by nearby fields (fig. 1) points to sharp

difference of the paragenetic garnet types set in kimerlites of given field. This is expressed in nearly full absence of eclogitic garnets and, in the first place garnets with high Ca-content from kyanite and the other types highaluminous eclogites, that are wide-spread in Udacnaya and the other pipes of Daldysky field [5]. The distribution of different paragenetic groups of garnets is shown on specifif diagram (Fig. 3). It is obvious a resemblence in relationship of paragenetic groups between garnets of Muna pipes and difference in comparison with garnet from the Mir pipe.

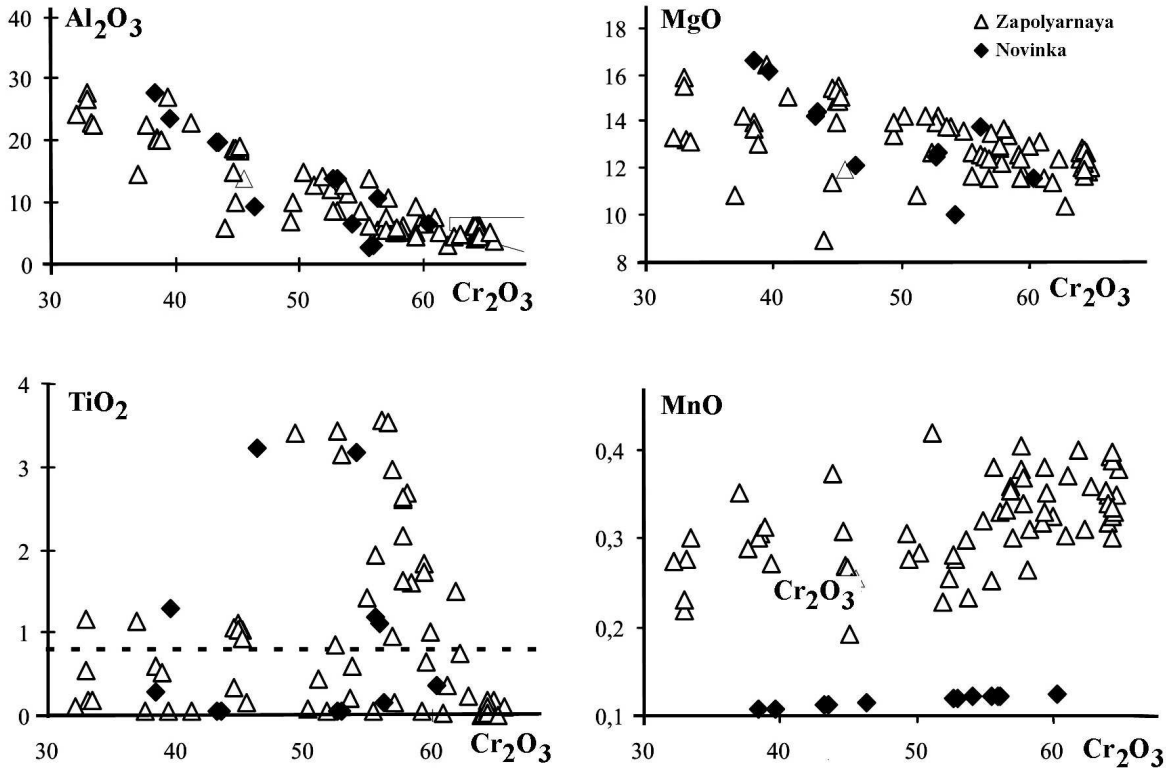

Fig.4. **Comparison of chromspinelides from the Zapolyarnaya and Novinka pipes.**

The particularity garnet from Upper-Muna field pipes is a broad development powerful kelyphite rims and presence in both petrographic types kimberlites of the quite a number garnet, has strained the substituted kelyphite by material. In PK their amount forms approximately one third from the general volume of the sample, in kimberlite brecchias approximately 1/5 parts.

The garnets basically orange or orange-red varieties, answerring two assotiations: mafic and ultramafic. Their seize seldom exceed 5 mms in diameter. Much grains are noted with size from 0,1 to 1 mm. Xenocrysts of 7-10 mms are single, their contents in the grond mass does not exceed 7 %.

Ilimenite meets seldom amongst indicator mineral (in single sign), contents of chromspinelides are less than 0.1 percent. Spinels from all pipes of Muna field are clode in composition. But there is fixed a rather obvious difference in content of Mn and other elements between chromspinelides of Zapolyarnaya and Novinka

pipes (Fig. 4). Chromspinelides of these pipes are really different in the presence of chromites of diamond assotiation. This statement is confirmed by low grade of the Novinka pipe.

Petrohimichal feature investigated kimberlites shown that composing their kimberlite phases are present itself formation. Their chemical composition varies within pipe from phase to phase and inwardly each phases. One of the petrohimichal particularities of studied pipes is a clear delimitation of petrographic rocks of the different introding phases on the contents of major oxydes (Table 2). Phorhiric kimberllites are characterized by raised contents of TiO_2, Fe_2O_3, MnO, MgO and K_2O. The kimberlite brecchias have high contents of CaO, in contrast with PK and contain more Al_2O_3, Na_2O. A high importance of SiO2 and MgO is determined by quite a numbers of fresh olivine. It is present in majority of porphiric kimberlites, will broadly develop in the ground mass in the manner of veins of different orientation.

Table 2.

Chemistry of kimberlites from Upper-Muna field (average, wt.%)

Pipe	Type of rocks	Num. of analyses	Avarage major composition											
			SiO_2	TiO_2	Al_2O_3	Fe_2O_3	MnO	MgO	CaO	Na_2O	K_2O	P_2O_5	ppp	total
Zapolyrnaya	PK	54	31,07	1,28	1,67	8,12	0,14	34,67	4,32	0,01	0,41	0,38	17,63	99,83
	KB	83	30,09	1,19	2,21	6,67	0,13	32,87	6,82	0,02	0,25	0,39	19,23	99,86
Deymos	PK	9	27,62	1,74	2,51	8,61	0,15	31,70	8,99	0,02	0,57	0,79	17,37	100,06
	KB	15	28,60	1,28	3,08	7,46	0,14	28,14	11,36	0,00	1,44	0,59	18,04	100,13
Poiskovaya	PK	31	29,99	2,46	1,97	8,93	0,15	33,68	4,01	0,01	0,65	0,42	17,60	99,87
	KB	9	30,84	1,62	2,88	7,17	0,13	29,79	7,35	0,01	0,65	0,36	18,60	99,42
Novinka	PK	103	30,34	1,41	2,12	8,82	0,15	33,64	6,61	0,01	0,76	0,47	16,02	100,35
Komsomol'skaya-Magnitnaya	PK	76	30,35	1,38	2,51	8,49	0,15	31,52	8,32	0,00	1,20	0,42	15,97	100,31
	KB	54	29,88	1,11	2,83	7,66	0,14	30,12	9,65	0,00	0,98	0,39	17,58	100,34

The other petrochemical particularity, inherent all five pipes, is concluded in firm negative relationship between CaO and MgO. At constancy of the amount CaO + MgO equal 40%, the graphs of the change the contentses oxides are bound mirror symmetry that reflects two arctic processes – serpentinisation and carbonatisation [6]. Low rocks carbonatisation is a typical sign of all pipes of Upper-Muna field.

In kimerlites these pipe is raised contents TiO_2 that is conditioned presence in them perovskite that well diagnosed in thin sections. Particularly much perovskite is present in kimerlites of the pipe Poiskovaya. The practice shows that there exists a certain relationship between contents of TiO_2 and productivity of kimberlite ores. Diatremes Internacionalinaya, Ayhal, Botuobinskaya, Nyurbinskaya are this petrochemical factor characterized by low importances (0,3 - 0,7 wt.%) that on mineral level is checked by low contents of ilmenite. In kimerlites of Verhne-Muna pipes ilmenite is also noted in rare single sign. However, importances of TiO_2 on result chemical test at the average change within the range of 1,2 - 2,5 mas.% on

miscellaneous pipe that is defined presence of perovskite in composition of the ground mass all pipe.

The typical particularity of kimberlites Zapolyarnaya, Deymos and Poiskovaya pipes is a broad development of magnetite mineralisation, unlike the other pipe, where in greater degree are shown processes of sulfidisation.

CONCLUSION

The complex study of the material composition kimberlite pipe Upper-Muna field has allowed revealing total and individual line of the composition of this field kimberlites:

- All diatremes built two structural types of kimberlites: porphiric kimberlites and kimberlitic brecchias, being derived independent phases of the introding. In favour of this witness are the discoveries of the more early of the phase in another.

- As a whole kimberllites of Verhne-Muna pipes are dense rocks, weakly changed by processse of secondary mineralisation. They contain the smaller amount of sedimentary rocks debris and greater amount of xenoliths of spinel-pyroxenite facies, unlike kimberlitees from the other pipes of West Yakutia. Kimberlites of Upper-Muna field could be refer to kimberlites with the absence of ilmenite.

- It is noted a big amount of garnet with powerful keliphytic rims, that is indicative of aggressive influence of kimberlitic melt on the xenocrystic mantle minerals, including diamonds.

- Amongst xenoliths of the deep rocks greatly dominate the ultramafic olivine bearing varieties. For kimberlites all studied pipes is characteristic of nearly full absence of mafic xenoliths of eclogite and garnet vhebstherite composition that is indicative of specificity of the lithospheric mantles under kimberlite pipes of this field.

High temperaturre nature and raised oxygen redox conditions on final stages of the crystallizations of kimberlitic magmas in Muna field pipes, probably, have defined the crystals corrosion and dissolution of a part of diamonds. On the other hand, comparatively low diamond grade of kimberlites given field, probably, has conditioned by selective seizure of mantle material or difference in the composition of the lithosphere with sharply subordinated position of eclogitic substratum and dominanting an ultramafic that in turn, has conditioned the absence of eclogitic paragenesis diamonds in diamond population of these pipes.

-

REFERENCES

1. **Fedorchuck Yana, Canil Dante and Carlson Jon A.** 2003. // Oxygen fugacity of kimberlite magmas and their relationship to the characteristics of diamond populations, Lac de Gras, N.W.T, Canada. Ext. Abstracts 8th IKC. FLA_0098.
2. **Kharkiv, A.D., Zinchuk, N.N., and Zuev, V.M.** 1998. // Primary diamond deposits of the world. Moscow, Nedra. 555 p (in Russian).
3. **Kornilova V.P., Nikishov K.N**. 1976. //Relations and nature of the varieties kimberlite rocks in pipe Novinka and Zapolyarnaya. Geology, petrography and geochemistry of magmatic rocks forming the northeast Siberian platform. - Jakutsk, AN USSR.122-130 pp.

4. **Serenko V.P. and others**. 1989. // Complex study of the material composition kimberlite tel Upper-Muna field (the pipes Novinka, Poiskovaya, Komsomolskaya-Magnitnaya, Zapolyarnaya). YANIGP CNIGRI, Mirny. 80p/
5. **Spetsius, Z.V**., 2004. Petrology of highly aluminous xenoliths from kimberlites of Yakutia. Lithos 77, 525-538 pp.
6. **Spetsius Z.V., Serenko V.P**. The Composition to continental upper mantle and bottom of the cortex under Siberian platform. M., Science, 1990, 272 p. (in Russian).
7. **Vladimirov B.V., Kostrovickiy S.I., Solovieva L.V**. 1981.//Categorization of kimberlites and internal construction of kimberlite pipes - M.: Science,. – 136 pp. (in Russian).
8. **Zankovich N.S.** 2004. //Material-indicator criteria of tipisation of kimberlite rocks and sequence of their shaping (on example complicated pipes of Yakutia) //Abstract of Dr. Thesises. Irkutsk. 23 p. (in Russian).
9. **Zankovich N.S., G.N. and Rudakova G.P.** 2005. // New evidence on petrography of kimberlites from pipe of Upper-Muna field (Yakutia). (Geology of diamond - a present and future). Voronesh,.790-806 pp. (in Russian).
10. **Yakovlev D.A.** 2004. // Particularities of mineralogy of kimberlite magmatism of Upper-Muna field (Yakutiya}. Abstract of Dr. Thesises. Irkutsk. 23 p. (in Russian).

UDK 550.42 + 552.321.6

Geochemical types of kimberlites and their mantle sources

Lapin A.V[1]., Tolstov A.V[2].

[1]*The Institute of Mineralogy, Geochemistry and Crystal Chemistry of Rare Elements, ul. Veresaeba15, Moscow, 121357 Russia;e-mail:lapin@imgre.ru*

[2]*Botuobinskaya Geological Prospecting Survey of the A/K ALROSA, ul. Lenina 44b, Mirnyi, Sakha Republic, 678170 Russia*

ABSTRACT

A number of kimberlite occurrences, that have been revealed during last decades in Russia, differ from classical representatives of this magmatic formation by some significant properties i.e. the absence of ilmenite, as well as by relatively small quantity of minerals-satellites of diamond, and that of pyrope, first of all. These occurrences include kimberlites of the Arkhangelsk diamond-bearing province and the Nakyn field in the Middle Markha region in Yakutia. It can be concluded from the cited petrochemical data, that the most strong evidence of abnormal character of these manifestations is the high degree of contrast of their geochemical parameters relative to rock parameters, that are traditionally considered as the formation petrotype of diamond-bearing kimberlites. Contrast differences are established, first of all, for contents of rare and radioactive HFS elements (Ce, Nb, Zr, U, Th) and for the ratios Ce/Y, Nb/Zr. They are manifested by individual features of correlation relations of elements (Ce-Y; Ce-P; Nb-Ti and oth.) in two kimberlite groups.

High degree of geochemical contrast in two kimberlite groups, which apparently has deep geonetic reasons, allows to distinguish a special geochemical type of these rocks, that is characterized by negative anomalies of HFS rare and radioactive elements (kimberlites of D-type) and by opposition to the rocks of the formation petrotype of kimberlites (kimberlites of N-type), that are characterized by moderately high HFS elements contents.

The main factor, determining distribution of noncoherent HFS elements in the mantle kimberlite source, is abyssal metasomatism, caused by juvenile fluids flows, which is always accompanied by significant introduction of alkalies, titanium, highly charged rare and radioactive elements. Thus, there is a good reason to consider the lithosphere substrate, metasomatized under the influence of juvenile abyssal fluids, as a mantle source of kimberlites, belonging to the geochemical type N. It is also clear, that generation of D-type kimberlites takes place under different conditions. Geochemical properties of this type of kimberlites and their confinement to the collision margins of ancient cratons and terrains allows to think, that these rocks with negative HFS elements and titanium anomaly are generated from the lithosphere substrate, that was metasomatized under the influence of volatiles, introduced from the subducted oceanic crust.

INTRODUCTION

Abyssal mantle magmas, that are generated inside plates, most typical of which are alkaline ultrabasic kimberlite and carbonatite magmas, are characterized by increased alkalinity, high saturation with fluids and increased concentrations of highly charged lithophile rare and radioactive elements. Fusion of such fluid saturated magmas out of relatively dry pyrolite is impossible, and thus, it is

thought, that the necessary condition of their generation is the abyssal metasomatism, initiated by fluid flows of the juvenile emanation; the main components of the latter are carbonic acid, water, phosphor pentoxide, alkalies, and rare elements. Thermofluid flows of juvenile emanation, that present a part of the common process, are associated with a series of phase transformations, taking place during convective transition of the mantle matter, and with decomposition of metastable phases under conditions of change from high pressures to lower ones. Perhaps, such abyssal phases as carbides, phosphides and hydrides of metals, as well as dense structural modifications of olivine and other silicates, participate in these transformations. Thus, according to these ideas, fusion of most deeply generated fluid-saturated alkaline ultrabasic magmas, typical of inside-plate conditions, results from fundamental processes of primary differentiation of the Earth composition and evolution of its structure.

Geological forms of juvenile fluid flows manifestation, alongside with scattered dissipation of abyssal emanations, can be caused by so called “hot spots” of the planet – areas of prolonged concentrated discharge of thermofluid flows, as well as, mantle plumes – extended areas of upward movement of heated mantle matter; it is accompanied by generation of large arc uplifts inside cratons, in axial parts of which, deep rift structures are developed; these structures are the zones of increased permability for abyssal fluids and melts. In recent years, with development of the theory of plate tectonics, the main part in generation of abyssal mantle magmas is assigned to the processes of the Earth’s crust matter recycling, including its volatile components within subduction mechanism. In subduction zones, features of penetration of the oceanic crust slabs are traced to the depth of 400-600 km, and horizontally they can extend to 1000 km and more, overlapping significant areas of cratons.

Thus, to the present, two possible methods of metasomatic preparation of the mantle substrate are outlined. One of them is associated with primary differentiation of the Earth’s matter – the process of the planet degassion; it occurs in the flows of juvenile fluid emanations, containing carbonic acid, phosphor pentoxide, alkalies and rare metals. The other includes secondary redistribution of the differentiated planet matter during subduction of the oceanic crust, accompanied by recycling of its matter and of its volatile components, first of all.

In spite of greater popularity of the second method of metasomatic preparation of the mantle substrate due to active expansion of the plate tectonics theory, the common sense does not allow to prefer a priori the second process over the first one, and actually, the target is to determine the real role of each mechanism. Obviously, solution of this problem proposes development of rather efficient criteria, allowing to distinguish magmatic products, generated with participation of juvenile fluids or volatiles, activated in the process of recycling of the matter of the subducted oceanic crust.

The aim of this publication is to reveal such criteria on the basis of the analysis of correlation relations between geochemical specific features of deeply generated magmatites and their geodynamic position.

GEOCHEMICAL TYPES OF KIMBERLITES AND GEODYNAMIC CONDITIONS OF THEIR FORMATION

The important development of the past years is the detection of the geochemical heterogeneity of kimberlites, which was established for the first time, during investigation of the Arkhangelsk province. The geochemical parameters of kimberlites from this province appeared to be significantly different from those of diamodiferous rocks from traditional diamond-bearing regions of Yakutia, which are considered as standard of diamondiferous kimberlite [1]. Later, after the discovery of diamond-bearing kimberlite pipes in the Middle Markha region (Nakyn field), the heterogeneity of kimberlites was established within the Yakutian dimondiferous province [2, 5, 7, 9]. Geochemically anomalous kimberlites, similar to Arkhangelsk and Nakyn rocks, were recently reported from the Slave province of Canada [15, 26].

The reason of so close in time and relatively late discovery of a number of unusual occurrences of kimberlites probably lies in anomalous properties of these rocks. They have rather low contents of ilmenite and, thus, week magnetic ability and low contrast in the magnetic field. Contents of pyrope, the main indicator mineral of kimberlites, often is a little higher than diamond content, which makes it difficult to use the traditional slime method of exploration. These specific features at once attracted attention and make it necessary to develop a special estimation-exploration complex for anomalous kimberlites of this type [15].

The subsequent detailed studies revealed the unusually high degree of contrast of geochemical parameters of these recently discovered kimberlite occurrences in relation to the parameters of the rocks, which are traditionally considered as a formation petrotype of diamondiferous kimberlites. The revealed heterogeneity of kimberlites as a formation type and distinguishing of contrast geochemical types in it, is important for efficient mineragenic estimation and potential evaluation of alkaline ultrabasic magmatites, because it allows to detect more precisely the parameters of potential diamond-bearing objects. At the same time, detection of the nature of geochemical heterogeneity of kimberlites presents the real scientific interest, because it provides the necessary conditions for creation of adequate petrological models for the most deeply generated magmatic formations. The preliminary analysis show, that heterogeneity of kimberlites is directly connected with the problem under consideration, and can point to the possible variation under conditions of the abyssal magma generation.

In order to scrutinize this problem, obtain reliable characteristics of contrasting geochemical types of rocks, and analyze the probable nature of

Major element compositions (wt.%) and trace element contents (ppm) of kimberlites Yakutia

Table 1.

Field	Mirnynskoye				Alakit-Markhinskoye			Daldyn		Nakyn			
Pipe	Mir (10)*	Interna-tional (10)	23rd CPSU Congress (6)	Taezh-naya (13)	Yublei-naya (6)	Aikhal (4)	Komso-mols-kaya (6)	Udach-naya (4)	Mean1-8	Botyo-biya (10)	Nyurbins-kaya (10)	May (3)	Mean 10-12
Compo-nent	1	2	3	4	5	6	7	8	9	10	11	12	13
SiO_2	31.3	33.40	23.60	33.47	32.62	25.05	32.46	25.13	29.64	30.55	29.80	32.55	330.97
TiO_2	1.06	0.40	0.66	1.06	1.01	0.62	1.69	0.98	0.94	0.58	0.42	0.41	0.47
Al_2O_3	2.57	2.52	2.56	3.12	1.10	2.21	2.71	2.15	2.37	3.42	3.75	3.71	3.63
Fe_2O_3	6.54	6.21	3.78	4.32	6.10	4.87	9.22	5.43	5.81	6.30	5.65	7.99	6.65
MnO	0.13	0.12	0.12	0.09	0.10	0.05	0.10	0.07	0.10	0.11	0.14	0.03	0.09
MgO	28.7	28.67	20.32	21.81	32.52	23.19	25.75	20.43	25.17	27.16	22.72	25.94	25.27
CaO	10.2	7.96	21.87	13.57	7.81	16.64	8.05	20.45	13.32	11.61	13.29	11.57	12.16
Na_2O	0.07	0.62	0.21	0.11	<0.003	0.14	0.03	0.06	0.18	0.01	0.00	0.17	0.06
K_2O	0.88	1.16	0.52	0.71	0.12	0.97	0.49	0.94	0.72	1.58	0.92	1.45	1.32
P_2O_3	0.45	0.44	0.51	0.75	0.24	0.42	0.22	0.32	0.42	0.67	0.41	0.67	0.58
L.O.I.	17.8	18.32	24.09	19.57	18.20	25.70	19.23	23.90	20.85	16.56	22.36	15.54	18.15
Total	99.8	99.80	99.40	100.33	99.79	99.84	99.94	99.83	99.52	98.55	99.45	100.02	99.34
Be	2.90	2.97	2.43	1.38	1.17	2.33	1.42	1.56	2.02	5.59	2.67	3.06	3.77
Ti	6717	2819	3506	6493	6363	40.97	10987	6110	5887	4102	2655	2460	
V	103	63.95	69.65	91.50	76.40	68.86	122	87.93	85.41	74.28	55.08	50.53	59.96
Cr	618	774	1475	1127	842	607	811	570	853	899	465	1852	10.72
Mn	751	550	389	970	844	556	746	518	666	572	584	302	486
Co	74.4	68.16	47.31	57.65	90.21	75.00	92.04	65.75	71.32	69.08	66.49	55.20	63.59
Ni	1189	1355	762	814	1698	1258	1295	1060	1179	1261	1546	1906	1571
Cu	27.8	32.86	17.14	30.24	23.18	26.61	59.91	27.41	30.65	20.52	24.10	26.15	23.59
Zn	161	40.22	172	52.46	45.69	32.19	77.36	77.58	82.31	81.51	42.72	18.93	47.72
Ga	7.56	6.65	5.70	4.48	5.02	6.42	6.77	5.90	6.06	7.18	7.45	5.50	6.71
Rb	30.1	23.66	10.43	17.28	8.64	27.82	31..50	31.66	22.64	38.01	12.11	47.07	32.40
Sr	1017	990	836	467	111	636	226	787	634	767	314	1115	732

Table 1 (Contd)

	1	2	3	4	5	6	7	8	9	10	11	12	13
Y	12.1	11.43	13.26	12.39	5.11	11.24	7.54	8.41	10.19	11.14	7.45	4.50	7.70
Zr	152	143	153	106	78.73	133	110	95.02	121	89.33	63.28	49.77	67.46
Nb	148	122	129	109	129	138	121	136	129	36.67	20.27	24.30	27.08
Mo	2.60	4.60	0.93	1.71	1.98	2.18	2.97	2.33	2.41	1.54	1.12	0.30	0.99
Cs	0.26	0.10	0.23	0.24	0.13	0.26	0.55	0.80	0.32	0.23	0.22	0.80	0.42
Ba	783	701	707	488	106	1215	361	602	620	681	145	589	472
La	68.5	80.23	105	73.17	50.96	80.58	42.03	59.79	70.04	17.18	20.02	8.51	15.24
Ce	136	153	185.7	141	97.44	152	72.06	110	131	35.10	29.45	17.97	27.51
Pr	14.9	16.43	19.78	14.98	10.16	16.04	7.65	11.55	13.94	4.63	4.25	3.06	3.98
Nd	52.0	55.64	67.34	51.45	33.57	54.97	26.39	38.96	47.55	19.33	16.30	13.33	16.32
Sm	7.51	7.59	8.97	7.35	4.44	7.57	3.77	5.33	6.57	4.01	2.83	3.14	3.3
Eu	1.91	1.87	2.14	1.62	1.06	2.05	1.04	1.33	1.63	1.15	0.80	0.86	0.94
Gd	4.74	4.63	5.45	4.61	2.62	4.45	2.38	3.15	4.00	3.23	2.23	2.70	2.72
Tb	0.59	0.56	0.65	0.56	0.31	0.56	0.32	0.40	0.49	0.44	0.30	0.39	0.38
Dy	2.81	2.57	2.90	2.65	1.34	2.55	1.53	1.87	2.28	2.26	1.54	1.86	1.89
Ho	0.45	0.41	0.46	0.43	0.20	0.41	0.27	0.31	0.37	0.38	0.27	0.33	0.33
Er	1.05	0.94	1.02	0.94	0.44	0.97	0.69	0.75	0.85	0.93	0.67	0.80	0.80
Tm	0.14	0.12	0.13	0.13	0.05	0.12	0.10	0.09	0.11	0.12	0.09	0.11	0.11
Yb	0.79	0.69	0.72	0.63	0.33	0.69	0.57	0.55	0.62	0.69	0.55	0.67	0.64
Lu	0.11	0.10	0.10	0.09	0.04	0.09	0.08	0.07	0.09	0.10	0.07	0.10	0.09
Hf	3.47	2.99	3.46	2.29	1.96	3.01	2.71	2.23	2.77	1.97	1.44	1.58	1.66
Ta	2.60	1.77	7.79	8.47	2.70	1.34	1.95	3.50	3.77	0.72	0.50	1.32	0.85
W	1.04	96.70	-	-	1.01	3.20	1.68	1.76	17.56	0.83	0.65	0.34	0.61
Pb	0.88	0.83	-	-	0.88	0.60	3.30	0.92	1.23	1.39	1.2	1.56	1.39
Th	7.60	7.44	14.96	11.92	6.13	7.70	4.12	6.77	8.33	1.17	0.91	1.46	1.18
U	2.76	2.94	1.54	1.99	1.98	2.87	1.72	2.42	2.28	0.52	0.52	0.63	0.56

*In brackets – number of samples

The main components are determined with X -ray fluorescent method in the Institute of Geology and Mineralogy, Siberian branch of RAS, Novosibirsk, analyst L.D.Kholodova; trace elements – with ICP -MS method in IMGRE, Moscow, analyst D.Z.Zhuravlev.

the geochemical heterogeneity of kimberlites, the authors carried out a comparative petrochemical investigation of kimberlites from the Middle Markha region of the traditional diamond-bearing areas in Yakutia. In discussion of the results the authors used the data on geochemistry of kimberlites from the Arkhangelsk diamond- bearing province [1, 8, 22].

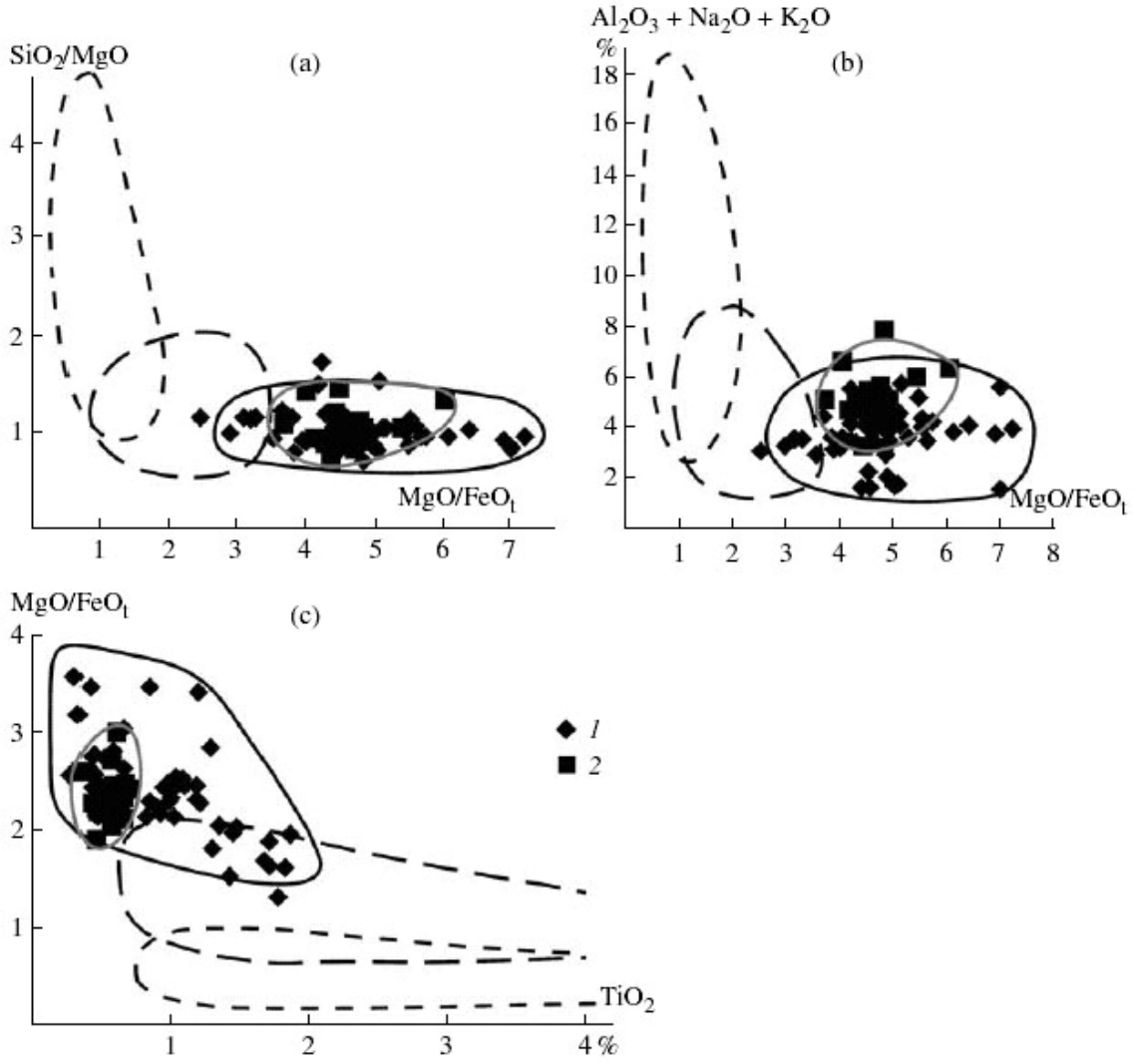

Fig. 1. **Compositions of kimberlites from the traditional diamond-bearing areas and the Middle Markha region of Yakutia.**

In the (a)SiO2/MgO–MgO/FeOt, (b)(Al2O3+Na2O+K2O) –MgO/FeOt, and (c) MgO/FeOt–TiO2diagrams. Kimberlite pipes: (*1*) Mir,Internatsional'naya, Udachnaya, Aikhal, Yubileinaya, Komsomol'skaya, 23rd Party Congress, Taezhanaya, Dachnaya, (*2*) Botuobiya,and Nyurbinskaya. The solid line shows the field of diamondiferous kimberlites, the long-dashed line shows the field of kimpicrites,and the short-dashed line shows the field of alpicrites. The solid gray line encloses the field of kimberlites from the MiddleMarkha region (Nakyn field).

Table 1 presents average kimberlite compositions from different pipes; however, the graphical interpretation of the results and construction of petrochemical and geochemical diagrams involved the analysis of individual

samples of kimberlites. Ratios of the compositions of new kimberlites occurrences and composition of the formation petrotype are clearly seen on previously proposed by us the diagnostic petrochemical diagrams for kimberlites and

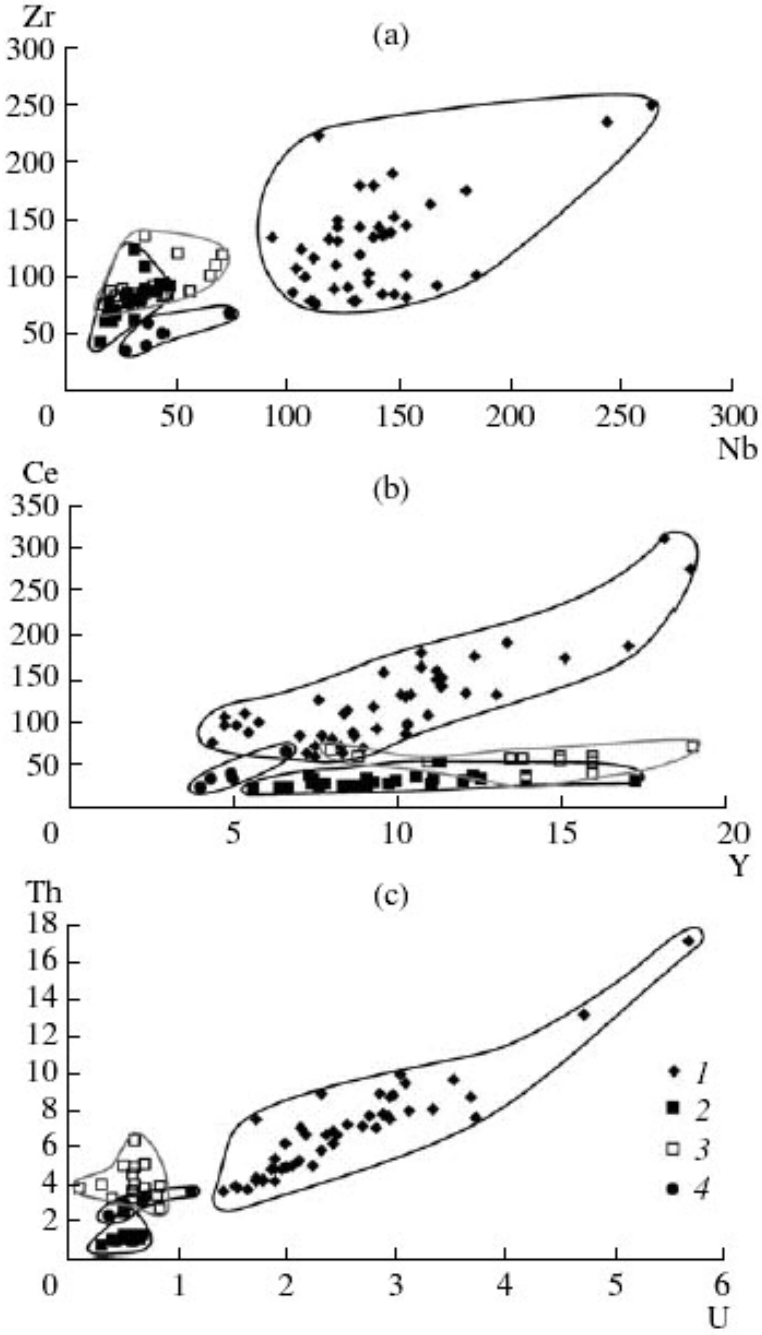

Fig. 2. **Correlations between the contents of (a) Zr and Nb,(b) Ce and Yb, and (c) Th and U in the kimberlites of the Nakyn and Zolotitsa fields and traditional diamond-bearing regions of Yakutia.**

(*1*) Kimberlites from the traditional diamond-bearing regions of Yakutia (Mir, International,Udachnaya, Aikhal, Yubileinaya, Komsomol'skaya, 23rd Party Congress, Taezhnaya, and Dachnaya pipes); (*2*) kimberlites from the Nakyn field of Yakutia (Botuobiya and Nyurbinskaya pipes); (*3*) kimberlites of the Zolotitsa field of the Arkhangelsk province (Lomonosovskaya, Pionerskaya, and Karpinskii pipes). (*4*) V. Grib pipe in the Verkhotina field of the Arkhangelsk province.

convergent rocks [10]. Fig.1 shows the compositions of kimberlites in the Nakyn field and compositions of rocks in the traditional diamond-bearing regions of Yakutia, that are considered as a formation standard. This figure demonstrates, that indicator petrochemical parameters of kimberlites in the Nakyn field in most cases are in the limits of value limits, typical of the rocks of the formation petrotype. The kimberlites of the Nakyn field are somewhat peculiar because their figurative points are confined to low-Ti part of the kimberlite field (Fig. 1c) and are slightly shifted toward elevated parameter values (Al_2O_3+Na_2O+K_2O) (Fig. 1c). However, these features are not sufficient to distinguish contrasting petrochemical groups of kimberlites; our data suggest, that their compositions are rather uniform.

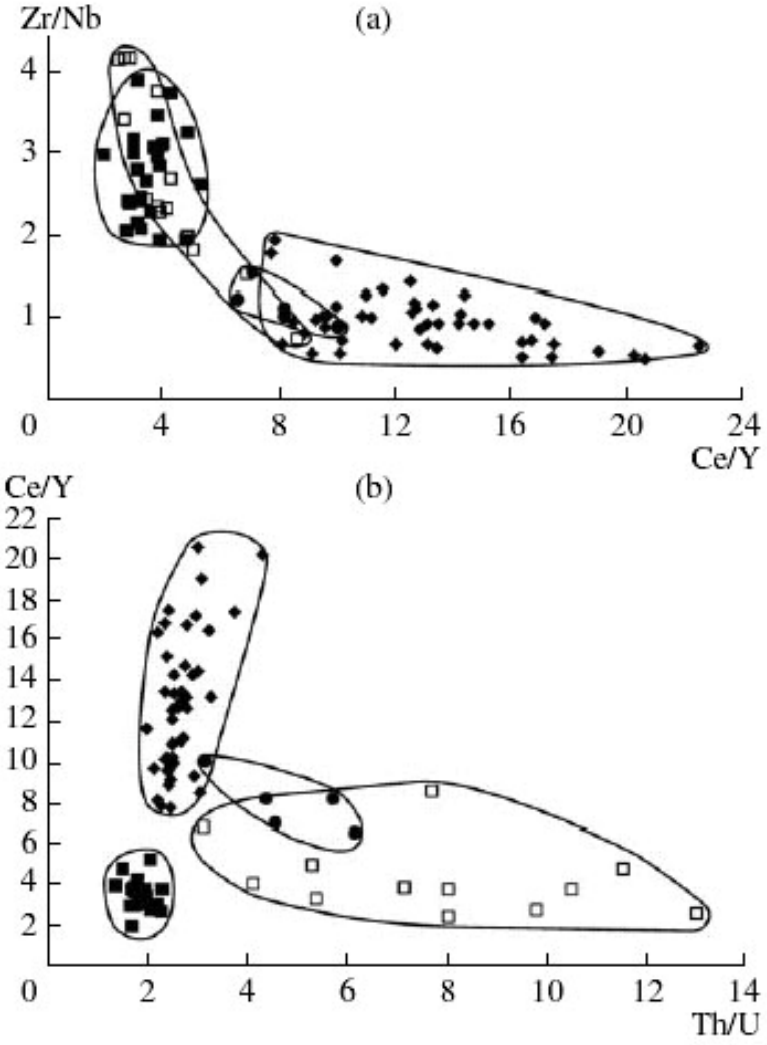

Fig. 3. **Correlations between the element ratios (a) Zr/Nb– Ce/Y and (b) Ce/Y–Th/U in the kimberlites of various geochemical types.**

The symbols are the same as in Fig. 2.

At the same time the most significant differences between the recently revealed kimberlite occurrences and the rocks of the formation petrotype are established by comparison of their geochemical parameters. According to a number of geochemical parameters, these groups of kimberlites are so contrast that this allows to distinguish two geochemical types of rocks. The main geochemical type corresponds to the petrotype of the kimberlites and can be represented by the rocks of the traditional diamond-bearing-regions of Yakutia: Malaya Botuobiya, Daldyn–Alakit, and Upper Muna. The rocks of this type show moderately high contents of highly charged trace and radioactive elements.

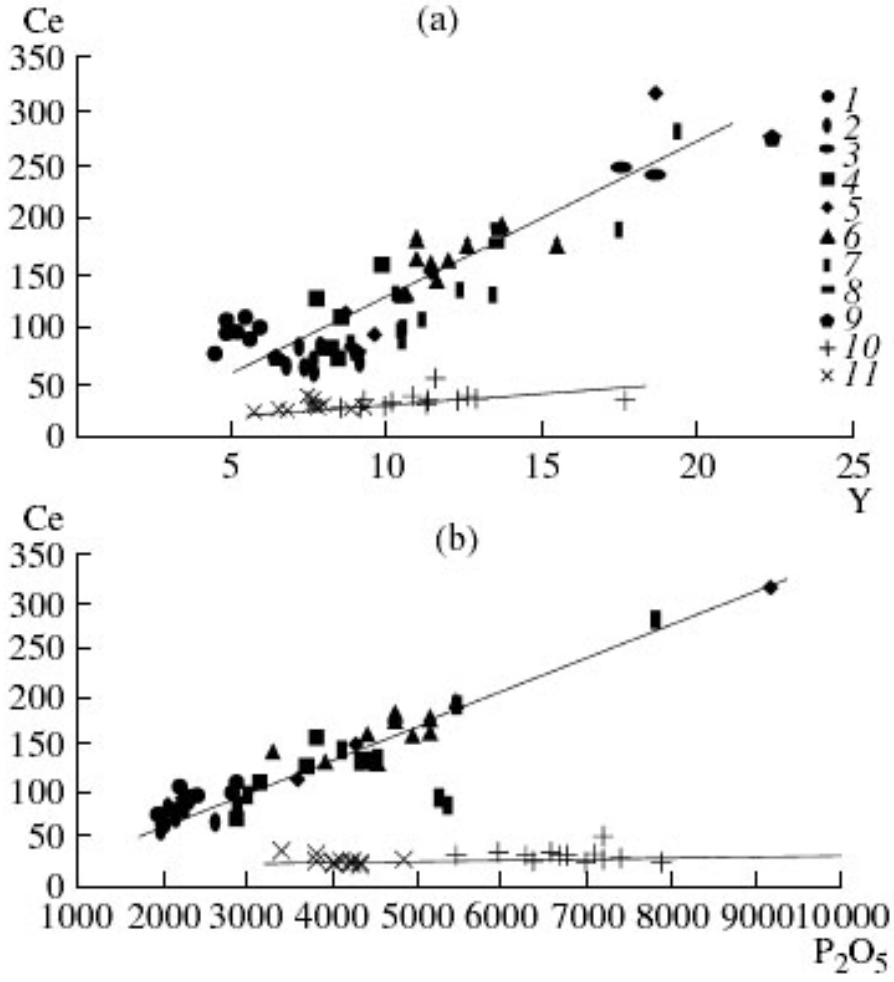

Fig. 4. **Correlations between the contents of (a) Ce and Y and (b) Ce and P2O5 in the kimberlites of the Middle Markha region and traditional diamond-bearing regions of Yakutia.**

Kimberlite pipes: (*1*) Yubileinaya, (*2*) Komsomol'skaya, (*3*) Dachnaya, (*4*) Udachnaya, (*5*) Aikhal, (*6*) International, (*7*) Mir, (*8*) 23rd Party Congress, (*9*) Taezhnaya, (*10*) Botuobiya, and (*11*) Nyurbinskaya.

These rocks are in sharp contrast to the kimberlites of the Nakyn field, which show significantly lower contents of Nb, Ta, Ce, U, and Th. This geochemical type of kimberlites is distinguished by the negative anomaly of highly charged trace and radioactive elements, relatively low (compared with other occurrences of

kimberlite rocks) concentrations of titanium, and low Ce/Y, Nb/Zr, and Th/U values. In addition to the kimberlites of the Nakyn field, similar characteristics were observed in the rocks of diamondiferous pipes from the Arkhangelsk province [1, 2, 8, 9].

The division of kimberlites into two geochemical types is clearly manifested in the covariation diagrams of highly charged lithophile elements: Zr–Nb (Fig. 2a), Ce–Y (Fig. 2b), and U–Th (Fig. 2c) and their indicator ratios: Zr/Nb–Ce/Y (Fig. 3a) and Ce/Y–Th/U (Fig. 3b). In all of these diagrams, the rocks of the Nakyn field are clearly distinguished from the kimberlites of the traditional diamond-bearing regions of Yakutia, falling near the rocks of the Zolotitza field and the V. Grib pipe in the Verkhotina field of the Arkhangelsk diamondiferous province.

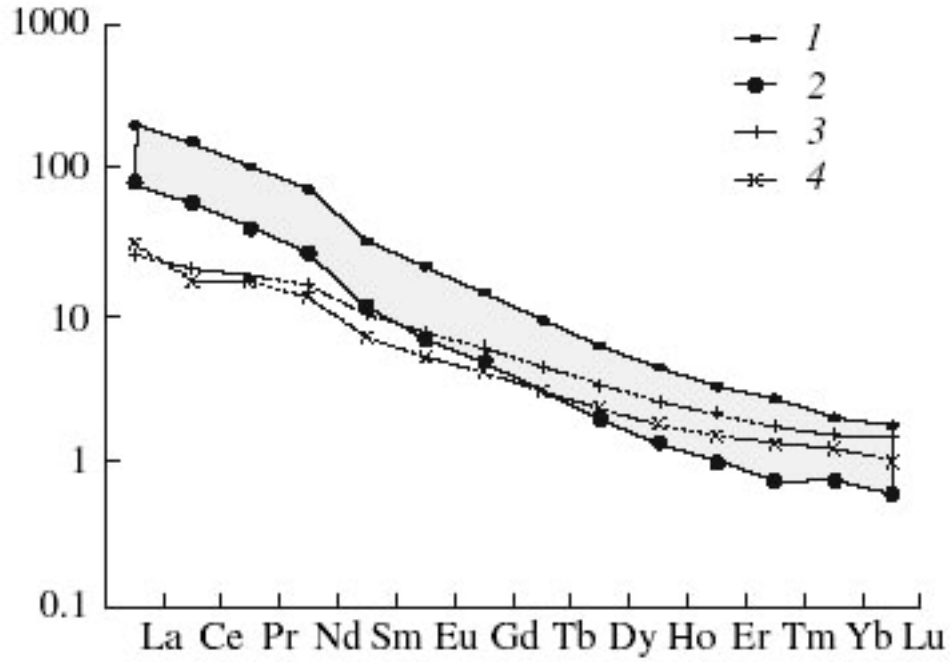

Fig. 5. **Pyrolite-normalized (McDonough and Sun, 1995) distribution of rare earth elements in the kimberlites of the traditional diamond-bearing regions (Malaya Botuobiya and Daldyn–Alakit) and the Middle Markha region of Yakutia.**

The gray shading indicates the field of kimberlites from the traditional diamond-bearing regions; (*1*) and (*2*) extreme compositions of this field (*1*, kimberlites of the Dachnaya pipe and *2*, kimberlites of the Yubileinaya pipe); (*3*) and (*4*) kimberlites of the Middle Markha region (*3*, Botuobiya pipe and *4*, Nyurbinskaya pipe).

The analysis of geochemical differences between the two types of kimberlites suggests that they are related to fundamental genetic distinctions reflecting the specific character of mantle sources for these rocks. This is indicated by the Ce–Y (Fig. 4a) and Ce–P_2O_5 (Fig. 4b) relationships in the two groups of kimberlites. In the Ce–Y diagram (Fig. 4a), the rocks of each pipe from the traditional diamond-bearing regions of Yakutia occur mainly in their own characteristic field; all of

these fields are confined to a common regression line. The rocks from the Botuobiya and Nyurbinskaya pipes of the Nakyn field also fall within individual fields, which overlap in part and form a common regression line. The slope of the line is significantly different from that of the above-described trend for the traditional diamond-bearing regions of Yakutia and the Ce content is significantly lower. The Ce–Y diagram (Fig. 4a) illustrates considerable differences both in the concentration of Ce-group REE and in the composition of REE in the kimberlites of the two groups. This is supported by Fig. 5, which shows the distribution patterns of REE in the kimberlites. The less fractionated REE patterns of the rocks of the Nakyn field reflect a substantial decrease in the concentration of light lanthanides and a relatively high role of heavy lanthanides and yttrium in their composition, as compared with the kimberlites of the traditional diamond-bearing regions of Yakutia.

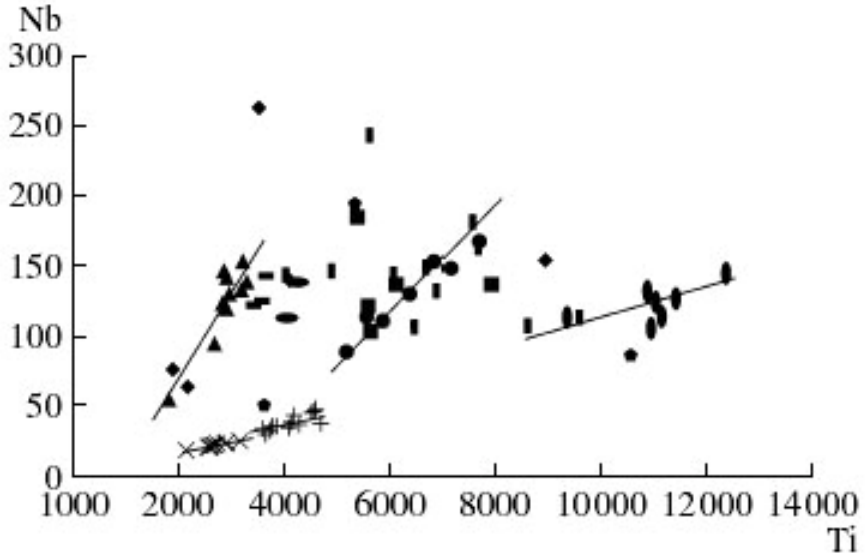

Fig. 6. **Covariations of Nb and Ti contents in the kimberlites of the Middle Markha region and traditional diamond-bearing regions of Yakutia.**

The symbols are the same as in Fig. 4.

Similar relationships can be observed in the Ce–P_2O_5 diagram (Fig. 4b), where two correlation lines, one for the kimberlites of the traditional diamond-bearing regions of Yakutia and the other for the rocks of the Nakyn field, indicate that different modes of Ce-group REE occurrence dominate in the two kimberlite types: mostly phosphates in the former case and silicates or oxides in the latter case.

Important relationships were observed in the Nb–Ti diagram (Fig. 6). The rocks of the Nakyn field cluster in the region of low Nb contents along a distinct regression line, which is restricted to low Ti contents. In contrast, the kimberlites of the traditional diamond-bearing regions of Yakutia plot at much higher Nb ontents and show considerably variable Ti contents, from low to moderately

Table 2.

Average contents of characteristic elements (ppm) and their indicator relations in contrast geochemical types of kimberlites

Rocks	Nb	Ta	Zr	Hf	Ce	Y	U	Th	Sr	Ba	Rb
Kimberlites from traditional diamond-bearing regions of Yakutia: pipes Mir, International, Udachnaya, Aikhal, Yubileinaya, Komsomolskaya, 23th CPGU Congress, Dachnaya (79)	136.1	3.8	118	2.2	140.5	10.5	2.66	7.95	700	621	27.8
Kimberlites from Nakyn field: pipes Botuobiya, Nyurbinskaya, May (23)	24.7	1.05	66.8	1.66	27.8	7.9	0.63	1.46	790	481	35.8
Kimberlites from Zolotitsa field, Arkhangelsk province: pipes Lomonosovskaya, Pionerskaya, Karpinskii (17)	39.4	1.8	100.3	2.74	55.07	14.04	0.58	4.13	415	708	26.4
Kimberlites V.Grib pipe, Arkhangelsk province (4)	44	2.09	50.2	1.1	41.16	4.99	0.67	2.97	239	248	17.3
Kimberlites Victor Nort pipe, Slave province, Canada (1)	42	1.12	24.0	0.62	30.5	2.5	0.55	1.98	384	252	4.5

Rocks	Cr	Ni	V	Ti	Zr/Nb	Nb/Ta	Ce/Y	Th/U	Rb/Sr	Sr/Ba
Kimberlites from traditional diamond-bearing regions of Yakutia: pipes Mir, International, Udachnaya, Aikhal, Yubileinaya, Komsomolskaya, 23th CPGU Congress, Dachnaya (79)	732	1260	87	7660	0.87	35.8	13.38	2.99	0.04	1.13
Kimberlites from Nakyn field: pipes Botuobiya, Nyurbinskaya, May (23)	1226	1364	57.6	2563	2.63	24.5	3.61	2.32	0.05	1.65
Kimberlites from Zolotitsa field, Arkhangelsk province: pipes Lomonosovskaya, Pionerskaya, Karpinskii (17)	1077	1296	95	5555	2.5	21.9	3.9	7.14	0.08	0.59
Kimberlites V.Grib pipe, Arkhangelsk province (4)	1100	1610	109	5996	1.14	21.1	8.25	4.43	0.07	0.96
Kimberlites Victor Nort pipe, Slave province, Canada (1)	904	1737	61.2	6437	0.58	37.5	12..3	3.63	0.01	1.52

high ones. In the general data set, the points of rocks from individual pipes are usually confined to rather narrow specific intervals of Ti contents, within which a direct correlation between Nb and Ti is often observed. The slopes of these correlation lines are different from that of the Nakyn field kimberlites. It is noteworthy that the character of correlation relationships between Nb and Ti in the kimberlites of this type varies depending on the level of Ti content. The regression line is steep at low Ti (International pipe), and a slight increase in Ti content is accompanied by a sharp increase in Nb. With increasing Ti content, the slope of the regression lines decreases, and at high Ti contents, a significant increase in Ti is accompanied by only a slight increase in Nb concentration. The regular change in the character of correlation relationships between Nb and Ti, which is manifested by a gradual decrease in the slope of regression lines with increasing Ti content, indicates common genetic features for the kimberlites of the traditional diamond-bearing regions of Yakutia. Such a character of the regression lines is probably related to the fact that Nb has a higher charge and a smaller effective ionic radius compared with Ti, which results in its preferential partitioning into Ti-bearing minerals during the early stages of their crystallization. The peculiar characteristics of the kimberlites of the Nakyn field, which do not follow the general trend of Nb and Ti relationships formed by the kimberlites of the traditional type, indicate that the two types of kimberlites are probably contrasting in terms of both geochemistry and genesis.

The average contents of characteristic elements and their indicator relations in contrast geochemical types of kimberlites are summarized in table 2.

ON THE NATURE OF THE GEOCHEMICAL HETEROGENEITY OF KIMBERLITES

As follows from our analysis, the geochemical parameters of kimberlites are much more variable compared with their petrochemical characteristics and vary within broad limits. The systematic character of these variations allows us to distinguish contrasting geochemical types of rocks. The existence of contrasting geochemical types of diamondiferous kimberlites indicates both geochemical and genetic heterogeneity of this association and metallogenic type of igneous rocks. The origin of kimberlite heterogeneity is not fully understood and deserves special consideration. It is evident that it is connected with some specific features of the sources of these rocks or different conditions of their generation.

The share geochemical differences between the kimberlites with rather similar petrochemical properties allow us to conclude that the geochemical and petrochemical parameters of these rocks are decoupled and were probably controlled by different factors. The major element composition of rocks depends mainly on the composition of the magma-generating mantle source. Under the condition of incipient melting and fluidization, this material is extensively incorporated into the kimberlite. Thus, the petrochemistry of kimberlites is a

function of the parameters that, similar to the diamond content of rocks, are controlled by the depth of generation. This is why the diamond content of kimberlites is always correlated with their petrochemical parameters and distribution of compatible elements [13, 17, 29].

On the other hand, the main factor controlling the geochemistry of rocks, including the distribution of incompatible HFS elements, is probably the metasomatic alteration of mantle rocks, which occur repeatedly under the influence of deep fluids or volatiles released during the recycling of subducted crustal materials. The processes of mantle metasomatism, which operate both long before the generation of kimberlites and immediately prior to their formation, could be responsible for the formation of geochemically heterogeneous source materials and subsequent generation of geochemically specialized types of deep-derived magmas showing signatures of individual mantle sources.

An alternative mechanism that is often proposed for the formation of geochemical and isotopic heterogeneities in mantle rocks and their magmatic derivatives is the mixing of a primitive mantle source with a lithospheric reservoir of the EM-1 or EM-2 type. This suggestion was invoked, for example, to interpret the isotopic signatures of lamproites and orangeites, which are strongly different from those of group 1 kimberlites. Given the similarity of the isotopic characteristics of the enriched sources to those of the lower crust, one possible scenario is the subduction of crustal material, younger (Pr_3) in the case of the EM-2 source or older (Ar_3-Pr_1) for the EM-1 source. It is believed that the subduction of the crust could supply volatile components (promoting melting) and incompatible elements.

Although the theoretical possibility of the occurrence of the subduction mechanism cannot be denied, there are a number of arguments for a more universal role of deep flows of thermal fluids (mantle jets) and metasomatism caused by these flows. The results of these phenomena are similar to those of subduction processes. There is direct evidence that in many cases the chemical heterogeneity of mantle material affecting the geochemical characteristics of kimberlites and related rocks is caused by mantle metasomatism, which is most commonly manifested in the development of the phlogopite–ilmenite assemblage. This assemblage occurs in kimberlites as inclusions of phlogopite–ilmenite and phlogopitized ultrabasic rocks, deformed phlogopite xenocrysts, and coarse-grained ilmenite clots and nodules.

It can be shown that the geochemical characteristics of kimberlites are directly related to the presence and amount of the minerals of metasomatic phlogopite–ilmenite assemblages. For instance, the rocks that are almost free of ilmenite (kimberlites of the Nakyn field of Yakutia and the Zolotitsa field of the Arkhangelsk province) have anomalously low contents of not only titanium but also niobium, zirconium, thorium, uranium, and cerium. In contrast, elevated contents of ilmenite in kimberlites and kimpicrites are usually accompanied by

enrichment in niobium, zirconium, and some other elements. This is clearly illustrated by the kimpicrites of Liberia containing abundant ilmenite xenocrysts [12]. An increase in titanium content in these rocks is correlated with an increase in niobium, zirconium, and chromium, i.e., the elements that reside primarily in ilmenite (Fig. 7).

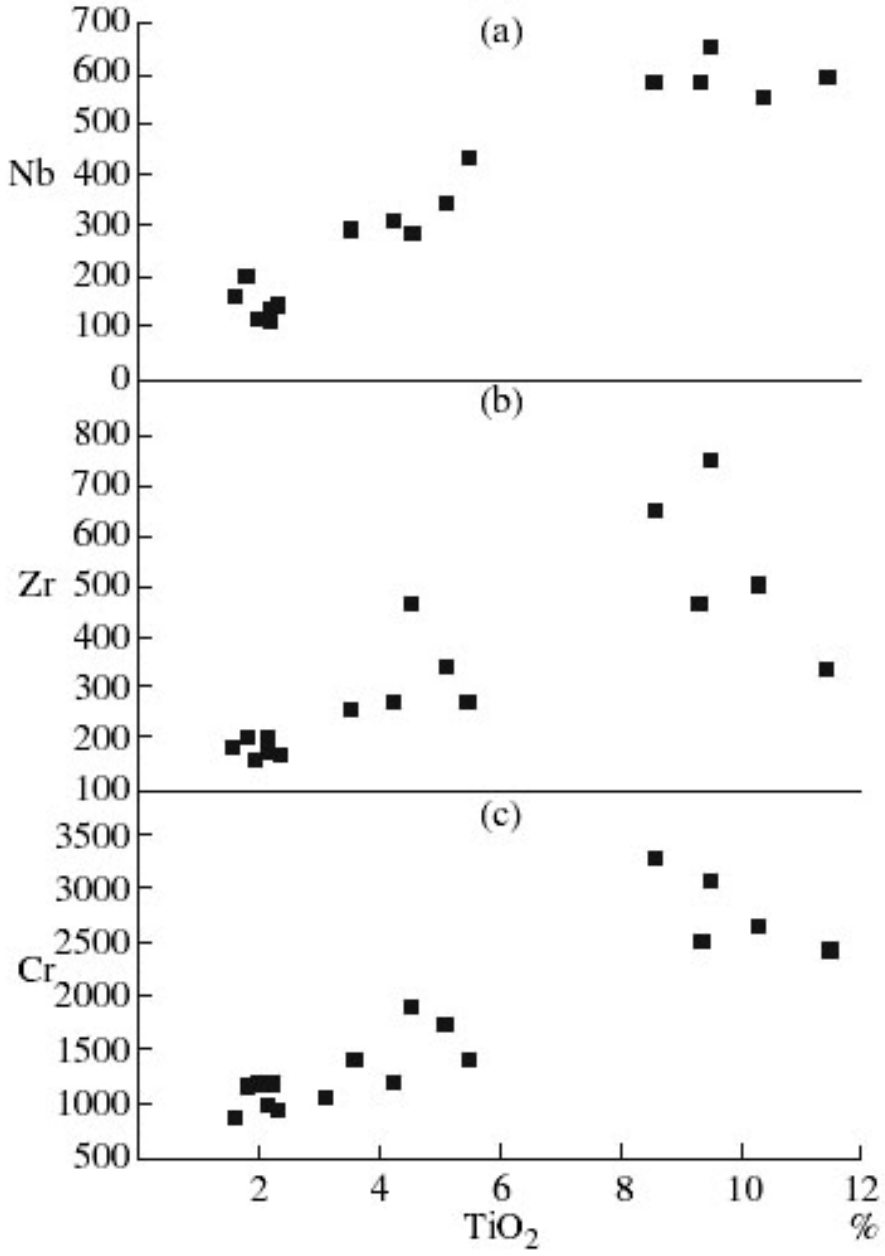

Fig. 7. **Correlation between the concentrations of TiO2 (wt %) and (a) Nb, (b) Zr, and (c) Cr in the kimberlites of Liberia.**

As was noted above, there were probably several deep metasomatic events, which might have different geochemical signatures and significantly different concentration levels and proportions of incompatible elements. The repeated

occurrence of metasomatic processes deep in the mantle is supported by strongly variable model ages of the mantle sources of kimberlites, lamproites, and rocks convergent with them (Table 3). As follows from Table 3, each regional and association group of kimberlites and related rocks, as well as each geochemical type of kimberlite, corresponds to a certain interval of the model ages of the mantle source.

Such intervals were established for the kimberlites from the majority of pipes of the traditional diamond-bearing regions of Yakutia (~600–700 Ma). The kimberlites of the Udachnaya and Aikhal pipes (~700–900 Ma) are conspicuous within this group. The model age of the Nakyn field kimberlites is from 800 to 1240 Ma, and each pipe shows its individual model age (1180–1240 Ma for the Nyurbinskaya pipe and 832–979 Ma for the Botuobiya pipe). The model ages of kimberlites from the Zolotitsa field (~1200–1300 Ma) and V. Grib pipe (~880–1050 Ma) are close to these intervals. Noteworthy are markedly older model ages of the source rocks of the lamproite family, olivine lamproites of Kostamuksha and madjgawanites of India, which are usually higher than 2 Ga and occasionally up to 2.6–2.7 Ga.

The geochemical signature of metasomatic processes is probably affected by a number of factors, including the temporal and geochemical stage of Earth evolution, the character of phase transitions in the interiors, the depth of origin and source of juvenile emanations,etc. The existence of geochemically specialized metasomatic processes in the mantle is supported by the compositions of the alkaline ultramafic rocks of the lamproite clan, olivine lamproites and madjgawanites. The geochemical peculiarity of these rocks includes the extremely high (for ultramafic rocks) concentrations of Ti, Zr, Ce, K, Rb, Ba, P, and F at elevated Zr/Nb, Ce/Y, and Ba/Sr values [6, 11]. The fact that the concentrations of most of these elements in the rocks of the lamproite clan are much higher than those of crustal rocks is difficult to explain in terms of the mixing and recycling of crustal materials. On the other hand, these data and the old model age of the source of lamproitic rocks suggest a contribution from ancient deep-seated metasomatism to the formation of a geochemically peculiar source material enriched in incompatible elements and radiogenic isotopes.

The existence of ancient mantle metasomatism with a geochemical signature similar to that of lamproitic rocks is directly supported by the metasomatic phenomena that were documented by Z.Spetsius [19] in a garnet–orthopyroxene nodule from the kimberlites of the Udachnaya pipe. The nodule contains a secondary assemblage of metasomatic minerals (phlogopite +rutile + zircon), which developes between the garnet and orthopyroxene grains and often intersects the garnet. The modal composition of the inclusion is the following: *Opx* – 30.4%; *Gr* – 29.4%; *Fl* – 36.6%; *Ru* –3.0%, and *Zr* – 0.6%. The U–Pb age of the zircon was estimated by Z.Spetsius as 1.8 Ga. Judging from the composition of the

metasomatic assemblage, this ancient metasomatic process had a K–Ti–Zr specialization similar to that of lamproite magmas.

Examples of geochemically specialized occurrences of kimberlites and related rocks were found in various provinces of the world. Among them are the rocks of the Koidu complex in Sierra Leone (Nb, Ce, Th, and U), the Aries pipe in Western Australia (Nb and Th), and the Alto Paranaiba province in Brazil (Zr, Ce, and U) [9, 21, 23, 24].

Based on these data and the results of the geochemical investigation of xenoliths of metasomatically altered ultrabasic rocks in kimberlites [12], it can be concluded that the metasomatic alteration of mantle rocks under the influence of deep fluids is always accompanied by enrichment in indicator trace elements, primarily incompatible highly charged trace and radioactive elements. This allows us to propose a more comprehensive interpretation of the origin of the peculiar geochemical type of kimberlites which is represented by rocks of the Nakyn field of Yakutia and the Zolotitza field and V.Grib pipe of the Arkhangelsk province. These rocks are characterized by a negative anomaly of highly charged trace and radioactive elements. The kimberlites of this type show very low titanium contents and are almost fee of ilmenite. These observations cast doubt on the significant role of deep metasomatism in formation of these rocks and their mantle source and allow us to prefer the variant of a lithosphere source metasomatized under the influence of fluids supplied from the subducted crust [5]. This example can probably be considered as a geochemical precedent reflecting the contribution of the processes of subduction and recycling of crustal material to the genesis of kimberlites.

The possible participation of subduction processes in the genesis of diamond-bearing kimberlites of the Zolotitza field and the Arkhangelsk province are testified by investigations carried out by O.G. Sorokhtin and oth. [17]According to this source, the analysis of the tectonic development of the Karelo-Kolsky region, as well as interpretation of the available geological data from the point of view of plate tectonics, show, that the Karelo-Kolsky Archean megablock of the continental crust is framed in the north-west by two seamed zones of oceanic lithosphere plates of subshift belonging to the Svecofennian age (1900 million years ago), generated as a result of the Svecofennian paleoocean closure.Both zones are dipping to the North-East under the Karelo-Kola Archean megablock. The authors extrapolated the dipping plane of the eastern subduction zone, which allowed to outline the areas of potential location of oversubducted alkaline ultrabasic carbonatite and kimberlite magmatism in the north-west part of the Baltic Shield and the adjacent territory of the northern part of East-European platform; the noteworthy is coincidence of these areas with real territories of carbonatites and kimberlites development in this region.

As for geohemically anomalous kimberlites of the Middle Markha region on the Sibreian diamond-bearing province, the subduction model also does not meet significant contradictions. Kimberlites are located within the Markha granite-

greenbelt terrain, which is connected with the adjacent terrains and forms the Siberian craton in the collision 1,8-1,9 million years ago during closure of the Paleoproterozoic ocean. This was preceded by generation of island arcs in the Paleoproterozoic ocean and formation of metamorphized sedimentary and volcanogenic belts similar to the deposits of active and passive margins [16]. These conditions were probably favorable for wide manifestation of subduction processes in the ancient oceanic crust. Participation of subduction processes in formation of kimberlites in the Middle Markha region is indirectly confirmed by predominance of diamond paragenesis of eclogitic compositions (pyrope-almandines from magnesio-ferrous eclogites) among garnets [20] as well as by the fact that eclogitic paragenesis constitutes above 50% of all inclusions in the diamond pipe Botuobiya [14].

CONCLUSION

The geochemical investigation of kimberlites from the Middle Markha region and their comparison with kimberlites from the traditional diamond-bearing areas of Yakutia supported the discrimination between two geochemical types of kimberlites. One of them is represented by the rocks of the traditional diamond-bearing regions of Yakutia, whose parameters correspond to the petrotype of the kimberlite association. In addition to the kimberlites of the Middle Markha region, the second type includes the rocks of the Zolotitsa field and V. Grib pipe of the Arkhangelsk province and the kimberlites of the Slave province of Canada. This type can be considered as geochemically anomalous. The obtained representative parameters of the two kimberlite types indicate a considerable geochemical contrast between these rocks, and the individual features of correlation relationships of elements in the two types of rocks suggest that their differences are related to essential genetic reasons.

Contrasting differences were established primarily for the group of incompatible highly charged trace and radioactive HFS elements, including Ce, Nb, Zr, U, and Th. The Ce/Y, Nb/Zr, and Th/U ratios can be used as geochemical indicators. The contrasting geochemical differences between petrochemically uniform kimberlites emphasize the heterogeneous nature of these rocks and their mantle source.

High degree of geochemical contrast of kimberlites belonging to two groups, that has deep genetic reasons, allows to distinguish a special geochemical type of these rocks which is characterized by negative anomaly of HFS rare and radioactive elements (kimberlites of D-type). These rocks can be opposed to the rocks of the formation petrotype of kimberlites (kimberlites of N-type), which are characterized by moderately high contents of HFS elements.

In contrast to the major components and geochemically similar compatible trace elements (Cr, Ni, Co, V, etc.), whose contents are controlled by the

composition of the mantle source and depend on the depth of kimberlite generation, the main factor controlling the distribution of incompatible HFS elements is probably the metasomatic alteration of mantle rocks under the influence of deep-derived fluids or volatiles released during the recycling of subducted crustal material. The processes of mantle metasomatism that occurred both long before the derivation of kimberlites and immediately prior to their generation could promote the appearance of geochemically heterogeneous materials and subsequent generation of geochemically specialized types of deep magmas showing the signatures of individual mantle sources.

The geochemical specialization of deep metasomatic processes probably depends on a number of factors, the detailed study of which will be a subject of future studies. The real existence of geochemically specialized metasomatic processes can be proved by some occurrence of kimberlites and convergent rocks, such as Koidu in Sierra Leone, Aries in Western Australia, Alto Paranaiba in Brazil, as well as the olivine lamproites of Western Australia and other alkaline ultramafic occurrences of lamproitic rocks. The metasomatic alteration of mantle rocks under the influence of fluids of deep-seated origin is always accompanied by a considerable increase in the concentrations of alkalis, titanium, and highly charged incompatible trace and radioactive elements. This can be considered as an additional argument for the suggestion that the rocks of the Middle Markha field, as well as other kimberlite occurrences with negative HFSE anomalies are generated in a lithospheric source region metasomatized by fluids released from the subducted crust.

Petrochemical study of kimberlites and analysis of their geochemical heterogeneity allows to oppose two groups of components, participating in the composition of these rocks. One of them includes main rock forming components as well as coherent trace elements (Cr, Ni, Co, V and oth.); their contents depend on the composition of the mantle substrate in the areas of magma generation – garnet peridotites, which are incorporated into kimberlites under conditions of fusion and fluidization, and make up the substantial part of its matter. This is associated with the observed correlation between diamond mineralization of kimberlites and their petrochemical parameters and distribution of coherent trace elements. The second group includes highly charged incompatible rare and radioactive elements, as well as titanium and alkalies; the latter are distributed mainly as a result of reheating processes of metasomatic transformation of the mantle rocks, influenced by abyssal fluids, or the volatiles, separated during recycling of the subducted crust matter.

Thus, the received data emphasize the heterogeneous nature of kimberlites and their mantle source. It is noteworthy that according to the diagrams with participation of HFS elements kimberlites of the anomalous geochemical D-type form separate fields independent of the fields of N-type. This confirms the concept of the genetic peculiarity of each of two geochemical types of kimberlites under various conditions of their generation. This is another argument in favor of special

investigations of all the aspects of D-type kimberlites generation, including peculiarities of their structural–tectonic position.

So, it should be noted, that this subdivision into two contrast geochemical types was previously established for lamproites too. According to O.A. Bogatikov and V.A. Kononova [3] lamproites were formed inside the plates in presence of higher contents of titanium and highly charged rare elements (Zr, Nb, Ce, La and oth.) , while low-titanium rocks , rather poor of HFS elements, are formed under oversubduction collision conditions of continental margins. This heterogeneity of most abyssal generated formations probably reflects global laws of the mantle magmatism, resulted both from substrates, metasomatized under the influence of juvenile abyssal fluids, and substrates, transformed under the influence of the volatiles from the subducted crust.

The analysis and the data based on it, have a number of important results. Among kimberlites of N-type and D-type both highly dimondiferous and low dimondiferous rocks occur; this means, that diamond mineralization of kimberlites is not dependent on the mechanism of metasomatic preparation of the substrate. This suggests that diamond is a protomineral of the mantle substrate, which is formed in the process of primary differentiation of the earth substrate prior to the influence (on mantle rocks) of juvenile fluids and volatiles, associated with the recycling of the matter of subducted oceanic rock. The subsequent processes of metasomatism and fusion of the mantle matter as well as its transportation with kimberlite magma to the surface, can be accompanied by crushing, growth and solution of the dimondiferous protocrystals. This conclusion is consistent with the isotope data, pointing the ancient age of the most part of diamonds in kimberlites (3,1-3,5 Ma).

The fact that all known diamond-bearing kimberlite bodies of the Nakyn and Zolotitza fields are composed of the anomalous D-type rocks, while the traditional diamond-bearing regions of Yakutia are presented only by N-type kimberlites, points to the trend for spatial separation of two geochemical types of kimberlites. At the same time, one can’t exclude the potential spatial contact of two types of kimberlites, when both juvenile fluids and volatiles, generated in the process of the oceanic crust subduction take part in the metasomatic preparation of the mantle substrate. This possibility is indirectly confirmed both by the transient character of kimberlites in the V.Grip pipe and the presence in the Arkhangelsk province in association with diamond-bearing kimberlites of kimpercrites; according to their geochemical parameters they correspond both to the rocks moderately enriched by HFS elements and the rocks with negative anomaly of these elements. The prevailing tendency is the preferred confinement of N-type kimberlites to the inner parts of ancient cratons and D-type kimberlites – to the marginal parts.

The above data substantially change the ideas of kimberlites as a geochemical object. They have a number of petrological and prospecting results. For petrology it is important to get reliable criteria of subduction processes

partcipation in the mantle metasomatism and magmatism. It is important for the diamond minerageny, that the degree of diamond mineralization of kimberlites doesn't depend on their geochemical type and, consequently, diamond, most likely , refers to protominerals of the mantle substrate; the subsequent metasomatism and fusion of the latter, as well as transportation of the abyssal matter of the kimberlite magma, can be accompanied by crushing ,growth and solution of diamond. At last, the adequate geochemical image of kimberlites, which is substantially different from the traditional ideas, presents great importance for forecasting of the diamond mineralization of new occurrences of magmatites and diamond prospecting geochemistry.

REFERENCES

1. **Arkhangelsk Diamondiferous Province:** Geology, Petrography, and Mineralogy, (Ed. by O. A. Bogatikov) Mosk. Gos. Univ., Moscow, 2000, [in Russian].
2. **Bogatikov O. A., Kononova V. A., Golubeva Yu. Yu., et al.** Variations in Chemical and Isotopic Compositions of the Yakutian Kimberlites and Their Causes// Geokhimiya, 2004, №. 9, 915–939, [in Russian].
3. **Bogatikov O.A.., Rjabchikov I.D., Kononova V.A..,** et al.// Lamproites. M, Nauka, 1991. 301pp. [in Russian].
4. **Verzhak V.V.**Geological structure, matter composition, conditions of formation and methods of exploration in diamond deposit M.V Lomonosov. // The author's abstract of Diss.. M. Moscow State University. 2001. p.36 [in Russian].
5. **Golubeva Yu. Yu., Pervov V. A., Kononova V. A..** Low-Ti Diamondiferous Kimberlites - a New Petrogeochemical Type// in Proceedings of Scientific and Applied Conference on 50th Anniversary of the Discovery of the First Diamondiferous Pipe Zarnitsa, VSEGEI, Russia, 2004 (VSEGEI, St. Petersbur), 2004, pp. 96–99 [in Russian].
6. **Jaques L., Lewis J. D. Smith B. D.,** The Kimberlites and Lamproites of Western Australia, Geol. Surv.W. Aust. Dep. Mines Bull. 1986,132, [in Russian].
7. **Kononova V. A., Golubeva Yu. Yu., Bogatikov O. A., et al**., Geochemical Diversity of Yakutian Kimberlites: Origin and Diamond Potential // Petrologiya, 2005, 13, 493–509 [in Russian].
8. **Kononova V. A., Levsky L. K., Pervov V. A.,** et al., Pb–Sr–Nd Isotopic Systematics of Mantle Sources of Potassic Ultramafic and Mafic Rocks in the North of the East European Platform// Petrologiya,2004, .№10, 493–509 [in Russian].
9. **Lapin A.V., Tolstov A. V.,** Problems of the Geochemical Heterogeneity of Kimberlites, //Prikl. Geokhim. 2005,2 (7), 77–93 [in Russian].
10. **Lapin A.V., Tolstov A. V., and Lisitsin D. V.** Kimberlites and Related Rocks. IMGRE, Moscow, 2004 [in Russian].
11. **Lapin A.V. Khar'kiv A. D.** Geochemical Features of Ilmenite–Phlogopite Ultramafic Xenoliths in Kimberlites and the Role of Fluids in Mantle Differentiation// Dokl. Akad. Nauk 1980, 255, 1269–1271 [in Russian].
12. **Lapin A.V. Khar'kiv A. D.** Majgawanites as a Special Petrochemical Type of Diamondiferous Igneous Rocks// Geokhimiya, 2003, No. 11, 1–10 [in Russian].
13. **Milashev V. A.,** Petrochemistry of the Yakutian Kimberlites and Factors of Their Diamond Potential. Nedra, Leningrad, 1965 [in Russian].
14. **Mitiukhin S.I.., Spetsius Z.V..** Inclusions in diamonds from kimberlite pipe Batuobinskaya.- Geologia I geophisika. 2005.T.46.N13. P.1246-1258. [in Russian].
15. **Pokhilenko N. P., Sobolev N. V., Zinchuk N. N.,** Essential Features of Anomalous Kimberlites from the Siberian Platform and Slave Craton with Application to the Problem of Forecasting and Prospecting// in Proceedings of All-Russia Conference on the Diamond Potential of the Timan–Ural Region Syktyvkar, 2001, p. 19-21 [in Russian].
16. **Rosen O.M.., Manakov O.V.., Suvorov V.D..** Collision system in the North-East of the Siberian craton and the problem of the diamond-bearing lithosphere kill.- Geotektonika. 2005.N6.P.42-67 [in Russian].
17. **Sarsadskikh N. N. Blagul'kina V. A.,** Petrographic and Petrogenetic Differences of Kimberlites from the Rocks Showing a Similarity in Some Characteristics// Zap. Vseross. Mineral. O-va 98, 415–421 (1969) [in Russian].

18. **Sorokhtin O.G., Mitrofanov F.P., Sorokhtin N.O..** Origin of diamonds and prospects of diamond mineralization of the Western Part of the Baltic shield. - Apatity. 1996. 146pp. [in Russian].
19. **Spetsius Z. V.** Metasomatism and Partial Melting in Xenoliths from the Kimberlite Pipes of Yakutia in the Context of Diamond Genesis// in Proceedings of 4th International Seminar on Sources of Deep-Seated Magmatism and Their Relations with Plume Processes, Irkutsk–Ulan Ude, Russia, 2004, pp. 107–143 [in Russian].
20. **Khar'kiv A.D., Zinchuk N.N. Kriuchkov A.I..** Original deposits of the world diamonds, M. Nedra. 1998. 555pp. [in Russian].
21. **Araujo L. N., Carlson R. W., Gaspar J. C., Bizzi L. A.,** Petrology of Kamafugites and Kimberlites from the Alto Paranaiba Alkaline Province, Minas Gerais, Brazil,// Contrib. Mineral. Petrol. **142**, 163–177 (2001).
22. **Beard A.D.,.Downes H, Hegner E., Sablukov S.M..** Geochemistry and mineralogy of kimberlites from the Arkhangelsk Region NW Russia: evidence for transitional kimberlite magma types.// Lithos. 2000, 51, , p.43-73.
23. **Carlson R.W., Esperance S, Svisero D.P**..Chemical and Os isotopic study of Cretaceous potassic rocks from Southern Brasill.// Contrib. Mineral. Petrol. 1996. 125. P.393-405.
24. Ed**wards D.,. Rock N. M. S, Tailor W. R.,** et al., Mineralogy and Petrology of the Aries Diamondiferous Kimberlite Pipe, Central Kimberley Block, Western Australia// J. Petrol. 1992, 33, 1157–1191.
25. **Mitchell R.N..** Kimberlites, orangites and related rocks. Us. Plenum Press. NY.1995. 410pp.
26. **Pokhilenko N. P., McDonald J. A.,. Agashev A. M,** et al. Kimberlites and Carbonatites of the Snap Lave/King Lake Dike System: Structural Setting, Petrogeochemistry and Petrology of a Unique Type of Association,// in Long Abstracts of 8th International Kimberlite Conference, Victoria, 2003, Canada,
27. **Smith S.B., Gurney J.J., Skinner E.M, Clement C.R., Ebrahim N..** Geochemical character of Southern African kimberlites: a new approach based on isotopic constraints. //Trans Geol. Soc. S. Africa. 1985.66.p.267-280.
28. **Taylor W. R., Tompkins L. A., Haggerty S. E,** Comparative Geochemistry of West African Kimberlites// Geochim. Cosmochim. Acta 1994, 58, 4017–4037.
29. **Vasilenko V. B., Zinchuk N. N., Krasavchikov V. O**., et al., Diamond Potential Estimation Based on Kimberlite Major Element Chemistry// J. Geochem. Explor. 2002. 76, 93–112.

UDK38.33.17 (476)

Geochemical features of alkali rocks of Palaeozoic magmatism of Belarus

Mikhailov N.D.[1], Vladykin N.V.[2], Laptsevich A.G.[1]

[1] *Institute of Geochemistry and Geophysics, Kuprevich str., 7, Minsk, 220141, Belarus e-mail: mihailov@igig.org.by*
[2] *A.P. Vinogradov Institute of Geochemistry, Siberian Branch of the Russian Academy of Sciences, Favorsky str., 1a, Irkutsk, Russia, e-mail:vlad@igs.irk.ru*

ABSTRACT

The genetic similarity of igneous rocks from the Pripyat graben, Zhlobin saddle and, to some extent, North-Pripyat zone of steps is suggested from the distribution of rare earth elements (REE) and some rare elements, as well as the Sr and Nd isotopic composition of Palaeozoic alkali igneous rocks occurring within two magmatism areas of Belarus. A peculiar feature of the REE distribution in rocks of the Gomel structural dam is the europium minimum. An analysis of the distribution of Nb/Y – Zr/Y ratios in various type alkali igneous rocks of Belarus could be indicative of two different magmatic sources probably involved in their petrogenesis. Isotope data of the Sr – Nd distribution in the studied samples form a field restricted between the isotope data of the primitive mantle (PREMA) and those of the enriched mantle source EM 1.

INTRODUCTION

The igneous activity in the southeast of Belarus during the Palaeozoic resulted in the location of all the magmaic formations within two areas: Pripyat graben including the Bragin–Loyev saddle, and the North-Pripyat magmatic region with the Gomel structural dam, North-Pripyat zone of steps and Zhlobin saddle distinguished within their limits in the present-day geotectonic plan (Fig.1).

The Upper-Devonian magmatic formations of Belarus have been studied over many years and were described in several papers published before [2-4, 9-10, etc.]. Showing a wide facies and petrographic diversity igneous rocks are described by a number of petrological and other peculiarities evidently suggesting their belonging to a genetically common igneous series of the continental alkali basic-ultrabasic formation of intracratonal rifting. Their wide petrographic range is due to a multiphase magmatism, diffentiation and contamination of the primitive mantle magmas, as well as to the difference in tectonic and geodynamic environments.

The aim of the present paper is to provide a geochemical description of alkali-ultrabasic – alkali-basaltoid rocks from two areas of Palaeozoic magmatism identified within the territory of Belarus using reliable isotopic and geochemical data.

All the igneous rocks distinduished in the platform cover composition in the southeast of Belarus are represented by alkali-ultrabasic and basic rocks of various petrographic families and, subordinately, by alkali and subalkali intermediate rocks. Of the whole petrographic diversity ultrabasic effusive and subvolcanic rocks of the Pripyat graben, namely, limburgites, alkali picrites, monchiquites;

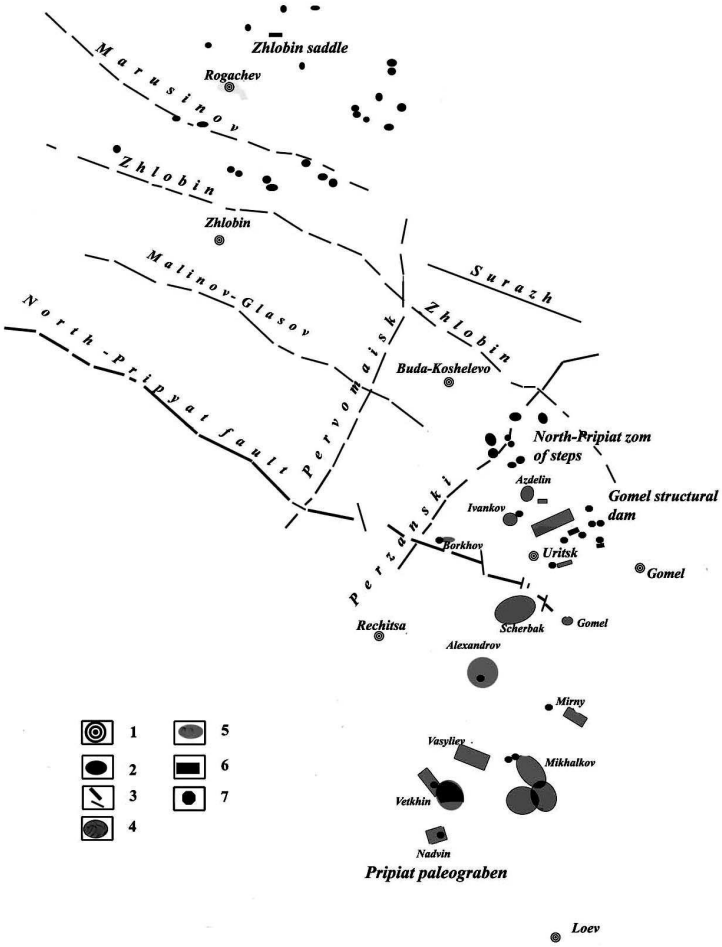

Fig. 1. **Sketch map of Palaeozoic alkaline magmatism evidences in the territory of Belarus: 1 – settlements; 2 – diatremes of the North-Pripyat magmatism area; 3 – faults; 4 – central-type volcanoes; 5 – fissure volcanoes and effusive rock sheets; 6 – subvolcanic and intrusive bodies of alkali igneous rocks.**

nephelinites, leucitic nephelinites, their tuffs and tuff breccias from the Gomel structural dam; alkali basaltoids from the North-Pripyat zone of steps and ultrabasic rocks of the Zhlobin saddle (Figs. 2A-2G) were selected for investigation.

METHODS OF INVESTIGATION

Trace elements and rare earth elements (REE) were determined by the ICP MS method at the V.I.Vinogradov Institute of Geochemistry of the Siberian Branch of the Russian Academy of Sciences, by the neutron activation analysis at the Institute of Nuclear Investigations of the National Academy of Sciences of Ukraine, using a spectrometer at the Department of Geology of the London University and by the ion method at the Pave University of Italia. The Sr and Nd isotope ratios were determined by M.Wilson using the mass-spectrometry method and by H. Downes using the ion-conductive plasma method at the London and Leeds Universities, as well as at the Laboratory of isotope geochronology and geochemistry of the Russian Academy of Sciences [5, 8, 11].

DISTRIBUTION AND AMOUNTS OF THE RARE EARTH AND RARE ELEMENTS

Igneous rocks of the Pripyat graben like alkali ultrabasic and basaltoid rocks from the other regions are enriched in REE relative to the primitive mantle (Fig. 3A), whereas the REE concentration in effusive rocks is similar to that in their subvolcanic analogues. The maximum REE concentrations are peculiar to alkali nephelinic basalts from the Borschevskaya 4 borehole (ΣTR=469.7 ppm) and to

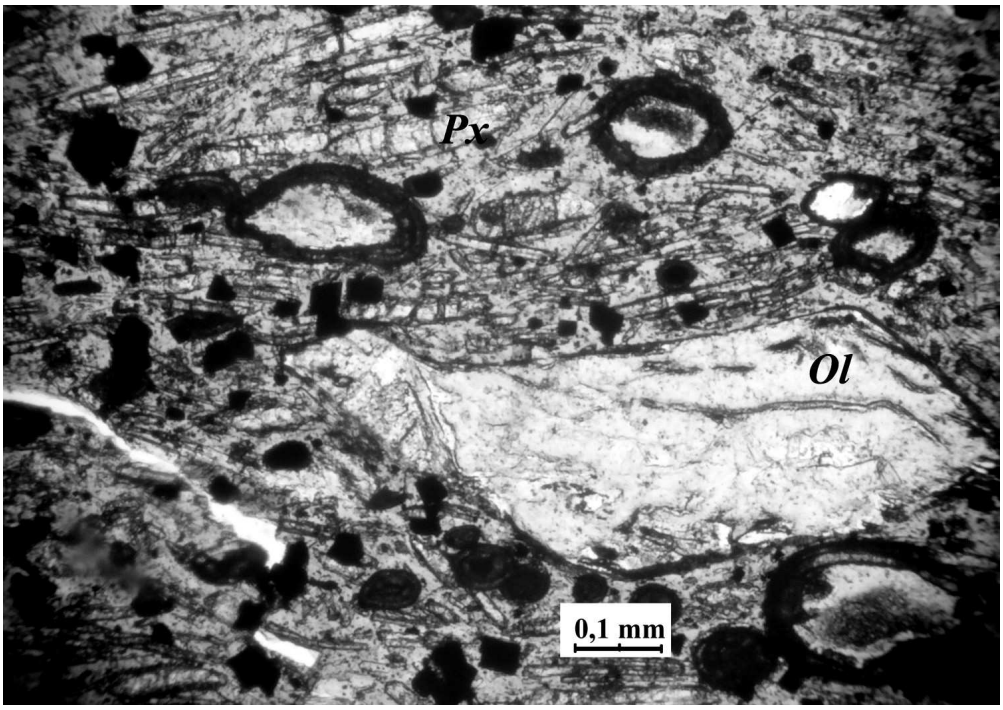

Fig. 2. **Photographs of microsections of some Palaeozoic alkali igneous rocks of Belarus. A – limburgite, Krasnoselskaya borehole 210, depth 3357 m, crossed nicols; B – olivine-pyroxenic alkali picrite, Mezhinskaya borehole 2, depth 1288 m, crossed nicols; C – monchiquite, Artukovskaya borehole 3, depth 4514 m, crossed nicols; D – leucitic nephelinite, Tsentrolit borehole 2, depth 545 m, parallel nicols; E – alkali basaltoid, Uvarovichi borehole 149, depth 355 m, parallel nicols; F – melanephelinite, Madorskaya diatreme 654, depth 270 m, parallel nicols; G – melilite-pyroxenic picrite changing to olivine melilitite, Luchin diatreme 637, depth range from 253 to 255 m, parallel nicols.**

alkali-pyroxenic picrites from the Vasilievskaya 1 borehole (ΣTR=416.8 ppm), and rather low concentrations – to nephelinites from the Vyshemirovskaya 11 borehole (ΣTR=182.4ppm) (see Table 1). Alkali rocks of the Pripyat graben are described by a predominance of light lanthanoids. A degree of fractionation of heavy/light (La/Yb) and light/medium (La/Sm) REE varies from 16 to 51 and from 2 to 10, respectively. The highest enrichment with light lanthanoids was noted in primitive ultrabasic rocks – alkali picrites (La/Yb=51-76), whereas it is smaller (about 15) in the case of differentiated nephelinites. The REE distribution ranges are of similar pattern, i.e. are approximately subparallel without distinct minima and the europium anomaly. And only monchiquit from the Artukovskaya 3

borehole is described by a rather high content of heavy REE (La/Yb=6). Potassic alkali rocks of the Gomel structural dam of the North-Pripyat region represented by leucitites, nephelinites, leucitic nephelinites and their tuffs and tuff breccias are correlated with nepheline-leucitic rocks of the graben in REE contents. These rocks are characterized by the smallest RE concentrations (on the average Σ=160-170 ppm) of all the rocks studied by the authors, and, consequently, by the lowest enrichment relative to the primitive mantle (Fig. 3B). At the same time alkali rocks of the Gomel

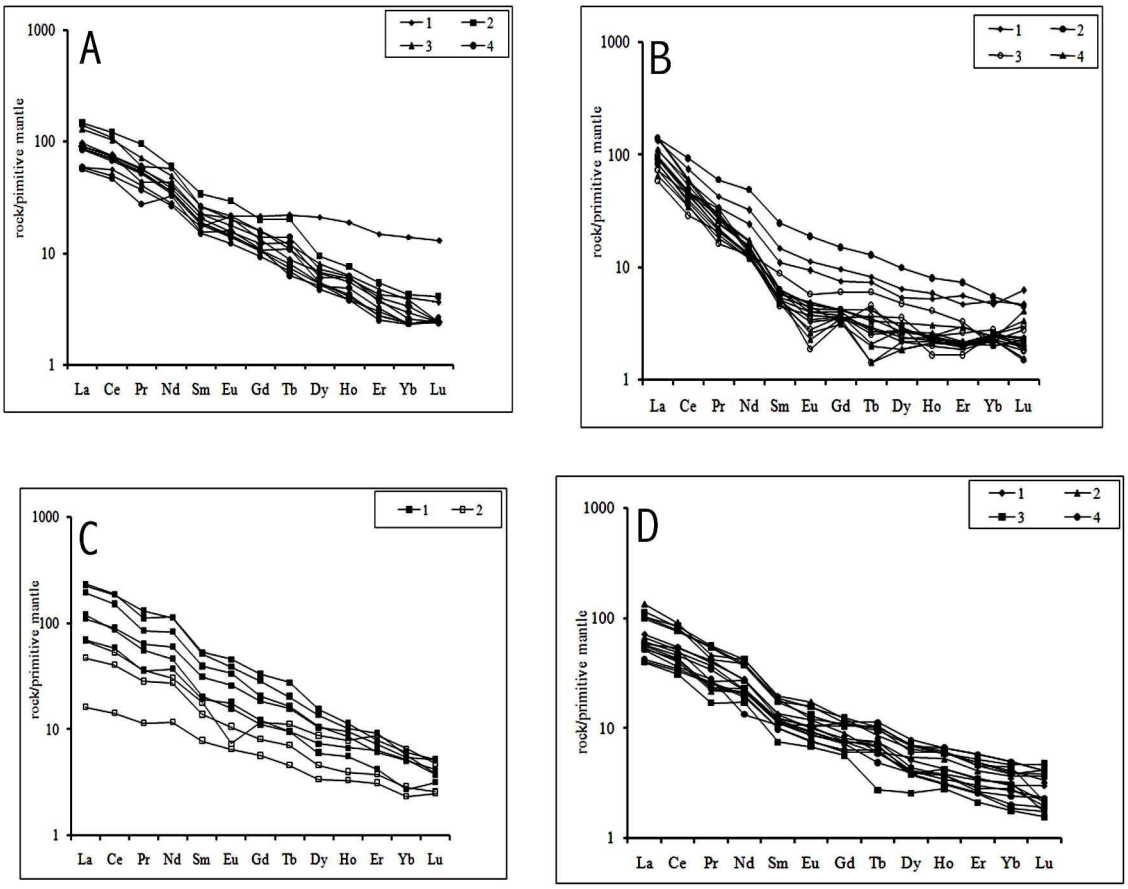

Fig. 3. **REE values of igneous rocks of Belarus normalized to the primitive mantle.**

A – Pripyat graben: 1-monchiquite, 2 – nepheline basalt, 3-limburgite, 4-alkali picrite; B – Gomel structural dam: 1-leucite, 2-leucitic nephelinite, 3- nephelinite, 4- leucitic nepheline tuff; C – North-Pripyat zone of steps: 1-basalt, 2-basaltic tuff; D – Zhlobin saddle: 1-melilitite, 2-melaleucitite, 3-melanephelinite, 4-alkali picrite.

structural dam differ from those of the Pripyat graben in the range of REE contained in both effusive and piroclastic rock. A peculiar feature of the rare earth distribution in these rocks is the europium minimum especially distinct in tuffs and tuff breccias. The difference in relative concentrations of europium (Eu/Eu*) can serve as a genetic evidence of rock classification: the standard Eu content of

REE content of Palaezoic alkali igneous rocks of Belarus (in ppm)

Table 1

Borehole	Depth, m	Rock	La	Ce	Pr	Nd	Sm	Eu	Gd	Tb	Dy	Ho	Er	Yb	Lu	ΣTR	La/Yb
Depth. m Rock																	
			Pripyat graben														
Vyshemirovskaya 11	1729	leucitic nephelinite	70,7	60,2	3,8	16,2	3,7	1,7	5,9	1,5	6,7	1,8	4,6	4,9	0,6	182,4	14
Krasnoselskaya 210	3360	limburgite	89,2	182,0	19,8	66,5	11,7	3,4	9,3	1,3	5,9	1,0	2,3	1,9	0,2	394,4	48
Vetkhinskaya 1	4565	monchiquite	66,2	131,4	11,9	58,4	9,8	3,4	8,0	0,9	4,9	1,0	2,1	2,0	0,3	300,2	33
Artukovskaya 3	4518	"	40,0	100,0	11,1	37,5	7,7	3,6	12,8	2,3	15,6	3,1	7,1	6,8	0,2	247,9	6
Dnieprovskaya 1	3565	"	62,0	131,1	15,8	51,6	9,2	2,6	7,3	1,3	4,5	1,0	1,9	1,6	0,2	290,0	38
Borschevskaya 4	2125	nepheline basalt	101,4	213,5	26,3	81,5	14,9	4,9	11,9	2,2	6,9	1,2	2,6	2,1	0,3	469,7	48
Artukovskaya 3	4515	ulkali picrite	62,2	128,6	15,4	54,4	10,0	3,0	8,2	1,5	5,3	1,0	1,8	1,5	0,2	292,9	43
V, Borschevskaya 3	2925	"	40,6	87,2	10,1	35,7	6,6	2,0	5,5	0,8	3,5	0,6	1,4	1,2	0,2	195,4	35
V, Borschevskaya 3	2921	"	38,5	81,5	7,6	43,9	6,9	2,7	6,5	0,7	3,7	0,8	1,5	1,1	0,2	195,7	34
Vasilievskaya 1	1785	"	95,7	192,5	16,4	77,4	11,6	3,6	9,3	1,2	4,9	0,9	1,8	1,3	0,2	416,8	76
Mezhinskaya 2	1274	"	57,9	119,1	14,3	46,3	7,9	2,3	6,1	0,8	3,9	0,6		1,1	0,2	261,8	51
Mezhinskaya 2	1282	"	59,5	123,6	14,7	47,8	8,3	2,4	6,4	1,2	4,0	0,7	1,3	1,2	0,2	271,2	51
			Gomel structural dam														
Tsentrolit 1	420	leucite	91,3	131,5	11,7	43,4	6,6	1,9	5,7	0,9	4,7	0,9	2,2	2,4	0,3	303,7	37
Tsentrolit 2	475	"	74,3	102,7	9,2	32,3	4,9	1,6	4,5	0,8	4,0	0,9	2,7	2,3	0,5	240,6	32
"	650	"	57,4	67,4	5,4	16,2	2,2	0,6	2,1	0,3	1,6	0,4	0,9	1,2	0,2	155,8	47
"	432	leucitic nephelinite	96,3	164,5	16,4	66,3	10,9	3,2	8,9	1,4	7,2	1,3	3,5	2,7	0,3	382,8	36
"	568	leucitic nephelinite	62,4	81,6	9,2	18,6	2,8	0,8	2,5	0,5	2,2	0,4	1,0	1,3	0,2	183,3	50
"	545	nephelinite	50,2	62,7	4,4	17,3	2,4	0,7	1,9	0,5	1,7	0,4	1,0	1,1	0,1	144,4	47
"	565	"	63,8	84,3	6,7	20,8	2,1	0,5	2,2	0,3	1,7	0,4	1,0	1,1	0,1	184,9	57
"	568	"	62,4	81,6	8,3	18,6	2,8	0,8	2,5	0,5	2,2	0,3	0,8	1,3	0,2	182,1	50
"	653	"	40,0	51,0	5,7	16,9	2,0	0,6	2,1	0,4	2,6	0,4	1,0	1,2	0,2	124,1	33
"	750	"	56,8	70,8	5,8	17,9	2,8	0,6	2,2	0,3	2,0	0,4	1,3	1,4	0,1	162,2	42
"	777	"	50,0	79,0	8,0	17,8	3,9	1,0	3,6	0,7	3,5	0,7	1,6	1,0	0,2	170,8	51
"	596		98,0	108,1	7,7	23,2	2,9	0,7	2,5	0,4	2,0	0,4	1,0	1,1	0,1	248,1	87
"	630	leucitic nepheline tuff	77,0	94,3	7,2	20,0	2,6	0,8	2,5	0,4	2,4	0,5	1,4	1,2	0,1	210,5	64
"	701	"	44,7	60,9	5,0	16,4	2,3	0,7	2,2	0,2	2,1	0,4	1,4	1,1	0,1	137,5	40
"	827	"	62,5	76,2	6,0	17,2	2,2	0,4	1,9	0,2	1,4	0,3	1,0	1,0	0,2	170,6	62
"	827	"	65,8	80,2	6,0	17,3	2,1	0,4	2,1	0,2	1,4	0,3	1,0	1,1	0,3	178,1	59

Table 1. Continued

Borehole	Depth, m	Rock	La	Ce	Pr	Nd	Sm	Eu	Gd	Tb	Dy	Ho	Er	Yb	Lu	ΣTR	La/Yb
North-Pripyat zone of steps																	
Uvarovichi 58/2	289	basalt	160,7	333,0	31,2	154,8	23,5	7,7	19,8	3,0	11,4	1,9	3,8	3,0	0,4	753,9	54
"	299	"	155,4	332,0	35,9	153,4	22,8	6,5	17,1	2,2	10,0	1,7	4,4	2,8	0,3	744,5	56
"	382	"	76,0	161,2	17,7	81,4	13,9	4,3	11,0	1,7	7,6	1,5	3,4	2,7	0,4	383,0	28
Uvarovichi 173	360	basaltic tuff	32,2	71,5	7,8	36,8	6,1	1,8	4,8	0,8	3,3	0,6	1,8	1,4	0,2	169,2	23
Uvarovichi 109	380	"	47,0	94,5	10,0	41,3	7,9	1,2	7,0	1,2	6,4	1,3	4,1	3,2	0,3	225,6	15
Uvarovichi 144	324	"	11,1	25,0	3,1	15,9	3,4	1,1	3,4	0,5	2,5	0,5	1,5	1,2	0,2	69,4	10
Uvarovichi 162	490	"	51,0	105,1	9,6	47,5	7,7	2,9	6,7	1,1	4,2	0,9	2,0	1,9	0,3	240,9	26
Uvarovichi 149	358	alkali basalt	132,4	268,7	23,5	112,2	17,4	5,6	12,3	1,8	7,8	1,4	2,9	2,5	0,3	588,9	52
Uvarovichi 169	515,5	"	47,5	102,7	9,8	49,6	8,6	3,0	7,2	1,0	4,4	0,9	2,0	1,3	0,2	238,2	36
Uvarovichi 148	367	"	82,0	152,7	15,3	62,1	9,0	2,6	6,6	1,0	5,4	1,1	3,0	2,5	0,3	343,5	32
Zhlobin saddle																	
Krasnitskaya 693	415	leucite-olivine melilitite	48,9	96,8	10,9	37,8	5,9	1,7	4,8	0,8	3,7	0,7	1,7	1,5	0,2	215,3	33
"	300	melaleucitite	36,3	71,3	6,0	28,6	5,0	1,4	4,6	0,7	3,0	0,6	1,6	1,6	0,1	160,9	23
Kustovitskaya 530	474	"	91,8	161,7	12,6	56,8	8,7	2,9	7,3	0,9	4,8	1,0	2,3	2,0	0,2	353,0	46
Fedorovskaya 716	329	"	46,0	90,7	7,4	36,7	6,0	2,0	5,3	0,6	4,0	0,9	2,0	1,8	0,3	203,7	26
Bliznetsovskaya 665*	265	melanephelinite	67,3	133,6	14,7	49,9	7,7	2,2	6,2	1,1	5,1	1,0	2,5	2,3	0,4	293,8	29
Kniazhinskaya 712	443	"	38,2	76,1	6,4	30,6	5,4	1,7	4,5	0,8	2,8	0,7	1,7	1,5	0,2	170,5	25
Madorskaya 654	314	"	78,0	144,9	11,5	51,7	7,8	2,7	6,6	1,1	4,5	1,0	2,2	2,2	0,2	314,4	35
Madorskaya 654*	438	"	70,6	136,8	15,1	52,1	8,2	2,0	6,4	1,0	5,1	1,0	2,3	1,9	0,3	302,8	37
Madorskaya 654*	449	"	71,2	150,4	15,6	57,5	8,3	2,6	7,4	1,1	5,2	1,0	2,2	1,9	0,3	324,8	37
Nizhevskaya 667	301	"	27,1	54,6	4,7	23,1	3,3	1,1	3,4	0,3	1,9	0,5	1,0	0,9	0,1	121,9	31
Sluchajnaya 750	394	alkali picrite	35,9	74,2	6,3	29,0	5,0	1,5	4,3	0,5	2,9	0,6	1,3	1,4	0,1	163,2	26
Asoya 497*	618	"	29,0	61,8	7,3	27,2	4,5	1,3	3,8	0,7	2,8	0,5	1,2	0,9	0,1	141,0	31
Asoya 497*	635	"	27,3	57,7	6,9	25,8	4,4	1,3	3,6	0,7	2,8	0,5	1,2	1,0	0,1	133,3	28
Deniskovichi 552**	226	"	35,0	64,0	7,7	18,0	4,7	1,8	6,2	1,1	5,0	1,1	2,8	2,4	0,3	150,0	14
Deniskovichi 552**	307	"	40,0	95,0	11,4	36,4	5,5	1,7	6,7	1,2	5,7	1,1	2,8	2,4	0,3	210,2	16
Deniskovichi 555***	373-555	"	39,3	81,8	9,4	29,4	5,2	1,6	4,4	0,8	3,2	0,6	1,3	1,2	0,2	178,3	33
Senozhatka 501***		"	41,5	85,7	10,1	30,1	5,2	1,5	4,4	0,6	3,0	0,6	1,4	1,3	0,2	185,6	31

Note: Analyses were performed at: A,P, Vinogradov Inst itute of Geochemistry of the Siberian branch of the RAS by ICP_MS method in 2007; * - Royal Holloway University of London by ICP -AES method in 2001;**- Institute for Nuclear Investigations of NAS of Ukraine (Kiev) by neutron -activation in 1995; ***- Royal Holloway University of London by ICP method at RHUI in 1996,

primitive mantle series is nearly close or identical to the chondrite one (that of the primitive mantle). In the case under study this evidence was noted in ultrabasic

rocks of the Pripyat graben. Anomalies of the relative europium content should be noted in rocks formed by fractional crystallization. Besides, the europium content of the more recent igneous rock differentiates decreases, therefore, these show the

smaller Eu/Eu* ratio values. Similar conditions would be expected in potassic rocks of the Gomel structural dam. Concentrations and the REE distribution pat

tern studied in rocks of the North-Pripyat zone of steps show that in general the REE contents of alkali basaltoids of the zone of steps coincide very closely with those of analogous graben rocks (Fig. 3C). Alkali basaltoids of the Azdelin and Ivankovo palaeovolcanos (Uvarovichi 58/2 and Uvarovichi 149 boreholes) are exceptional, as their rocks show rather high REE concentrations (ΣTR=753.9 and 588.9 ppm, respectively) as compared to those determined in all the other studied alkali rocks. The REE distribution range in the rocks of the North-Pripyat zone of steps is of similar pattern without distinct minima and the europium anomaly. The europium minimum was noted only in the borehole 109, which is located at the Gomel structural dam border.

Rocks of diatremes from the Zholobin field do not considerably differ from each other in the total REE content. Their highest amounts are peculiar to ultrabasic foidites (up to 325 ppm in melanephelinites), but these are 1.5-2 time smaller in alkali picrites averaging 150 ppm. Diatreme rocks like alkali rocks of the Pripyat graben typically show predominance of light lanthanoids with the rather stable REE spectrum and light and heavy REE differentiation pattern. Ultrabasic foidites differ therewith from alkali picrites in their light REE content. So, the La content of melanephelinites averages 68 ppm, Ce – 123 ppm, in melilitites La – 48 ppm, Ce -81, in alkali picrites – 21 and 75 ppm, respectively. The light REE (La, Ce) content of rocks is 140-280 times and that of heavy TR (Yb, Lu) – 6-11 times the chondrite level. Plots of REE distribution are of similar pattern without distinct minima, which is indicative of their common origin (Fig. 3D). Diatreme rocks are described by a rather low HREE and LREE (La/Yb) fractionation averaging 35 and by the absence of europium extremes, which suggest their mantle origin, and some deviations of its actual values from the standard ones are insignificant (Eu/Eu*≈0.9).

The geochemical data cited above are in agreement with well-known trends of REE distribution in the alkali igneous rock series. Therefore, alkali basalts and picrites as essentially sodium rocks, as well as their subvolcanic analogues widespread within the Pripyat graben are described by the higher REE concentrations, as compared to those peculiar to potassic rocks (leucitites, leucitic nephelinites) of the Gomel structural dam. The REE concentrations and their distribution (see Fig 3) suggest the genetic similarity of igneous rocks from the Pripyat graben, Zhlobin saddle and, to certain extent, North-Pripyat zone of steps.

Rocks from these regions show the similar slope of the REE distribution curves and close values of the HREE and LREE (La/Yb) fractionation. However, the curves of rocks from the graben and zone of steps deviate toward the higher concentrations as compared to REE spectra of ultrabasic rocks from the Zhlobin saddle diatremes.

The exact formation belonging of extrusive and explosive rocks is important for reconstructing environments when the Palaeozoic magmatism became evident, as well as for elucidating the question whether the rocks of the Pripyat graben and North-Pripyat areas of magmatism derived from a common magma source. The Nb/Y – Zr/Y ratio in alkali igneous rocks can serve as one of geochemical indices to solve this question. This ratio was choosen because these elements are rather insensitive to rock transformation processes, the fractional crystallization and degree of partial melting [1].

The Nb/Y –Zr/Y diagram shows variations of these coefficients in alkali igneous rocks of the Pripyat graben and in those from all the parts of the North-Pripyat area (Fig. 4). The distribution of these ratios in various type alkali igneous rocks of Belarus suggests that at least two different magmatic sources could be involved in their petrogenesis. Low Nb/Y – Zr/Y values (field I) are typical of just the majority of alkali igneous rocks of the Pripyat graben, the Zhlobin saddle and

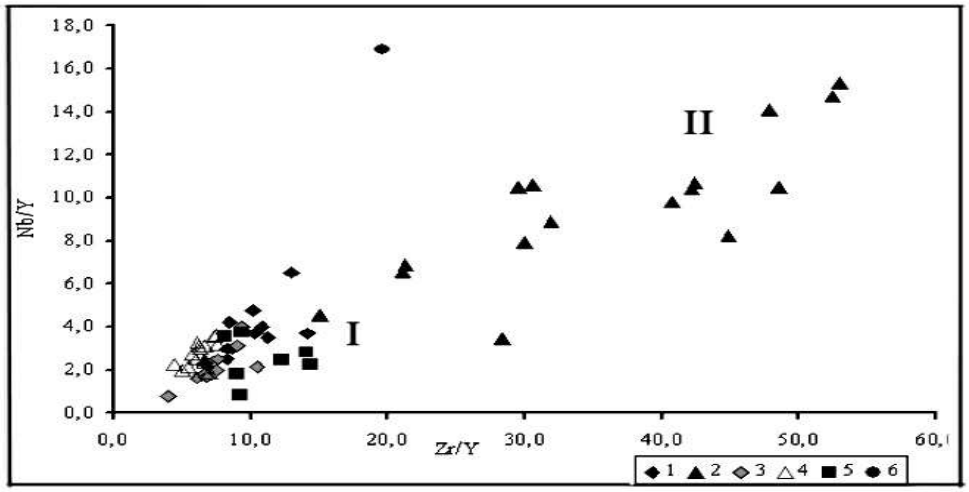

Fig. 4. **Correlation of the Nb/Yb – Zr/Y ratios of Palaeozoic alkali igneous rocks of Belarus.** 1-ultrabasic rocks of the Pripyat graben; 2- ultrabasic rocks of the Gomel structural dam; 3- ultrabasic and basic rocks of the North-Pripyat zone of steps; 4- ultrabasic rocks of the Zhlobin saddle; 5-intermediate rocks of the Pripyat graben; 6- olivine melilitite of the Zhlobin saddle.

the most part of the zone of steps. The arrangement of points of Nb/Y – Zr/Y ratios in these rocks can imply a source similar to the upper mantle, which participated in their petrogenesis. The higher ratios of these elements (field II) noted in potassic rocks of the Gomel structural dam, in alkali olivine picrite from

the easternmost part of the graben (Borschevskaya 3 borehole) and olivine melilitite from the southeastern part of the Zhlobin saddle (Luchin 518 borehole) can extend the trend of the field I values. High Nb/Y – Zr/Y ratios in alkali rocks (field II) including ultrabasic rocks of the Gomel structural dam can be due to an enriched mantle source, which participated in the rock formation in this zone.

ROCK ISOTOPIC COMPOSITION

Isotope data of the Sr-Nd distribution in rocks of the Palaeozoic igneous formation (370 Ma) of Belarus were published in the literature [6-8, 11] and presented in the Table 2. Isotope data of Sr-Nd distribution in the studied samples of the Palaeozoic alkali igneous rocks of Belarus form a field restricted between the isotope data of the primitive mantle (PREMA) and those of the enriched mantle souce EM 1, some of the isotopic composition points falling within the EM1 field (Fig.5). It

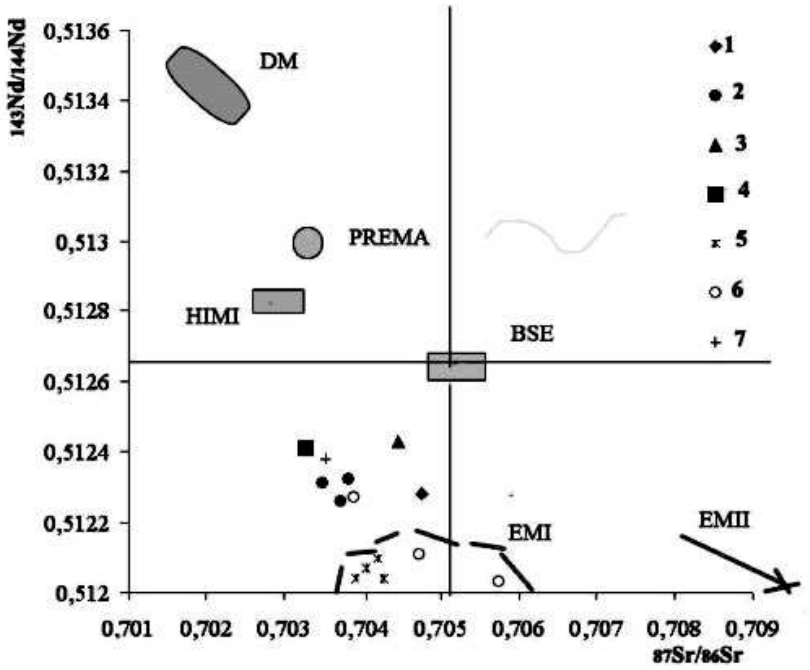

Fig. 5. **Diagram showing the $^{143}Nd/^{144}Nd$ – $^{86}Sr/^{87}Sr$ relationship for Palaeozoic alkali igneous rocks of Belarus (with data by [5, 8, 11]). All data are corrected to an age of 370 Ma.**
1- Pripyat graben, monchiquite, 2- Pripyat graben, olivine-pyroxenic alkali picrite, 3-Dnieper graben, alkali basalt, 4 - Gomel structural dam, nephelinite, 5- Zhlobin saddle, melanephelinite, 6- Zhlobin saddle, melilite-pyroxenic picrite, 7- Zhlobin saddle, olivine melilitite.

Table 2.

Sr and Nd isotopic composition of Palaezoic alkali igneous rocks of Belarus

Borehole	Depth, m	Rock	Rb/Sr	$^{87}Sr/^{86}Sr$	$^{87}Sr/^{86}Sr$ 370 Ma	εSr	Sm/Nd	$^{143}Nd/^{144}Nd$	$^{143}Nd/^{144}Nd$ 370 Ma	εNd
Pripyat graben										
Mezhinskaya 2*	1274	ulkali picrite	0,0333	0,70398	0,70348	-8,2	0,171	0,51256	0,51231	2,8
“	1274	"	0,0139	0,70403	0,70382	-3,4	0,172	0,52258	0,51232	3,1
“	1282	"	0,0135	0,70394	0,70373	-4,6	0,173	0,51252	0,51226	1,9
Artukovskaya 3*	4515	monchiquite	0,0520	0,70555	0,70476	9,9	0,184	0,51255	0,51228	2,3
Gomel structural dam										
Tsentrolit 2*	570	leucitic nephelinite	0,1523	0,70560	0,70328	-11,1	0,148	0,51263	0,51241	4,8
Zhlobin saddle										
Madorskaya 654***	449	melanephelinite		0,70469	0,70420	1,61		0,512321	0,512097	-1,27
Kniazhinskaya 712**	440	"	0,033	0,70478	0,70427	0,2	0,170	0,51229	0,51204	-2,4
Sluchajnaya 747**	361-367	"	0,043	0,70471	0,70404	-3	0,167	0,51231	0,51207	-1,8
Luchin518**	151,5	olivine melilitite	0,089	0,70489	0,70353	-10,3	0,125	0,51256	0,51238	4,20
Asoya 497***	618	alkali picrite		0,70905	0,70657	35,66				
Bliznetsovskaya665***	265	"		0,70559	0,70486	11,37				
Senozhatka 501*		"	0,0518	0,70551	0,70472	9,4	0,171	0,51237	0,51211	-1,0
Deniskovichi555*	373	"	0,1763	0,72016	0,71747	50	0,178	0,51254	0,51228	2,3
Tsuper 486**	391	"	0,070	0,70681	0,70574	21	0,171	0,51228	0,51203	-2,6
Marusino 589**	490	"	0,086	0,70519	0,70389	-5,1	0,179	0,51253	0,51227	2,1
Olejnikovskaya 550**		"	0,076	0,70646	0,70531	15	0,166	0,51223	0,51199	-3,3

Note: Sr and Nd isotopic ratios were determined: * Sr– with a VG54E Isomass mass-spectrometer and Nd – with a VG MM30 mass-spectrometer at the University of Leeds in 1996; ** - with a Finnigan MAT-261 mass-spectrometer at the IGGD RAN of Saint-Petersburg in 2004; *** - with a VG 354 mass-spectrometer at the Royal Holloway University of London in 2001,

is seen from the diagram of the Sr-Nd isotopic composition and the Table 2 that the studied rocks having rather similar $^{87}Sr/^{86}$ Sr values (0.7030-0.7050) form two fields due to the Nd isotope distribution. The εNd values vary from 50 to 14.5, the first (positive) field with εNd=1.9-4.2 being occupied by rocks from the Pripyat
is seen from the diagram of the Sr-Nd isotopic composition and the Table 2 that the studied rocks having rather similar $^{87}Sr/^{86}$ Sr values (0.7030-0.7050) form two fields due to the Nd isotope distribution. The εNd values vary from 50 to 14.5, the first (positive) field with εNd=1.9-4.2 being occupied by rocks from the Pripyat graben, Gomel structural dam and, partly, Zhlobin saddle. The positive εNd values suggest that the rocks derived from the residual solid phases of a reservoir after the magma had been removed from it over some early time interval. Such reservoir parts are depleted in lithophile elements of a large ion radius (LIL), which pass into the liquid phase in the course of partial melting. The second field is formed by alkali-ultrabasic rocks of the Zhlobin saddle, which are similar to those from the EM I field in their isotopic composition and contain an insignificantly increased amount of the radiogenic Sr isotope as against its content of rocks from the Pripyat graben and Gomel structural dam. This may be indicative of the secondary transformation of these rocks. However, the $^{87}Sr/^{86}Sr$ ratio of volcanic rocks that penetrated through the continental crust is usually higher than that of volcanites from oceanic basins, which is caused by an interaction of these magmas with old crustal rocks (or magma formation due to crustal rock melting). Therefore, on the other hand, high $^{87}Sr/^{86}Sr$ ratios may be indicative of the contamination of alkali-ultrabasic rocks of the Zhlobin saddle by the crystalline crust rock fragments. Rather low εNd values (-0.1 – 3.3) in alkali rocks of the North-Pripyat magmatic area found mainly in the negative field also could suggest their formation in the course of the crustal rock reworking or assimilation. This is seen more distinctly from the isotopic composition of rocks from the Deniskovichi volcanic pipe, where the strontium isotope ratio is sharply increased ($^{87}Sr/^{86}Sr$ – 0.72016) (see Table 2). Negative εNd values also testify to the fact that rocks derived from a source which showed the lower Sm/Nd ratio than that of the chondrite reservoir.

CONCLUSIONS

Hence the distribution of some mostly revealing geochemical and isotope parameters suggests that alkali ultrabasic and basaltoid rocks from two areas of Palaeozoic magmatism of the territory of Belarus form a rather homogenous group. This is generally indicative of a comagmatic origin of igneous formations from the Pripyat graben and those from the North-Pripyat zone of steps, which suggests a common source of Palaeozoic rifting magmatism in Belarus. The exceptions are rocks from the Gomel structural dam and some varieties of alkali-ultrabasic rocks from the southern part of the Zhlobin saddle (Luchin bunch), that differ from the main group of alkali magmatic rocks in their Nb/Y – Zr/Y ratio and strontium and neodymium isotopic composition. This enable an assumption about one more

source different in the composition and similar to the enriched mantle (EM I), which could be possibly involved in the magmatism process and could contribute to the formation of rocks of these types.

The research was performed with the financial backing of the BRFFI (grant №X08P-087) and RFFI (grant 08-05-90002).

REFERENCES

1. **Fitton G., Hardarson B. S., Saunders A. D., Norry M. J.** The chemical distinction between depleted plume and N-MORB mantle sources. Abstract 1996.167 p.
2. **Khomich P.Z., Nikitin Ye. A., Grishko A.I. et al.** A new range of kimberlite magmatism development in the west of the East European Platform. Doklady NAN Belausi, 1993, Vol. 37, №1, pp. 83-86(in Russian).
3. **Korzun V.P., Makhnach A.S.** Late-Devonian magmatism of the Pripyat aulacogen. In: Tectonics and Magmatism of the East European Platform. Minsk, 1994, pp. 195-195 (in Russian).
4. **Korzun V.P., Makhnach A.S.** Upper-Devonian alkali volcanogenic formation of the Pripyat Trough. Minsk, Nauka I Technika Publ., 1977, 164 p. (in Russian).
5. **Markwick A.L., Downes M., Veretennikov M.V.** The lower crust of SE Belarus: petrological, geophysical and geochemical constraints from xenolits. Tectonophysics, № 339 (2001). P. 215-237.
6. **Mikhailov N.D., Laptsevich A.G.** The question of the genesis of Devonian alkaline magmatism in Belarus (geochemical aspect). In: Geochemistry of Magmatic Rocks. Transactions of the scientific school “Alkaline magmatism of the Earth”. Moscow, 2005, pp.105-108 (in Russian).
7. **Mikhailov N.D., Laptsevich A.G., Veretennikov N.V., Korzun V.P.** Nd-Sr isotopic features of the Late- Devonian magmatism in Belarus. XX Seminar “Geochemistry of Magmatic Rocks”. Moscow, 2002, p. 71 (in Russian).
8. **Pervov V.A., Nikitin Ye. A., Levsky L.K.** Ultrabasic alkaline volcanites of the Zhlobin field (Republic of Belarus). In: Magma sources and evolution. Petrologiya, 2004. Vol. 12, №4, pp.354-373 (in Russian).
9. **Veretennikov N.V., Korzun V.P., Laptsevich A.G., Mikhailov N.D.** Petrology of volcanic pipes of the Zhlobin field (Belarus). Lithosphere, 2001_1, №1(14), pp.46-55 (in Russian with English abstract).
10. **Veretennikov N.V., Korzun V.P., Makhnach A.S., Laptsevich A.G.** Upper-Devonian volcanogenic formations of the Uvarovichi district. Doklady NAN Belausi, 2001_2, Vol. 45, №1, pp. 100-102 (in Russian).
11. **Wilson M., Lyashkevich Z. M.** Magmatism and geodynamics of rifting of the Pripyat-Dnieper-Donets rift, East European Platform // Tectonophysics.1996.V.268. № 1-4. P.65-81.

UDK 552.33 + 548

Variations of Chemical composition in platinum-group minerals and gold of the Konder alkali-ultrabasic massif, Aldan Schield, Russia

Lennikov A.M., Zalishchak B.L., Oktyabrsky R.A. and Ivanov V.V.

Far East Geological Institute, Far East Division, RAS, 159, prospect 100-letya, Vladivostok, 690022, Russia, anortozit@mail.ru, galgen51@mail.ru

The platinum-group minerals (PGM) of the Konder zoned alkali-ultrabasic massif, located east of the Aldan Shield, in far-eastern Russia, are predominantly represented by isoferroplatinum of two generations, both with Fe contents ranging from 7.5 to 11.5 wt. %. A high-temperature isoferroplatinum is saturated with platinum-group-element (PGE) impurities: up to 5.3 Ir, 2.9 Os, and 1.8 Rh (all in wt. %). In contrast, the later isoferroplatinum contains lower levels of Ir, Os and Rh: less than 1.9 Ir, 1.0 Os, 0.6 Rh (in wt. %). The minor PGM are represented by a wide range of solid solutions in the system Os-Ir-Rh-Pt, tetraferroplatinum, tulameenite, hongshiite, minerals of erlichmanite-laurite and irarsite-hollingworthite series, sperrylite, bismuthides, antimonides, tellurides, stannides, and hydroxides. There are possibly new mineral species: native ruthenium, the Pd-dominant analogue of hongshiite, Pt_2As_3, the Pt-dominant analogue of konderite and inaglyite, and others minerals, which form rims around grains of isoferroplatinum and inclusions in it. A similar morphology and distribution as found with Pt_3Fe are observed with gold, related to rare lenses of sulfide and impregnations in dunite (Cu-, Pt-, and Pd-bearing high-grade gold) and monzodiorite cutting dunite (low-impurity middle- and low-grade gold).

Keywords: platinum-group minerals, gold, rare minerals, Konder massif, Aldan Shield, Russia.

INTRODUCTION

The Konder alkali-ultrabasic massif, in far-eastern Russia, belongs to a set of platform analogues of the Ural-Alaska type of zoned platinum-bearing intrusive complexes [3]. The accessory platinum-group minerals (PGM) from the primary and placer occurrences associated with the Konder intrusion are mainly represented by isoferroplatinum, as indicated by numerous electron-microprobe analyses and examinations by X-ray diffraction [12, 20]. Except in rare instances [38], reflections attributed to the superstructure were revealed in diffraction patterns of Pt_3Fe samples obtained in long-exposure studies. These lines pertain to a primitive cubic cell. Claims of the widespread presence in the Konder massif of ferroan platinum having a disordered face-centered cubic cell [44] have been called in question [13, 12].

Inclusions of Os-Ir-Ru and Os-Ir-Pt solid solutions are usually present in the isoferroplatinum. The minor minerals of the platinum-group element (PGE) are tetraferroplatinum, tulameenite, hongshiite, sulfides, sulfoarsenides, arsenides, bismuthides, antimonides, tellurides, stannides, Pd germanide, oxides and

hydroxides, forming a rim around isoferroplatinum or incorporated as inclusions. Together with these minerals, accessory gold invariably occurs in outcrops and also in placers along streams draining the Konder massif.

Original results of a study of accessory PGE minerals in the Konder alkaline-ultrabasic massif are briefly described in this paper. More details are provided in a monograph of the authors [20], which was published in a very limited number of copies (300). It became inaccessible almost immediately, even for Russian geologists studying PGM. Before of this monograph was published, all the information about the mineralogy of the noble metals in the Konder alkaline-ultrabasic massif was scattered in separate articles, either by the monograph's authors or by other specialists.

GEOLOGICAL SETTING

In addition to the Konder central-type massif with a dunite core, a few other concentrically zoned platiniferous massifs of ultramafic and alkaline rocks are known in the central part of the Aldan Shield (Inagli) and in its southeastern part (Chad and Sybakh). All such massifs were formed at a depth of 1-2 km [2, 5] and are eroded to some extent, giving rise to variable proportions of specific rocks exposed at the present-day surface [20]. The Sybakh and Inagli massifs are the least eroded, whereas the Konder and especially the Chad massifs are eroded to a greater depth.

The Konder annular alkaline-ultrabasic massif is located on the eastern margin of the Aldan Shield, in the middle reaches of the Maya River, approximately 250 km northwest of the coast of the Okhotsk Sea (Fig. 1). Most of the massif is composed of ultrabasic rocks, represented by dunite, forming a rounded core about 6 km across. Olivine clinopyroxenite surrounds the dunite and grades to olivine-free magnetite-bearing pyroxenite, gabbro-pyroxenite, and further to melanocratic gabbro toward the periphery of the massif. The coarse-grained phlogopite-bearing magnetite clinopyroxenite occurs as dikes up to 40 m across in the southwestern sector of the dunite core. The dunite core and the enveloping pyroxenite contain numerous thin dikes (up to 1-2 m) of syenite and nepheline syenite. The enveloping clinopyroxenite is cross-cut in places by intrusive bodies of granodioritic, monzonitic or monzodioritic composition [6]. According to geological data, the Konder intrusive body formed at a shallow depth (about 1.5 km) [1]. No reliable evidence for the age of the Konder massif is available [20, 43]. The ultrabasic suite is considered to have formed not later than the Upper Protero-zoic [33], but the alkaline and monzonitic rocks may be partly of Mesozoic age [6, 23].

The contact aureole

Igneous rocks of the Konder intrusive complex have metamorphosed the enclosing Middle Riphean clastic sedimentary rocks. At the present-day level of erosion, the contact-metamorphic rocks are in the pyroxene-hornfels and

muscovite-hornfels facies. In its outer part, the contact aureole, commonly more than 500 m across [2], is in the cordierite-biotite hornfels facies, with andalusite developed at the expense of sandstones and siltstones. The hornfelses at the inner part of the contact aureole (more 100 m wide) were deformed owing to the intrusion of ultrabasic magma and also were subjected with acid leaching due to the late intrusion of granodioritic magma [9, 10].

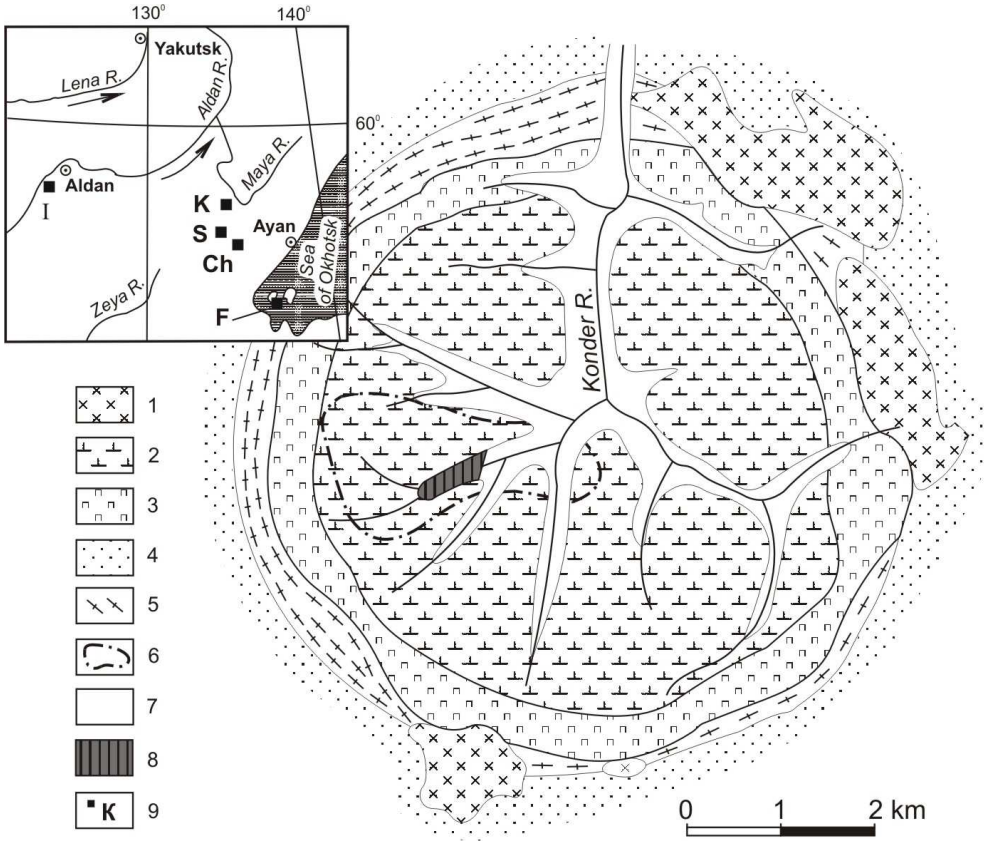

Fig. 1. **Geological map of Konder alkali-ultrabasic massif, after Andreev (1987) and Sushkin (1995), with simplifications and additions.**

1) granodiorite, monzonite, monzodiorite; 2) dunite cut by dikes of syenite and nepheline syenite in the southern half of the dunite core; 3) olivine and magnetite-bearing pyroxenite with dikes of syenite and nepheline syenite; 4-5) massive (4) and gneissic (5) andalusite- and sillimanite-bearing biotite-cordierite hornfels formed at the expense of Riphean siltstones and sandstones; 6) area injected by phlogopite-pyroxenite dykes; 7) platinum- bearing alluvium; 8) platinum-gold-bearing alluvium; 9) site of the Konder massif (K) and its associated bodies Inagli (I), Chad (Ch), Sybakh (S) and Feklistov (F).

Associated carbonate rocks consist of periclase -forsterite - brucite marble and calc-silicate assemblages containing qandilite, the rare Ti-Mg spinel-group mineral [42], as well as monticellite + melilite, vesuvianite + clintonite, grossular + diopside and scapolite-bearing varieties of skarn [9, 10].

Petrography of the Konder massif

The dunite is a massive, fine- to medium-grained inequigranular rock, with olivine grains varying in size from fractions of a millimeter to tens of millimeters.

Olivine crystals up to 5-7 cm in length can be seen in sporadic bodies of pegmatitic dunite. The fine-grained dunite occurs in marginal parts of the core. The main body is composed of medium-grained dunite locally grading into a coarse-grained variety. According to the results of drilling, the coarse-grained dunite becomes predominant at a depth of more than approximately 200m.

Olivine from the fine- and medium-grained dunite corresponds to $Fo_{87.9-9.93.1}$ [20]. Olivine in clinopyroxene-bearing dunite from the marginal zone of the core is somewhat richer in Fe ($Fo_{86.-87.6).}$The pegmatitic dunite in the central part of the core and dunite inclusions in olivine clinopyroxenite contain $Fo_{84.-85.3}$ and $Fo_{81.6-84.0}$, respectively. Schlieren of pegmatitic olivine clinopyroxenite hosted in dunite contain $Fo_{87.3}$, whereas the composition of olivine in clinopyroxenite surrounding the dunite core and forming dikes therein attains Fo_{70}.

Table 1.

Composition of isoferroplatinum and ferroan platinum, Konder alkaline-ultrabasic massif (wt. %).

No.	Pt	Ir	Os	Pd	Rh	Ru	Cu	Ni	Fe	Total
Dunites with accessory chromite-isoferroplatinum impregnation										
A. The least eroded zone of the massif										
1	84.59	3.03	1.17	0.45	1.18	0.13	0.75	0.43	9.70	101.43
2	84.46	0.76	2.64	1.51	0.77	-	1.65	0.36	9.25	101.40
3	84.74	0.88	2.86	1.44	1.03	-	1.72	0.38	9.25	102.30
4	85.65	1.94	0.57	-	-	-	0.12	-	10.97	99.25
5	80.39	3.37	-	-	1.66	0.14	1.06	0.83	11.47	98.92
B. The most eroded zone of the massif										
6	86.57	1.87	0.89	0.90	0.76	-	0.69	0.37	8.27	100.32
7	87.09	1.74	0.72	0.99	0.68	-	0.52	0.13	8.03	99.90
8	83.36	5.28	-	-	0.85	-	0.50	-	8.77	98.76
9	85.51	2.22	-	0.20	1.06	-	0.36	-	9.26	98.61
10	86.87	1.95	-	0.53	0.41	-	0.70	-	9.00	99.46
Chromite segregations in dunites with accessory isoferroplatinum										
11	83.87	0.70	-	-	1.37	0.12	1.02	0.71	11.40	99.19
12	86.98	0.58	-	-	0.70	-	0.50	0.53	10.92	100.21
13	89.23	-	0.32	0.17	0.16	-	0.82	-	9.11	99.81
14	89.93	0.08	-	0.39	-	0.18	0.52	0.53	8.64	100.27
15	88.59	0.31	0.45	-	0.36	-	1.75	0.25	8.04	99.75
Pyroxenites (dikes in dunites) with accessory ferroan platinum										
16	87.07	0.41	0.27	0.33	0.56	-	0.48	-	10.27	99.39
17	87.46	-	0.33	0.37	0.23	-	0.71	-	10.04	99.14
18	87.71	-	0.43	0.58	0.47	-	1.00	-	9.56	99.75
19	88.02	-	0.30	0.61	0.54	-	0.77	-	9.50	99.74

The chromian spinel, abundant in dunite and olivine clinopyroxenite from the central part of the Konder massif, is largely composed of ferrian chromite, both accessory and ore-forming. The accessory chromian spinel occurs as disseminated octahedra and, less commonly, flattened and rounded equant grains

from 0.01 to 2-3 mm across. Rounded and lenticular schlieren, .vein-like bodies and pockets (up to 0.7 x 1.5m^2 across) of densely impregnated chromian spinel ore are distributed throughout the massif, without apparent systematic pattern in spatial distribution.

The chromian spinel is associated with $Fo_{87.1-92.9}$ in dunite and $Fo_{87.3-87.6}$ in olivine clinopyroxenite of the central facies. The chemical composition of the chromian spinel covers a range from a sporadically encountered high-Cr variety (61.7-63.7 wt. % Cr_2O_3; [26], *via* the main mass of ferrian chromite, to the Cr-bearing magnesian magnetite. The Cr content of the chromian spinel from dunite varies from 55.0 to 19.6 wt. % C_2O_3 in magnesian magnetite. In the magnetic fraction of densely impregnated chromian spinel, the respective ranges are 7.6-8.6 and 10-12 wt. % C_2O_3 *(i.e.,* chromian magnetite). The Mg content varies to a lesser extent, from 3 to 11 wt. % MgO. The ore-zone chromite is distinguished by the highest Mg content.

The chromian spinel from dunite and olivine clinopyroxenite of the central facies contains an appreciable quantity of titanium. The lowest Ti content is typical of ore-zone chromian spinel, and the highest is found in octahedra of chromite (0.4-0.8, and up to 1.55 wt. % TiO_2, respectively). The accessory chromian spinel from pegmatitic and coarse-grained dunite and from olivine clinopyroxenite of the central facies is somewhat richer in Ti (1.07-1.95 wt. % TiO_2). The range in TiO_2 in Cr-bearing magnetite is narrower, but higher (1.80-2.12 wt. % TiO_2).

The chromian spinel from Konder is relatively poor in Al. The highest Al content (5.9-7.9 wt. % $A1_2O_3$) was detected in the ore-zone chromian spinel and accessory spinel of the first generation in dunite. The Al content of chromite from the pegmatitic olivine clinopyroxenite and from the fine-grained rocks drops to 5.2-3.3 and from 4.6-2.4 to 0.8 wt. % $A1_2O_3$, respectively. The Al content in the Cr-bearing magnetite (1.8-2.5 wt. % $A1_2O_3$) and densely impregnated chromite schlieren in dunite (1.97-2.49 wt. % $A1_2O_3$) varies over approxmately the same range.

Clinopyroxene of the ultrabasic suite of the Konder massif is distributed as widely as the chromian spinel. Within dunites, it forms schlieren-like accumulations and thin veinlets, but in the pyroxenites, it is a rock-forming mineral.

The pyroxene in the intercalated suite of dunites and olivine pyroxenites of the central facies, as in the magnetite-free pyroxenites of the ring unit, is low in ferrous iron ($4.5 < f_{total} < 20.6\%$) [$f_{total} = 100(Fe^{2+} + Fe^{3+})/(Mg + Fe^{2+} + Fe^{3+})$], moderately aluminous (0.5-2.2 wt. % $A1_2O_3$) and low in titanium (0.1-0.44 wt. % TiO_2). It is enriched in Cr (0.25-0.76 wt. % Cr_2O_3).

The clinopyroxene in magnetite-bearing pyroxenites and within dikes of pyroxenite in dunite contain significantly more Ti (to 1.14 wt. % TiO_2) and less Cr (0.1 wt. % Cr_2O_3), but is more ferrous (f_{totl} to 30%) and moderately aluminous (to 2.4 wt. % Al_2O_3). A characteristic feature of the ring clinopyroxenites of the Konder massif is the high value of the oxidation ratio ($48 < f_o < 56$ %) [$f_o = 100Fe^{3+}/(Fe^{2+}$ +

Fe^{3+})], which is evidence of the presence of the aegirine end-member; the pyroxene contains up to 0.85 wt. % Na_2O.

The clinopyroxenite in dikes cross-cutting dunite at the southwestern part of the core of the complex differs from ring clinopyroxenites by their significantly lower Cr content (0.02 wt. % Cr_2O_3) and by the greater proportion of ferrous iron ($20 < f_{total} < 23.5$ %). In these pyroxenites, opaque minerals along with apatite are represented by titaniferous magnetite (4.7-5.8 wt. % TiO_2), in some cases intergrown with oxidized (5.9-8.8 wt. % Fe_2O_3) ilmenite with appreciable Mg (3.7-3.8 wt. % MgO) in solid solution, with pyrrhotite and chalcopyrite.

As for the dikes of clinopyroxenite, they can be subdivided according to the minerals present into phlogopite-, hornblende- and magnetite-bearing varieties. Large (up to 2 mm) red-brown single crystals of vesuvianite and faintly pink xenomorphic grains (1-2 mm) of titanite are present within the coarse-grained units.

The formation of the dunite core was completed by crystallization of native metals (Si-bearing and pure α-iron, tin, copper, and antimony), along with rare grains, polymineralic veinlets and lenses of pentlandite, pyrrhotite, chalcopyrite, pyrite, and arsenopyrite.

ANALYTICAL TECHNIQUES

The PGM were analyzed quantitatively with a JXA-5A electron microprobe under the following conditions: acceleration voltage 25 kV, beam current 30 nA, counting time 10 seconds. We used the *L* series of X-ray lines and pure metals as standards. Concentrations of elements other than the PGE were determined using the following X-ray lines and standards: S*Kα* Bi*Lα*, *Mα:* Bi_2S_3; Fe*Kα:* FeS_2; Cu*Kα*, Sb*Lα:* $CuSbS_2$; Sn*La:* SnO_2; Ni*Kα,* Au*Lα* Ag*Lα*, Ge*Lα:* pure elements; Pb*Lα*, *Ma:* PbS; Se*Ka*, *Lα:* Zn, Se; Hg*Lα*: HgS; Te*Lα*: Cd, Te; As*Kα, Lα:* FeAsS. Overlaps of X-ray lines (Laputina 1980) were taken into account with a correction program using the relative intensities of X-ray lines. The detection limit for PGE is 0.1-0.3 wt. %. The precision of analyses was evaluated on PGM with a stoichiometric composition, and deviations were at the 2-3 % limit in the most cases. Analyses were made by V.I. Sapin and V.I. Taskaev; a dash indicates that the element was not detected. The proportion of the elements is expressed in wt. %.

PGE MINERALS OF THE KONDER MASSIF

According to the results of prospectors' activities [34], the major portion of the platinum-rich heavy-mineral concentrate consists of irregular, lump-shaped, angular, and perfectly faceted grains of variable dimensions, up to nuggets (that weigh more than 10 g). Euhedral crystals of platinum mainly are cubic in habit. Hexahedral crystals dominate in small-size fractions. The proportion of various twins and intergrowths of two or three individuals, up to 17 mm in dimension, increases among coarser grains. Films of gold, 0.05-1.0 mm thick, surround many

small grains of platinum. In some cases, these films are coupled with a crystalline gold dust. The gold films are without doubt endogenic, because they consist of closely intergrown tiny crystals of Cu-bearing gold, Au- and Te-bearing sulfide, and some Pd and Pt compounds. The films on crystal edges are abraded during transport, and thus provide additional morphological evidence for their relatively high-temperature origin [34]. However, the micrometer-thick gold films of high fineness on rounded platinum nuggets most likely are of low-temperature origin [20]. Native gold, silver, lead, tin, copper, nickel, iron, antimony and bismuth occur along with platinum in both bedrock and stream placers [6].

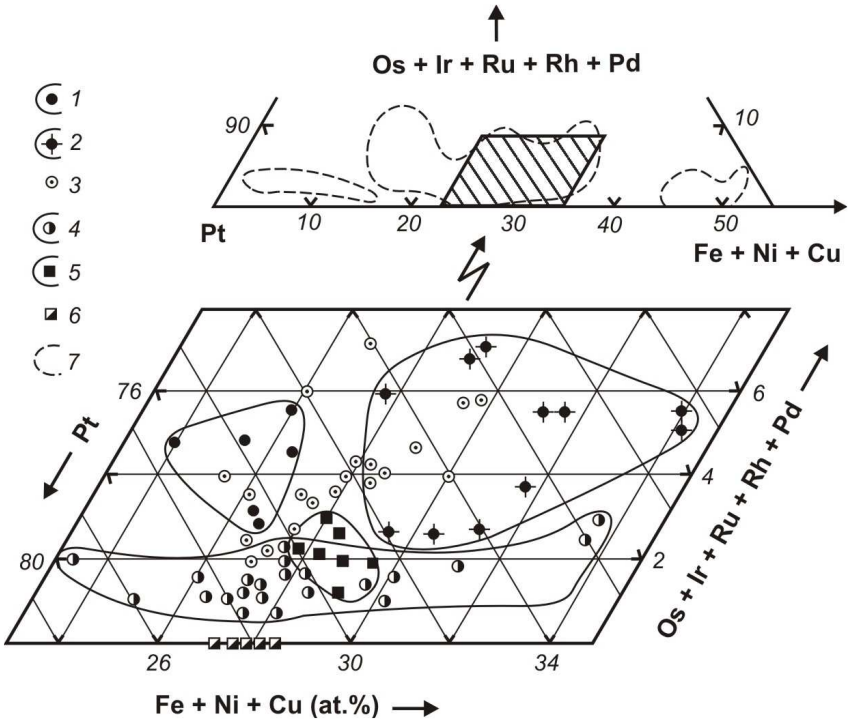

Fig. 2. **Composition of native accessory isoferroplatinum from chromite-bearing dunite.**

Of more (1) and less (2) eroded and other (3) parts of the dunite core of the Konder massif; massive chromite veins and schlieren in dunite (4), and ferroan platinum from phlogopite-magnetite pyroxenites (5), forming dikes in dunite (Table 1), and from cubic nuggets of platinum (6) locally coated with a film of Cu-bearing gold (after Cabri & Laflamme 1997, Shcheka et al. 2004). Contours of fields of native Pt-Fe solid solutions from chromite-bearing dunite of ultramafic formations (7) are shown (after Zhernovsky et al. 1985).

More than 50 PGE, Au- and Ag-bearing minerals, including new and rare species, were identified in loose sediments over 20 years of systematic study of noble-metal mineralization. Discovery of new PGE minerals continues to this day [45]. Many of these minerals were also detected in bedrock. The specific assemblages of minerals are related to one of two principal sources of platinum: chromite-bearing dunite in the core of the massif and the adjacent clinopyroxenite, and dikes of phlogopite-magnetite clinopyroxenite that intrude dunite and spatially associated sulfide lenses in the southwestern part of massif. Other PGM occur in

extremely small quantities as tiny (commonly, no larger than a few tens of micrometers), globular and tabular inclusions within platinum and as an outer rim around these grains. Segregations of such abases are extremely sporadic. Nevertheless, these micro-inclusions turn out to be very diverse and attract the lost interest.

Isoferroplatinum and ferroan platinum

Isoferroplatinum, the main PGM, is very heterogeneous in terms of amount of iron and the other PGE. Two varieties of this mineral were identified in the chromite-bearing dunite of the Konder massif [18]: an early, high-temperature variety in association with chromite accumulations (up to 64 wt. % Cr_2O_3) and Mg-rich olivine (6-9 % Fa), and a late variety that fills the interstitial space in lenses and veins of massive chromitite (up to 54 wt. % C_2O_3). Forsterite (Fo_{94-95}), chromian clinopyroxene, chromian amphibole, Cr-Na-bearing phlogopite, chromite inclusions are commonly included in the isoferroplatinum [30]. The early isoferroplatinum is relatively rich in other PGE and characterized by a variable Fe content, from 7.5 to 11.5 wt. % (24-35 at. %) that decreases with depth (Table 1, Fig. 2). Inclusions of Os, Ir, Ru, and Pt minerals are typical. In conrast, the late Pt-Fe alloy is free of such inclusions and is depleted in other PGE (except Pt), retaining the same Fe content (Table 1).

Table 2.

Composition of Os-Ir-Ru-Rh-Pt solid solutions included in isoferroplatinum, Konder alkaline-ultrabasic massif (wt. %).

No.	Pt	Ir	Os	Rh	Ru	Total
1	2.10	10.10	84.96	0.55	2.00	100.46
2	2.06	2.05	91.64	0.85	1.25	98.18
3	1.79	21.14	72.12	0.73	2.78	99.39
4	1.64	2.44	94.52	0.80	0.38	99.59
5	2.11	12.97	81.88	0.64	1.11	98.98
6	4.39	41.55	27.55	-	25.47	98.96
7	3.20	36.35	39.78	-	20.44	99.77
8	0.84	29.64	68.61	-	-	99.09
9	3.51	34.88	41.25	-	19.03	98.67
10	26.78	38.09	19.11	-	14.40	99.75
11	9.22	54.49	30.12	1.59	2.98	99.16
12	10.37	31.06	56.44	-	1.03	99.26
13	9.85	57.32	30.58	-	0.96	98.99
14	10.64	52.87	37.16	0.29	-	101.11
15	14.04	62.91	20.91	-	0.30	98.97
16	2.20	18.68	76.88	0.40	1.37	99.53
17	0.13	24.26	72.53	0.33	2.42	99.69
18	-	0.60	0.23	-	98.87	99.70
19	-	8.45	55.11	-	35.88	99.44

Note. A selection of the 56 available analyses is given [20]. Additional determinations have been included in the totals: Pd in compositions 1 (0.28), 2 (0.33), 3 (0.13), 4 (0.33); Cu in compositions 1 (0.19), 3 (0.25), 5 (0.27), 11 (0.50), 17 (0.15); Fe in compositions 1 (0.12), 3 (0.45), 10 (1.37), 11 (0.26), 12 (0.36), 13 (0.28), 14 (0.15) and 17 (0.12).wt. %

The ferroan platinum from dikes of phlogopite-magnetite clinopyroxenite that intrude dunite typically consists of cubic crystals locally coated with a film of Cu-bearing gold. The level of PGE impurities in the cubic crystals is close to that in isoferroplatinum in the late Pt-Fe alloy, but the iron content is higher (Fig. 2): 9.5-11.5 wt. % Fe (27-30 at. %). Amphibole, calcic clinopyroxene, aegirine-augite, aegirine, phlogopite, magnetite and apatite inclusions are common in the ferroan platinum [45].

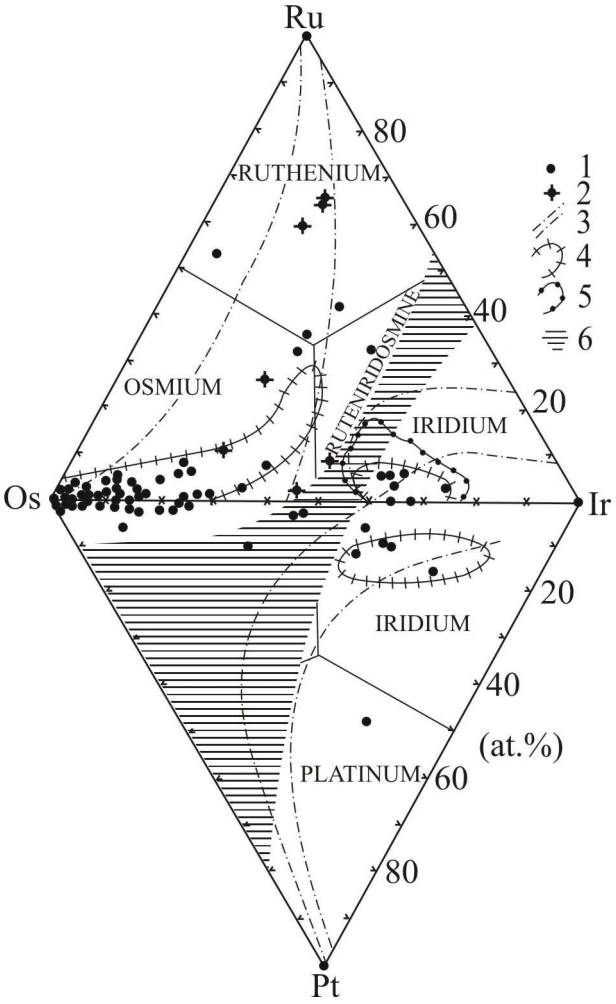

Fig. 3. **Diagram representing solid solutions of Os-Ir-Ru-Pt system of Konder massif.**

1) Data of Table 2; 2) after Mochalov (1994), 3) fields of solid-solution compositions of PGE from alpine-type ultrabasic rocks (after Dmitrenko et al. 1985), 4) the same from the massifs of alkali-ultrabasic formation (after Rudashevsky 1989), 5) the same from Konder massif (after Mochalov 1994), 6) miscibility gaps (after Harris & Cabri 1991).

In the Konder massif, in which the depth of erosion in dunite reaches 350-400 m [20], the maximum Fe content (up to 11.5 wt. %) in the Pt-Fe solid solution is encountered in the uppermost part of the massif. In the isoferroplatinum associated with chromite accumulations, found in the deepest levels of the dunite body, the Fe content falls to 8-9 wt. %. The content of other PGE impurities in the Pt-Fe alloy shows a dependence on depth of crystallization. In the least eroded areas of the dunite, isoferroplatinum contains (wt. %): 0.8-3.8 Ir, up to 2.9 Os, up to 1.5 Pd, and 0.5-1.8 Rh; in the most deeply eroded zone of the dunite, it contains 2.5-5.3 Ir, 0.7-0.9 Os, 0.2-1.OPd, and 0.7-1.1 Rh. The PGE contents in isoferroplatinum show intermediate values in the other parts of the massif.

Os-Ir-Ru-Pt solid solution

As the end member of two solid-solution series Os-Ir-Ru and Os-Ir-Pt, osmium is the more common, on the contrary, platinum and ruthenium are very rare (Table 2). Impurity-free platinum occurs in the Konden massif as isolated inclusions (10-15 μm) of isoferroplatinum and tetraferroplatinum grains, whose margins! have undergone low-temperature alteration. It is associated with micro-inclusions of gold and aggregates of porous Pt-oxide (see below).

Impurity-free iridium (up to 30 μm) and ruthenium (30 x 170 μm) also form rare inclusions in isoferroplatinum. Ruthenium in the Konder massif was first noted by Nekrasov et al. [16].

Table 3.

Chemical composition of hongshiite and its pd-dominant analogue, Konder alkaline-ultrabasic massif (wt. %).

No.	Pt	Pd	Cu	Fe	Ag	Total
1	25.20	40.97	26.16	5.23	0.42	97.98
2	25.65	41.02	26.41	5.20	0.26	98.54
3	67.33	8.62	15.06	7.97	-	98.98
4	71.42	5.91	13.68	8.80	-	99.81
5	67.58	7.98	15.63	8.21	-	99.40
6	58.73	14.68	19.04	7.53	-	99.98
7	48.78	21.75	20.81	6.78	0.19	98.31
8	20.32	45.83	28.44	5.06	0.38	100.03

Osmium is the most commonly encountered, and exhibits one of three habits. It may form rare, predominantly laminar, and in some cases roundish or worm-like inclusions in cumulate isoferroplatinum of the first generation, enriched in PGE impurities. As a rule, this osmium has a high level of Pt and Ir, up to 6 and 17 wt. %, respectively. The second variety of osmium forms disk-shaped and roundish

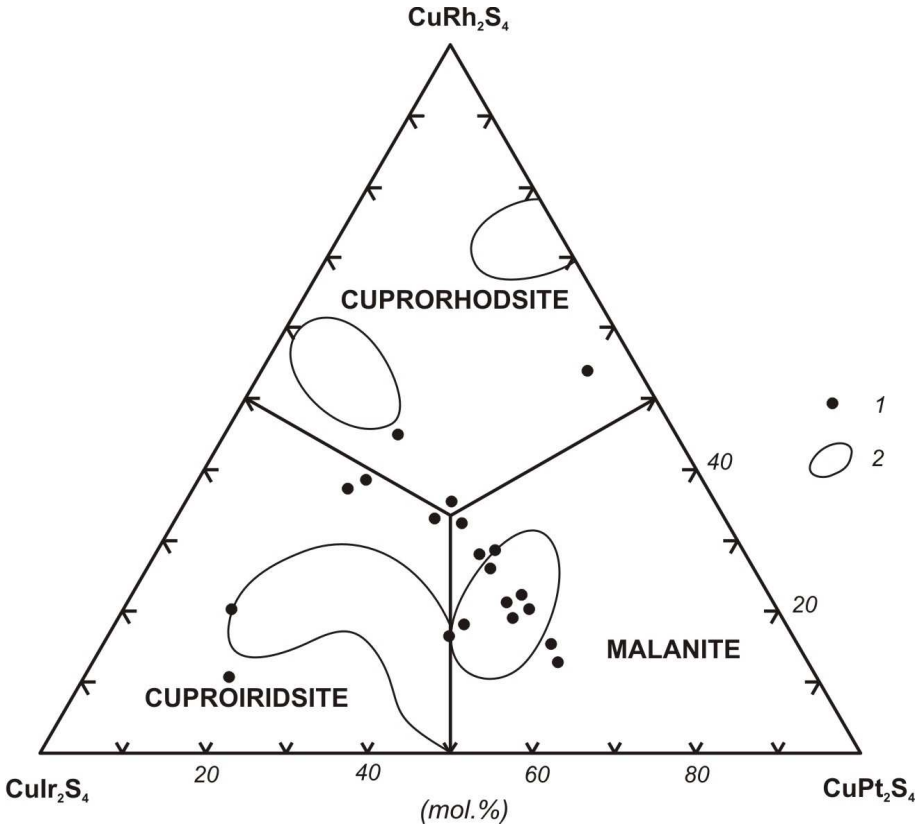

Fig. 4. **Compositions of PGE thiospinels 1) PGE thiospinel of Konder massif according to our data (Table 5); 2) fields of PGE thiospinel composition (after Rudashevsky et al. 1985).**

grains. It has a low level of Pt and Ir, less than 3 and 11 wt. %, and reveals a zonal distribution of Ir in the largest grains, with maximum Ir in the core. This variety of osmium forms inclusions in the low-impurity isoferroplatinum of the second generation. The third variety of osmium forms isolated lamellar aggregates of relatively coarse-grained osmium (50 x 350 μm) with a low level of impurities (up to 2 wt. % of Ir, Pt); it fills interstices in isoferroplatinum of the second generation.

In the Konder massif, solid solutions in the system Os-Ir-Ru-Pt consist mainly of compounds with Os or Ir dominant (Fig. 3), and are named in accordance with the nomenclature of Harris & Cabri [40]. Isolated grains of rutheniridosmine and ruthenium-dominant solid solutions with wide variability are present but rare. There are single occurrences of solid solutions whose compositions occupy the miscibility field. Such an anomaly may be the result of the influence of the Pt matrix during electron-microprobe analysis. It is possible that the field of miscibility of the compositions of natural Pt-Os-Ir and Ru-Os-Ir solid solutions is less significant, in agreement with the analytical data on alpine-type ultrabasic rocks in northeastern Russia [11, 24]. The solid solutions form isolated grains 30-75 μm to 250 μm in size. Note that they are distributed in the high-temperature isoferroplatinum only exceptionally.

The crystallization of PGM at the magmatic stage is limited to isoferroplatinum and solid solutions in the system Os-Ir-Ru-Pt. The postmagmatic stage of evolution is characterized by a much greater variety of mineral species.

Tetraferroplatinum, tulameenite and hongshiite

Platinum-dominant solid solutions are tetraferro-platinum, tulameenite, and hongshiite. They are rare in the Konder massif and most commonly form a rim of variable thickness on isoferroplatinum, but may completely replace it. Tetraferroplatinum exhibits the most consistent composition, invariably containing Cu (up to 3 wt. %) and Ni (up to 1.5 wt. %). Tulameenite forms a rim on grains of isoferroplatinum; it contains variable Fe (8.5-13 wt. %) and Cu (8.8-12.8 wt. %), but constant Pt contents. In rare isolated segregations of tulameenite associated with bornite, irregularly distributed impurities of Ni (up to 3.5 wt. %) and Ir (up to 2.5 wt. %) occur, showing an enrichment as the rim is approached. Variants of tulameenite enriched in Sn and Sb also are found [25]. Even within the same rim around isoferroplatinum, the tulameenite is represented by both marginal and intermediate members of the solid-solution series Pt(Fe,Cu)-Pd(Cu,Fe). Hongshiite seems to be the most variable in composition (Table 3).

PGE sulfides and sulfoarsenides

PGE sulfides and sulfoarsenides are much more widespread at the postmagmatic stage in the Konder massif. Members of the laurite-erlichmanite series and .sulfoarsenides of the irarsite-hollingworthite series are the most common. Monosulfides and compound sulfides of malanite-cuprorhodsite-cuproiridsite composition are less common. Sulfides such as inaglyite and konderite are much rarer. All these compounds form a fragmentary rim (10 μm

wide or more) or lens-like and equidimensional segregations (5-75 μm) at grain boundaries and at the margins of isoferroplatinum grains.

Table 4.

Composition of monosulphides of PGE and iron-group elements, Konder alkaline-ultrabasic massif (wt. %).

No.	Pt	Ir	Rh	Fe	Ni	Cu	S	Total
1	2.13	26.23	2.21	19.21	17.93	2.88	27.66	98.24
2	1.09	25.54	2.71	19.96	18.31	2.87	28.29	98.77

PGE monosulfides are represented by cooperite and a nickel-rich variety of a pentlandite-like phase. Electron-microprobe analyses show that cooperite has a composition close to PtS. Its block-shaped and needle-shaped segregations form a rim around grains or veinlets of isoferroplatinum in tulameenite in some instances. However, the bulk of the cooperite is related to concentrations of pentlandite, chalcocite, bornite, chalcopyrite, and cubanite that form rare lenses and veinlets in dunite in the southwestern part of the Konder massif [6].

Table 5.

Chemical composition of PGE thiospinels, Konder alkaline-ultrabasic massif (wt. %).

No.	Cu	Fe	Pt	Ir	Rh	S	Total
1	8.18	1.38	11.34	49.08	3.08	24.08	97.14
2	5.04	1.15	13.63	33.76	14.59	23.74	99.82
3	9.94	1.70	30.27	26.60	7.97	23.59	101.06
4	8.83	3.41	17.98	25.54	17.77	25.13	98.66
5	10.56	0.51	25.19	24.04	13.62	26.35	100.27
6	10.64	0.77	33.42	20.38	9.11	25.32	99.64
7	11.69	-	38.11	17.36	6.76	25.47	99.39
8	8.28	1.77	30.27	6.21	21.45	26.63	100.98

Pentlandite-like monosulfides have been found intergrown with magnetite and pyrrhotite in dikes of magnetite-phlogopite pyroxenite. In the last case, the PGE (Ir mainly) account for only 26 wt. % of the monosulflde fraction (Table 4). This material is isotropic, and has a microhardness in the range 180-220 kg/mm^2. Analogues of pentlandite-type phases described earlier are enriched in Ir and Rh, or rarely only in Rh, or in a single case, Rh and Ru. Along with Fe and Ni, it contains Co and Cu (up to 2.5 and 5.8 wt. %) also [37, 7].

Compound sulfides, represented largely by thiospinel of the malanite-cuprorhodsite-cuproiridsit group and, rarely, by a Cu- and Pb-bearing mineral o the inaglyite-konderite group [26, 27, 28], form equidimensional inclusions am veinlet-like grains of isoferroplatinum and a thin rin around them. Individual rounded grains, up to 0.3 mm in size, and polymineralic intergrowths with iridosmine, erlichmanite, laurite and, in some cases, with sperrylite, bismutharsenide, irarsite, and hollingworthite, are much rarer. These minerals occur predominantly in the same samples of dunite in which lenses and veinlets of

Cu, Fe, Ni sulfides with Co, Ft impurity up to 0.8 wt. % Co, *2.5* wt. % Pt were found.

The maximum Pt, Ir, and Rh content in the thiospinel is 38, 49 and 21 wt. %, respectively (Table 5). Most grains of thiospinel correspond to malanite with a high concentration of Rh and Ir, but others are cuproiridsite, the rhodium analogue, iridian cuprorhodsite, and an essentially platinum-rich variety of the cuprorhodsite (Fig. 4). Fe (up to 3,4 wt. %) is invariably present in these thiospinels.

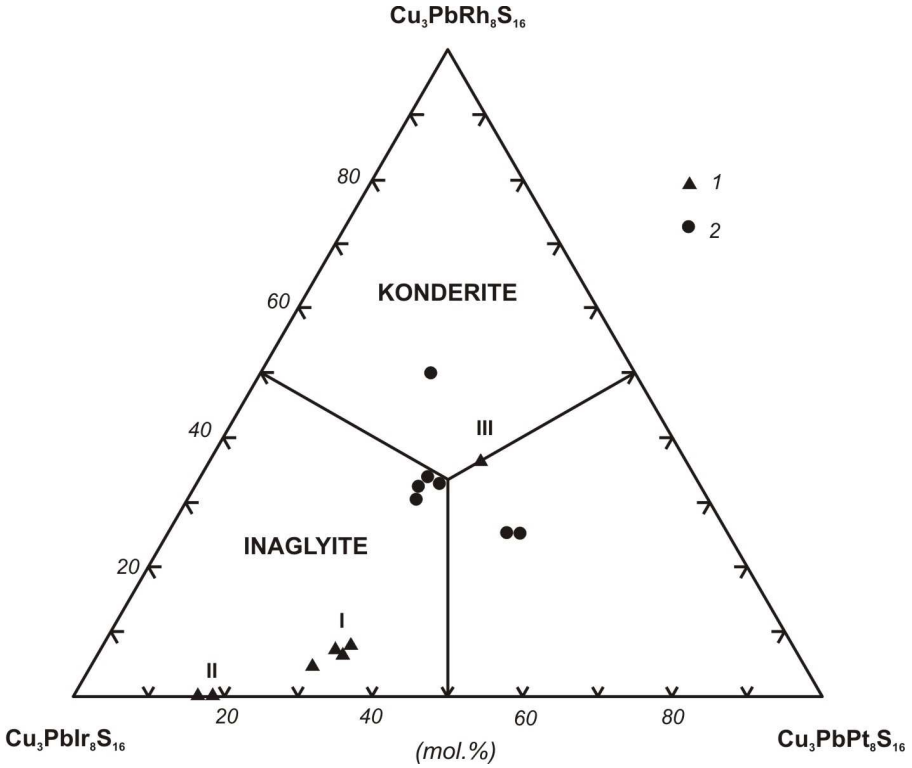

Fig. 5. **Compositions of Cu-Pb-bearing sulfides of PGE.**

1 inaglyite (I, II) and konderite (III) from Inaglinsky (I), Nizhne-Tagilsky (II) and Konder (III) massifs (after Rudashevsky et al. 1984a b); 2) inaglyite, konderite, and w is likely to be a new platinum analogue (Table 6).

Among the Cu- and Pb-bearing sulfides we have studied (Table 6), inaglyite saturated with rhodium is the most prevalent. One of these sulfides is konderite, with much less iridium than that described earlier [28], and the other two varieties are enriched in the $Cu_3PbPt_8S_{16}$ end-member (up to 46 %) and represent a new mineral, the Pt-dominant analogue of inaglyite and konderite (Fig. 5). Like the other two minerals, this sulfide has a microhardness of 412-435 kg/mm^2 and contains little Fe, and no Ni; however, we established the essential impurity as As (up to 3.96 wt. %).

In the Konder River placer, we have found a complex sulfide that contains palladium and gold (in wt. %: 52.47 Pd, 11.53 Au, 4.94 Ag, 15.64 Bi, 8.46 Pb, 0.69 Ni, 7.34 S, total: 101.07) with the general formula $(Pd,Au,Ag,Ni)_{11}(Bi,Pb)_2S_4$.

Together with palladium germanide (Pd_2Ge), discovered probably for the first time, it forms a heterogeneous rim of variable composition around grains of hongshiite. Experimental investigations of the systems Au-Ag-S and Au-Bi-S [15] show that the gold-bearing sulfide could have originated only at relatively low temperature (200-350°C) and extremely high $f(S_2)$ (10^2 - lO^3 Pa).

Table 6.

Chemical composition of Cu- and Pb-bearing sulphides of PGE, Konder alkaline-ultrabasic massif (wt. %).

No.	Pb	Cu	Ir	Pt	Rh	S	Total
1	8.12	9.32	18.73	29.15	9.25	24.12	99.43
2	7.60	10.12	18.20	30.67	9.14	24.47	100.92
3	8.84	7.96	24.32	21.54	12.56	24.43	99.65
4	8.43	9.32	23.45	22.31	11.73	24.17	99.41
5	8.18	8.92	20.12	16.58	18.70	25.12	100.40
6	7.44	7.92	26.15	19.72	11.05	24.17	100.41
7	8.07	8.16	26.32	19.84	11.34	23.91	99.87

Note: Additional determinations have been included in the totals: Fe in compositions 1, 2 (0.74, 0.72) and As in compositios 5-7 (2.78, 3.96, 2.23).

Disulfides of the erlichmanite-laurite series are represented by both end members and less common examples of intermediate compositions (Fig. 6). Zoned

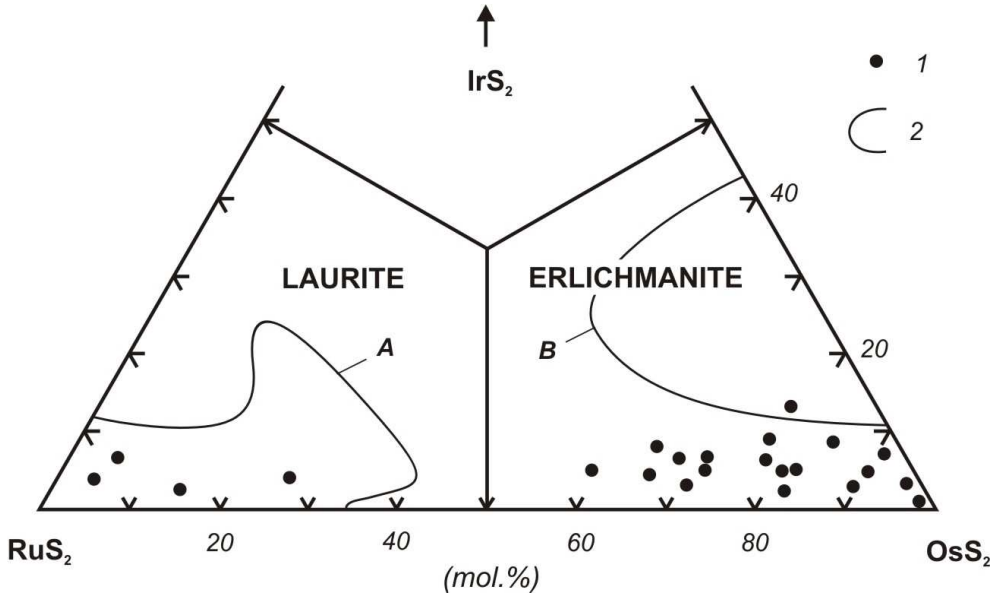

Fig. 6. **Compositions of PGE disulfide of the erlichmanite-laurite series.**

1) PGE disulfides of Konder massif according to our data (after Nekrasov et al. 1994); 2) fields of mineral compositions of laurite (A) - erlichmanite (B) series from alpine-type ultrabasic rocks (after Dmitrenko et. al 1985).

grains are the general case, with osmian laurite and ruthenian erlichmanite both enriched in Ru near the rim compared with the center. These minerals contain a

variable level of Pt (0.2-2.1), Rh (0.5-5.1), Ir (0.2-9.9), Pd (0.5-2.7), and As (0.4-2.2 wt. %). Analogous disulfides of Pt and Rh have been noted in alpine-type ultrabasic massifs [4]. However, the latter contain less Pd and commonly more Ir.

A sulfarsenide of the irarsite-hollingworthite series is as common as Os-Ru disulfides and formed almost simultaneously with these, on the basis of observations of interrelations in polymineralic grains.

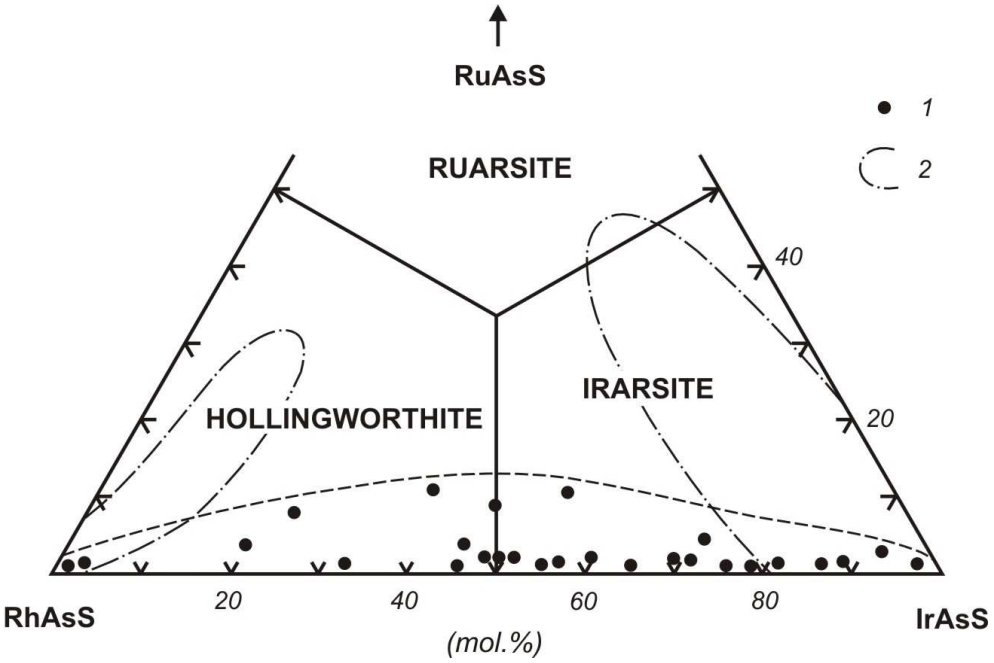

Fig. 7. **Compositions of sulfoarsenide of Rh-Ir-Ru system of Konder massif.**

1) PGE sulfoarsenides of Konder massif according to our data (after Nekrasov et al. 1994); 2) fields of sulfoarsenide compositions from alpine-type ultrabasic rocks (after Dmitrenko et al. 1985).

Like the disulfides, the sulfarsenides are represented by both the end members and intermediate compositions, which is not typical of PGM occurrences related to alpine-type ultrabasic massifs (Fig. 7). Along with isolated homogeneous inclusions of irarsite and hollingworthite, their zonally arranged segregations, in which the marginal part is enriched in Ir and the center in Rh, are commonly found in isoferroplatinum. Much more complicated formations, with a zonal structure (50-200 μm in size) also are present. Their core is composed of iridosmine, which gives way to irarsite enriched in osmium toward the periphery, and then to hollingworthite, forming a narrow (5-8 (μ) rim. Platarsite occurs as isolated grains [11, 25].

The content of Pt, Os, and Ru impurities in the Konder irarsite-hollingworthite sulfarsenides varies less widely (0.2-4.6 wt. %) than in their analogues from alpine-type ultrabasic rock, in which the maximum concentrations of these PGE are twice as large [4], except for Pd, which seems saturated (0.4-4.8 wt. %).

Sperrylite and Pt_2As_3

PGE arsenides are represented mainly by sperrylite. The compound Pt_2As_3, first found here, and complex Sb-, Bi-, and Te-bearing Pd and Pt arsenides are rare. Sperrylite occurs as fine (50-250 μm) inclusions in isoferroplatinum and composite grains with tulameenite. Single octahedra up to 1.5 mm across are much rarer. The association of sperrylite with antimonpalladinite, irarsite, and cooperite has been also encountered. The chemical composition of sperrylite is close to being stoichiometric $PtAs_2$, with a negligible proportion of sulfur in most samples; this finding does not contradict the experimental data of Makovicky *et al.*[41], according to which the solubility of S in $PtAs_2$ at 850° and 470°C attains 2.5 wt. %.

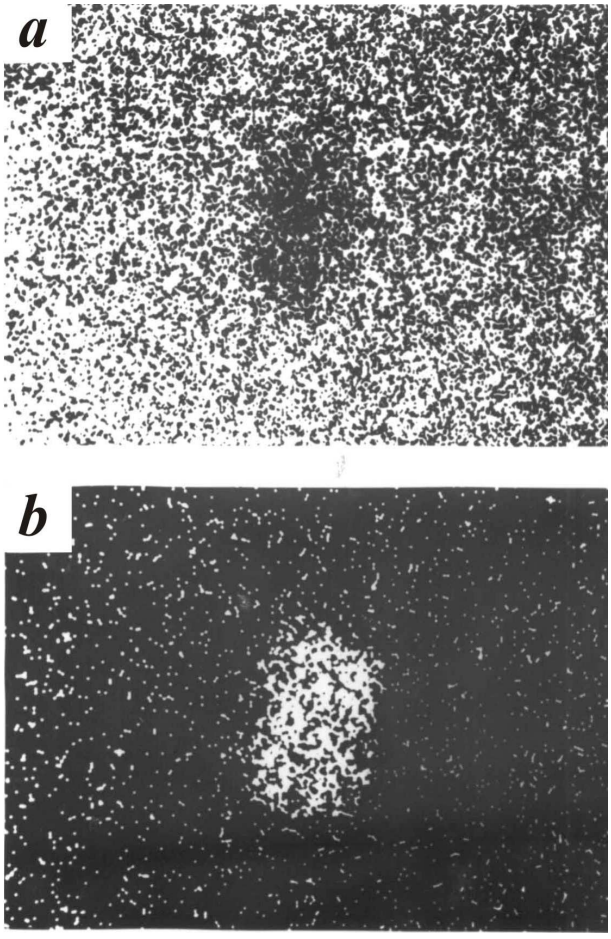

Fig.8. **X-ray maps of the isoferroplatinum grain enclosing new platinum arsenide (1200x); a) PtL*α*, b) AsK*α*.**

In their experiments, sulfur-bearing sperrylite precipitated in association with cooperite, pyrrhotite, and platarsite, which may be an indication of high $f(S_2)$ in the natural ore-forming system. Although the associations of sperrylite are diverse within the system Fe-Pt-As-S, these experiments showed that $PtAs_2$ is the only stable binary phase. In other words, we did not expect to find the fine inclusions of the compound $Pt_{1.5}Ir_{0.5}As_3$ (in wt. %: 51.62 Pt, 1.08 Rh, 10.57 Ir, 0.28 Os, 0.16 Cu, 2.2 S, 33.14 As, total: 99.05; approximately 25 μm, microhardness 500 kg/mm^2) with a calculated formula $(Pt_{1.57}Ir_{0.33}Rh_{0.06})_{\Sigma 1.96}(As_{2.63}S_{0.40})_{\Sigma 3.03}$ (Fig. 8) in isoferroplatinum. A close analogue of this mineral is a phase enriched in Rh and S with the formula $(Pt,Rh)_2(As,S)_3$, discovered in a gold-platinum placer in Russia [32]. In this connection, it seems that the presence of Ir (up to 10.6 wt. %) or Rh (up to 6.2 wt. %) as impurities in the Pt_2As_3 compound must stabilize its structure.

Composite palladium and platinum arsenides

In composite palladium and platinum arsenides (Table 7), in spite of considerable variations in the content of all components, the ratio of Pd (or Pd + Pt + Ag) to S(As, Bi, and Sb) in most of minerals approximates 3:1, as in the discredited species "guanglinite", and correspond to the generalized formula

$(Pd,Pt)_3(Bi,Sb, Te,As)$. Among these, the antimony and bismuth arsenides predominate. The exceptions are two antimony arsenides (Table 7, anal. 1, 2), two bismuth arsenides (anal. 10, 11), and both bismuth tellurarsenides. One of the antimony arsenides (anal. 1) exhibits the isomertieiteformula, $(Pd_{9.66}Pt_{1.34})_{\Sigma 11}(Sb_{2.18}As_{1.73}Te_{0.05})_{\Sigma.96}$. The other antimony arsenide is similar to the previous case; however, its inferred chemical composition gave a somewhat different formula,

Table 7.

Chemical composition of composite Sb-, Bi-, and Te-bearing arsenides of palladium and, Konder alkaline-ultrabasic massif (wt. %).

No.	Pd	Pt	Ag	Sb	Bi	Te	As	Total
1	61.63	15.67	1.30	13.95	-	0.43	7.80	100.78
2	73.03	1.32	2.38	12.46	1.68	0.32	7.60	98.79
3	70.27	1.12	2.59	19.59	0.55	-	5.54	99.66
4	69.63	0.40	0.84	23.26	-	-	2.28	99.25
5	67.61	-	0.72	15.95	-	0.12	9.44	98.00
6	69.87	-	-	25.51	-	-	3.01	100.01
7	64.94	2.10	1.05	3.75	17.58	1.46	6.64	98.35
8	65.67	1.11	0.62	0.66	22.38	1.89	6.20	99.81
9	66.87	0.94	1.05	2.65	16.88	1.95	6.06	99.02
10	63.69	12.43	0.65	-	13.87	-	9.49	100.13
11	64.48	11.78	0.54	-	13.56	-	9.26	99.62
12	72.11	4.45	0.16	0.42	9.46	6.13	4.74	97.47
13	72.76	3.18	0.31	1.87	7.01	6.94	5.33	97.40

Note: Additional determinations have been included in the totals: Sn in compositios 4(1.43), 9(0.19), Cu in compositions 4(1.41), 5(4.16), 6(1.62) and Pb in compositios 7(0.83), 8(1.28), 9(2.43). 1-6 – antimonarsenides, 7-11 – bismutharsenides, 12-13 – bismuthtellurarsenides.

$(Pd_{9.59}Pt_{0.10}Ag_{0.31})_{\Sigma 10}(Sb_{|1.43}As_{1.41}Bi_{0.11}Te_{0.04})_{\Sigma 2.99}$. One of the bismuth tellurarsenides seems to be similar to "guanglinite" and has an inferred formula $(Pd_{3.89}Pt_{0,09}Ag_{0.02})_{\Sigma 4}(Bi_{0.16}\ Sb_{0.09}\ Te_{0.31}As_{0.40})_{\Sigma 0.96..}$The other bismuth arsenide ranges in composition (Table 7) and cation : anion ratio from 7:2 (anal. 10, 11) to 9:2 (anal. 12), and is similar to arsenopalladinite [39], and more precisely to its Bi-bearing (anal. 10, 11) and Bi-Te-bearing (anal. 12) variants. Most of the composite Pd and Pt arsenides are found in the form of fine isolated inclusions in isoferroplatinum, the palladium-dominant analogue of hongshiite, and palladium-, copper-bearing gold, where they usually are associated with sobolevskite and other bismuthides and antimony bismuthides of palladium, which form in some cases polymineralic aggregates up to 90 μm in size. The associations with sperrylite are rarer.

Bismuthides, antimonbismuthides, antimonides and tellurides

Bismuthides, antimonbismuthides, and antimonides I of palladium, represented by minerals of sobolevskite (PdBi) - sudburyite (PdSb) series, are rare at Konder. Fine inclusions (10-25 μm) of sobolevskite close to the t stoichiometry PdBi (Table 8) are common in copper- bearing gold, and rarer in isoferroplatinum.

Many bismuthide grains are zoned. The central part is composed of PdBi, whereas the margin is enriched in palladium, up to a composition corresponding to the stoichiometry Pd_3Bi_2 and Pd_3Bi. We found both as individual phases and in a grain of tetra-auricupride containing 8.69 wt. % Pt and 0.36 wt. % Pd, and as rare inclusions in froodite, $PdBi_2$ (Table 8). As long as Sb is available to replace Bi in sobolevskite, sudburyite eventually forms. Several small grains of this mineral (Table 8), up to 25 μm in size, were found in composite grains with sobolevskite and the phase $Pd_3(Bi,Sb)$, enclosed in gold. In some cases, needle-shaped inclusions of native antimony are present in the gold. Antimonides, arsenide-antimonides, surfantimonides, and phases of more complex composition, with the ratio of the PGE to the "anion" portion from 5:2 and 3:1 to 1:2, also were found closely intergrown with bismuthides of the sobolevskite-sudburyite series.

Table 8.

Chemical composition of bismuthides and antimonbismuthides of palladium and platinum, Konder alkaline-ultrabasic massif (wt. %).

No.	Mineral and its generalized formula	Pd	Pt	Sb	Bi	Total
1	Sobolevskite-PdBi	31.83	-	-	69.94	101.77
2	The same	31.33	-	-	70.58	101.91
3	– „ –	31.35	-	-	64.88	99.02
4	– „ –	23.69	9.82	-	64.98	99.77
5	Pd_5Bi_2*	57.69	-	-	43.68	101.37
6	Bismuthpalladinite-Pd_3Bi_2*	44.27	-	-	55.31	99.58
7	The same	47.27	-	-	52.00	99.27
8	$Pd_3(Bi,Sb)$*	77.26	-	15.01	8.14	100.41
9	The same	77.34	-	15.03	8.54	100.91
10	(Pt,Pd)(Bi,Sb)*	12.23	34.10	13.64	39.95	99.92
11	Frudite - $PdBi_2$	19.76	8.80	3.60	64.94	100.59
12	Sudburyite - Pd(Sb,Bi)	42.25	-	42.43	14.34	99.02
13	The same	41.34	-	41.08	16.16	98.58
14	Insizwaite -$PtBi_2$	-	31.39	3.57	66.09	101.05

Note: Additional determinations have been included in the totals: Cu in compositions 3 (0.52), 11 (3.49), Au in compositions 3 (2.27), 4 (1.28). Probably new minerals are shown by an asterisk.

Rhodium-iridium sulfantimonide, (Rh,Ir)SbS, similar to tolovkite (ideally, IrSbS) was first discovered at Konder by Mochalov [11]. Later, a similar mineral was discovered by Evstigneeva *et al.* [7] at Yubdo, Ethiopia. Many grains of these minerals are zoned.

Minerals of sobolevskite (PdBi) - kotulskite (PdTe) series have a limited distribution. Owing to the complete solid-solution between Te and Bi, even within the same host-mineral (tetra-auricupride or isoferroplatinum), inclusions of two or three phases may be present. These phases differ from one another in composition, as a result of complete substitution involving Te and Bi, and are intermediate compounds between sobolevskite and kotulskite (Table 9). In some of them, the impurity elements are Pb (to 2 wt. %) and Pt (to 2.7 wt. %). Members of the series

kotulskite (PdTe) - sudburyite (PdSb) contain a bismuth-free phase with a high concentration of Sb (more than 15 wt.%), which may be a new mineral (Table 9).

The Bi-Te-bearing palladinite that we found is a much more widespread mineral than the members of the sobolevskite-kotulskite solid solution (Table 9). It occurs as fine inclusions (10-15 μm) in bornite from the sulfide lenses in the Konder dunite, mentioned above, and in low-grade gold. This mineral is characterized by striking heterogeneities, with small-scale variations of .2-3 wt. % Pd and 0.5-1.5 wt. % in other elements. Some Bi-Te-enriched domains of palladinite have decompsosed into two or three phases, one of which is Pt oxide and other two are identified as Bi_3Te and native bismuth. The Bi_3Te compound occurs also as individual mica-like accumulations up to 5 μm across. In aggregates with high-grade Au (fineness 880-920), the Bi_3Te precipitated later and cemented segregations of gold.

Table 9.

Chemical composition of bismuth-and antimontellurides of palladium, Konder alkaline-ultrabasic massif (wt. %).

No.	Pd	Ag	Sb	Bi	Te	Total
1	44.24	-	-	13.62	38.19	97.99
2	44.72	0.19	-	12.39	39.45	98.87
3	42.42	0.57	15.64	-	38.81	98.31
4	32.42	-	-	55.17	11.34	101.62
5	69.92	0.94	0.35	9.14	16.69	97.04

Note: Additional determinations have been included in the totals: Pb in compositions 1 (1.94), 2 (2.12), 3 (0.87) and Pt in composition 4 (2.69).

Insizwaite, PtBi2, occurs in isoferroplatinum (Table 8), earlier first described at Konder by Mochalov, [11], and in geversite, $Pt(Sb,Bi)_2$, as discovered by Rudashevsky *et al.* [25]; it is not common in the Konder massif. A palladium bismuth plumbide is present as single grains. We found it in copper-bearing gold as inclusions 5-15 μm in size. The chemical composition of this presumably new phase (wt. %) is: 57.52 Pd, 34.74 Pb, 7.02 Bi, 1.2 Pt, total 100.48. Rare inclusions of zvyagintsevite are present in tetra-auricupride.

Platinum and palladium stannides

Platinum and palladium stannides are relatively widespread, in the form of fine (15-60 μm) inclusions in tetra-auricupride, tulameenite, and isoferroplatinum. Their chemical composition (Table 10) allows us to subdivide them into three groups. The first one (Table 10, anal. 1 and 2) has a negligible level of Sb (up to 1 wt. %) and is free of Cu. The sum of Pt and Pd is 82 wt. %, with about 17 wt. % Sn, and the composition as a whole was calculated on the basis of the formula of rustenburgite, $(Pt,Pd)_3Sn$. The second group includes the multicomponent copper-enriched (up to 14 wt. %) alloys of the system Pt-Pd-Sn-Cu-Fe (Table 10, anal. 3 to 9). Impurities are Ni (up to 0.4 wt. %) and Bi (up to 1.3 wt. %). The compounds of this group are characterized by notable variations in Sn content (9-17.2 wt. %),

relatively constant Pt (63-73.4 wt. %), and the almost invariant presence of Fe (up to 5.8 wt. %). These phases are associated with sobolevskite and palladium-bearing gold. High-palladium solid solutions, which have been described already from the Konder massif (Mochalov 1986), represent the third group of stannides.

Table 10.

Chemical composition of platinum and palladium stannides, Konder alkaline-ultrabasic massif (wt. %).

No.	Pt	Pd	Cu	Sn	Sb	Fe	Total
1	66.12	15.40	-	16.90	0.66	-	99.08
2	62.84	17.68	-	16.96	1.07	-	98.55
3	63.02	5.00	14.05	16.64	-	0.18	99.83
4	68.12	3.18	13.09	13.82	-	1.75	99.96
5	63.48	4.69	13.50	16.27	-	0.36	99.59
6	72.49	0.34	12.16	9.01	-	5.78	99.78
7	63.41	5.32	13.75	17.18	-	-	99.66
8	72.66	-	12.51	10.75	0.36	3.30	99.98
9	73.44	-	12.95	10.28	0.35	2.52	99.54

Note: Additional determinations have been included in the totals: Bi in compositions 3, 5 (0.94, 1.29) and Ni in composition 8 (0.4).

Palladium germanide

As was noted above, we found palladium germanide (Pd_2Ge) in the Konder massif. It is a new, as yet unnamed mineral, which together with a new palladium-gold-bearing sulfide, make a narrow (5-17 μm) rim around a grain of the palladium analogue (PdCu) of hongshiite (Fig. 9). Although high magnification reveals an optical heterogeneity, consisting of a rhythmic alternation of fine strips of the germanide, all eight analyses of the same grain show similar results, that on average are described by the composition (wt. %): 75.62 Pd, 1.12 Ag, 23.89 Ge, total: 100.63. The experiment carried out by I.Ya. Nekrasov (unpubl. data) at dry conditions at 700°C shows that in the system Ge-Pd, along with Pd_2Ge, three other phases, PdGe, Pd_4Ge, and Pd_5Ge, are stable, which allow

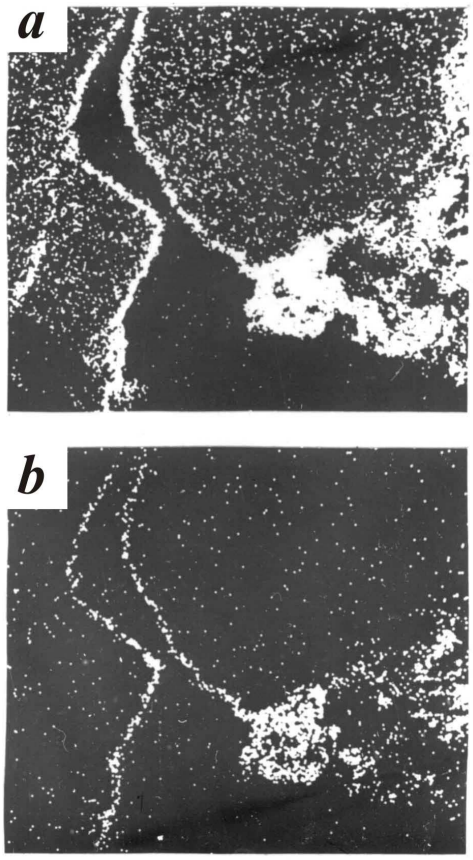

Fig. 9. **X-ray maps of edge part of the Pd-bearing hongshiite grain in contact with palladium germanide, which forms heterogeneous units continuous into a rim (1000x); a) PdL*α*; b) GeL*α*.**

us to anticipate their existence in nature.

PGE oxide and hydroxide

PGE oxide and hydroxide compounds formed at the final stage [36]. They are the products of supergene events in most cases; however, they may also be hypogene, in part as a result of interaction of PGM of an early (magmatic) stage with postmagmatic solutions.

Table 11.

Chemical composition of PGE oxides, Konder alkaline-ultrabasic massif (wt. %).

No.	Pt	Pd	Ir	Os	Rh	Cu	Fe	Total
1	3.76	54.10	-	-	-	22.43	7.93	88.22
2	65.86	-	-	-	-	13.61	5.89	85.36
3	81.18	-	-	-	-	1.54	6.94	89.66
4	64.09	-	-	-	-	15.20	4.44	83.73
5	63.51	-	-	-	-	19.64	6.63	83.78
6	66.96	-	-	-	-	9.91	11.99	88.86
7	77.74	-	-	-	-	-	6.93	86.72
8	74.08	-	-	-	-	-	6.08	84.54
9	-	-	21.28	51.16	0.14	-	3.31	83.94
10	3.68	-	34.72	1.27	31.26	2.02	12.03	84.98

Note: Additional determinations have been included in the totals: Ru in composition 9 (8.05) and Au in compositions 7 (2.05), 8 (4.38).

In most cases, oxides and hydroxides developed at the expense of isoferroplatinum, tulameenite, and hongshiite. In addition to Pt(Pd), they preserve the high Fe and Cu contents. Palladium, Os, Rh, and Ir oxides are much rarer in the Konder placer (Table 11). For example, Pd oxide coats the palladium analogue of hongshiite, Pd(Cu,Fe), as a thin film, but Pt, Ir, Os, and Rh oxides result from the partial replacement of hongshiite, minerals of irarsite-hollingworthite series and other PGM. The analytical totals in the case of the hydroxides vary over the range 70-80 wt. % (Table 12), depending on the amount of H_2O in the structure [11, 20].

Table 12.

Chemical composition of PGE hydroxides, Konder alkaline-ultrabasic massif (wt. %).

No.	Pt	Pd	Ir	Os	Rh	Cu	Fe	Total
1	6.35	0.69	48.57	-	6.71	2.04	6.08	70.44
2	8.07	-	53.16	0.32	4.28	-	7.92	73.92
3	4.19	-	40.27	0.44	28.62	-	0.76	74.51
4	75.52	1.92	-	-	-	-	6.93	77.45
5	1.76	-	26.53	6.01	30.02	10.20	2.84	77.56

Note: Additional determinations have been included in the totals: Ru in compositions 2, 3 (0.17, 0.23) and Bi in composition 4 (0.31).

Gold mineralization

The gold mineralization in the Konder massif is extremely diverse. Numerous electron-microprobe results indicate not only native and Ag-bearing

gold, but also Cu-, Cu-Pd-, and Cu-Pt-enriched varieties [20, 19], which are exceptionally rare in nature [21,22].

The gold minerals formed later than the cubes of platinum and, probably, somewhat later than the PGE sulfides and sulfoarsenides, but contemporaneously with various Pd-bearing compounds including hongshiite and its Pd-dominant analogue, complex sulfides, arsenides, antimonides, bismuthides, tellurides, stannides, plumbides, and palladium germanide.

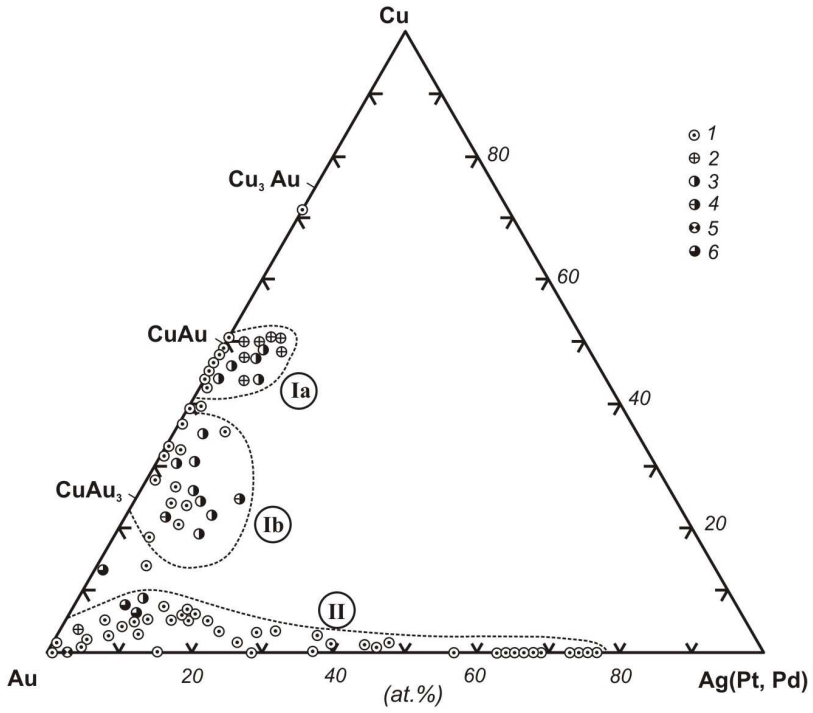

Fig. 10. **Compositions of the gold solid solution of Konder massif.**

Au-Cu, Au-Cu-Ag and Au-Ag (1), Au-Cu-Pt (2), Au-Cu-Pd (3), Au-Cu-Pt-Pd (4), Au-Cu-Pt with Ag (5), and Au-Cu-Pd with Ag (6). See text for other explanations.

The compounds of gold and other metals can be divided into three broad groups (Fig. 10), distinguished by proportions of Au, Cu, Ag, Pd, and Pt [19]. The first group of solid solutions comprises the compounds based on Au and Cu, belonging to the systems Au-Cu, Au-Cu-(Pd,Pt), and Au-Cu-Ag. They form fine tabular and spindle-shaped inclusions in Ag-bearing gold of high fineness, or serve as host minerals containing inclusions of Ag-bearing gold. In addition to forming discrete grains, both types of Cu-bearing and native gold intergrowths occur as zonal rims around the platinum crystals, and occasionally around other minerals. The Cu-bearing gold from Konder reveals a bimodal distribution of Cu (Fig. 10, 1a, b) that demonstrates a high abundance of cupro-auride (AusCu), which is lacking in other natural assemblages [14, 21, 22, 31], and tetra-

auricupride (AuCu) with a whole range of Cu contents from 6.89 to 24.99 wt. % (Table 13). The Cu content, 44.27 wt. %, corresponding to auricupride (CuAu),

Table 13.

Composition of Au-Cu solid solution, Konder alkaline-ultrabasic massif (wt. %).

No.	Au	Ag	Cu	Total
1	75.03	-	24.42	99.45
2	79.05	-	21.50	100.55
3	78.14	-	21.92	100.06
4	76.38	-	23.75	100.13
5	76.29	-	23.02	99.31
6	83.99	-	16.12	100.11
7	86.55	0.34	11.37	98.26
8	86.64	-	14.34	100.98
9	86.20	0.55	13.56	100.31
10	89.15	2.84	7.44	99.43
11	86.12	3.27	9.47	98.86
12	55.50	-	44.27	99.77

Note: A portion of the 50 compositions available is given [19].

was detected in one sample only. Auricupride in association with tetra-auricupride is more typical of some other occurrences of Cu-bearing gold in the absence of cupro-auride [21]. Some phases of Cu-bearing gold contain Ag (0.33-5.39 wt. %),

Table 14.

Composition of Au-Cu-Pt and Au-Cu-Pd solid solution, Konder alkaline-ultrabasic massif (wt. %).

No.	Au	Ag	Cu	Pt	Pd	Total
1	63.41	-	23.52	11.79	-	98.72
2	62.54	-	24.40	10.33	-	97.27
3	70.17	-	19.62	9.56	-	99.35
4	65.19	-	24.69	9.27	-	99.15
5	67.09	-	23.86	7.55	-	98.50
6	72.54	-	24.28	3.12	-	99.54
7	95.87	0.68	1.16	2.35	-	100.06
8	79.17	-	10.25	0.22	10.27	99.91
9	82.84	-	8.86	-	7.79	99.49
10	84.67	1.10	6.08	-	7.43	99.28
11	84.12	0.50	7.66	-	6.81	99.09
12	83.35	-	9.84	-	5.82	99.01
13	70.03	-	24.99	-	4.27	99.29
14	83.27	0.27	13.66	-	3.32	100.52

Note: A portion of the 23 compositions available is given (19).

which replaces Cu where Au content is no lower than 14 wt. %. The Pt and Pd in solid solution (0.22-11.79 wt. % and 0.18-10.27 wt. %, respectively) were established in a broader range of compositions within the Au-Cu series (8-25 wt. % Cu). Pt and Pd are present in various proportions, either separately or together (Table 14). The elevated Pt content is present only in AuCu, *i.e.*, in compositions enriched in Cu. The Cu-free Pd-bearing gold (wt. %: 94.32 Au, 2.58 Pd) was

detected at the margin of a complex grain of Pd-Cu-bearing gold with inclusions of zvyagintsevite $(Pd,Pt,Au)_3(Sn,Pb)$.

The second broad group of natural Au compounds comprises its solid solutions with Ag (1.71-62.73 wt. %). This is mainly low-Cu (0.58-3.13 wt. %) native gold of moderate and high fineness (Table 15). The Au-Ag solid solutions richer in Ag also occur in heterogeneous grains (Fig. 10, II).

Table 15.

Composition of Au-Ag alloys, Konder alkaline-ultrabasic massif (wt. %).

No.	Au	Ag	Cu	Total
1	98.31	1.09	0.46	99.86
2	97.86	1.71	0.71	100.28
3	94.82	2.84	1.92	99.58
4	89.68	7.11	3.02	99.81
5	88.89	8.70	2.09	99.68
6	86.23	14.08	-	100.31
7	84.79	12.31	2.01	99.11
8	81.48	17.14	1.56	100.18
9	75.70	23.46	-	99.16
10	69.71	29.83	0.11	99.65
11	69.97	30.29	0.12	100.38
12	59.30	41.13	-	100.43
13	50.35	47.96	-	98.31
14	45.78	53.21	-	98.99
15	39.07	61.37	-	100.44

Note: A portion of the 39 compositions available [19] is given.

In the third broad group are the three-component compositions containing 3-5 wt. % Cu and 5-9 wt. % Ag. Where the concentration of these elements in gold is still higher, then the three-component alloy becomes unstable below 370-410^{o}C [15] and breaks down into Au-Cu-(Ag) and Au-Ag-(Cu) phases. The proportions of phases in representative exsolution- induced intergrowths and the distribution of data points in the Ag-Cu-Au diagram show that the initial composition of the Au-Ag-Cu alloy that underwent exsolution during post-crystallization cooling was (at. %): from SI-55 to 72-75 Au, from 5-8 to 20-22 Ag, and from 12-14 to 32-35 Cu.

In addition to the close intergrowths of Cu- and Ag-bearing gold in heterogeneous grains and the gold dusting on platinum grains, gold of high fineness occurs as a film coating platinum nuggets in the Konder placers [19, 45]. Individual grains of gold with a high fineness (up to 990) at the margin and a lower fineness (750-820) in the core are sporadically found. The gold of high fineness was likely formed within the placer as a result of different solubility of Ag and Au in groundwater [20]. Gold grains with a high fineness in the core and low fineness at the margin are probably related to felsic rocks in the outer zones of the Konder massif.

CONCLUSIONS

A review of the PGM and gold encountered in the Konder alkaline-ultrabasic massif reveals an extremely diverse assemblage of accessory minerals related to the massif. This mineralization resembles the dispersed impregnations, predominantly of isoferroplatinum, in moderately chromium-enriched gabbro-pyroxenite-dunite intrusive bodies of the Urals and Alaska. At the same time, it resembles the manifestations of chalcogenides of PGE connected with the complex copper-nickel deposits in the layered intrusive bodies of basic rocks. Such a peculiarity of the Konder precious-metal mineralization is caused by the existence of several stages of PGM formation at Konder, at magmatic and postmagmatic temperatures. For example, at the highest-temperature stage, mineralization occurred in low-chromite dunite of the core zone of the Konder intrusive complex; the crystallization of accessory isoferroplatinum enriched in minor PGE and of more unusual alloys in the system Ir-Os-Ru-Pt took place. Later, high-purity isoferroplatinum filled the interstices in lenses of massive chromite, chromite veins in dunites, and in dikes of magnetite clinopyroxenite. Formation of the more restricted but compositionally more widely variable chalcogenides of PGE occurred at the postmagmatic stage, with the participation of a residual fluid phase containing, along with platinum and palladium, Pb, Sn, Cu, Au, Ag, S, As, Bi, Sb, Te, and Ge. As a result of interaction of isoferroplatinum of the first stage of crystallization along its margin and along fractures with such a fluid phase, the PGE chalcogenides, tetraferroplatinum, tulameenite, hongshiite, as well as copper-bearing, platinum-copper-bearing, palladium-copper-bearing gold, and high-grade (fineness: more then 750) gold-silver solid solutions formed at the same time. The process of PGM formation at Konder ended with oxide and hydroxide compounds of supergene origin, mostly. Middle- and low-grade gold-silver solid solutions, found in placers, formed later than their high-grade analogues, and are related genetically with monzonite, which intruded the Konder ultrabasic suite.

ACKNOWLEDGEMENTS

Drs. Louis J Cabri and Thierry Auge provided constructive criticism and many incisive comments, including language corrections; their help is greatly appreciated. Robert F Martin provided helpful comments, editorial serenity, support and encouragement. The authors are grateful to Galina G. Zubkova and Valentina A. Piskunova for help in computer processing of the manuscript and translation. We are also grateful to Sergey A. Shcheka for his critical review of the paper, and help in its revision.

REFERENCES

1. **Andreev G.V.** (1987): The Konder Massif of Ultramafic and Alkaline Rocks. Nauka, Novosibirsk, Russia (in Russ.).
2. **Bogomolov M.A.** (1964): Nature of crystalline schists and carbonate rocks near the Konder massif. In Petrography of Metamorphic and Igneous Rocks of Aldan Shield, Nauka, Moscow, Russia (32-56; in Russ.).
3. **Cabri l.J., Naldrett A.J.** (1984): Pattern of distribution and concentration of platinum-group elements in different geological settings. 27th Int. Geol. Congress, Mineralogy Reports 10. Nauka, Moscow, Russia (10-26; in Russ.).
4. **Dmitrenko, G.G., Mochalov, A.G., Palandzhyan, S.A. & Goryacheva, E.M.** (1985): Chemical Compositions of Rock-Forming and Accessory Minerals of Alpine-Type Ultramafic Rocks of Koryak Plateau. 2. Minerals of Platinum Elements. USSR Acad. Sci., Far East Centre, North-Eastern Compound Research Inst., Magadan, Russia (in Russ.).
5. **El'ynov A.A. & Moralev V.M**. (1972): Massifs of ultramafic and alkaline rocks: depth of formation and erosion level. Geologia Rudnykh Mestorozhdenii 5, 32-40 (in Russ.).
6. **Emel'yanenko E.P., Maslovsky A.N., Zalishchak B.L., Kamaeva L.V. & Fomenko A.S.** (1989): Regularities of the location of ore mineralization at the Konder alkaline-ultrabasic massif. In Geological Conditions of the Localization of Endogenetic Ore Formation. Far Eastern Branch, Academy of Sciences, Vladivostok, Russia (100-113; in Russ.).
7. **Evstigneeva T.L., Kudryavcev A.C. & Rudashevsky N.S.** (1992): Platinum-group element minerals of Yubdo (Ethiopia): new data. Mineral. Zh. 14, 29-41 (in Russ.).
8. **Laputina I.P**. (1980): Microprobe analysis of the platinum group minerals. In Electron-Probe Microanalysis in Mineralogy. Int. Mineral. Assoc., Proc. XI Gen. Meeting. Nauka, Leningrad, Russia (42-52; in Russ.).
9. **Lennikov A.M., Oktyabrsky R.A., Sapin V.I., Taskaev V.I., Kiselev V.I. Demchenko V.S**. (1991): New data on rocks in metamorphic framework of the Konder massif. Dokl. Akad. Nauk SSSR 319, 1187-1191 (in Russ.).
10. **MArakushev A.A., Emel'yanenko E.P., Nekrasov I.YA., Zalishchak B.L. & Maslovsky, A.N.** (1990): Formation of concentrically zoned structure of the Konder alkaline-ultramafic massif. Dokl. Akad. Nauk SSSR 311, 167-170 (in Russ.).
11. **Mochalov A.G.** (1986): Mineralogy of Platinum Elements of Alpine-Type Ultramafic Rocks. Dissertation, Department of Geological and Mineralogical Sciences, Leningrad State Univ., Leningrad, Russia (in Russ.).
12. **Mochalov A.G.** (1994): Mineralogy of platinum-group elements from dunites. In Geology, Petrology, and Ore Presence in the Konder Massif. Nauka, Moscow, Russia (92-106; in Russ.).
13. **Mochalov A.G., Zhernovsky I.V. & Dmitrenko G.G**. (1988): Composition and spreading of platinum and ferrum native minerals in ultramafics. Geol. Rudnykh Mestorozh. 5, 47-58 (in Russ.).
14. **Murzin V.V., Kudryavtsev V.I., Berzon R.O. & Sustavov S.G.** (1987): The Cu-bearing ore in rodingite zones. Geol. Rudnykh Mestorozh. 5, 96-99 (in Russ.).
15. **Nekrasov I.Ya.** (1991): Geochemistry, Mineralogy, and Genesis of Gold Deposits. Nauka, Moscow, Russia (in Russ.).
16. **Nekrasov I.Ya., Ivanov V.V., Lennikov A.M., Oktyabrsky R.A., Sapin V.I. & Taskaev V.I**. (1993): About specificity of solid solutions of system Os–Ir–Ru–Pt in

alkaline-ultrabasic massifs. Doklady Akademii Nauk SSSR. 328, 382-385 (in Russ.).

17. **Nekrasov I.Ya., Ivanov V.V., Lennikov A.M., Oktyabrsky R.A., Sapin V.I. & Taskaev V.I., Zalishchak B.L. & Khitrov V.V.** (1991a): New data on PGE mineralization of alkaline-ultrabasic concentrically zoned massifs of the Far East. Dokl. Akad. Nauk SSSR 320, 705-709 (in Russ.).
18. **Nekrasov I.Ya., Ivanov V.V., Lennikov A.M., Oktyabrsky R.A.,, Zalishchak B.L., Sapin V.I. & Taskaev V.I**. (1991b): Composition of Pt–Fe solid solutions as indicator of erosional level of platinum-bearing alkaline-ultrabasic ring intrusives. Dokl. Akad. Nauk SSSR 321, 1049-1053 (in Russ.).
19. **Nekrasov I.Ya., Ivanov V.V., Lennikov A.M., Sapin V.I., Safronov P.P. & Oktyabrsky R.A.** (2001c): Rare natural polycomponent alloys based on gold and copper from a platinum placer in the Konder alkaline-ultrabasic massif, southeastern Aldan Shield, Russia. Geol. Rudnykh Mestorozh. 5, 406-417 (in Russ.).
20. **Nekrasov I.Ya., Lennikov A.M., Oktyabrsky R.A., Zalishchak, B.L. & Sapin V.I**. (1994): Petrology and Platinum Mineralization of the Alkaline-Ultrabasic Ring Complexes. Nauka, Moscow, Russia (in Russ.).
21. **Novgorodova M.I.** (1983): Native Metals in Hydrothermal Ores. Nauka, Moscow, Russia (in Russ.).
22. **Novgorodova M.I.** (1994): Crystal chemistry of native intermetallic compounds. In Achievements of Science and Engineering, Seria Crystal Chemistry 29 (in Russ.).
23. **Orlova M.P.** (1991): Geological structure and genesis of the Konder ultramafic massif. Tikhookeanskaya geologia 10(1), 80-88 (in Russ.).
24. **Rudashevsky N.S.** (1989): Evolution of chemical composition of osmium, ruthenium, and iridium hexagonal solid solutions in different formation of ultramafites. Geologia i Geofizika 10, 68-74 (in Russ.).
25. **Rudashevsky N.S., Burakov B.E., Malich K.N. & Khaetsky V.V.** (1992): Accessory platinum mineralization of chomitites from Konder alkaline-ultrabasic massif. Mineral. Zh. 14(15), 12-32 (in Russ.).
26. **Rudashevsky N.S. & Mochalov A.G**. (1985): Composition of cromespinels inclusions into PGM grains from rocks of ultramafic formations. Geologia i Geofizika 8, 56-69 (in Russ.).
27. **Rudashevsky N.S. & Mochalov A.G. Begizov V.D., Men'shikov Yu.P. & Shumskaya N.I**. (1984b): Inaglyite $Cu_3Pb(Ir,Pt)_8S_{16}$ – a new mineral. Zap. Vses. Mineral. Obshchest. 113, 712-717 (in Russ.).
28. **Rudashevsky N.S. & Mochalov A.G., Trubkin N.V., Gorshkov A.M., Men'shikov YU.P. & Shumskaya N.I.** (1984a): Konderite $Cu_3Pb(Rh,Pt,Ir)_8S_{16}$ – a new mineral. Zap. Vses. Mineral. Obshchest. 113, 703-711 (in Russ.).
29. **Rudashevsky N.S., Men'shikov Yu.P., Mochalov A.G., Trubkin N.V., Shumskaya N.I. & Zhdanov V.V**. (1985): Cuprorhodsite $CuRh_2S_4$ and cuproiridsite $CuIr_2S_4$ – new natural thiospinels of platinum elements. Zap. Vses. Mineral. Obshchest. 114, 187-195 (in Russ.).
30. RUDASHEVSKY N.S., MEN'SHIKOV YU.P., MOCHALOV A.G., TRUBKIN N.V., SHUMSKAYA N.I., **Mochalov A.G. & Orlova M.P**. (1982): Inclusions of silicate in natural iron-platinum alloys of the Konder massif. *Dokl, Akad. Nauk SSSR* 266. 977-981 *(in Russ.)*
31. **Sazonov A.M., Romanovsky A.E., Grinev O.M., Lavrent'ev Yu.G., Mayorova O.N. & Pospelova L.N.** (1994): The noble-metal mineralization of the Guli intrusion, Siberian Platform. Geologia i Geofizica 9, 51-65 (in Russ.).

32. **Shcheka S.A., Vrzhosek A.A., Sapin V.I. & kiryukhina, N.I.** (1991): Transformations of platinum group minerals from placers of Primorye. Mineral. Zh. 13(13), 34-40 (in Russ.).
33. **Shnai G.K. & Kuranova V.N.** (1981): New evidence for age of dunite in composite massifs of ultramafic-alkaline composition. Dokl. Akad. Nauk SSSR 261, 950-952 (in Russ.).
34. **Sushkin L.B.** (1995): Characteristic features of native elements of the Konder deposit. Tikhookeanskaya Geologia 14(5), 97-102 (in Russ.).
35. **Zhernovsky I.V., Mochalov A.G., Rudashevsky N.S.** (1985): Phase heterogeneity of isoferroplatinum rich in iron. Dokl. Akad. Nauk SSSR 283, 196-200 (in Russ.).
36. **Augé T. & Legendre O.** (1992): Pt–Fe nuggets from alluvial deposits in eastern Madagascar. Can. Mineral. 30, 983-1004.
37. **Cabri L.J., Criddle A.J., Laflamme J.H.G., Bearne G.S. & Harris D.C.** (1981): Mineralogical study of complex Pt–Fe nuggets from Ethiopia. Bull. Minéral. 104, 508-525.
38. **Cabri L.J. & Laflamme J.H.G.** (1997): Platinum-group minerals from the Konder massif, Russian Far East. Mineral. Rec. 28, 97-106.
39. **Fleischer M. & Mandarino J.A**. (1995): Glossary of Mineral Species (seventh ed.). The Mineralogical Record, Tucson, Arizona.
40. **Harris D.C. & Cabri L.J.** (1991): Nomenclature of platinum-group element alloys: review and revision. Can. Mineral. 29, 231-237.
41. **Makovicky E., Karup-Møller S., Makovicky M. & Rosehansen J**. (1990): Experimental studies on the phase systems Fe–Ni–Pd–S and Fe–Pt–Pd–As–S applied to PGE deposits. Mineral. Petrol. 42, 307-319.
42. **Oktyabrsky R.A., Shcheka S.A., Lennikov A.M. & Afanas'yeva T.V.** (1992): The first occurrence of qandilite in Russia. Mineral. Mag. 56, 385-389.
43. **Pushkarev Yu.D., Kostoynov A.I., Orlova M.P., Bogomolov E.S. & Guseva V.F**. (2001): Sm–Nd, Rb– Sr, K–Ar and Re–Os isotopic constraints on the origin of PGE mineralization in the Konder massif, Khabarovsk region, Russia. In Mineral Deposits at the Beginning of the 21st Century. Swets and Zeitlinger Publ., Lisse, The Netherlands (677-680).
44. **Razin L.V.** (1976): Geologic and genetic features of forsterite dunites and their platinum-group mineralization. Econ. Geol. 71, 1371-1376.
45. **Shcheka G.G., Lehmann B., Gierth E., Gömann K. & Wallianos A.** (2004): Macrocrystals of Pt–Fe alloy from the Kondyor PGE placer deposit, Khabarovskiy Kray, Russia: trace-element content, mineral inclusions and reaction assemblages. Can. Mineral. 42, 601-617.

UDK 550.42

Alkaline and ultramafic lamprophyres in Italy: Distribution, mineral phases, and bulk rock data

Stoppa F.

Dipartimento di Scienze della Terra, Università G.d'Annunzio, Chieti, Italy

ABSTRACT

Several lamprophyre outcrops occur in Italy paralleling the European cycles. Lamprophyre occurrences from the lower Cretaceous to the Oligocene are comprised primarily of dykes and rarely lavas, generally emplaced in isolation. They are ultramafic or alkaline lamprophyres located in eight different places ranging from the eastern Alps to the areas of Tuscany, Sardinia, Abruzzi, and Puglia and exhibit similar geochemistry, suggesting that they originated from the same mantle source, despite different tectonic conditions. Lamprophyres relate to partial melting of a mantle source rich in large-ion lithophile-elements (LILEs) and C-O-H. Distribution of high-field-strength elements (HFSEs) and their ratio to LILEs depends upon the presence of specific scavenger phases, which makes the geochemistry of these and similar rocks very different with respect to that of basalts. Italian Lamprophyres preserve different specific isotopic features that can be described in term of mixing of two mantle end-members, one of which is highly radiogenic. Lamprophyre magma emplacement should occur during structural extension after major compression episodes. However, this tectonic model seems much too simple for the Italian lamprophyres and is inconsistent with the Mediterranean Tethys geodynamic evolution. On the other hand, Italian lamprophyres evolved into lamproites after the Lower Oligocene era and finally into leucitites and kamafugites (plus carbonatites), ultrapotassic rocks which could be considered anhydrous, petrologic equivalents of lamprophyres. Certainly this requires very specific source conditions, possible related to a mature stage of mantle metasomatisms triggered by repeated episodes of (alkaline) carbonatite invasion, melt extraction, and upper mantle decompression. Italian lamprophyres demonstrate, with their long-term constant geochemistry and isotopic features, that the metasomatic agent is unrelated in time and space to the relatively shorter subduction phases of the Mediterranean Sea area and better fits with the presence of a large, long-lived, pulsing deep plume.

INTRODUCTION

Lamprophyres are related to ultrabasic magmas rapidly emplaced at the crustal level during regional stages of crustal relaxation. Among lamprophyres' peculiarities are their cyclic emplacement and their genetic affinity with diamond-bearing lamproites and kimberlites. Only deep-mantle contribution accompanied by repetition of cutting of the entire lithosphere system can explain the existence of these melts which cut across different structural domains. Several lamprophyre occurrences have been recognised in Italy, but they may have been misclassified

and little is known about their composition and general distribution, as they are part of larger lamprophyre repetitions occurring around the Mediterranean Sea. Notably, similar repetitions were observed in Africa [4] where four different magmatic cycles well fit with those of the Mediterranean Sea area. The first one is the Lower Cretaceous cycle (130-120 My); the second is the Upper Cretaceous cycle (85 My); the third one is the Upper Eocene-Oligocene cycle (40 My); and the last one is the Miocene to Recent (<20 My). In Italy, alkaline (potassic) lamprophyres dominated the Cretaceous-lower Eocene cycles and occur in largely

Fig.1. **Italian lamprophyres schematic localization.**

Eastern Alps: Calceranica and Corvara in Badia, Upper Cretaceous (70–68 My); Val Fiscalina, Upper Eocene (34 My). Southern Tuscany: Castiglioncello del Trinoro, Murci, Senna River, Fosso Ripiglio, Rapolano Terme, Lower Cretaceous (109–90 My) Abruzzo Region: Monte la Queglia, Eocene (54 My); Puglia Region: Punta delle Pietre Nere, Lower Paleocene (62–58 My); Sardinia: Nuraxi Figus, Lower Paleocene (62–60 My).

distributed, en echelon dyke swarms. From the Pleistocene era, lamproites were associated with ultrapotassic mafic rocks, namely leucitites and kamafugites and carbonatites, which characterize this magmatic cycle. This evolution seems largely irrespective of geodynamic evolution of the Tethyan-Mediterranean area

and lamprophyric cycles do not correlate with main Tethyan events. Early Cretaceous to lower Oligocene lamprophyres in Italy are represented by occurrences of eleven alkaline lamprophyres (ALs) and one ultramafic lamprophyre (UML) (Fig.1). Italian lamprophyres (ILs) are nonequigranular melanocratic to ultramafic rocks and, often, carbonatitic [40]. Phenocrysts are often altered. Quench, comb, and spiniphex or fealty/branching textures are typically observed, as is widespread presence of ocellar structures (Plate 1 and 2). Mineral abundances are typical but variable (Tab.1) The ILs are classified following the International Union of Geological Sciences (IUGS) criteria [22] and the more recent classification criteria for ultramafic lamprophyres proposed by Tappe et al. [38]. ILs represent a

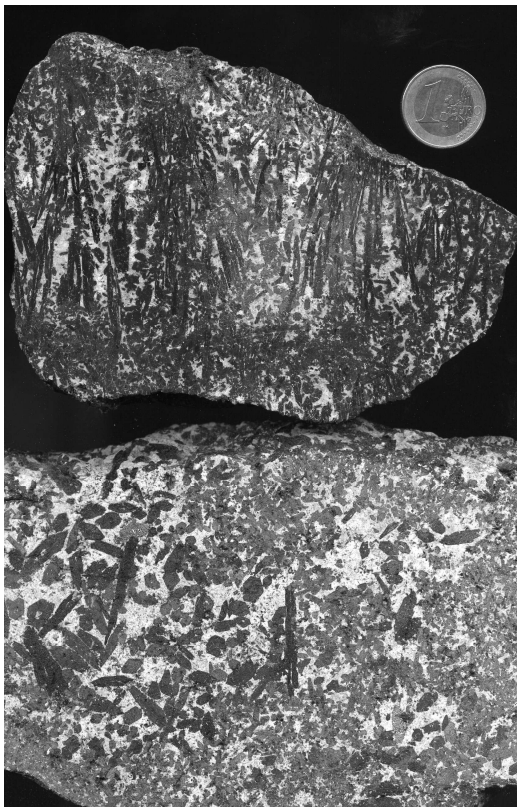

Plate 1. **Alkaline lamprophyres samples from Punta delle Pietre Nere (see text).**

Upper picture: comb texture, lower picture: central coarsening and a dyke rock. ! euro coin for scale, diameter is 22 mm.

challenging test for deep-mantle phenomena and unconventional, large-plume activity and their consequences on lithospheric tectonics. The aim of this paper is to spur the discussion of new petrological and mineralogical data addressing sensible hypotheses about Ils' geological significance.

FIELD OCCURRENCE AND LITHOLOGY

Southern Tuscany

The southern Tuscany lamprophyres are Albian in age (ca. 110 Ma) and occur in an Early Cretaceous sequence of flysch [9, 15]**.** Lamprophyre dyke swarms are composed of several en echelon occurrences ranging from a meter to a few meters in thickness and several tens of metres in length. The inner parts of the dykes are coarser-grained than at the contacts with the surrounding rocks. Notably, the lamprophyre dykes are associated with pillow-lava in three localities. Pillows form

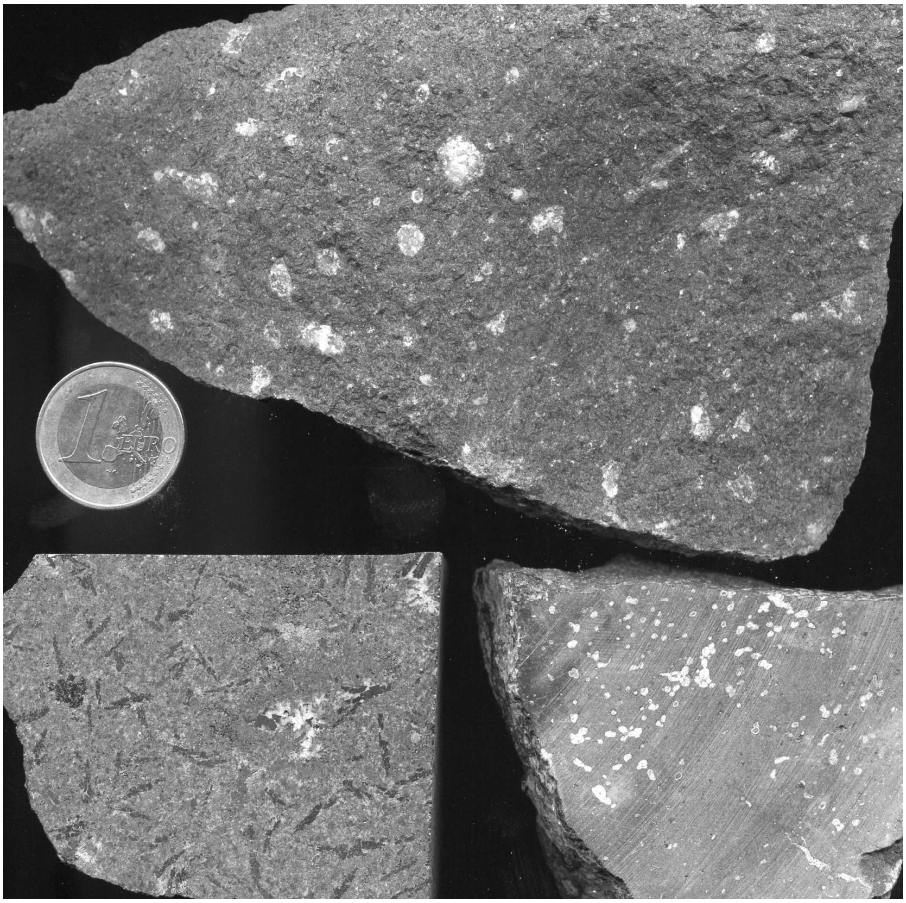

Plate 2. **Various examples of ocelli and patch structures in Italian lamprophyres.**
Upper picture : Val Fiscalina, down left: Punta delle Pietre Nere, down right: La Queglia.

lenses with a maximum thickness of about 50 metres. Rocks are fine-grained to medium-grained and show quench texture. Medium-grained facies have 16-22% (by vol.) diopside up to 12-20% (by vol.) mica plus amphibole, and 3-4% (by vol.) olivine, set up in a groundmass mainly formed by 35-47% (by vol.) alkali feldspar and 7-20% (by vol.) calcite or dolomite, with the rest comprised of analcite, sphene, carbonate, and opaques. Apatite forms up to 3 mm-long prisms. Fine-grained facies have 52-62% (by vol.) glomerocrystic Ti-diopsides, 12-18% (by

vol.) olivine, up to 12% (by vol.) titaniferous eastonite-annite plus kaersutite amphibole. Felt-like groundmass contains, in addition, up to 10% (by vol.) branching/spherulitic or poikilitic K-feldspars, albite, analcite, apatite, micas, and opaques. Opaques are Ti-spinel or trevorite. Chromite occurs as inclusions inTable 1.

Modal abundances (%vol.) of Italian lamprophyres.[1]=include melilite in Monte la Queglia

Location	Olivine[1]	Diopside	Micas	Amphibole	Alkali feldspar	Apatite	Analcite + foids[2]	Calcite	Accessory phases[3]
Senna River	3	20-22	12-16	0-4	35-47	2-3	<1	7-20	2-4
Murci	4-15	18-57	<1-20	0-12	6-36	1-2	<1	9-15	4
Fosso Ripiglio	13-18	55-62	<1-10	2-10	2	<1	<1-17	4-5	/
Castiglioncello	3-12	16-57	4-12	9-42	3	<1	<1-15	4-6	/
Corvara	11-15	32-34	13-21	/	/	3-5	15-21	3-23	1-4
Val Fiscalina	4	38-43	26-35	/	<1	2	<1	12-21	1-3
Calceranica	3-4	27-28	2-4	46-49	5-9	1-2	<1-2	5-8	3-4
Nuraxi Figus	10	41	20	12	3	2	7	5	/
Punta PietreNere	1-10	38-44	25-32	2-7	3	8-17	1-6	3-6	/
La Queglia	19-20	54-55	3-8	/	<1	2	2	10-15	4

Note: samples; [2]= include nepheline; [3]=include Ti-magnetite, chromite, rutile, ilmenite, pyrite, perovskite and chalcopyrite.

olivine. Euhedral titanite, pyrite (up to 30 μm in diameter), chalcopyrite (up to 10 μm in diameter), and ilmenite crystals and glass are also present in the groundmass. Carbonate occurs as interstitial material and forms veins and pseudomorphs after olivine and diopside, as well as ocelli and segregation patches. Taxonomy of Southern Tuscany lamprophyres is difficult because of theb abundance of mica, which may indicate a minette. However, all the other aspects of their mineralogy - kaersutite, groundmass aegirine, aegirine and augite-rimmed diopside phenocrysts, and the presence of analcite - clearly indicates that these rocks are AL; in particular, they are evidence of an affinity with sannaites [22].

Eastern Alps-Corvara

The lamprophyric rock outcroppings in Corvara in Badia (Eastern Alps) form a sill about 4 metres in thickness and 50 metres in length, intruded into Triassic marly limestones (of the Upper Ladinian era) at the base and dolomitic limestone (of the Lower-Upper Carnian era) at the top. The contacts are characterized by white to pink ocelli and, although the cross-cutting relationships with the host rocks are always sharp and regular, there are also carbonate ocelli within the first 30 cm of the wall rocks. Potassium-argon (K/Ar) dating indicated an age of 68-66 ± 2 Ma, while Rubidium-Strontium (Rb/Sr) dating indicated an age of 69.8 ± 3 Ma [23]. Fresh samples are melanocratic and fine-grained near the contact and coarse-grained in the central part of the sill. The rock has a Mafic (M) index of between 74 and 82. The average modal composition (Tab.1) is 33% (by vol.) diopside, 18.5% (by vol.) nepheline plus analcite, 18.5% (by vol.) phlogopite/biotite, 13% (by vol.) olivine, 3% (by vol.) opaques, and 4% (by vol.) apatite; modal carbonate is up to 23% (by vol.). Percentages of mica and apatite increase towards the centre

of the sill, up to 21% and 5%, respectively. Chromite inclusions are present in the olivine. The groundmass is comprised of diopside/aegirine, Ti-rich phlogopite/biotite, Ti-spinel, apatite, carbonate, and analcite, plus small crystals (up to 10 μm in diameter) of pyrite, chalcopyrite, and brookite-rutile. Analcite is formed in a late-stage phase and is occasionally associated with quartz in the groundmass and co-precipitated with Sr-bearing calcite in the ocelli. Scanning electron microscope (SEM) analyses attest to the presence of perovskite crystals (<10 μm in diameter) included in the diopside. Spherical and coalescent ocelli with carbonate and/or analcite are widespread but increase towards the dyke contact with the surrounding rocks. Due to the absence of feldspars, the rock was correctly classified as a monchiquite [23].

Eastern Alps-Calceranica

A dyke swarm described by Galassi et al. [16] occurs around the Caldonazzo Lake near Calceranica. A discrete, large dyke intrudes into the Palaeozoic phyllitic basement at the location of Maso Pradi. Maximum thickness of the dyke is approximately 3.5 metres, with a length of approximately 10 metres. The visible contact with the hosting rocks is sharp. The central section of the dyke has white to pink ocelli near the contact with the hosting rock. Argon-39/Argon-40Ar dating indicated an age of 71 ± 2 Ma. The rock has an M index ranging from 87 to 95. The average modal composition (Tab.1) is 48% (by vol.) amphibole (and subordinate mica), 27% (by vol.) euhedral diopside, 6% (by vol.) feldspars (plagioclase, K-feldspars), 6.5% (by vol.) carbonates, 3.5% (by vol.) opaques, 3 % (by vol.) euhedral olivine crystals (up to 0.5 cm), and apatite 1% (by vol.). Diopsides have a cribrous, colourless core and a well-defined darker, pleocroic and zoned rim. Euhedral amphiboles—kaersutites, Fe-pargasites, pargasites, and Mg-hastingsite—subordinate diopsides, and rare Ti-biotites from the groundmass. Ti-magnetite is abundant in the groundmass, as well as in inclusions of phenocryst and microphenocryst rims; apatite is rare. Intergranular spaces are filled by co-precipitated K-feldspars, carbonates, and nepheline. Pyrite and calcopyrite form crystals up to 10 μm in diameter. Coarse-grained samples contain carbonate ocelli and segregation patches filled by diopsides and amphiboles set up in a matrix made of K-feldspars and carbonates. Globular structures, filled by carbonates, are widespread in fine-grained samples.

Sardinia

A sill approximately 2 metres thick has been drilled by four boreholes in the Sulcis coalfield, near Nuraxi Figus in southwestern Sardinia. The sill lies into an Upper Paleocene limestone sequence and it is slightly dipping (about four degrees) toward the south-southeast (24). Carbonate ocelli form discontinuous trails a few centimetres thick that irregularly pervade the sill at various levels. K/Ar radiometric dating [24] indicated an average age of approximately 61.1 ± 3.1 Ma. The Mafic index of the sill's composition is 83. The modal composition (Tab.1) is 41% (by vol.) Ti-diopside with a cribrous, colorless core and darker pleocroic and

zoned rim, 20% (by vol.) pargasite plus Ti-Ba phlogopite and biotite, 12% (by vol.) feldspars (plagioclase, K-feldspars), 10% (by vol.) olivine altered to chlorite and carbonate, 5% (by vol.) opaques, 3% (by vol.) apatite, 7% (by vol.) carbonates, and 2% (by vol.) analcite. Groundmass is made up of phlogopite and biotite, pargasite, Fe-pargasite, and Mg-hastingsite, rarely supplemented by aegirine-augite, apatite, and Ti-magnetite, set in an intergranular matrix of co-precipitating K-feldspar and plagioclase, analcite, and carbonate, together with small crystals (<20 μm in diameter) of pyrite and members of the barite-celestina solid solution. Feldspars often show pecilitic texture. Carbonate ocelli rim is usually formed by small crystals of green aegirine-augite, sometimes growing towards the center. Rarely, the ocelli are filled by K-feldspar and analcite, co-precipitated with carbonate. The rock has been correctly classified as camptonite [24] having plagioclase/K-feldspars >1 [22], even if feldspathoids/feldspars <1.

Puglia Region

The Punta delle Pietre Nere occurrence, near Marina di Lésina, has been described in several papers [1, 10, 12]. This occurrence probably refers to a large intrusion along a strike-slip fault system of regional significance. Among Italian lamprophyres, this one is the most complex and there is some evidence of magma evolution and eruption. However, the exposure is very poor and was recently spoiled by construction of a harbour. A dyke, approximately 4 metres in thickness and discontinuously traceable for approximately 500 metres, intrudes a sequence of Triassic, dark marly-limestone, gypsum, and anhydride. K/Ar dating indicates the igneous rocks are 58-62 My in age [8]. The dyke rock is fresh, melanocratic with an M index of 83 to 89. Grain size increases progressively towards the central part of the dyke, where phenocrystals of mica and amphibole are up to several centimetres in length (Plate 1). The modal composition (Tab. 1) is: 40% (by vol.) glomerules of Ti-diopsides, 30% (by vol.) Ti-micas with a phlogopitic core and biotitic rim plus Mg-hastingsite, 10% (by vol.) sodalite, 6% (by vol.) olivine, 5% (by vol.) opaques, 3% (by vol.) apatite up to several millimeters in diameter, 4% (by vol.) carbonates, and 2% (by vol.) K-feldspar. Small crystals of chromite are present as inclusions in olivine and diopside. Diopside and aegirine-augite, sphene, Ti-magnetite, ilmenite, apatite, carbonate, K-feldspar and sodalite, locally altered in analcite, form the groundmass. Calcite co-precipitating with K-feldspars and sodalite fill the intergranular spaces. Pyrite and calcopyrite are abundant in the groundmass and form crystals up to 1 cm. Locally is present a mesocratic to melanocratic facies (with an M index up to 73) with phenocrysts of diospide, micas, and amphiboles up to 3 cm set in a groundmass formed by sodalite, calcite, and K-feldspars. This facies forms small stokes along the main dyke or comb-textured dykelettes or cemented, dyke-rock breccia. The average modal composition is 43% (by vol.) clinopyroxene, 25% (by vol.) amphiboles and micas, 17% (by vol.) sodalite, 8% (by vol.) carbonates plus K-feldspar, 3% (by vol.) spinels up to 0.5mm in diameter, and 3% (by vol.) apatite up to 4mm in diameter.

Altered relicts of olivine are present as inclusions in mica and amphiboles. The diopside contains inclusions of Mg-hastingsite and mica. Kaersutite or Fe-pargasitic amphibole forms aureole structures around the diospide and are mantled, in turn, by aegirine-augite. The surrounding groundmass is composed of mica and aegirinic clinopyroxene, abundant apatite, titanite, and opaques immersed in a matrix comprised of sodalite, often altered to analcite, carbonates, and feldspar.

The foids/K-feldspar ratio >1 indicates that these rocks as monchiquites; however, it is quite difficult to assign them within the classification scheme proposed by Le Maitre [22]. Even if the K-feldpsars/plagioclase ratio >1 suggests affinity with sannaite, these lamprophyres are characterised by a high modal abundance of foids (mainly sodalite), in which case they should be classified as a camptonite/monchiquite series.

Abruzzo

The Monte la Queglia lamprophyre forms an en echelon system with dikes from 1.5 to 6.5 metres in thickness. It intrudes into the Upper Cretaceous-Eocene limestone. Contacts with the surrounding rocks are sharp and there is no evidence of thermal metamorphism. The igneous rock is brecciated and is pervaded by veins of calcite. Ocellar structures, up to 0.5 cm across, are widespread. Argon-39/Argon-40 dating of separated mica indicated an age of 54 My. (Laurenzi M., personal communication). The lamprophyre is ultramafic, presenting an M index ranging from 95 to 97. The average modal composition (Tab.1) is 58% (by vol.) Ti- and Cr-rich diopside, 20% (by vol.) olivine and melilite altered into chlorite and carbonates, 4% (by vol.) micas, 2% (by vol.) K-feldspars, 4% (by vol.) opaques with perovskite and garnet, 2% (by vol.) apatite up to 6mm in length, 11% (by vol.) carbonate, and 2% (by vol.) analcite/nepheline. Chromite inclusions occur in olivine and Cr-rich diopside. Microphenocrysts are titaniferous pyroxene, ranging in composition from those with diopsidic cores to aegirine rims, titaniferous mica with eastonitic cores and tetraferriannitic rims, and altered melilite plus fresh apatite. Perovskite is a frequent inclusion in melilite and pyroxene. Aegirine, Ti-rich phlogopite with biotitic rims, apatite, spherulitic K-feldspar, carbonates, zeolites, a minor amount of nepheline, Ti-magnetite, and altered glass form the groundmass. Pyrite, chalcopyrite, and brookite-rutile also occur as small crystals (up to 10 μm in diameter) in the groundmass. Carbonate forms segregation patches in the groundmass where branching diopsides are well developed. The rock is an ålnöite [14, 38]. UML with melilite could be also named melnoite, or rocks making transition to carbonatites, according to Mitchell [25].

Eastern Alps -Val Fiscalina

This is a brecciated dyke intruded along vertical joints in the Triassic era limestone. Glacial deposits and debris hide in situ exposure and contain several fresh lamprophyre blocks. Dating by Rb/Sr yielded an age of 34 My [23]. The rock has an M index of 97, is ultramafic, medium- to fine-grained, and nonequigranular,

sometimes with a fluidal texture formed by lineation of clinopyroxene laths. The average modal composition (Tab. 1) consist of 40.5% (by vol.) diopside, 30.5% (by vol.) eastonitic mica, 17% (by vol.) carbonates, 6% (by vol.) fresh olivine (Fo90-85) with chromite inclusions, 3% (by vol.) opaques, and 1% (by vol.) K-feldspar. Apatite and Ti-magnetite are abundant as inclusions in micas and in the intergranular spaces where pyrite (up to 100μm in diameter) and brookite-rutile (up to 10 μm in diameter) are also present.

MINERAL CHEMISTRY

We conventionally distinguish among phenocrysts (>0.5 mm in diameter, euhedral), microphenocrysts (>0.05mm in diameter, subhedral), and groundmass minerals (<0.05mm in diameter, euhedral to anhedral). Essential minerals in ILs are diopside, amphibole, mica, and olivine phenocrysts from a few millimetres to several centimetres long, settled in a fine-grained matrix of the same minerals, plus feldspar and/or foids, calcite and/or dolomite, plus accessory apatite, sphene, perovskite, and Ti-spinels. More rare is the occurence of pyrite and calcopyrite (< 50 μm in diameter), zircon (10 μm in diameter), zeolites, barite-celestine in solid solution phase, and rutile in acicular crystal up to 20 μm in diameter. Melilite and schorlomite garnet occurrence is limited to UMLs of the La Queglia. Minerals in ILs show notable complexity due to intense zoning, coronas, and occurrences in several generations and specific compositions. These complexities have been interpreted as derived from the mixing of crystal-rich magma batches of similar composition but that have suffered different degrees of crystal fractionation [27]. Alternatively, these abrupt changes in composition during emplacement could be due to volatile exolution and separation of immiscible carbonate fractions at crustal pressure [40]. ILs' quenched nature may indicate non-equilibrium or a "patch" composition produced by rapid crystallisation and only those with an average composition have been considered as representative. Mineral analyses were performed by a CAMECA SX50 electron microprobe, operated at 20 kV, 20 nA, and spot size of 1μm for silicates, and 15kV, 15nA, and spot size of 20μm for silicates, using a selection of mineral and synthetic standards and a PAP matrix correction routine at EMMA labs of The Natural History Museum, London. Representative analyses of minerals are in Tables 2 through 14. Space limitations preclude the mineral recalculations, providing instead a greater number of analyses.

Olivine

Fresh olivine crystals have been analysed from Calceranica, Punta delle Pietre Nere, Nuraxi Figus, and Val Fiscalina samples, but these are often relicted or replaced by cholorite, serpentine, and carbonate. These chrystals contain ubiquitous chromite inclusions. Phenocryst margins are often corroded and show engulfment bays indicating disequilibrium and reaction with the hosting melt. Olivine exhibits a relatively narrow range in Mg/Fe ratios (83-90 with average

Fo86) and is chrysolite. CaO is 0.23% (by wt.) on average, up to 0.49% (by wt.). MnO is approximately 0.2% (by wt.). Cr_2O_3 is present up to 0.1% (by wt.) and NiO is present up to 0.47% (by wt.). Higher Ni and Cr olivines plot inside the field

Table 2.

Selected analyses of olivine from Italian Lamprophyres.

	Calceranica				**N.F**	**Pietre nere**						**Val Fiscalina**			
SiO_2	39.5	39.4	39.4	39.3	40.2	39.0	40.0	39.8	39.3	37.7	38.1	40.0	40.1	40.8	40.9
Al_2O_3	0.06	0.06	0.07	0.04	0.05	0.04	bdl	bdl	bdl	0.06	0.07	0.03	0.05	0.07	bdl
FeO	14.2	14.2	15.4	15.9	13.2	12.0	11.2	12.0	11.7	13.4	14.9	12.2	12.5	10.3	9.17
MnO	0.18	0.19	0.24	0.28	0.18	0.17	0.15	0.12	0.18	0.22	0.21	0.17	0.13	0.13	0.13
MgO	44.9	44.6	44.3	43.7	46.1	47.9	48.0	47.3	47.4	47.1	45.6	46.5	46.7	49.0	48.8
CaO	0.27	0.29	0.32	0.39	0.19	0.25	0.23	0.26	0.25	0.28	0.49	0.10	0.15	0.11	0.10
NiO	0.33	0.31	0.38	0.26	0.33	0.32	0.29	0.29	0.30	0.28	0.20	0.47	0.37	0.26	0.39
Cr_2O_3	bdl	bdl	0.05	bdl	bdl	bdl	0.05	0.05	bdl	bdl	bdl	bdl	0.09	bdl	0.05
Total	99.4	99.1	100.1	99.9	100.3	99.7	99.9	99.8	99.1	99.1	99.6	99.4	100.2	100.7	99.5

Note: Mg#= $Mg/(Mg+Fe^{2+})$; Ca#=$Ca^{2+}/(Mg+Ca^{2+})$; bdl=below detection limit

of olivine in mantle nodules [35]. Olivines with a higher CaO content than normal olivines from the mantle are known from carbonatitic lavas at Fort Portal and Polino [37], from olivine-biotite-pyroxenite xenoliths at Oldoinyo Lengai and Loluni, in garnet and spinel peridotites from Lashaine, as well as from Ruri Volcano in Kenya. The inverse correlation of Mg# and CaO is interpreted as the result of a reaction of the xenocrystic olivines with the host carbonate-rich liquid or carbonatite metasomatisms in the mantle [21].

Pyroxene

Clinopyroxenes usually are euhedral and zoned. Phenocrysts (up to >1 cm in diameter) have sharp, cribrous, colourless cores containing small crystals of chromite. The rims are pleocroic with light brown-pink-green brown color schemes and generally contain Ti-magnetite inclusions. Microphenocrysts cluster in glomerules of euhedral laths. Groundmass clinopyroxenes are strongly pleocroic and without inclusions. According to the Wo-En-Fs diagram [28], they range from diospide to aegirine-augite to aegirine. Clinopyroxenes have Si+Al in T <2 atoms per formula unit (afu), thus allowing Ti and/or Fe2+ entering it up to 0.15 afu, the larger T-undersaturation occurs in diopside. Phenocrysts and microphenocrysts are diopsides. Diopsidic cores contain Cr_2O_3 up to 1.4% (by wt.). Core-to-rim compositional variation occurs in individual phenocrysts and microphenocrysts and comprises an increase in Al_2O_3 (from 0.6% by wt. to 11.95% by wt.), in TiO_2 (up to 7.8% by wt.) and FeO (from 3.3% by wt. to 12.5% by wt.) and decrease in SiO2 (from 55.9% by wt. to 35.8% by wt.), as well as in MgO (from 17.4% by wt. to 8.7% by wt.). Mg# ranges from 0.75% to 1.0% (by wt.), with the higher values belonging to the cores. Diopsides from groundmass have much lower percentages (by weight) of Mg# (from 0.46 to 0.69) and higher percentages (by weight) of Ca# (from 0.60 to 0.67). These clinopyroxenes have a generally higher TiO_2/Al_2O_3 ratio if compared with the diopside pheno-micro crystals. Some of the

high Mg# and high Cr_2O_3 diopsides could be from mantle or HP xenocrysts [13]. Lamprophyric melt seems able to crystallise in very high Al_2O_3-CaO diopsides with high fassaite or esseneite molar solution [12], coupled with high TiO_2. Some microphenocryst
rims and groundmass clinopyroxenes are aegirine-augite, having up to a 94.4 Ae

Table 3.

REPRESENTATIVE ANALYSES OF CPX FROM ITALIAN LAMPROPHYRES

cpx	*Nuraxi Figus*				*Punta delle Pietre Nere*										
SiO_2	48.7	53.5	52.7	51.6	47.4	46.1	51.4	55.9	46.1	46.9	49.4	49.2	48.0	47.9	47.7
TiO_2	1.29	0.11	0.26	1.52	1.90	2.56	1.14	0.14	2.16	3.29	0.72	0.66	0.46	1.20	1.28
Al_2O_3	6.56	0.11	0.39	0.21	4.93	7.04	2.78	0.63	6.01	5.25	2.17	2.05	1.70	2.67	2.98
FeO	6.84	7.31	9.69	20.5	9.42	10.1	4.69	5.00	6.22	8.01	21.7	21.0	18.5	21.8	19.7
Cr_2O_3	0.18	0.00	0.00	0.00	0.00	0.00	0.65	0.00	1.39	0.00	0.00	0.00	0.00	0.00	0.00
MnO	0.16	0.21	0.23	0.25	0.20	0.21	0.11	0.15	0.05	0.12	0.42	0.46	0.66	0.59	0.51
MgO	13.7	14.8	12.9	5.70	11.8	10.5	15.7	15.2	14.0	12.3	4.18	4.45	6.36	3.44	5.17
CaO	22.2	23.1	21.3	12.3	22.7	22.6	23.0	22.0	23.4	23.2	15.2	15.1	19.1	15.7	17.6
Na_2O	0.74	0.51	1.48	6.57	0.73	0.83	0.39	0.96	0.47	0.77	4.87	4.93	2.70	4.89	3.73
Totale	100.4	99.7	99.0	98.7	99.2	99.8	99.9	99.9	99.8	99.9	98.7	97.9	97.6	98.1	98.7
cpx	*La Queglia*												*Val Fiscalina*		
SiO_2	35.8	35.9	36.5	45.4	47.3	48.9	48.2	49.7	52.1	52.3	53.6	51.9	50.5	39.6	49.8
TiO_2	8.46	7.79	7.35	4.70	3.51	3.51	4.02	3.62	0.54	3.85	1.51	4.01	1.65	5.90	1.73
Al_2O_3	11.5	10.8	11.9	3.23	2.47	0.99	0.93	1.21	0.04	0.41	0.48	0.84	3.14	8.69	3.25
FeO	10.2	10.5	9.90	13.4	10.1	13.8	22.1	25.9	28.7	28.5	28.2	26.1	5.28	14.8	7.49
Cr_2O_3	0.02	0.00	0.02	0.02	0.00	0.00	0.00	0.00	0.00	0.03	0.05	0.02	0.46	0.02	0.02
MnO	0.09	0.09	0.09	0.40	0.29	0.45	0.56	0.69	0.96	0.76	0.95	0.70	0.12	0.35	0.18
MgO	9.16	9.08	9.03	8.98	12.02	9.01	3.17	0.88	0.04	0.02	0.05	0.13	15.35	6.94	13.03
CaO	23.9	23.6	23.4	21.3	22.8	19.7	14.1	5.59	2.79	0.80	1.43	2.85	23.0	22.2	23.4
Na_2O	0.49	0.56	0.55	2.18	1.12	2.09	5.45	10.94	12.72	12.96	12.98	13.06	0.38	1.54	0.68
Total	99.6	98.3	98.7	99.6	99.6	98.4	99.5	98.5	97.9	99.6	99.2	99.6	99.9	100.0	99.6
cpx	*Fosso Ripiglio*			*Castiglioncello*			*Senna River*			*Corvara in Badia*			*Calceranica*		
SiO_2	51.8	47.8	46.0	47.7	44.7	43.5	51.6	51.9	50.4	52.2	47.0	40.0	51.5	48.5	42.4
TiO_2	0.64	2.95	3.44	2.91	4.39	5.23	4.67	3.11	2.62	0.49	2.01	4.08	0.49	1.86	3.64
Al_2O_3	1.25	5.09	6.17	3.83	6.13	6.97	1.23	1.50	0.82	3.23	5.98	11.4	0.26	5.59	9.80
FeO	4.82	6.13	6.90	5.20	8.63	7.52	24.8	26.5	26.2	7.84	6.50	9.34	16.9	6.93	9.69
Cr_2O_3	0.10	0.27	0.12	0.76	0.00	0.27	0.00	0.00	0.00	0.08	0.00	0.05	n.a.	0.03	0.02
MnO	0.05	0.11	0.09	0.07	0.11	0.08	0.20	0.02	0.43	0.22	0.09	0.10	0.92	0.09	0.14
MgO	16.9	13.8	13.5	14.7	12.0	12.2	0.51	0.59	0.63	13.3	13.2	10.0	8.05	13.2	10.7
CaO	23.4	23.3	23.2	23.8	23.0	23.5	2.38	3.27	7.08	20.8	24.5	23.9	19.8	23.3	22.2
Na_2O	0.35	0.53	0.54	0.55	0.81	0.62	12.23	11.88	9.47	1.49	0.30	0.34	1.77	0.50	0.70
Total	99.3	99.9	99.9	99.6	99.8	99.9	97.6	98.8	97.7	99.6	99.6	99.1	99.7	100.0	99.3

molar solution. TiO_2 ranges up to 6.2% (by wt.), Al_2O_3 is present at up to 3% (by wt.), FeO is present at 13.8% to 28.6% (by wt.), and Na_2O is present at 2.7% to 9.8% (by wt.). All the Al occupies the tetrahedrally coordinated site, which is always undersaturated. Mg# is lower than 0.73 and correlates positively with Ca# of between 0.6% and 0.9% (by wt.). Aegirine is limited to groundmass in the Tuscany and Abruzzo lamprophyres. In these lamprophyres, Mg# is lower than 0.54% (by wt.), while Ca# is higher than 0.77% (by wt.). TiO_2 is present at up to 6% (by wt.), Al_2O_3 is present at up to 1.5% (by wt.), FeO is present at 24.8% to 28.7% (by wt.), and Na_2O is present from 10.8% to 13.1% (by wt.). MnO_2 concentrates in aegirine at up to 1% (by wt.). BaO and SrO generally correlate to an Ae molar solution percentage and are present at up to 0.2% (by wt.) and 0.7% (by wt.), respectively. An evolution trend from diospide to aegirine is typical of SiO_2-undersaturated alkaline rocks but. if coupled with high Al and Ti content is

typical of lamprophyres [33]. Drastic TiO_2 and Al_2O_3 reductions in groundmass-diopsides with respect to phenocrysts and microphenocrysts is probably due to the extensive crystallization of titanates and feldspars, abundant in pheno-microphenocrysts rims and groundmass, respectively.

Micas

Mica forms pleochroic euhedral phenocrysts and microphenocrysts, usually brown or dark brown. The crystals are always zoned, with light cores and dark

Table 4.

Representative analyses of micas from Italian Lamprophyres.

mica	***Fosso Ripiglio***			***Murci***		***Castiglioncello del T.***			***Senna River***				***Corvara in Badia***		
SiO_2	34.9	38.5	37.0	35.5	34.9	35.9	34.4	45.5	34.6	34.3	33.8	33.6	32.7	34.8	34.7
TiO_2	9.74	8.08	9.80	7.62	8.39	7.65	8.91	5.01	8.85	7.74	8.90	9.10	4.24	3.56	3.52
Al_2O_3	13.7	14.2	14.6	14.8	15.2	14.7	14.5	14.3	14.2	13.7	14.2	13.7	16.7	16.7	16.3
Cr_2O_3	0.00	0.00	0.00	0.00	0.00	0.00	0.00	0.00	0.00	0.00	0.00	0.00	0.00	0.00	0.00
FeO	19.9	16.5	17.6	12.4	12.6	12.6	12.9	11.4	14.4	22.5	14.1	20.8	9.28	9.17	8.96
MnO	0.15	0.13	0.15	0.08	0.04	0.12	0.10	0.12	0.16	0.23	0.16	0.27	0.12	0.13	0.10
MgO	9.36	8.16	8.60	15.73	15.0	15.9	14.7	8.11	11.9	7.38	12.2	7.74	17.9	18.6	18.7
CaO	0.08	0.21	0.15	0.02	0.09	0.11	0.08	0.43	0.00	0.04	0.07	0.06	0.00	0.12	0.06
BaO	0.94	0.94	0.92	1.38	1.87	1.44	2.06	0.96	1.92	0.13	2.10	1.71	5.43	3.83	3.75
Na_2O	0.66	1.09	2.04	0.59	0.59	0.58	0.56	1.73	0.73	0.52	0.64	0.59	0.59	0.56	0.57
K_2O	8.88	8.16	8.39	8.29	7.57	9.09	8.98	8.65	8.51	9.51	8.52	8.75	7.84	8.29	8.50
F	0.00	0.00	0.00	0.00	0.00	0.00	0.00	0.00	0.00	0.42	0.42	0.00	0.00	0.00	0.22
Cl	0.00	0.00	0.00	0.00	0.00	0.00	0.00	0.00	0.00	0.00	0.00	0.00	0.00	0.00	0.00
Ce_2O_3	0.28	0.35	0.32	0.39	0.56	0.47	0.67	0.25	0.60	0.00	0.68	0.60	n.a.	n.a.	n.a.
Total	98.5	96.4	99.6	96.8	96.8	98.5	97.8	96.5	96.0	96.7	95.9	97.2	95.0	95.9	95.1
	Calceranica		***Nuraxi Figus***							***Pietre Nere***					
SiO_2	33.8	34.9	37.0	36.6	34.0	36.7	34.4	36.6	33.6	40.4	41.5	38.7	35.7	35.2	33.0
TiO_2	4.04	3.69	2.48	0.77	4.79	0.00	3.55	0.77	4.70	0.60	0.43	2.97	3.40	3.74	4.95
Al_2O_3	15.0	16.1	14.2	17.3	17.0	14.5	16.6	17.3	15.8	12.7	11.5	12.5	13.5	14.1	13.2
Cr_2O_3	0.00	0.00	0.00	0.00	0.00	0.00	0.00	0.00	0.00	0.00	0.00	0.00	0.00	0.00	0.00
FeO	16.3	15.1	20.6	12.0	11.6	12.1	15.0	12.0	18.2	4.27	4.58	15.1	21.2	21.1	23.2
MnO	0.23	0.20	0.33	0.18	0.19	0.18	0.24	0.18	0.44	0.08	0.08	0.24	0.50	0.37	0.42
MgO	12.9	13.6	11.3	18.0	16.1	19.6	14.1	18.0	11.6	25.3	25.2	16.1	11.5	11.4	9.76
CaO	2.42	0.18	0.20	0.13	0.02	0.91	0.01	0.13	0.10	0.03	0.03	0.19	0.03	0.07	0.04
BaO	2.60	2.65	0.12	2.04	3.86	0.56	2.82	2.04	3.28	0.36	0.14	0.08	0.15	1.00	0.67
Na_2O	1.07	1.04	0.21	0.94	1.07	0.84	0.98	0.94	0.78	1.40	1.94	0.45	0.57	0.40	0.57
K_2O	7.23	7.24	9.90	8.66	7.51	8.56	8.11	8.66	7.98	8.01	7.40	9.56	9.47	9.50	9.20
F	0.79	0.27	0.00	0.30	0.00	0.33	0.34	0.30	0.00	n.a.	n.a.	0.98	0.26	0.00	0.00
Cl	0.06	0.05	0.00	0.00	0.00	0.00	0.09	0.00	0.00	n.a.	n.a.	0.09	0.00	0.20	0.31
Ce_2O_3	0.81	0.89	n.a.	n.a.	n.a.	n.a.	n.a.	n.a.	n.a.	n.a.	n.a.	0.00	0.00	0.31	0.17
Total	97.3	96.0	96.5	97.0	96.3	94.5	96.3	97.0	96.5	93.2	92.8	96.9	96.5	97.5	95.6
	Pietre Nere			***La Queglia***							***Val Fiscalina***				
SiO_2	34.8	34.9	36.7	39.6	37.9	37.5	33.9	34.1	33.6	34.7	35.5	33.9	35.0	36.1	37.0
TiO_2	3.63	3.51	5.62	4.22	5.52	5.10	4.09	3.67	5.38	5.03	6.96	5.88	7.33	6.62	6.87
Al_2O_3	13.6	14.2	15.9	10.9	11.9	13.2	3.76	4.10	2.94	2.43	14.9	12.8	15.1	14.7	15.0
Cr_2O_3	0.00	0.00	0.00	0.00	0.00	0.00	0.00	0.00	0.00	0.00	0.00	0.00	0.00	0.00	0.00
FeO	23.23	25.12	10.57	11.30	11.86	11.00	42.58	41.27	40.70	39.33	10.03	26.97	9.89	9.67	9.31
MnO	0.52	0.64	0.12	0.21	0.23	0.19	1.06	1.06	1.12	1.14	0.09	0.54	0.06	0.06	0.07
MgO	9.69	8.17	17.7	19.6	17.7	17.9	1.14	1.53	1.58	1.41	17.0	5.61	16.6	17.3	17.6
CaO	0.11	0.02	0.03	0.20	0.27	0.13	0.34	0.49	0.13	0.48	0.04	0.05	0.04	0.06	0.03
BaO	0.86	0.03	1.17	0.97	2.05	2.22	0.88	0.80	1.43	1.13	1.27	0.29	1.66	1.16	1.36
Na_2O	0.29	0.42	1.18	0.23	0.22	0.29	0.26	0.26	0.55	0.60	0.58	0.18	0.57	0.62	0.50
K_2O	9.42	9.52	8.28	9.52	9.32	9.27	7.90	7.70	8.60	8.64	9.41	9.33	9.36	9.56	9.58
F	0.00	0.35	0.00	0.91	1.06	1.03	0.00	0.00	0.00	0.00	0.55	0.24	0.54	0.45	0.61
Cl	0.73	0.00	0.47	n.a.	n.a.	n.a.	n.a.	n.a.	n.a.	n.a.	0.00	0.00	0.00	0.00	0.00
Ce_2O_3	0.22	0.00	0.31	n.a.	n.a.	n.a.	n.a.	n.a.	n.a.	n.a.	0.39	0.11	0.54	0.44	0.44
Total	97.2	97.1	98.2	97.6	98.1	98.0	96.0	95.0	96.1	95.1	96.8	96.0	96.7	96.7	98.4

rims. Sometimes, mica can grow on the olivine and pheno-micro clinopyroxenes. Inclusions of apatite and Ti-magnetite are very frequent. Reverse pleocroism has been observed as a typical feature of micas in lamprophyres [33]. Basing on the $Mg:Fet^{2+}$=2:1 ratio, the mica core is phlogopite with a minor eastonite molar solution, the rim is biotite with a molar solution of siderophillite and annite, with high Fe-enrichment in Monte la Queglia UML. In general, passage from phlogopite to biotite is marked by a strong decrease of Al and Mg. Phenocrysts cores are generally phlogopite, having FeO, MgO, and Al_2O_3 contents ranging from 4.3% to 20.6%, 8.1% to 25.2%, and 11.5% to 17.5% (by wt.), respectively. Cr_2O_3 is generally <0.1% (by wt.), BaO is up to 5.4% (by wt.), and TiO_2 is present at up to 9.8% (by wt.), inversely correlated to MgO content. Light rare earth elements (LREEs) were consistently detected in the cores at levels generally ≥ 1% (by wt.). F is present at up to 1.1% (by wt.) in phlogopitic cores. The mica rim is biotite, consisting of FeO, MgO, and Al_2O_3 at ranges from 14.9% to 43.0%, 1.1% to 15.1%, and 2.4% to 17.6% (by wt.), respectively. BaO is present up to 3.3% (by wt.) and TiO2 up to 9.1% (by wt.). MnO is up to 1.4% (by wt.) and is inversely correlated to MgO. Mg# is present at levels from 0.91% to 0.63% (by wt.) in phlogopite cores and from 0.63% to 0.5% (by wt.) in biotite rims. High Al_2O_3 content in phlogopitic cores yields the T site saturation; moving towards the biotitic rims, Al_2O_3 progressively decreases and it is usually insufficient to fill the tetrahedral site, with major undersaturation belonging to the extreme tetraferriannite compositions. Micas from Punta delle Pietre Nere AL a have high Cl content, up to 0.7% (by wt.). Al_2O_3- and TiO_2-rich micas are typical of L and Ti-Fe-Mn enrichment, along with differentiation is a typical feature of L and lamproites, kimberlites, and other Italian ultrapotassic rocks [3, 27, 39].

Amphiboles

Amphiboles form euhedral phenocrystals or are in the groundmass minerals. Amphibole coronas are widespread on olivine and diopside phenocrysts. Pleocroism is light-yellow to dark brown. They are calcic and can be further subdivided by their Ti content as kaersutite (Ti>0.5 afu) and further into pargasite (Ti<0.5 afu, Fe_3< VI Al) and Mg-hastingsite (Ti<0.5 afu, Fe_3>VI Al). Ferroan pargasite and Mg-hastingsite are confined to the groundmass. Kaersutitic cores have between 36.3% and 40.6% (by wt.) SiO_2, 4.4% to 7.6% (by wt.) TiO_2, 10.4% to 15.2% (by wt.) Al_2O_3, 9.6% to 17.4% (by wt.) FeO, 1.2% to 3.6% (by wt.) Na_2O, and 0.6% to 1.9% (by wt.) K_2O. F+Cl is present at up to 0.6% (by wt.). Even if Ti clearly correlates with Ba, kaersutites have a Ba content lower than 0.3 afu. Sr is detectible in both kaersutite and pargasites and up to 0.5 afu. ILs' kaersutites are subsilicic, having in general level of TSi<6% (by wt.). Pargasite and ferroan pargasite have between 37.1% and 40.6% (by wt.) SiO_2, 1.9% to 6.4% (by

wt.) TiO_2, 9.7% to 14.4% (by wt.) FeO, 11.8% to 15.4% (by wt.) Al_2O_3, 0.8% to 1.9% (by wt.) K_2O, and 2.2% to 3.3% (by wt.) Na_2O. Pargasites have a higher level of BaO, generally higher than 0.3 afu and up to 2.6% (by wt.). F and Cl are detectible and up to 0.4% (by wt.). Mg-hastingsite has between 36.3% and 46.5% (by wt.) SiO_2, 0.3% to 7.0% (by wt.) TiO_2, 8.1% to 13.7% (by wt.) Al_2O_3, 8.6% to

Table 5a, b.

Representative analyses of amphyboles from Italian Lamprophyres

	Pargasite											***Mg-Hastingsite***							
	Calceranica				***Nuraxi Figus***				***Punta Pietre Nere***			***Calc.***	***NuF***	***Punta Pietre Nere***					
SiO_2	37.9	40.6	37.6	37.9	39.5	37.7	39.0	38.4	39.4	40.6	39.1	39.83	37.99	39.7	40.1	40.1	39.5	38.7	39.46
TiO_2	4.14	3.94	4.11	4.14	4.39	4.34	3.81	3.58	3.52	2.38	4.17	2.35	2.87	2.95	3.90	2.58	3.76	3.14	3.82
Al_2O_3	14.6	13.8	14.4	14.6	13.6	15.2	14.1	14.4	11.8	11.7	13.4	13.2	14.0	11.5	11.5	12.2	12.5	13.1	11.9
FeO	12.2	10.8	13.7	12.2	10.0	10.8	11.7	11.4	12.9	16.9	10.9	11.5	15.0	11.2	9.80	9.42	10.4	9.44	12.3
Cr_2O_3	0.09	0.12	0.02	0.09	0.02	0.01	0.04	0.00	0.11	0.00	0.09	0.00	0.02	0.00	0.00	0.00	0.00	0.00	0.07
MnO	0.22	0.25	0.24	0.22	0.23	0.20	0.27	0.23	0.19	0.19	0.13	0.20	0.40	0.22	0.14	0.11	0.16	0.06	0.22
MgO	11.7	13.6	11.2	11.7	13.1	12.3	12.2	12.7	12.2	10.9	13.4	13.8	11.2	14.8	15.1	15.1	14.3	14.6	12.9
CaO	11.5	11.5	12.2	11.5	13.3	12.1	12.0	11.7	11.6	11.4	12.0	11.3	11.1	11.7	11.8	12.2	12.1	12.3	11.4
Na_2O	2.96	3.24	2.88	2.96	2.19	2.41	2.69	2.41	2.83	3.28	2.62	3.11	2.75	3.23	3.01	2.64	2.88	2.43	3.05
K_2O	1.00	0.98	1.01	1.00	1.05	1.29	1.25	1.23	1.63	1.33	1.55	0.88	1.32	1.03	1.20	1.22	1.52	1.37	1.30
F	0.30	0.00	0.00	0.30	0.00	0.00	0.00	0.00	0.18	0.15	0.17	0.00	0.00	0.00	0.00	n.a.	0.17	n.a.	0.03
La_2O_3	0.00	0.00	0.00	0.00	0.00	0.00	0.00	0.00	0.00	0.00	0.00	0.00	0.00	0.02	0.00	n.a.	0.00	n.a.	0.00
Ce_2O_3	0.00	0.12	0.12	0.00	0.00	0.00	0.00	0.00	0.00	0.00	0.00	0.16	0.00	0.03	0.08	n.a.	0.00	n.a.	0.00
SrO	0.36	0.34	0.16	0.36	0.51	0.30	0.30	0.35	0.00	0.00	0.00	0.25	0.19	0.00	0.00	0.00	0.00	0.00	0.00
BaO	0.37	0.26	0.22	0.37	0.41	0.47	0.39	0.45	0.00	0.00	0.10	0.28	0.32	0.00	0.09	0.00	0.11	0.12	0.00
Cl	0.00	0.00	0.11	0.00	0.00	0.00	0.00	0.00	0.00	0.00	0.00	0.00	0.00	0.00	0.00	n.a.	0.00	n.a.	0.00
Total	97.5	99.7	98.0	97.5	98.6	97.3	97.8	97.0	96.6	97.0	97.7	97.1	97.4	96.7	96.9	95.7	97.5	95.3	96.8

	Kaersutite																	
	Senna river						***Calceranica***						***Pietre Nere***					
SiO_2	40.9	39.4	38.3	38.2	38.0	37.9	38.3	38.3	37.7	37.2	36.9	36.3	39.9	37.8	39.8	38.9	37.6	
TiO_2	6.88	7.62	7.03	7.25	6.88	6.47	4.74	5.02	5.17	5.22	4.88	5.57	4.57	5.52	4.58	4.49	5.78	
Al_2O_3	12.6	12.3	11.3	11.7	13.2	12.2	14.0	13.2	14.8	14.5	14.5	14.7	12.3	13.7	12.6	12.8	13.5	
FeO	11.4	12.6	12.4	11.4	12.3	17.4	11.1	11.6	11.1	11.4	12.5	14.5	9.68	10.0	12.9	10.9	10.9	
Cr_2O_3	0.00	0.00	0.10	0.08	0.00	0.00	0.00	0.08	0.03	0.01	0.01	0.01	0.00	0.00	0.00	0.00	0.00	
MnO	0.14	0.18	0.20	0.17	0.20	0.24	0.20	0.19	0.16	0.20	0.19	0.28	0.15	0.12	0.22	0.16	0.10	
MgO	12.7	11.6	11.1	11.4	11.1	8.10	13.0	12.0	12.8	12.4	11.5	10.2	14.8	14.0	12.2	13.7	12.5	
CaO	11.8	11.9	11.9	12.0	11.8	11.6	11.6	12.4	11.7	11.8	11.6	11.7	12.0	11.9	11.9	12.1	12.2	
Na_2O	2.49	2.43	2.48	2.27	2.15	2.39	2.99	2.64	2.86	2.73	3.02	2.85	2.80	2.54	2.86	2.64	2.47	
K_2O	1.75	1.77	1.78	1.81	1.85	1.83	1.05	0.98	1.00	1.07	1.10	1.06	1.51	1.72	1.39	1.60	1.84	
F	0.00	0.00	0.35	0.00	0.00	0.00	0.00	0.26	0.00	0.00	0.00	0.00	0.00	0.00	0.04	0.12	0.02	
La_2O_3	0.00	0.00	0.00	0.00	0.00	0.00	0.00	0.00	0.00	0.00	0.00	0.00	0.00	0.00	0.00	0.00	0.00	
Ce_2O_3	0.00	0.00	0.00	0.00	0.00	0.00	0.14	0.00	0.14	0.17	0.17	0.00	0.00	0.00	0.00	0.00	0.00	
SrO	0.00	0.08	0.30	0.39	0.08	0.18	0.11	0.40	0.08	0.19	0.13	0.00	0.00	0.00	0.00	0.00	0.00	
BaO	0.23	0.27	0.27	0.27	0.27	0.23	0.21	0.24	0.22	0.34	0.20	0.05	0.13	0.18	0.15	0.10	0.17	
Cl	n.a.	n.a.	n.a.	n.a.	n.a.	n.a.	0.12	0.00	0.00	0.00	0.00	0.00	0.00	0.00	0.00	0.00	0.00	
Total	101.0	100.3	97.6	97.2	97.8	98.7	97.7	97.8	97.9	97.3	96.7	97.4	98.1	97.7	98.8	97.6	97.8	

15.1% (by wt.) FeO, 1.2% to 4.1% (by wt.) Na_2O, and 0.5% to 1.4% (by wt.) K_2O. MnO concentrates in Mg-hastingsite at up to 0.63% (by wt.). Fl+Cl are alway very low and near the detection limit. TiO_2 content positively correlates with Al_2O_3 andnegatively with SiO_2 and Na_2O. Mg and Fe contents are inconclusive with respect to other elements' variations and Mg# is detected ranges of between 0.8% and 0.55% (by wt.) in all the three groups. Even if the T site has Si< 6 afu, Ti is always sufficient to saturate it. Titanian amphiboles are typical of lamprophyres (33). Kaersutite is typical of AL amphiboles and TSi<6 afu (subsilicic) it is strongly diagnostic of AL and UML [33].

Feldspars

K-feldspar, albite, and oligoclase/andesine are only found in the groundmass, where they form laths of between 100 and 200 μm in length. Anorthoclase was found only in Southern Tuscany rocks. It si associated with carbonate, nepheline and/or sodalite, with coprecipitation relationship. K-feldspars are also found in

Table 6.

Representative analyses of feldspars from Italian Lamprophyres.

Feldspars	*Fosso Ripiglio*		*Senna*	*Castiglioncello del T*			*Calceranica*		*Nuraxi Figus*		*Punta Pietre Nere*				*La Queglia*		*Val Fiscalina*	
SiO_2	69.4	68.1	65.8	65.3	64.2	63.8	58.1	54.0	66.1	59.3	68.3	65.5	56.1	56.0	64.7	62.4	71.6	64.6
TiO_2	0.00	0.00	0.00	0.09	1.24	0.08	0.21	0.12	0.00	0.00	0.00	0.00	0.00	0.00	0.00	0.00	0.00	0.00
Al_2O_3	19.9	19.6	18.2	18.7	18.1	19.9	23.8	26.4	18.7	24.7	20.2	17.8	30.7	30.6	18.5	18.0	21.2	18.5
Fe_2O_3	0.09	0.74	0.57	1.52	3.61	1.10	0.79	0.61	0.40	0.48	0.11	0.29	0.07	0.09	0.34	0.81	0.59	0.22
MnO	0.00	0.00	0.00	0.00	0.00	0.00	0.00	0.00	0.00	0.00	0.00	0.00	0.00	0.00	0.00	0.00	0.00	0.00
MgO	0.00	0.80	0.00	1.06	1.72	0.00	0.00	0.00	0.00	0.00	0.00	0.00	0.00	0.00	0.00	0.00	0.28	0.00
BaO	0.00	0.00	0.16	0.00	0.16	0.00	0.73	0.49	0.00	1.06	0.00	0.00	0.00	0.00	0.70	0.80	0.11	0.00
CaO	0.03	0.10	0.00	0.09	0.16	0.00	5.19	9.16	0.09	5.60	0.41	0.00	0.03	0.02	0.00	0.02	0.24	0.00
Na_2O	11.4	11.5	3.50	6.59	8.84	0.86	7.23	5.44	3.15	6.94	11.0	1.82	12.0	12.3	0.30	0.33	5.71	1.40
SrO	0.00	0.00	0.00	0.00	0.00	0.00	1.36	1.68	0.00	1.24	0.00	0.00	0.00	0.00	0.00	0.00	0.56	0.00
K_2O	0.04	0.05	12.31	7.08	2.20	13.8	0.72	0.32	12.9	1.36	0.07	14.5	0.00	0.00	16.8	16.8	0.60	15.5
Total	100.9	100.9	100.6	100.5	100.2	99.6	98.2	98.2	101.4	100.7	100.2	99.9	99.0	99.1	101.5	99.2	100.9	100.2

ocelli. Plagioclases with albite twining form varioles and K-feldspar is pecilitic of aegirine, biotite, apatite, and Ti-magnetite. They co-precipitate with sodalite, nepheline, and carbonate. Sanidine has a notable An molecule up to 43% (by wt.). Selected analyses are reported in Tab. 6. K-feldspar has moderate Fe and Ba levels of up to 2.4% and 1.2% (by wt.), respectively. Plagioclase has Fe_2O_3< 1 and high

Table 7.

Representative analyses of feldspatoids from Italian Lamprophyres.

	nepheline			*sodalite*							*analcite*			
	La Queglia			*Punta Pietre Nere*										
SiO_2	42.7	42.4	42.0	37.6	37.5	37.4	37.3	37.3	37.2	36.7	47.4	47.4	46.9	50.8
Al_2O_3	31.1	31.6	30.5	30.0	30.9	30.8	29.7	29.5	29.7	30.9	0.00	0.00	0.00	0.00
Fe_2O_3	2.64	2.60	2.58	0.17	0.28	0.12	0.00	0.11	0.05	0.14	27.2	27.4	28.2	26.1
MnO	0.00	0.07	0.00	0.04	0.00	0.00	0.00	0.00	0.00	0.00	0.30	0.00	0.20	0.00
MgO	0.70	0.29	0.65	0.00	0.00	0.00	0.00	0.00	0.00	0.00	0.00	0.00	0.06	0.00
CaO	0.27	0.28	0.25	0.05	0.07	0.00	0.00	0.09	0.03	0.06	0.00	0.00	0.00	0.00
Na_2O	10.9	12.8	14.3	26.2	25.3	25.2	25.7	25.4	26.1	24.8	0.08	0.04	0.22	0.12
K_2O	8.81	8.88	8.79	0.00	0.00	0.00	0.09	0.09	0.00	0.06	15.8	16.2	16.5	15.2
SrO	0.00	0.00	0.00	0.00	0.00	0.00	0.00	0.00	0.00	0.00	0.15	0.07	0.05	0.05
BaO	0.00	0.10	0.00	0.00	0.00	0.00	0.00	0.00	0.00	0.00	0.00	0.00	0.00	0.00
Cl	0.00	0.00	0.00	7.26	7.17	7.43	7.14	7.20	7.25	7.20	0.00	0.00	0.00	0.00
SO_3	0.00	0.00	0.00	0.00	0.08	0.25	0.00	0.00	0.00	0.18	0.00	0.00	0.44	0.00
Total	97.3	99.1	99.0	101.3	101.3	101.2	100.0	99.6	100.4	100.1	91.1	91.3	92.6	92.3

SrO and BaO levels up to 1.7% and 1.3% (by wt.), respectively. K-feldspar and plagioclase association, having this chemical features, is typical of AL [32].

Foids

Fresh nepheline is reported in small euhedra in the groundmass at Monte La Queglia, Calceranica, and Corvara in Badia. Sodalite was recognised as a

groundmass mineral associated with K-feldspar and carbonate. Analcite was detected in Corvara in Badia, Punta delle Pietre Nere, Nuraxi Figus, and reported from Tuscany. Analcite is present in the ocelli, where it coprecipitates with carbonate and/or K-feldspar. The above association is contrary to leucite occurrence as diagnostic of UML or AL. Analyses of fresh nepheline are available only from UML of Monte La Queglia. This nepheline has a high Ks molar solution of 30.3% to 33.1% (by wt.) and variable TSi leading to a Qmol of between 2.6% and 10.9%. Mn, Ba, and Sr are generally near the detection limits. Fe_2O_3 and CaO are present up to 0.5% and 0.3% (by wt.), respectively. Sodalite from Punta Pietre Nere (Tab. 8) has Cl up to 7.5% (by wt.) and very low SO_3 averaging 0.07% (by wt.). SrO and BaO are below the detection limit. Analcite has NaO up to 16.5% (by wt.), variable FeO up to 0.3% (by wt.), and low K_2O and CaO. Sr and Ba are below detection limits.

Spinel group

Spinels are Ti-magnetite and trevorite, frequently found in mica and amphiboles, and are abundant in the groundmass where they are associated with

Table 8.

Representative analyses of spinels from Italian Lamprophyres.

spinels	***Murci***		***Senna river***		***Fosso Ripiglio***			***Castiglioncello***		***Corsara in badia***			***Calceranica***			
SiO_2	0.98	0.00	1.57	1.52	0.00	1.18	2.20	0.40	0.30	0.06	0.09	0.12	1.91	2.60	4.37	7.86
TiO_2	16.6	13.1	24.2	26.3	11.5	7.46	5.82	5.11	2.80	9.45	8.68	9.01	11.4	9.42	12.9	7.91
Al_2O_3	0.53	3.99	0.71	0.15	0.00	0.00	0.00	10.1	18.0	5.05	8.60	8.96	9.48	9.95	10.14	11.56
FeO	72.6	46.7	63.8	63.6	59.8	53.1	49.3	42.6	28.7	72.6	70.5	68.0	63.6	63.5	58.1	55.2
MnO	0.04	0.00	0.25	0.12	0.00	1.15	0.00	1.54	0.31	1.13	0.83	0.71	0.73	0.35	0.33	0.25
MgO	0.00	0.00	0.03	0.03	0.00	0.00	0.00	5.88	12.2	3.98	5.81	6.61	3.66	5.69	5.90	8.93
CaO	0.15	0.00	0.22	0.22	0.68	0.00	0.80	0.29	0.19	0.14	0.16	0.05	1.14	0.62	0.36	0.31
Cr_2O_3	0.00	15.7	0.00	0.05	0.00	0.00	0.00	29.2	35.5	0.00	0.00	0.00	0.00	0.00	0.00	0.06
NiO	0.00	0.00	0.00	0.00	28.01	37.15	41.88	0.13	0.17	0.07	0.10	0.11	0.00	0.18	0.19	0.19
ZnO	0.39	11.9	1.83	0.08	0.00	0.00	0.00	1.06	0.00	0.00	0.00	0.12	0.13	0.06	0.14	0.06
Total	91.4	91.3	92.6	92.2	100	100	100	96.3	98.3	92.6	94.9	93.7	92.1	92.4	92.5	92.3
Sample	***Nuraxi Figus***		***La Queglia***		***Punta delle Pietre Nere***							***Val Fiscalina***				
SiO_2	0.10	0.08	0.14	0.26	0.19	0.50	0.00	0.00	0.93	0.97	0.09	2.99	3.30	0.72	0.27	0.00
TiO_2	9.99	9.97	11.02	2.52	2.46	1.10	0.00	0.00	15.42	5.22	6.08	4.48	1.87	0.00	2.55	1.31
Al_2O_3	8.33	8.58	8.86	22.5	22.5	0.04	0.00	0.00	0.67	11.56	9.43	0.80	10.10	0.00	15.78	0.00
FeO	73.5	72.5	71.2	25.7	25.2	90.0	80.8	80.5	72.7	40.8	53.7	80.9	36.9	35.1	33.4	31.7
MnO	1.12	1.05	0.95	0.40	0.38	0.26	0.00	0.00	3.36	0.26	0.51	0.00	0.88	0.00	0.37	0.00
MgO	2.93	3.28	4.10	13.53	13.42	1.05	0.03	0.00	0.00	10.42	7.63	0.00	3.99	4.78	9.01	6.60
CaO	0.05	0.07	0.03	0.09	0.05	0.13	0.00	0.00	0.33	0.99	0.02	0.15	0.25	0.00	0.10	0.51
Cr_2O_3	0.00	0.00	0.00	33.0	33.2	0.70	0.00	0.00	0.00	26.3	19.8	0.08	37.2	55.4	35.5	49.6
NiO	0.06	0.00	0.00	0.13	0.12	0.00	0.69	0.93	0.00	0.21	0.09	0.62	0.00	0.00	0.16	0.00
ZnO	0.16	0.14	0.15	0.00	0.00	n.a.	n.a.	n.a.	0.00	0.00	0.18	0.83	0.56	0.00	0.19	0.00
Total	96.2	95.7	96.5	98.3	97.6	93.8	81.5	81.4	93.6	96.7	97.6	90.9	95.1	96.0	97.3	89.7

apatite, K-feldspar, and carbonate. The most abundant type is a complete solid solution between magnetite and ulvospinel, which form a continuous series. This ulvospinel-magnentite serie contains a franklinite solid solution up to 5% (by vol.) (ZnO = 1.8% by wt.) and jacobsite up to 11% (by mol.) (MnO = 3.4% by wt.). Other composition are from 5% to 20% (by mol.) ulvospinel and 40% to 80% (by mol.) magnetite with up to 20% of quandilite or up to 24% (by mol.) spinel.

Trevorite with NiO up to 42% (by wt.) was found at Fosso Ripiglio. Solid solutions of chromite and spinel have 30% to 50% (by mol.) chromite and up to 41% (by mol.) spinel. In addition, these solid solutions can contain up to 34% (by mol.) ulvosopinel, 16% (by mol.) quandilite, 2% (by mol.) hercinite, and 6% (by mol.) franklinite. Chromite is found only as inclusion in olivine and diospide.

Ilmenite

Ilmenite is abundant in ILs from Tuscany and Puglia, and is only found in groundmass. Ilmenite-hematite solid solution has Hem up to 33% (by mol.) and

Table 9.

Representative analyses of ilmenite from Italian Lamprophyres.

ilmenite	*Pietre Nere*					*Fosso Ripiglio*									
SiO_2	0.33	0.10	0.32	0.68	1.01	0.06	0.24	0.00	0.09	0.06	0.07	0.09	0.00	0.15	0.18
TiO_2	45.6	31.8	38.3	41.2	43.8	49.8	49.55	49.3	49.2	49.0	48.9	48.7	48.7	48.6	48.5
Al_2O_3	0.31	1.05	0.23	0.87	1.73	0.07	0.03	0.06	0.07	0.07	0.07	0.06	0.07	0.08	0.08
FeOt	45.8	56.3	52.4	49.5	45.4	37.6	36.3	36.1	36.2	36.9	36.9	36.1	37.5	36.1	37.7
MnO	4.13	1.33	2.13	1.84	1.81	10.83	10.79	12.13	11.60	11.11	11.39	11.47	11.38	11.75	10.61
MgO	0.71	4.81	1.24	3.32	3.92	0.00	0.00	0.00	0.00	0.00	0.03	0.04	0.00	0.00	0.00
CaO	0.11	0.03	0.32	0.10	0.04	0.32	0.67	0.25	0.28	0.34	0.25	0.36	0.12	0.39	0.49
Cr_2O_3	0.01	2.23	0.02	0.00	0.01	n.a.	n.a.	n.a.	n.a.	n.a.	n.a.	n.a.	n.a.	n.a.	n.a.
NiO	0.02	0.02	0.00	0.04	0.03	0.00	0.00	0.06	0.00	0.06	0.00	0.00	0.00	0.00	0.00
ZnO	0.19	0.09	0.01	0.04	0.11	0.00	0.00	0.00	0.00	0.00	0.00	0.00	0.00	0.00	0.00
Total	97.1	97.8	95.00	97.6	97.8	98.7	97.7	98.0	97.6	97.7	97.8	96.9	97.8	97.1	97.6

minor amounts of geikielite up to 15% (by mol.) and pyrophanite up to 26% (by mol.) (= 12.1% by wt. MnO). Cr_2O_3 is present at <0.1% by wt. and MgO is present at up to 3.9% by wt.. ZnO is present at up to 0.4% (by wt.), with other compounds near the detection limit.

Titanite and Perovskite

Analyses of titanite have detected Al_2O_3 at levels of up to 2.4% (by wt.) and Fe_2O_3 up to 2.9% (by wt.). La_2O_3+Ce_2O_3 is present at up to 1.2% (by wt.), ZrO is present at up to 1.8% (by wt.), BaO is present at up to 0.4% (by wt.). Fluorine content is detectible and present at levels up to 0.6% (by wt.). Perovskite is the dominat Ti-phase in the Southern Tuscany and Punta delle Pietre Nere lamprophyres and it is subordinated in the Corvara in Badia lamprophyres. It forms octahedra in the groundmass or inclusions into melilite and pyroxenes. Perovskite contains 1.7% (by wt. FeO, with SrO present at up to 0.4% (by wt.), Nb_2O_3 and La_2O_3 at levels up to 0.5%, and Na_2O and Ce_2O_3 at levels of up to 1% (by wt.).

Garnet

Garnet forms small, red-brown, high- relief, euhedra in the groundmass of UML of the Monte La Queglia. It is a titanian garnet with a 45% to 75% pyrope, 25% to 34% andradite molar solution with a detectible grossular molecule up to 23.7%. TiO_2 is present at up to 8.3% (by wt.) and Na_2O is present at up to 0.7% (by wt.). This composition should be stable only at high pressures and high

temperatures, but La Queglia UML seems to have crystallized garnet at much lower pressure.

Table 10a, b.

Representative analyses of titanite and perovskite from Italian Lamprophyres.

titanite	***Pietre Nere***													
SiO_2	30.7	30.4	30.3	30.1	30.1	30.0	30.0	29.9	29.9	29.7	29.7	29.6	29.0	28.9
TiO_2	35.8	35.6	36.1	35.3	33.0	36.8	36.5	36.1	38.2	35.9	37.4	37.4	36.6	36.8
Al_2O_3	2.37	1.14	1.51	0.91	1.49	1.28	0.78	1.01	1.11	1.07	1.17	1.23	1.34	1.25
FeO	1.36	2.52	2.87	1.69	2.62	1.88	1.66	1.79	1.30	1.87	1.63	1.40	1.88	1.54
MnO	bdl	0.04	bdl	bdl	bdl	bdl	0.07	0.04	0.05	bdl	0.05	bdl	0.05	0.06
MgO	bdl	0.03	0.02	bdl	0.04	bdl	bdl	bdl	0.02	0.11	0.05	0.05	0.09	0.02
CaO	28.7	27.7	28.1	27.6	27.0	28.5	27.7	27.8	27.9	27.8	27.9	28.1	27.9	27.2
Na_2O	bdl	0.15	bdl	0.20	0.10	bdl	bdl	0.10	bdl	0.11	0.09	bdl	bdl	bdl
SrO	bdl	bdl	bdl	bdl	bdl	bdl	bdl	bdl	bdl	0.11	bdl	bdl	bdl	bdl
BaO	0.28	0.26	0.22	0.25	0.24	0.36	0.32	0.21	0.33	0.24	0.34	0.22	0.28	0.29
La_2O_3	bdl	bdl	bdl	bdl	0.29	bdl	bdl	bdl	bdl	0.22	bdl	bdl	bdl	bdl
Ce_2O_3	bdl	0.40	0.25	0.38	0.90	0.25	0.33	0.30	0.24	0.48	0.26	0.36	0.33	0.29
ZnO	bdl	bdl	bdl	bdl	bdl	bdl	0.20	bdl	bdl	bdl	0.15	bdl	bdl	bdl
ZrO_2	bdl	0.66	bdl	1.35	1.45	bdl	1.78	0.88	bdl	0.48	0.78	0.46	0.80	0.53
F	bdl	bdl	0.60	0.62	bdl	bdl	0.26	bdl	bdl	0.30	bdl	bdl	bdl	bdl
Total	99.5	99.3	100.3	98.7	97.4	99.4	99.7	98.5	99.6	98.6	99.7	99.3	98.9	97.5

perovskite	***La Queglia***																
SiO_2	0.00	0.00	0.06	0.08	0.00	0.08	0.00	0.00	0.09	0.08	0.00	0.06	0.06	0.07	0.08	0.00	0.09
TiO_2	57.1	57.1	56.9	56.9	56.9	56.8	56.7	56.7	56.7	56.7	56.7	56.7	56.6	56.6	56.5	56.6	56.4
Al_2O_3	0.00	0.00	0.03	0.05	0.00	0.00	0.03	0.03	0.00	0.00	0.03	0.00	0.00	0.00	0.08	0.03	0.07
La_2O_3	0.32	0.31	0.34	0.27	0.43	0.30	0.32	0.40	0.25	0.37	0.41	0.27	0.21	0.27	0.26	0.32	0.39
Ce_2O_3	0.58	0.66	0.62	0.53	0.88	0.51	0.74	1.00	0.32	0.80	0.92	0.54	0.29	0.77	0.72	0.86	0.82
FeO	1.11	1.13	1.18	1.14	1.11	1.17	1.24	1.22	1.48	1.17	1.24	1.11	1.20	1.20	1.34	1.31	1.48
MnO	0.03	0.03	0.02	0.03	0.03	0.02	0.02	0.01	0.04	0.02	0.01	0.04	0.04	0.01	0.02	0.03	0.03
MgO	0.02	0.02	0.03	0.04	0.02	0.00	0.02	0.04	0.02	0.02	0.05	0.00	0.00	0.00	0.00	0.07	0.02
CaO	39.7	39.5	39.5	39.4	39.5	39.5	39.4	39.2	39.1	39.3	39.0	39.7	39.4	39.3	39.0	39.0	39.3
Na_2O	0.26	0.18	0.27	0.28	0.22	0.26	0.29	0.31	0.31	0.19	0.29	0.24	0.38	0.18	0.29	0.21	0.22
SrO	0.29	0.23	0.26	0.34	0.23	0.29	0.21	0.21	0.40	0.22	0.19	0.27	0.38	0.22	0.20	0.18	0.18
Y_2O_3	0.03	0.03	0.04	0.03	0.02	0.04	0.03	0.02	0.04	0.04	0.04	0.03	0.04	0.04	0.01	0.03	0.05
ZrO_2	0.02	0.03	0.00	0.02	0.02	0.02	0.00	0.00	0.04	0.03	0.03	0.03	0.06	0.03	0.02	0.03	0.02
Nb_2O_3	0.31	0.26	0.27	0.39	0.35	0.40	0.27	0.23	0.48	0.31	0.26	0.32	0.44	0.30	0.24	0.21	0.26
Ta_2O_5	0.04	0.03	0.03	0.01	0.03	0.02	0.06	0.01	0.03	0.02	0.03	0.02	0.01	0.03	0.03	0.03	0.07
ThO_2	0.02	0.07	0.01	0.02	0.07	0.04	0.07	0.07	0.00	0.06	0.10	0.05	0.00	0.09	0.06	0.09	0.10
Totale	99.8	99.6	99.6	99.5	99.8	99.4	99.4	99.4	99.3	99.3	99.4	99.4	99.2	99.0	98.9	99.0	99.4

Apatite

Apatite is abundant and forms several millimeter-long prisms or inclusions in mica and amphiboles. It coprecipitates with calcite, K-feldspar, and analcite in the groundmass. Most of the analyses are hydroxyfluor-apatite but F-apatite and Cl-apatite are also present and relate to specific outcrops. Apatite modal abundance is evident up to 5% (by vol.) and reflects variable but high P_2O_5 content in the IL. Silica content averages 1% (by wt.),up to 3.5% (by wt.); Sr averages 0.7% (by wt.), up to 1.6% (by wt.); La_2O_3+Ce_2O_3 averages 0.5% (by wt.) and is up to 1.8% (by wt.). F averages 1.6% (by wt.), up to 4.6% (by wt.); SO_3 averages 0.4% (by wt.), up to 1.6% (by wt.), while Cl averages 0.4% (by wt.), up to 1.6% (by wt.). Generally speaking, high Si+LRE+Sr inversely correlates with P_2O_5 and volatile content. High but variable content of Si+LREE+Sr is typical of lamprophyres,

kimberlites, lamproites, melilitites, and carbonatites [17, 18, 19, 20, 26, 27, 31, 33]. Even if CO_2 is not readily detected in apatite, some IL apatites may contains detectible amounts of CO_2, as suggested by consistent P-site occupancy <6.

Table 11.

Representative analyses of garnet from Italian Lamprophyres.

garnet	*La Queglia*					
SiO_2	42.6	39.5	39.0	37.3	36.8	36.0
TiO_2	5.13	5.79	7.03	7.31	7.61	8.32
Al_2O_3	8.36	10.2	9.66	10.4	11.5	11.5
Cr_2O_3	n.a.	n.a.	n.a.	n.a.	n.a.	n.a.
FeO	6.31	9.08	9.44	10.7	9.36	9.97
Fe_2O_3	n.a.	n.a.	n.a.	n.a.	n.a.	n.a.
MnO	0.05	0.17	0.16	0.23	0.13	0.18
MgO	11.8	10.0	9.79	9.00	9.10	8.88
CaO	23.4	23.1	22.7	22.7	22.9	22.6
Na_2O	0.47	0.68	0.68	0.57	0.63	0.65
Total	98.1	98.6	98.5	98.2	98.0	98.2

Carbonate

Carbonates are ubiquitous as very fine-grained carbonate patches in the groundmass or forming the bulk of it. Ocelli (up to 2 mm in diameter) and globular structures are widespread. Small veins of secondary calcite can be present, as well as pseudomorphs after olivine, melilite, and pyroxenes. Carbonate proved to be mostly calcite with MgO, generally up to 2.6% (by wt.), dolomite with MgO

Table 12.

Representative analyses of apatite from Italian Lamprophyres.

apatite	*Calceranica*		*Corvara*		*Nuraxi Figus*		*Pietre nere*		*La Queglia*					*Val Fiscalina*		
SiO_2	0.69	0.78	1.79	2.29	1.09	0.75	0.12	0.34	3.50	3.21	1.64	1.94	1.99	1.98	1.57	2.01
FeO	0.65	0.57	0.17	0.24	0.39	0.27	0.41	0.45	0.32	0.48	0.22	0.17	0.24	0.36	0.28	0.52
MnO	0.00	0.05	0.05	0.05	0.00	0.00	0.08	0.03	0.00	0.04	0.03	0.00	0.00	0.03	0.05	0.04
MgO	0.31	0.22	0.20	0.10	0.27	0.22	0.25	0.34	0.23	0.13	0.13	0.14	0.17	0.24	0.16	0.29
CaO	53.6	53.1	55.4	53.4	55.0	54.5	52.6	52.7	57.1	56.0	55.8	55.8	55.7	55.0	54.5	54.3
Na_2O	0.15	0.12	0.13	0.30	0.16	0.13	0.36	0.37	0.05	0.04	0.09	0.00	0.04	0.07	0.05	0.06
SrO	0.52	0.50	0.67	1.23	0.49	0.70	1.54	0.93	0.38	0.65	0.40	0.51	0.40	0.56	0.73	0.56
BaO	0.00	0.00	0.00	0.00	0.00	0.00	0.00	0.01	0.00	0.00	0.00	0.00	0.00	0.00	0.00	0.00
Ce_2O_3	0.00	0.17	0.49	1.17	0.31	0.42	0.35	0.36	0.16	0.19	0.00	0.00	0.00	0.56	0.65	0.51
La_2O_3	0.00	0.00	0.25	0.61	0.00	0.21	0.21	0.22	0.00	0.00	0.00	0.00	0.00	0.34	0.33	0.29
P_2O_5	41.0	42.0	38.9	38.5	39.6	40.2	40.8	40.9	36.1	37.1	39.9	40.0	39.2	37.7	38.2	37.8
SO3	n.a.	n.a.	0.89	0.28	0.89	0.45	0.47	0.55	1.55	1.19	0.95	0.95	0.97	0.73	0.50	0.77
F	3.72	4.62	1.20	1.03	1.25	1.47	0.42	0.59	1.45	1.92	1.35	1.62	1.42	1.55	1.62	1.48
Cl	0.44	0.49	0.29	0.18	0.88	0.76	1.64	1.08	0.24	0.16	0.24	0.24	0.27	0.19	0.23	0.21
O=F,Cl	1.68	2.07	0.58	0.48	0.73	0.80	0.55	0.49	0.67	0.86	0.62	0.74	0.66	0.70	0.74	0.68
Total	99.6	101	99.9	99.0	99.7	99.4	98.6	98.0	101	100	100	101	100	98.7	98.1	98.2

between 12.6% and 20.9% (by wt.), and ankerite molar solution up to 40% (Tab. 14). Siderite-rich carbonate also occurs and contains up to 70% (by mol.) $FeCO_3$+$MnCO_3$. Dolomite and calcite contain SrO up to 2.2% (by wt.) and up to 1.8% (by wt.), respectively. LREEs are generally low but can be detected at up to 0.6% (by wt.) (2,000 ppm) in calcite. MnO is present at up to 1.5% (by wt.) in

calcite and up to 19.2% (by wt.) in dolomite. Siderite contains MnO at up to 38.3% (by wt.). In general, greater amounts of Sr, Ba, LREE, and MnO indicate higher temperature and igneous origins of the calcite and dolomite. Calcite composition in the various textural occurences in ILs is described in Vichi et al. [40].

Table 13.

Representative analyses of carbonates from Italian Lamprophyres.

carbonate	*Murci*		*Castiglioncello*		*Senna*		*Corvara*		*Calceranica*			
SiO_2	0.00	n.a.	0,47	0,06	0.00	0,09	0,94	0.00	0,04	0.00	0.00	0.00
FeO	0,14	8,48	1,10	6,08	0,63	0.00	0,64	0,05	2,87	7,29	1,97	1,32
MnO	0,21	0,53	0,29	0,71	0,20	0,05	0,74	0.00	0,89	0,40	0,36	0,35
MgO	0,02	14,16	1,08	14,89	0,97	0,00	0,59	0,00	18,87	16,34	0,71	1,10
CaO	55,1	31,5	51.0	31,6	52,3	54,1	50,8	55,2	30,2	28,8	51,0	50,6
SrO	0,95	0,04	0,36	0.00	0,15	0,93	0.00	0,86	0,65	0,19	0,12	0,05
BaO	0.00	0.00	0.00	0.00	0.00	0.00	0.00	0.00	0.00	0.00	0.00	0.00
La_2O_3	0.00	0.00	0.00	0.00	0.00	0.00	0,27	0.00	0.00	0.00	0.00	0.00
Ce_2O_3	0.00	0.00	0.00	0.00	0.00	0.00	0,32	0.00	0.00	0.00	0.00	0.00
Total	56,5	54,8	54,5	53,4	54,3	55,3	54,4	56,2	53,6	53,4	54,26	53,48
	Nuraxi Figus				*Pietre Nere*		*La Queglia*		*Val Fiscalina*			
SiO_2	0.00	0.00	0,08	0,16	0,12	0,06	0,06	0,06	n.a	n.a	n.a	n.a
FeO	0,06	0,09	0,45	1,49	0,17	0,19	0.00	0.00	42,62	21,42	6,50	6,62
MnO	0,24	0,23	0,09	0,28	0,07	0,28	0,12	0.00	10,6	33,3	19,1	16,6
MgO	0,19	0,08	20,40	20,90	0,05	0,03	2,63	1,49	0.00	0,85	0,19	0,15
CaO	54,4	54,5	30,9	29,4	53,4	55.0	51,2	54,0	1,86	0,12	27,8	27,8
SrO	0,48	0,87	2,20	2,16	1,78	0,37	0,08	0,07	0.00	0.00	1,46	0.00
BaO	0.00	0.00	0.00	0.00	0.00	0.00	0.00	0,11	0.00	0.00	0,09	bd
La_2O_3	0.00	0.00	n.a.	n.a.	n.a.	n.a.	0.00	0.00	0.00	0.00	0.00	0.00
Ce_2O_3	0.00	0.00	n.a.	n.a.	n.a.	n.a.	0.00	0.00	0.00	0.00	0.00	0.00
Total	55,6	56,0	54,1	54,3	55,6	55,9	54,1	55,7	55,1	55,7	55,2	51,1

Ocelli

Ocelli concentrate at the contacts, where they can form 25% (by vol.) of the igneous rock. Usually are smaller than 2 mm in diameter, spherical, and sometimes coalescent. The ocelli structure is made of concentric mica, clinopyroxenes, sulphides, and rarely brookite. Clinopyroxene prisms (aegirine-augite) can also grow towards the ocellus centre. The inner part is filled with mosaic-textured calcite and/or analcite and apatite. Calcite exsolves myriads of strontianitie grains concentrated at the crystal boundaries. Concentrations of ocelli towards the contact indicate primary carbonate migration towards the cooler contact rock, as seen typically in lamprophyres. Segregation patches are specific to lamprophyres and are better seen into coarser-grained facies. The presence of selective alteration patches in the matrix contrasts with some fresh mineral species, giving the typical autometasomatic look of ILs.

BULK ROCK GEOCHEMISTRY

Major elements

The ILs have a consistent silica undersaturation and are ultrabasic or basic, having between 36.6% and 49.8% (by wt.) SiO_2 for rocks with carbonates lesser than 10%

(by wt.), wheras carbonatitic ILs (containing carbonates at levels of 10% to 50% by wt/) have from 27.4% to 42.5% (by wt.) SiO_2. Al_2O_3 averages 10.5% (by wt.). Na_2O and K_2O are detected at up to 5.7% and 4.4% (by wt.), respectively. The ILs have Alk/Al averaging 0.54 in atoms. They are metalluminous rocks

Table 14.

Location	***Fos. Ripiglio***		***Murci***		***Castiglion.***		***Senna River***			***Corvara***			
SiO_2	46.1	49.7	39.6	39.6	44.2	42.5	27.3	40.2	43.9	29.1	40.7	41.7	41.3
TiO_2	2.39	2.38	2.95	2.89	2.70	2.85	1.73	2.36	2.26	1.80	1.79	1.78	1.80
Al_2O_3	10.7	11.0	11.1	11.6	10.5	11.8	9.39	11.7	13.3	10.0	10.1	9.71	10.0
Fe_2O_3	5.03	5.24	4.29	2.79	4.98	3.63	1.82	2.58	4.12	2.38	5.75	5.76	5.51
FeO	4.40	3.90	5.50	6.30	5.00	4.60	3.00	6.20	3.70	8.00	5.00	5.10	5.40
MnO	0.14	0.14	0.09	0.10	0.14	0.10	0.28	0.17	0.09	0.18	0.15	0.15	0.16
MgO	11.6	8.11	11.3	10.3	11.6	6.74	1.98	6.71	8.87	12.0	10.1	11.7	12.3
CaO	7.45	9.36	7.99	8.62	9.00	9.60	26.9	11.1	6.07	14.6	15.4	15.0	14.3
Na_2O	1.35	1.94	1.56	2.11	0.88	2.36	3.25	2.06	3.47	1.12	2.71	2.33	1.81
K_2O	2.74	3.68	0.70	0.81	3.08	1.76	0.46	2.48	3.31	0.57	0.79	1.06	1.07
P_2O_5	1.01	0.97	1.01	0.99	1.28	1.33	0.76	1.00	1.13	1.36	1.36	1.34	1.36
CO_2	0.16	0.73	5.79	6.60	0.06	6.24	20.25	7.72	2.55	9.75	2.07	0.93	1.02
LOI	6.74	3.77	7.21	6.80	6.24	6.36	2.35	5.08	7.15	6.95	3.43	3.57	4.38
Total	99.8	101	99.2	99.5	99.7	99.8	99.5	99.4	99.9	97.8	99.3	99.7	100
Mg#	0.82	0.79	0.79	0.75	0.81	0.72	0.54	0.66	0.81	0.73	0.78	0.80	0.80
$^{87}Sr/^{86}Sr$	0.70476		0.70574		0.70551		0.705945			0.70775			
$^{143}Nd/^{144}Nd$	0.51278		0.51276		0.51282		0.512782			0.51243			

Location	***Calceranica***			***N. Figus***	***Pietre Nere***			***La Queglia***			***Val Fiscalina***		
SiO_2	42.9	41.9	43.2	43.4	41.5	41.1	47.5	36.1	36.9	33.5	42.4	41.0	40.3
TiO_2	1.76	2.01	2.08	1.68	2.65	3.00	2.99	3.48	3.75	3.52	3.05	2.66	2.63
Al_2O_3	12.3	11.3	11.7	11.6	10.7	9.89	15.0	9.81	8.31	7.74	11.1	8.95	8.93
Fe_2O_3	4.04	4.57	4.40	4.39	4.61	4.91	4.60	6.38	8.08	5.91	3.71	3.51	2.61
FeO	7.10	6.50	6.30	5.80	6.40	6.70	6.20	3.70	3.40	4.10	6.40	6.60	7.30
MnO	0.18	0.14	0.15	0.17	0.19	0.17	0.18	0.18	0.13	0.15	0.15	0.14	0.14
MgO	8.84	8.04	8.15	9.83	9.25	9.45	3.88	12.5	10.8	13.1	8.14	12.3	11.8
CaO	11.7	13.3	12.4	12.1	13.7	14.3	7.28	13.4	14.3	15.3	12.0	10.3	10.1
Na_2O	3.40	1.99	2.00	2.39	3.54	2.70	5.70	0.89	0.44	0.68	1.60	0.88	0.62
K_2O	1.00	1.50	1.96	1.67	2.17	1.46	2.22	1.25	0.90	0.91	3.55	4.08	4.42
P_2O_5	1.28	1.57	1.66	1.31	1.35	1.34	1.12	1.40	1.14	1.04	1.04	0.84	0.84
CO_2	3.36	2.41	1.78	2.71	1.42	0.97	0.39	3.09	3.21	5.60	4.79	7.08	9.00
LOI	1.54	3.39	2.92	3.09	1.58	2.53	1.51	7.41	8.79	7.60	1.51	0.92	0.50
Total	99.4	98.7	98.8	100	99.1	98.6	98.6	99.5	100	99.2	99.4	99.2	99.3
Mg#	0.69	0.69	0.70	0.642	0.61	0.60	0.40	0.70	0.64	0.72	0.69	0.77	0.74
$^{87}Sr/^{86}Sr$	0.70370			0.70475	0.70355			0.70393			0.70603		
$^{143}Nd/^{144}Nd$	0.51297			0.51281	0.51283			0.51274			0.51264		

Bulk rock composition in major oxides of Italian lamprophyres.

having (Ca+Alk)/Al>1. The ILs are generally potassic rock [K_2O>(Na_2O-2)] with a K_2O/Na_2O ratio averaging 1.3, but ultrapotassic types have K_2O/Na_2O ratios up to 7.8. TiO_2 averages 2.5 and is present at up to 3.8% (by wt.). CaO ranges between 6.7% and 15.4% (by wt.) in non-carbonatitic ILs and 8% to 26.9% (by wt.) in carbonatitic ILs. P_2O_5 is 1.2% (by wt.) and up to 1.7% (by wt.). Most of the rock types represent primitive melts, with Mg# values ranging between 66 and 86. Only a very limited number of samples have Mg# values as low as 53-54 and still show a relatively evolved felsic composition. Compatible element content

correlates positively with Mg#. These values are in range with primary mantle melts such as kimberlites. The hydroxilated and CO_2-rich nature of ILs prevent the use of the TAS diagram [22]. Major element discriminating diagrams proposed by Rock [32] for kimberlites, lamproites, and lamprophyres indicate these rocks are

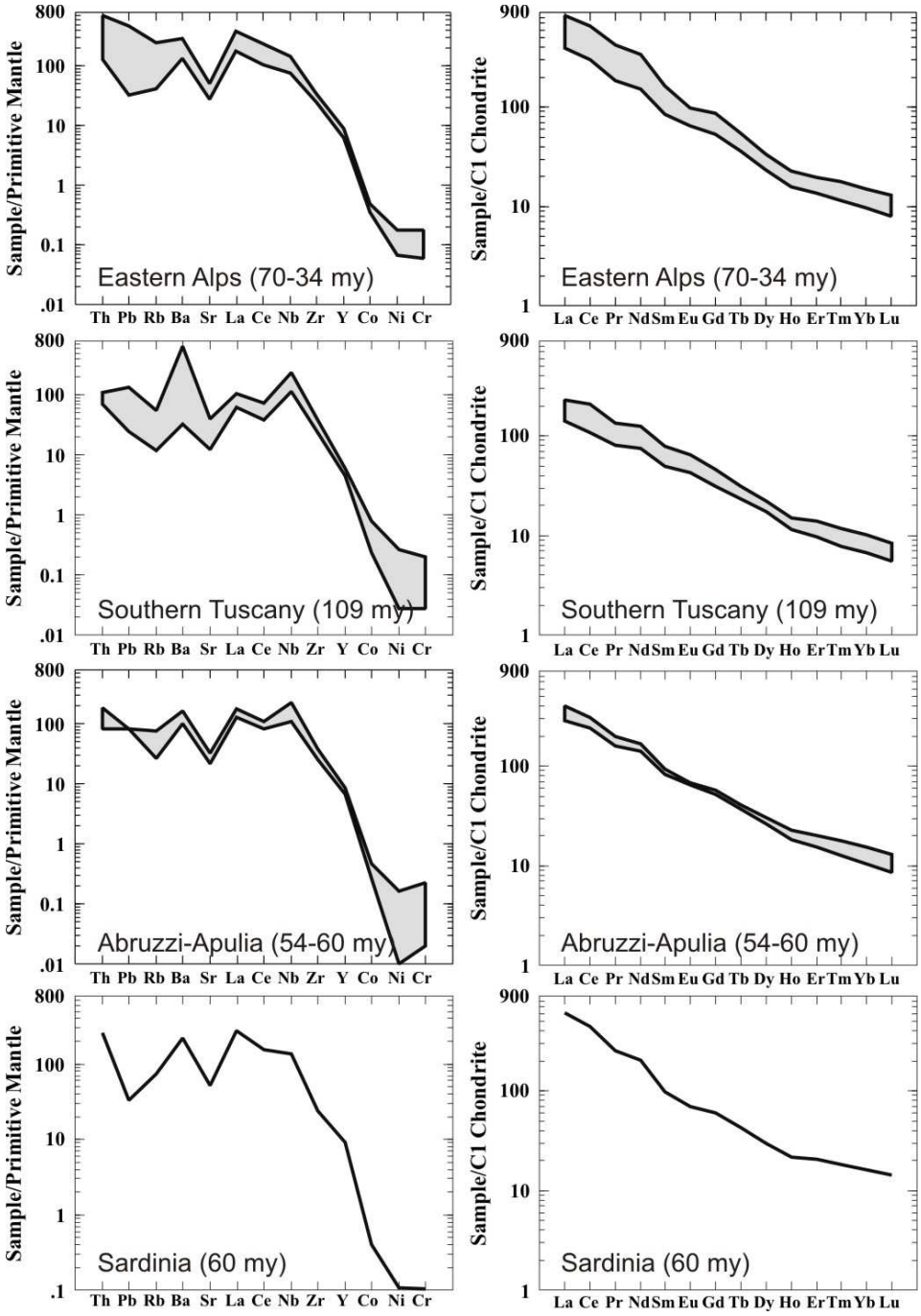

Fig. 2. **Mantle-normalised trace elements and chondrite-normalised REE spider diagrams for Italian Lamprophyres**

lamprophyres, belonging to the alkaline and ultramafic lamprophyre groups. ILs are well-separated by lamproite in their K_2O-MgO-Al_2O_3 content, having lower K_2O, and are separated by CAL, having lower SiO_2 in the SiO_2/10-CaO-TiO_2*4

diagram. Chemical distinction between Al and UML is not easy on a purely chemical basis, but they are clearly different in their taxonomy.

Trace elements and isotopes

All lamprophyres have very high content of both incompatible and compatible elements. This is directly related to their content of mafic minerals and to a liquid

Table 15.

Trace element composition of Italian lamprophyres.

produced by very low partial-melting degrees of the mantle source. However, trace

	Calceranica			*N. F*	*Punta Pietre Nere*			*la Queglia*			*Val Fiscalina*			*F.Ripiglio*		*Murci*		*C.Trinoro*		*Senna River*			*Corvara in Badia*			
Ba	876	755	1470	1250	848	498	617	919	562	852	1300	1110	1010	780	755	478	515	3630	715	181	608	755	1940	1470	1610	1610
Rb	31	46	55	55	43	26	32	56	20	44	120	170	184	33	27	16	18	40	36	9	35	41	19	29	35	32
Sr	1140	1160	1420	1420	817	611	616	829	923	692	1170	847	764	346	565	465	533	1090	852	539	912	874	833	1680	1050	1140
Cs	3.5	2.7	3.6	8.0	0.6	0.5	0.4	0.6	0.2	1.4	29.6	4.4	23.7	0.7	0.2	0.8	0.8	0.7	2.9	0.5	3.6	6.3	1.8	1.6	1.5	1.5
Ga	17	18	19	17	19	16	14	18	16	24	19	18	17	18	17	22	22	19	22	14	22	22	22	17	16	16
Tl	0.20	0.20	0.30	0.18	0.00	0.00	0.00	0.01	0.00	0.00	1.77	0.47	0.42	0.15	0.16	0.00	0.01	0.01	0.12	0.12	0.01	0.01	0.10	0.18	0.18	0.21
Ta	2.9	3.5	3.6	3.6	5.6	7.0	6.4	5.3	3.8	6.4	5.1	4.1	4.1	4.6	4.5	5.2	5.4	5.9	6.3	3.4	4.9	5.3	2.4	2.4	2.2	2.2
Nb	64.0	73.0	76.0	76.7	143	136	119	101	62.2	128	82.9	69.7	80.1	82.1	82.6	95.2	98.2	128	134	63.4	93.6	94.1	48.0	50.0	46.0	43.0
Hf	4.6	5.8	6.1	5.6	8.9	9.1	8.1	6.1	5.7	8.2	7.4	6.7	7.1	5.4	5.8	6.9	7.3	7.3	7.9	5.2	7.0	7.9	5.8	5.6	5.6	5.6
Zr	204	234	245	198	372	338	307	243	214	317	287	241	258	198	209	270	285	289	321	195	265	308	225	224	222	223
Y	29.0	29.0	30.00	30.9	28.8	26.2	22.8	25.8	23.0	29.4	24.6	21.6	22.1	15.4	15.4	17.1	17.5	19.5	19.1	20.5	17.6	20.2	29.0	32.0	31.0	30.00
Th	11.0	8.30	8.72	16.3	8.26	13.6	11.9	8.08	5.32	10.4	19.4	15.1	15.8	5.16	5.17	5.01	5.25	6.26	6.52	4.49	5.91	7.12	49.0	49.0	47.0	45.0
U	2.80	2.21	2.26	3.46	3.10	1.95	2.27	1.83	1.38	2.62	4.96	3.58	3.27	1.61	1.68	1.43	1.57	1.99	1.99	1.36	1.96	2.09	8.07	8.96	8.72	8.37
Cr	224	199	183	308	295	720	671	295	369	60	422	538	520	610	400	286	289	394	241	85	265	270	367	375	417	425
Ni	238	152	140	226	170	379	341	170	149	21	171	378	371	562	400	314	285	326	165	59	220	278	234	229	269	243
Co	42.9	38.7	36.8	42.8	38.9	50.00	49.4	43.1	38.8	28.3	37.6	52.0	51.7	82.8	60.7	44.2	40.2	39.8	57.2	25.0	34.4	52.6	45.0	47.0	48.0	45.0
Sc	18	17	16	22	16	25	23	20	23	7	20	21	20	13	12	11	12	13	12	9	11	12	22	21	23	23
V	188	173	177	200	316	264	251	236	255	199	256	221	219	152	154	154	151	165	157	107	137	132	218	214	209	215
Cu	101	57.2	84.4	64.0	64.7	38.7	47.2	80.5	69.8	33.3	70.5	60.9	60.7	46.1	45.4	44.1	50.7	77.6	49.7	41.7	38.6	55.4	67.0	67.0	68.0	76.0
Pb	0.00	0.00	0.00	4	3	0.00	0.00	0.00	0.00	10	0.00	4	5	6	0.00	8	0.00	0.00	0.00	16	3	0.00	0.00	57	49	57
Zn	118	123	126	109	91.8	100	81.8	124	107	133	108	94.5	96.8	114	120	121	126	132	115	71.6	119	125	150	113	97.0	105
Bi	0.1	0.00	0.00	0.1	0.1	0.2	0.00	0.00	0.00	0.1	0.1	0.1	0.1	0.00	0.00	0.00	0.00	0.00	0.1	0.1	0.00	0.00	0.4	0.3	0.3	0.4
Sn	0.00	2	2	1	2	2	2	2	2	2	3	2	2	2	2	2	3	3	3	9	2	2	2	2	2	2
W	2.2	2.2	2.1	1.4	1.0	0.6	0.8	1.1	0.7	0.7	2.0	2.2	2.8	207	144	1.3	1.6	2.0	158	68.7	1.4	158	4.8	2.2	3.0	3.4
Be	1.0	2.0	2.0	2.0	3.0	2.0	2.0	1.0	1.0	2.0	2.0	2.0	2.0	2.0	2.0	3.0	3.0	3.0	3.0	2.0	3.0	3.0	2.0	3.0	3.0	3.0
Ag	0.90	1.00	1.10	1.10	1.70	1.60	1.40	1.30	0.90	1.50	1.20	1.00	1.20	1.30	1.20	1.30	1.50	1.60	1.60	0.90	1.30	1.40	0.80	0.70	0.70	0.70
As	0.00	0.00	0.00	0.00	0.00	0.00	0.00	0.00	0.00	0.00	7.0	9.0	10.0	0.00	0.00	0.00	0.00	0.00	0.00	5.0	0.00	0.00	10.00	11.0	7.0	14.0
Sb	0.3	0.4	0.3	0.6	0.3	0.5	0.3	0.3	0.3	0.2	0.4	0.4	0.4	0.3	0.3	0.3	0.4	0.4	0.4	0.5	0.3	0.3	0.4	0.6	0.4	3.2
Ge	0.00	0.60	0.00	0.00	0.60	0.70	0.80	0.60	0.70	0.00	0.70	0.00	0.60	0.50	0.00	0.60	0.00	0.00	0.50	0.60	0.00	0.00	0.70	0.70	0.80	0.90
La	96.0	93.8	102	143	90.4	107	94.5	87.5	68.5	88.3	122	100	101	42.4	42.9	44.5	46.5	54.9	54.9	33.1	46.3	50.3	197	215	201	199
Ce	183	201	216	271	160	215	188	179	146	174	240	200	205	97.5	96.0	103	106	122	127	65.3	104	114	407	439	417	405
Pr	17.5	20.1	21.6	24.2	15.4	21.2	18.8	17.7	15.0	17.0	23.7	19.9	20.2	10.1	9.93	10.9	11.3	12.8	12.8	7.59	10.7	11.4	40.0	43.0	41.0	40.0
Nd	71.4	86.1	92.5	94.3	65.3	89.1	78.8	74.4	66.0	71.3	97.1	82.4	83.1	45.1	44.9	49.2	51.8	57.0	58.2	34.8	47.8	52.0	156	165	163	158
Sm	12.9	16.0	17.0	15.1	12.5	16.2	14.3	13.6	12.7	13.4	16.6	14.2	14.5	9.27	9.28	10.1	10.7	11.5	11.9	7.50	9.74	10.8	24.0	26.0	25.0	25.0
Eu	3.77	4.60	4.94	4.01	3.67	4.40	3.97	3.94	3.71	3.96	4.35	3.76	3.77	3.04	3.06	3.17	3.36	3.79	3.73	2.51	3.11	3.62	5.63	5.89	5.75	5.63
Gd	11.0	13.5	14.5	12.3	10.8	12.8	11.7	11.5	10.7	11.6	12.8	10.9	11.0	7.52	7.55	8.27	8.55	9.47	9.50	6.45	8.02	9.27	17.60	18.40	17.9	17.7
Tb	1.46	1.70	1.81	1.59	1.44	1.61	1.48	1.45	1.37	1.52	1.53	1.35	1.34	0.95	0.94	1.02	1.05	1.17	1.17	0.87	1.02	1.16	2.01	2.11	2.04	2.04
Dy	7.53	8.06	8.60	7.60	7.36	7.44	6.79	7.13	6.75	7.79	7.01	6.07	5.95	4.38	4.37	4.88	4.89	5.44	5.50	4.83	4.77	5.60	8.46	8.79	8.44	8.45
Ho	1.23	1.21	1.30	1.22	1.20	1.14	1.03	1.09	1.02	1.28	1.05	0.92	0.90	0.66	0.65	0.72	0.74	0.81	0.82	0.82	0.74	0.84	1.25	1.30	1.26	1.26
Er	3.24	2.96	3.15	3.41	3.10	2.92	2.66	2.87	2.56	3.35	2.61	2.27	2.28	1.64	1.60	1.77	1.83	1.96	1.94	2.29	1.85	2.12	3.20	3.31	3.18	3.16
Tm	0.45	0.37	0.39	0.47	0.41	0.36	0.32	0.36	0.32	0.45	0.34	0.29	0.29	0.21	0.20	0.21	0.23	0.25	0.24	0.30	0.22	0.27	0.41	0.43	0.41	0.41
Yb	2.54	2.06	2.13	2.72	2.30	2.05	1.80	2.01	1.77	2.60	1.93	1.65	1.63	1.20	1.13	1.19	1.25	1.33	1.35	1.72	1.26	1.47	2.37	2.38	2.30	2.33
Lu	0.33	0.26	0.28	0.36	0.28	0.26	0.23	0.26	0.22	0.33	0.25	0.20	0.20	0.15	0.15	0.14	0.15	0.16	0.16	0.21	0.15	0.18	0.30	0.31	0.30	0.33

elements are not very efficient for discriminating different ILs and intra- and infra-outcrop variations are comparable (Fig.2). ILs have Rb <100 ppm, excluding ultra-potassic lamprophyres from Val Fiscalina, which have up to 184 ppm; in general,

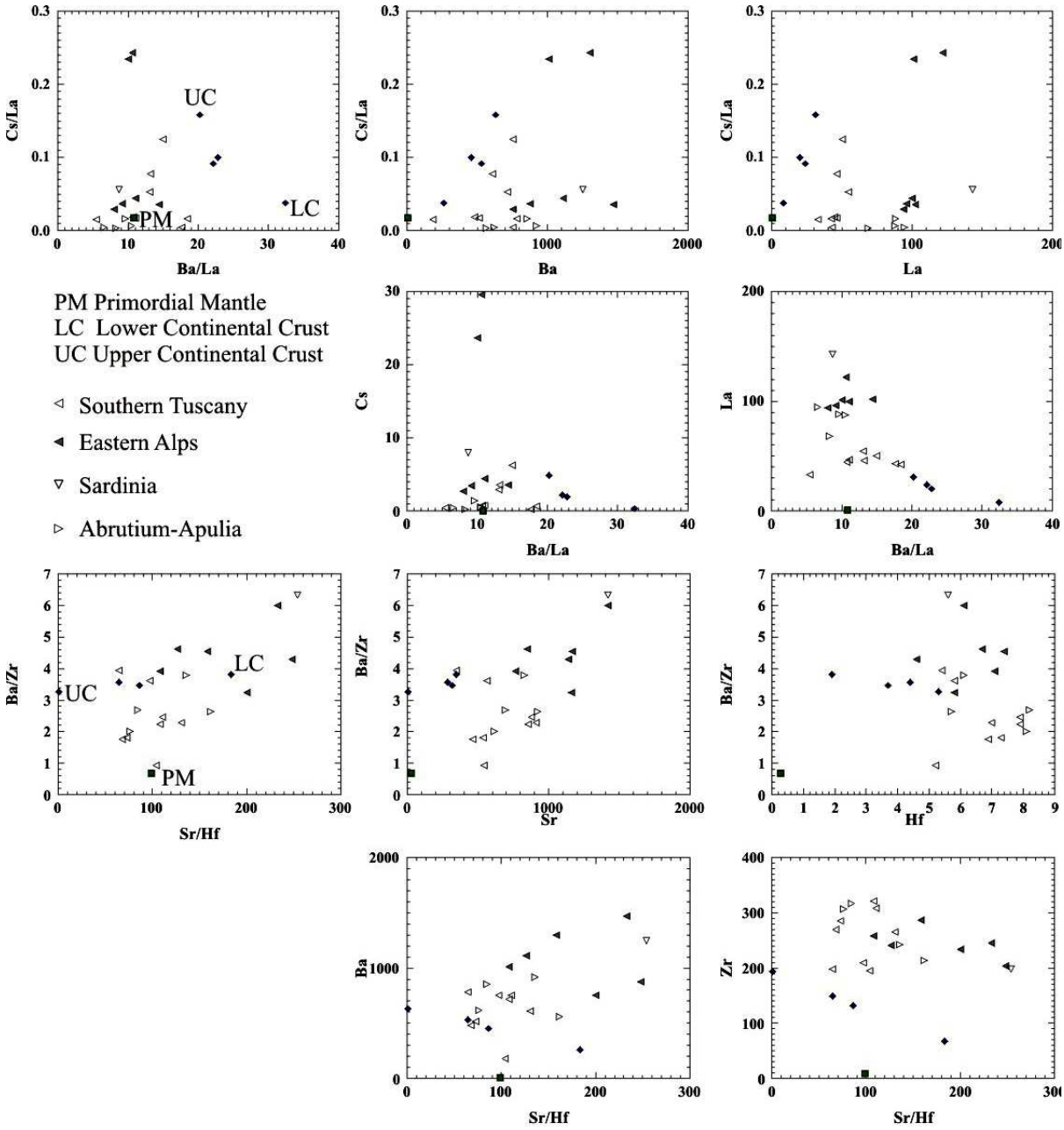

Fig. 3a. **Diagrams that combine LILE-HFSE ratios. HIMU, EMII and EMI are indicated.**

this distinction positively correlates with Ba and K. Ba and Sr are variable both in carbonatitic and non-carbonatitic lamprophyres, with Ba averages of >1,000 ppm and up to 3,630 ppm. The Sr average is 885 ppm and up to 1,680 ppm.

LILE distribution seems largely controlled by mica, amphibole, feldspar (Rb, Ba) and apatite-carbonate (Sr). $\sum LILE_{pm}$ average value is 684 ($_{pm}$ = normalised to the primitive mantle), having Cs_{pm} = 408, Rb_{pm} = 63, Ba_{pm} = 181, Sr_{pm} = 32. Zr averages 257 ppm and is up to 372 ppm. Hf averages 6.6 ppm and is up to 9.1 ppm. Ta averages 4.5 ppm and is up to 7 ppm. Nb averages 88 ppm and is up to 148 ppm.

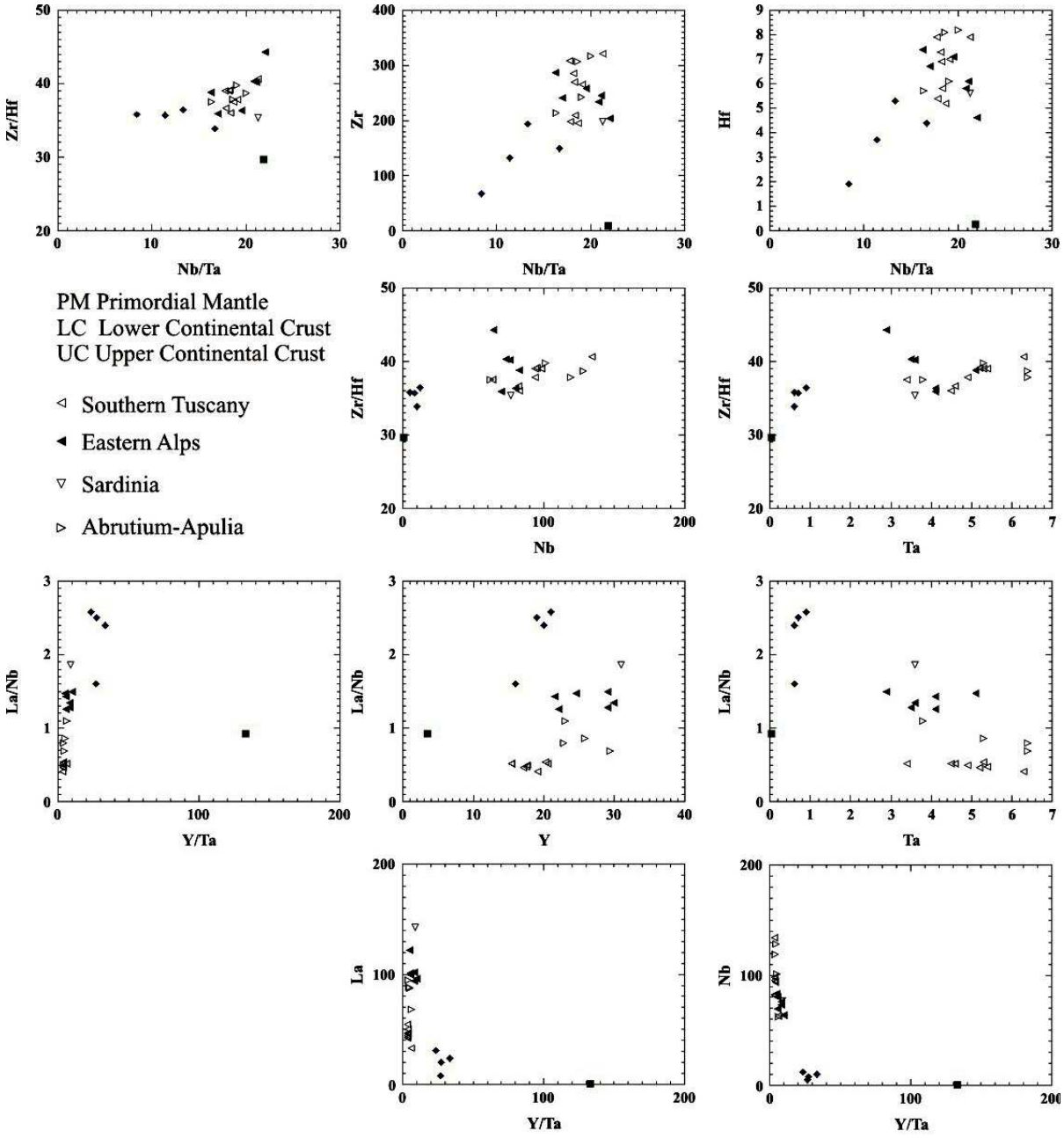

Fig. 3b, c. **$HFSE^{4+}$ /$HFSE^{5+}$, $HFSE^{3+}$ / $HFSE^{5+}$ diagrams.**

Smaller $HFSE^{4+}$ and $HFSE^{5+}$ have a strong positive correlation with Ti. Th averages 15 ppm and is up to 49 ppm. U averages 3 ppm and is up to 9 ppm. Th/U ratio is fairly constant at approximately 5. $\sum HFSE_{pm}$ average value is 607, while the La average is 95 ppm and up to 215 ppm, and Ce averages 193 ppm and is up to 439 ppm. LREEs are equally distributed among carbonatitic and non-carbonatitic lamprophyres and mainly relate to P_2O_5, thus apatite is likely the main acceptor for LREE in ILs. LREE/HREE average value is 62 and up to 112. Y correlates very well with HREE. Higher $HFSE^{4+}$ positively correlates with REE. $\sum REE_{cn}$ ($_{cn}$ = chondrite normalised) average value is 1431, having La_{cn} = 398, Ce_{cn} = 317, Pr_{cn} = 201, Nd_{cn} = 171, Sm_{cn} = 93, Eu_{cn} = 68, Gd_{cn} = 55, Tb_{cn} = 37, Dy_{cn} = 26, Ho_{cn} = 17, Er_{cn} = 15, Tn_{cn} = 13, Yb_{cn} = 11, Lu_{cn} = 9. Compatible elements Cr, Ni, Co, and V total up to 2,036 ppm. Cr and Ni content relates to chromite/olivine and Cr-pyroxene; Ni also relates to trevorite in some rocks. Incompatible elements, normalised to primitive mantle, show a distinctive negative spike of Rb, K, and Sr (Fig.2). Southern Tuscany has positive Nb-Ta spikes and Corvara in Badia (eastern Alps) has Nb-Ta-Ti negative spikes, whereas all the other outcrops do not show appreciable anomalies. Punta della Pietre Nere, Sardinia, and the outcrops of the eastern Alps show variable Zr-Hf negative spikes. REE_{cn} pattern shows a negligible Eu negative anomaly, LREE/HREE ratio increases with increasing $\sum$REE. ILs' incompatible element geochemistry and relationship with notional

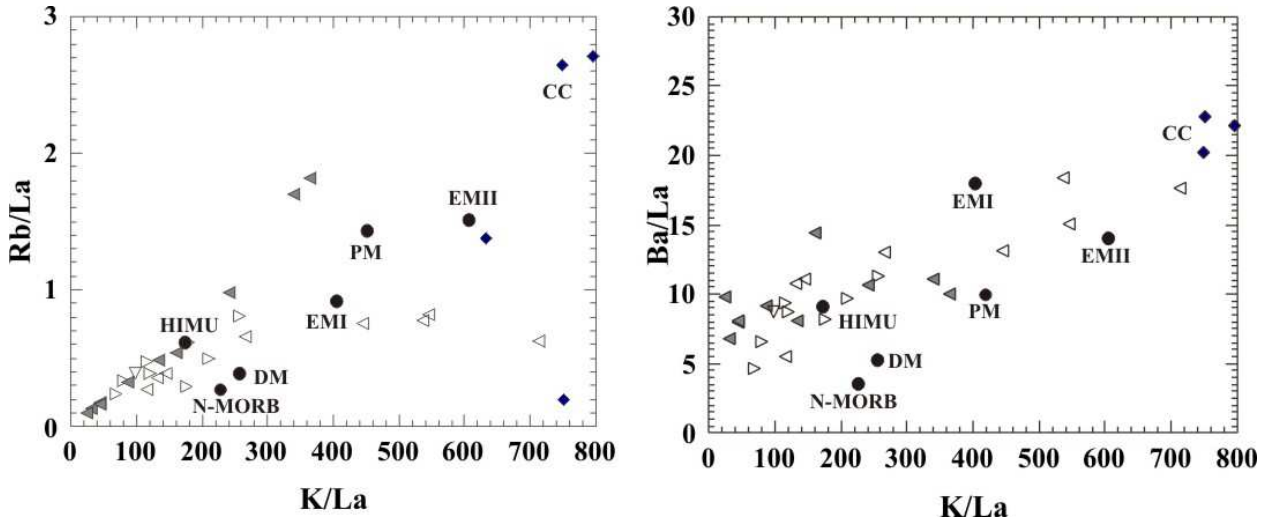

Fig. 3d. **Combined diagrams of radiogenic isotope ratios for Italian lamprophyres.**
FOZO, ITEM and otrher relavnt mantle end-memebrs discussed in the text are indicated.

crustal and primordial mantle compositions may be depicted using diagrams that combine LILE-HFSE ratios. ILs have relatively low LILE/HFSE ratios near the primitive mantle values and lower than HIMU; nevertheless, a clear enrichment trend towards EMII and EMI is apparent (Fig. 3a) [35]. LILE/HFSE ratios are

believed to preserve those of the source, but they certainly cannot be used for combining calculations of non-dimensional numbers. When they are plotted against the elemental concentration in ppm, it is easy to see that ILs' compositions are far apart from any possible crust-mantle mixing curve (Fig. 3b). This is confirmed by using "twin" nonvariable pairs of small ionic radius $HFSE^{4+}$ and $HFSE^{5+}$ (Fig. 3c). $HFSE^{3+}$ / $HFSE^{5+}$ fractionation is much greater in ILs if compared with basaltic rocks [29]. High HFSE content of lamprophyres makes these rocks capable of precipitating specific HFSE-rich mineral phases, a fact which is not observed in subalkaline rocks [11]. Thus, geochemistry of HFSE can be greatly influenced by the settling of crystals of heavy minerals (e.g., titanates).

Isotope taxonomy of ILs is described in term of focal zone (FOZO), which is best observed in Punta delle Pietre Nere and Calceranica outcrops [5-7] and the Italian enriched mantle (ITEM). In a conventional Sr-Nd-Pb isotope diagram, IL isotope ratios follow a trend from FOZO towards the enriched mantle, which greatly exceeds EMI-EMII and rests on a curve that links FOZO to an extremely ^{87}Sr- and ^{144}Nd-enriched radiogenic end-member ITEM. ITEM has isotopic value in excess of the average crust and must represent a very old Rb/Sr reservoir that is characteristic, even if not exclusive, of the Italian mantle. This is not surprising and confirms LILE additions from a very old and fertile source to justify such long-term ^{87}Sr decay.

CONCLUSIONS

The notable carbonatitic component of ILs could be a key feature in their interpretation but worldwide carbonatites have different trace element concentrations, including higher LREE/HREE. In addition, Vichi et al., [40] noted that there is no HFSE fractionation operated by the carbonatitic component. High SiO_2-undersaturation and high carbonate content of similar ultra-alkaline rocks have been considered by some authors to be a consequence of limestone assimilation or other crustal additions to the source via subduction [2, 30]. However, limestone assimilation cannot explain the distribution of strontium isotopes because Sr is at least one order of magnitude lower in sedimentary limestones if compared with lamprophyres and other ultra-alkaline rocks. This means that lamprophyres are virtually insensitive, from an isotopic point of view, to limestone addition. Furthermore, limestone assimilation would dilute the compatible elements of ILs, which are, instead, very high. There is no evidence of eruptive melts on the earth, with komatiite compostion and liquidus temperatures in excess of 1,700°C, which could retain such a high content of compatible elements and still be thermally capable of assimilating substantial amount of limestones. On the other hand, if high Sr crustal felsic rocks had been added, this would produce saturation -not understaturation- in SiO_2. These facts also discredit the old ideas for which lamprophyres would be "mafic" differentiates of felsic melts. Notional progressive undersaturation equations can be always written but, in

nature, this lead to limited skarn formation, that is, the turning of limestone into calcium silicate rocks by metasomatism on contact. This is because there is not sufficient heat in mafic magma to assimilate cold rocks on a large scale. The crustal rocks assimilation hypothesis is highly inconsistent with the observed major and trace element and isotope distribution in lamprophyres and other ultra-alkaline rocks. Addition via subduction is more complex to evaluate, especially if followed by further melt-mantle reactions but cannot be considered a truism. We note that only a few elements were added to the lamprophyre source and this certainly is not the case of a bulk crustal contribute via melting, which would have produced substantial chemical changes in the mantle. Of course, subduction models can be made more and more complex and complicated until they may partially respond to experimental conditions. However, geochemical signatures that are common in lamprophyres, carbonatites, kimberlites, lamproites, and other continental potassic rocks (kamafugites) has been not observed at all in subduction-related melts.

Basing on modern modal classification of lamprophyric rocks, taxonomy of Italian lamprophyres indicate they are carbonatitic, alkaline, and ultramafic lamprophyres. Mineralogy, geochemistry, and isotopic geochemistry indicate these rocks are largely a quenched primitive magma produced by a mantle modified by a deep-seated radiogenic component rich in LILE and carbonate. High Rb and K content of the enriched end-member suggests this may be radiogenic and ^{87}Sr-rich. ILs have variable high LILE/HFSE ratios, which cover virtually a range from FOZO to EMI-EMII to ITEM. The FOZO component, previously associated with the lower mantle, may be better understood as a highly heterogeneous mixture that constitutes the matrix in which larger plumes of LILE/HFSE-enriched material float. ITEM origin seems much more speculative, but it is rare and ILs distribution and chemistry do not seem to be constrained by lithosphere tectonics. The lower Cretaceous to lower Oligocene timespan covered by the ILs is much larger and earlier than the time of formation of the other alkaline Italian rocks and, if they share the same ITEM component, this implies that the source was constant over a very long period of time. These facts suggest that ITEM could be a long-term fed, very deep-seated component. In addition, ILs occur in wider cycles, which may refer to major perturbation of the deep earth better than upper-mantle tectonics. This aspect is germane to lamprophyre isolation or association with ultramafic ultrapotassic rocks [4]. The disappearance of lamprophyres may correspond, in the later cycle, to a source evolution in terms of dehydratation. In fact, lamprophyres are hydrated correspondents of kamafugite-leucitite, which occurs in the recent magmatism of Italy [25, 36]. Notably, carbonatite component seems a constant in all this story, maintained in both lamprophyres and kamafugitic associations. In theory, C-H-O-K-rich fluid could be released by the mantle/nucleous boundary during igneous “storms” as well as radiogenic elements accumulating during very long sealing period of the core-mantle interface. Only ultramafic, deep melts such as kimberlites, lamprophyres, lamproites, carbonatites, and leucitite-kamafugite

seem able to escape more superficial contributions which are seen in basalts and other upper-mantle magmas.

REFERENCES

1. **Amendolagine M., Dell'Anna L., Ventriglia U.** Le rocce ignee alla Punta delle Pietre Nere presso Lesina (provincia Foggia) // Periodico di Mineralogia, 1964, v. 33, p. 337-395.
2. **Anfilogov, V.N.** The hardnessing of the ADSM diagram for genetic analyses of magmatic rock series // In: Alkaline Magmatism: its sources and plumes, (N. V. Vladykin Ed.), Institute of Geography SB RAS, Irkutsk, 2007, p. 183-192.
3. **Bachinski S.W., Simpson E.L.** Ti-phlogopites of the Shaw's Cove minette: a comparision with micas of other lamprophyres, potassic rocks, kimberlites and mantle xenoliths // American Mineralogist, 1984, v. 69, p. 41-56.
4. **Bailey K., Woolley A.R.** Magnetic quiet periods and stable continental magmatism: can there be a plume dimension? // In: Anderson D.L., Hart S.R., Hofmann A.W. (Con.) "Plume 2", Terra Nostra, 1995, v. 3, p. 15-19.
5. **Bell K., Castorina F., Lavecchia G., Rosatelli G. and Stoppa F.** Is there a mantle plume beneath Italy? // EOS, 2004, v. 85 (50), p. 541-546.
6. **Bell K., Castorina F., Rosatelli G. and Stoppa F.** Plume activity, magmatism, and the geodynamic evolution of the eastern Mediterranean // Annals of Geophysics**,** 2006, v.49/1, 357-372.
7. **Bell K., Lavecchia G., and Stoppa F.** Reasoning and beliefs about Italian geodynamics // Boll. Soc. Geol. It., Volume Speciale, 2005, v. 5, p. 119-127.
8. **Bigazzi G., Laurenzi M.A., Principe C., Brocchini D.** New geochronological data on igneous rocks and evaporites of the Pietre Nere Point (Gargano Peninsula, Southern Italy) // Boll. Soc. Geol. It., 1996, v. 115, p. 439-448.
9. **Brogi A., Cornamusini G., Costantini A., Di Vincenzo G., Lazzarotto A.** Cretaceous volcanism of the Southern Tuscany: record of volcanic bodies from Tuscan succession of Rapolano Terme // Mem. Soc. Geol. It., 2000, v. 55, p. 329-337.
10. **Carella R.** Eruttivi di San Giovanni in Pane e della Punta delle Pietre Nere (Gargano) // Boll. Soc. Geol. It., 1963, v. 82, p. 97-110.
11. **Chakhmouradian A. R.** High-field-strength elements in carbonatitic rocks: Geochemistry, crystal chemistry and significance for constraining the sources of carbonatites // Chemical Geology, 2006, v. 235, p. 138-160.
12. **De Fino M., La Volpe L., Piccarreta G.** Geochemistry and petrogenesis of the Paleocene platform magmatism at Punta delle Pietre nere (Southeastern Italy) // N.Jb. Miner. Abh., 1981, v. 142, p. 161-177.
13. **Deer W.A., Howie R.A., Zussman J.** Rock forming minerals. Single chain silicates, Vol. 2A // The geological Society, London, 1997.
14. **Durazzo A., Taylor L.A., Shervais J.W.** Ultramafic Lamprophyre in a Carbonate Platform Environment, Mt. Queglia, Abruzzo, Italy // Neues Jahrbuch Miner. Abh., 1984, v. 150, p. 199-217.
15. **Faraone D., Stoppa F.** Petrology and regional implications of Early Cretaceous alkaline lamptophyres in the Ligure-Maremmano Group (southern Tuscany, Italy): an outline // Ofioliti, 1990, v. 15, p. 45-59.
16. **Galassi B., Monese A., Ogniben G., Siena F., Vaccaro C.** Age and nature of lamprophyric dykes at Calceranica (Trento) // Mineralogica et Petrographica Acta, 1994, v. 37, p. 163-171.
17. **Hogart D.D.** Pyrochlore, apatite and amphibole: distinctive minerals in carbonatite // In: Bell K (Ed.). Carbonatites: genesis and evolution. Unwin Hyman Ltd, London, 1989, p. 618.
18. **Jones A.P., Smith J.V.** Petrological significance of mineral chemistry in the Agata Peak and the Thumb minettes, Nevajo volcanic field // J. Geol., 1983, v. 91, p. 643-656.

19. **Kapustin Yu. L.** Distribution of Sr, Ba and the rare earths in apatite from carbonatite complexes // Geochemistry International, 1977, p. 71-80.
20. **Kapustin Yu. L.** Distribution of strontium, barium and rare-earth elements in minerals of ultramafic alkalic rocks // Doklady Akad. Nauk. SSSR, 1979, v. 252, p. 155-159.
21. **Kogarko L.N., Kurat G., Ntaflos T.** Carbonate metasomatism of the oceanic mantle beneath Fernando de Noronha Island, Brazil // Contrib. Mineral. Petrol., 2001, v. 140, p. 577-587.
22. **Le Maitre, R.E.** Igneous Rocks: A classification and Glossary of Terms. 2nd Edition // Cambridge University Press, Cambridge, 2002, 236 pp.
23. **Lucchini F., Simboli G., Zenatti A., Barbieri M., Nicoletti M., Petrucciani C.** Petrochimica e dati radiometrici K/Ar e Rb/Sr dei "filoni basici" di Corvara in Badia e dei lamprofiri di Val Fiscalina (Dolomiti orientali). Revisione classificativa ed implicazioni genetiche nel quadro del magmatismo filoniano delle Alpi // Miner. Petrog. Acta, 1983, v. 27, p. 233-249.
24. **Maccioni L., Marchi M., Salvadori A.** Eocene alkaline lamprophyre in south western Sardinia (Italy) (new occurrence) // Rendiconti Seminario Facoltà Scienze Università Cagliari, 1990, v. 60, p. 217-231.
25. **Mitchell R.H.** The lamprophyre facies // Mineralogy and Petrology, 1994, v. 51, p. 137-146.
26. **Mitchell R.H.** Kimberlites, orangeites and related rocks // Plenum Press, New York, 1995, 410 p.
27. **Mitchell R.H., Bergman S.C.** Petrology of lamproites // Plenum Press, New York, 1991, 447 pp.
28. **Morimoro N.** Nomenclature of Pyroxenes // Bull. Minéral., 1988, v. 111, p. 535-550.
29. **Muller D., Rock N.M. and Groves D.I.** Geochemical discrimination between shoshonitic and Potassic volcanic rocks in different tectonic settings: A pilot study // Mineral. Petrol., 1992, v. 46, p. 259-289.
30. **Peccerillo, A.** Mantle plume vs. subduction-realted origin of volcanism in Italy: A commentary // In: Alkaline Magmatism: its sources and plumes, (N. V. Vladykin Ed.), Institute of Geography SB RAS, Irkutsk, 2007, p. 57-70.
31. **Prins P.** Apatite from African carbonatites // Lithos, 1973, v. 6, p. 133-144.
32. **Rock N.M.S.** The nature and origin of lamprophyres: an overview // From: Fitton J.G., Ypton G.J. (eds) - Alkaline Igneous rocks, Geological Society Special Publication, 1987, v. 30, p. 191-226.
33. **Rock, N.M.S.** Lamprophyres // Blackie and Son Ltd, 1991, 285 pp.
34. **Rudnick R.L., McDonough W.T., Chappel B.W.** Carbonatite metasomatism in the Northern Tanzania mantle: petrography and geochemical characteristics // Earth Planet. Sci. Lett., 1993, v. 124, p. 463-475.
35. **Rudnick, R.L. and Gao, S.** Composition of the Continental Crust // In: Treatise on Geochemistry. Holland, H.D. and Turekian, K.K. (Editors), Elsevier, Amsterdam, 2004, v. 3, p. 1-64.
36. **Stoppa F., Lavecchia G.** Late Pleistocene ultra-alkaline magmatic activity in the Umbria-Latium region (Italy): an overview // J. Volcanol. Geotherm. Res., 1992, v. 52, p. 277-293.
37. **Stoppa F., Lupini L.** Mineralogy and Petrology of the Polino Monticellite Calciocarbonatite (Central Italy) // Mineral. Petrol., 1993, v. 49, p. 213-231.
38. **Tappe S., Foley S.F, Jenner G. A. and Kjarsgaard B. A.** Integrating Ultramafic Lamprophyres into the IUGS Classification of Igneous Rocks: Rationale and Implications // Journal of Petrology, 2005, v. 46 (9), p. 1893-1900.
39. **Velde D.** Minettes et kersantites. Une contribution a l'étude des lamprophyres // These de Doctorat des sciences naturelles, Paris, 1969, 235 pp.
40. **Vichi G., Stoppa F., Wall F.** The carbonate fraction in carbonatitic Italian lamprophyres // Lithos, Special Issue Eurocarb, 2005, v. 85, p. 154-170.